University of Alberta

Gas Phase Chemistry and Thermochemistry of Electrospray-Generated Ions

by

© John S. Klassen

A thesis submitted to the Faculty of Graduate Studies and Research in partial fulfillment of the requirements for the degree of **Doctor of Philosophy**.

Department of Chemistry

Edmonton, Alberta
Fall 1996

National Library of Canada
Acquisitions and Bibliographic Services Branch
395 Wellington Street
Ottawa, Ontario
K1A 0N4

Bibliothèque nationale du Canada
Direction des acquisitions et des services bibliographiques
395, rue Wellington
Ottawa (Ontario)
K1A 0N4

Your file Votre référence

Our file Notre référence

The author has granted an irrevocable non-exclusive licence allowing the National Library of Canada to reproduce, loan, distribute or sell copies of his/her thesis by any means and in any form or format, making this thesis available to interested persons.

L'auteur a accordé une licence irrévocable et non exclusive permettant à la Bibliothèque nationale du Canada de reproduire, prêter, distribuer ou vendre des copies de sa thèse de quelque manière et sous quelque forme que ce soit pour mettre des exemplaires de cette thèse à la disposition des personnes intéressées.

The author retains ownership of the copyright in his/her thesis. Neither the thesis nor substantial extracts from it may be printed or otherwise reproduced without his/her permission.

L'auteur conserve la propriété du droit d'auteur qui protège sa thèse. Ni la thèse ni des extraits substantiels de celle-ci ne doivent être imprimés ou autrement reproduits sans son autorisation.

ISBN 0-612-18055-7

Canada

University of Alberta

Library Release Form

Name of Author: **John Stephen Klassen**

Title of Thesis: **Gas Phase Chemistry and Thermochemistry of Electrospray-Generated Ions**

Degree: **Doctor of Philosophy**

Year this Degree Granted: **1996**

Permission is hereby granted to the University of Alberta Library to reproduce single copies of this thesis and to lend or sell such copies for private, scholarly or scientific research purposes only.

The author reserves all other publication and other rights in association with the copyright in the thesis, and except as hereinbefore provided, neither the thesis nor any substantial portion thereof may be printed or otherwise reproduced in any material form whatever without the author's prior written permission.

Signed: J. Klassen

Permanent Address: 3 Burrows Rd.
Gloucester, Ont.
Canada, K1J 6E5

Dated: Sept. 24, '96

University of Alberta

Faculty of Graduate Studies and Research

The undersigned certify that they have read, and recommend to the Faculty of Graduate Studies and Research for acceptance, a thesis entitled **Gas Phase Chemistry and Thermochemistry of Electrospray-Generated Ions** submitted by **John Stephen Klassen** in partial fulfillment of the requirements for the degree of **Doctor of Philosophy**.

P. Kebarle

Dr. Paul Kebarle

Gary Horlick.

Dr. Gary Horlick

Gordon Freeman

Dr. Gordon Freeman

M Klobukowski

Dr. Mariusz Klobukowski

John Gray

Dr. John Gray

Dr. Alex Harrison

Dated: Sept 12, 1996

TO MUM, DAD AND SARAH

Abstract

Using a modified triple quadrupole mass spectrometer equipped with a novel low pressure (10 Torr) interface, the energetics for the sequential hydration of a variety of singly and doubly charged electrospray-generated cations and anions ($M^{z+/-}$) have been determined from equilibrium measurements of the reaction: $M^{z+/-}(H_2O)_{n-1} + H_2O = M^{z+/-}(H_2O)_n$ where $M^{z+} = H_2N(CH_2)_pNH_3^+$ (p=2-8,10,12), $^+H_3N(CH_2)_pNH_3^+$ (p=7,8,10,12), $(Gly)_kH^+$, (k=1-4), $LysH^+$, $(Gly\text{-}Lys)H^+$, $(Lys\text{-}Tyr\text{-}Lys)H_2^{2+}$ and M^{z-} = fifty-five singly and doubly charged anions of the oxo acids of C, N, S, P, Cl and I. Measurement of the equilibrium constant ($K_{n-1,n}$) leads directly to the hydration free energy change ($-\Delta G^o_{n-1,n}$) for the reaction. Hydration of these ions involves the formation of ionic hydrogen bonds, *i.e.* $M^{z+}H\text{---}OH_2$, $M^{z-}O\text{---}HOH$, and is primarily electrostatic in nature. As a result, the hydration free energies are sensitive to the degree of charge localization and provide insight into substituent effects and intramolecular interactions which affect the stability of the ions.

Based on the temperature dependence of the equilibrium constants for the hydration of $^+H_3N(CH_2)_pNH_3^+$ (p=5-10,12) and $(CH_3)_3N(CH_2)_pN(CH_3)_3^{2+}$ (p=2,3), the hydration enthalpies ($-\Delta H^o_{n-1,n}$) and consequently the entropies ($-\Delta S^o_{n-1,n}$) were determined for n=1-2. The results obtained for the $^+H_3N(CH_2)_pNH_3^+$ ions indicate that the H_2O molecules add to alternate charged sites. Similar alternate occupation is indicated for $^+(CH_3)_3N(CH_2)_pN(CH_3)_3^+$ when p=2; however, the data obtained for p=3 suggest that the second H_2O molecule may add to same charged site as the first H_2O. These equilibria measurements were carried

out using a low pressure interface which has a temperature range of 273 to 473 K.

Using an apparatus similar to the interface used to study the hydration equilibria, the collision-induced dissociation (CID) threshold method has been successfully applied to measurement of binding energies of ion-ligand complexes generated by electrospray. From threshold measurements, the Na^+ and K^+ affinities of a series of amides and related compounds (CH_3COX, where x=NH_2, NHMe, NMe_2; $H_2NCO(CH_2)_2CONH_2$, H_2NCH_2COOH, $H_2NCH_2CONH_2$ $H_2NCH_2CONHCH_2COOH$) have been determined.

The CID threshold method has also been used to study the dissociation of protonated glycine (Gly), glycinamide, methylglycinamide, glycylglycine (Gly-Gly), glycylglycinamide, Gly-Gly-Gly and Gly-Gly-Gly-Gly. From the appearance curves, the activation energies of the major dissociation pathways have been determined. Based on the measured energetics and *ab initio* calculations, reaction mechanisms for some of the dissociation processes are proposed.

Acknowledgements

I would like to express my sincere gratitude to Professor Paul Kebarle for his guidance and encouragement throughout the course of my studies and for teaching me how to do good science. I would also like to extend a special thanks to Dr. Arthur Blades for all his help in the laboratory, in particular with the development of the low pressure interfaces and the many equilibrium measurements that he carried out. Thank you both for all that you have taught me and, more importantly, for your friendship.

I would also like to thank the members of my research group, both past and present, for all their help. In particular I would like to thank Dr. Yeunghaw Ho for putting up with my many questions over the past two years.

A special thanks goes to Professor Mariusz Klobukowski for assisting me the many theoretical calculations which are included in this work.

Many thanks to all the wonderful people whom I have met during my time in Edmonton, especially Christophe Ferry, Eric Cauchon, Steven Taylor, Edgar Arriaga and John Crabtree. A special thanks goes to Ian Stewart for the many interesting conversations about science and life as well as for being such a good friend.

Finally, I would like to thank those who are most important in my life: Mum, for all of the encouragement and support over the years; Sarah, for the many calls and email which really helped me through the tough times and lastly to my Dad, Dr. N. Klassen, for the inspiration.

Table of Contents

Page

Chapter 1. General Introduction....................1

Introduction....................1

a. Electrospray-mass spectrometry: a brief overview....................1

b. The electrospray process....................3

c. The present work....................5

References....................15

Chapter 2. Ions Produced by Electrospray. Hydration of Protonated Amines, Diamines and Some Small Peptides....................17

Introduction....................17

Experimental....................20

a. Apparatus....................20

b. Mass Analysis....................25

c. Conditions in forechamber and reaction chamber....................28

Results and Discussion....................33

a. Equilibria determinations involving systems for which equilibrium data are available in the literature....................33

b. Equilibria determinations involving ions produced by atmospheric pressure ionization, API....................42

c. Hydration equilibria of protonated alkylamines, diamines and small peptides....................43

References....................54

Chapter 3. Free Energies of Hydration in the Gas Phase of the Anions of Some Oxo Acids of C, N, S, P, Cl, I................58
Introduction...58
Experimental...59
Results and Discussion...62
  a. Ion abundances and $K_{n-1,n}$ determinations in some typical experiments..62
  b. Hydration of singly charged anions.............................64
  c. Hydration of singly charged anions of dicarboxylic acids..78
  d. Hydration energies of doubly charged anions...............84
  e. Enthalpy changes and temperature dependence of equilibria..91
References...92

Chapter 4. Determination of ion-solvent equilibria in the gas phase. Hydration of di-protonated diamines and bis-trimethylammonium alkanes.....................................96
Introduction...96
Experimental...97
Results and Discussion..100
  a. Determination of the equilibrium constans and ΔG^o, ΔH^o , ΔS^o values. Comparison with some data from the literature...100
  b. Sequential hydration of a doubly protonated diamine..103
  c. Changes of hydration thermochemistry with distance between the charged substituents, $H_3N(CH_2)_pNH_3{}^{2+}$...112

d. Hydration energies of $(CH_3)_3N(CH_2)_pN(CH_3)_3^{2+}$......117
References......122

Chapter 5. Reaction Enthalpies for: $M^+L = M^+ + L$ where $M^+(Na^+, K^+)$ and L(acetamide, N-methylacetamide, N,N-dimethylacetamide, glycine and glycyglycine) from Determinations of the Collision-Induced Dissociation Thresholds......125
Introduction......125
Experimental......128
a. Apparatus and conditions......128
b. Determinations of threshold energies, E_o......132
Results and Discussion......133
a. Evaluation of the threshold energies. Effect of kinetic shift......133
b. Comparison of threshold based energies with literature data. Types of bonding present in the complexes......153
References......163

Chapter 6. Collision-Induced Dissociation Threshold Energies of Some Protonated Amino Amides and Small Peptides......166
Introduction......166
Experimental......169
a. Apparatus......169
b. Determination of threshold energies E_o......171
c. Theoretical Calculations......172

Results and Discussion....173
a. CID of $^+H(H_2NCH_2CO\text{-}X)$ where X=OH, NH_2, NHMe $NHCH_2COOH$....173
b. $^+H(H_2NCH_2CONHCH_2CO\text{-}X)$ where X=NH_2, $HNCH_2COOH$ and $^-(HNCH_2CO)_2\text{-}OH$....200
Conclusions....208
References....210

List of Tables

Page

Table 2.1. Comparison with free energy data in literature.........39

Table 2.2. Hydration free energies of some protonated alkylamines, alkyldiamines and peptides..................44

Table 3.1. Free Energies of Hydration of Anions A^- and of Acid Dissociation, $AH = A^- + H^+$.

a. Carboxylates, RCO_2^-..66

b. Anions of some oxo acids of N, P, S, Cl, I..........67

Table 3.2. Hydration Free Energies of Singly Charged Anions of Dicarboxylic Acids................................79

Table 3.3. Hydration free energies of doubly charged anions.

a. Doubly charged ions of dicarboxylic acids...........85

b. Doubly charged anions of some oxo acids of sulphur and selenium..85

Table 4.1. Hydration energies of some singly charged ions......107

Table 4.2. Sequential hydration of $H_3N(CH_2)_{12}NH_3^{2+}$..............108

Table 4.3. Hydration of α, ω di-ammonium alkanes and di-methylammonium alkanes................................109

Table 5.1. Energies for reaction: $M^+L = M^+ + L$ from CID threshold determinations......134

Table 5.2. Vibrational Frequencies......135

Table 6.1. CID threshold energies, E_o......180

Table 6.2. Vibrational frequencies of precusor ions and transition states leading to a given fragment ion......183

List of Figures

Page

Figure 1.1. Illustration of the electrospray process......................4

Figure 2.1. Electrospray generator and ion source....................21

Figure 2.2. Electrospray ion source and front end of triple quadrupole mass spectrometer: CB, skimmer...........22

Figure 2.3a. Dependence of ion intensity on resolution RE3 setting of mass resolving quadrupole Q_3. Ion intensity of ion m/z = 242 $(n\text{-}C_4H_9)_4N^+$, versus RE3 where RE3 $\propto$ AC/DC potentials used in Q_3. Acceleration potential of ions: $V(OR) - V(Q_3) = 10$ V..............................26

Figure 2.3b. Ion transmission correction factors for different resolving powers on Q3 (RE3) versus ion mass to charge ratio..27

Figure 2.4. Mass spectrum of protonated diaminopentane BH^+ and hydrated $BH^+(H_2O)$ at equilibrium. Ions obtained from a 10^{-4} mol/L solution of diamino pentane 2×10^{-4} mol/L HCl in methanol. Water pressure in RCH 9 mTorr..29

Figure 2.5. Effect of drift potential reaction chamber, RCH, on ion intensity ratios at equilibrium......................31

Figure 2.6. Dependence of ion intensities of ions: $BH^+(H_2O)_n$ on drift potential in reaction chamber......................32

Figure 2.7. Equilibrium ratio plot. Plot of ion intensity ratio $I(Na^+(H_2O)_4)/I(Na^+(H_2O)_3)$ versus H_2O pressure....35

Figure 2.8. Ion intensities of $Na^+(H_2O)_n$ versus H_2O pressure....36

Figure 2.9. Equilibrium ratio plot for BH^+ = protonated n-propylamine. □ (1,2)-hydration equilibrium, ◆ (2,3)-hydration equilibrium..............................38

Figure 2.10. Mass spectrum showing hydrates of singly protonated BH^+ and doubly protonated BH_2^{2+} diaminooctane. 6.9 mTorr H_2O pressure..................45

Figure 2.11. Equilibrium ratio plot for , diprotonated diaminoheptane hydrates, $BH_2^{2+}(H_2O)_n$...................46

Figure 3.1. Electrospray Ion Source and Reaction Chamber........60

Figure 3.2. Ion intensities observed from a solution of $Na_2CO_2(CH_2)_6CO_2$, disodium suberate...................63

Figure 3.3. Ion intensities for $NO_3^-(H_2O)_n$ ions determined at different constant H_2O pressures in the reaction chamber.......65

Figure 3.4. Plots of ion intensities ratio, I_n/I_{n-1}, corresponding to ion intensities $NO_3^-(H_2O)_n$ and $NO_3^-(H_2O)_{n-1}$ versus partial pressure of H_2O, P_{H_2O}, in the reaction chamber.......70

Figure 3.5. Plot of the hydration free energies for A^-, $-\Delta G^\circ_{0,1}$, corresponding to the reaction $A^- + H_2O = A^-(H_2O)$ versus gas phase acidity of AH, $\Delta G^\circ_{ac}(AH)$.......73

Figure 3.6. Plot of hydration free energies, $-\Delta G^\circ_{0,1}$, for the dicarboxylates, $CO_2H(CH_2)_kCO_2^-$, ○, also shown are $-\Delta G^\circ_{0,1}$ for protonated diamines, $NH_2(CH_2)_kNH_3^+$, ●.......81

Figure 3.7. Hydration free energies $-\Delta G^\circ_{n-1,n}$ for several doubly charged anions.......86

Figure 3.8. Hydration free energies $-\Delta G^\circ_{n-1,n}$ for doubly charged dicarboxylates, $CO_2(CH_2)_kCO_2^{2-}$, with increasing chain length.......90

Figure 4.1. Ion source for determining ion-molecule equilibria involving electrospray generated ions.......98

Figure 4.2. Determination of equilibrium constants: Plot of ion intensity ratio $I_{M(H_2O)^+}/I_{M^+}$ for hydration equilibrium: $M^+ + H_2O = M(H_2O)^+$, (0,1), versus , P_{H_2O} pressure of water vapour in ion source reaction chamber, at a temperature T = 382 K for M^+ = n-$C_3H_7NH_3^+$ and M^+ = n-$C_6H_{13}NH_3^+$ 101

Figure 4.3. van't Hoff plots of ln $K_{0,1}$ vs reciprocal absolute temperature for hydration of n-$C_3H_7NH_3^+$, n-$C_6H_{13}NH_3^+$, and $NH_3(CH_2)_6NH_3^{2+}$ 102

Figure 4.4. van't Hoff plots for the sequential hydration (n-1,n) of $NH_3(CH_2)_{12}NH_3^{2+}$ 104

Figure 4.5. van't Hoff plots for the monohydration (0,1) of several diprotonated diamines $NH_3(CH_2)_pNH_3^{2+}$ 105

Figure 4.6. van't Hoff plots for the (0,1) and (1,2) hydration of $(CH_3)_3N(CH_2)_pN(CH_3)_3^{2+}$ 106

Figure 4.7. Enthalpy change, $-\Delta H^{o}_{0,1}$ for monohydration of $H_3N(CH_2)_pNH_3^{2+}$ as a function of chain length, p... 113

Figure 4.8. Plot of hydration free energy $-\Delta G^{\circ}_{0,1}$ for singly protonated alkyl amines BH^+ versus the gas phase basicity, GB (B) 115

Figure 4.9. Comparison of enthalpy change for monohydration of $H_3N(CH_2)_pNH_3^{2+}$ and $(CH_3)_3N(CH_2)_pN(CH_3)_3^{2+}$ ions............................119

Figure 5.1. Front end of apparatus. Electrospray generator, ES, consisting of electrospray capillary with stainless steel tip at high electric potential, generates charged droplets and ultimately gas phase ions.......130

Figure 5.2. Appearance curve of K^+ from CID of K^+Acetone. Also shown are three calculated cross section curves..140

Figure 5.3. Appearance curve of K^+ from CID of K^+N-Methylacetamide. The calculated curve (solid line), fitted from 1.1-2.5 eV, corresponds to n=1.02 and E_0=1.40 eV (32.2 kcal/mol)................141

Figure 5.4. Appearance curve of Na^+ from CID of Na^+N-Methylacetamide. The calculated curve (solid line), fitted from 1.4-4.0 eV, corresponds to n=1.25 and E_0=1.69 eV (38.9 kcal/mol)................142

Figure 5.5. Appearance curve of Na^+ from CID of Na^+Succinamide. The calculated curve (solid line), fitted from 2.8-4.5 eV, corresponds to n=1.25 and E_0=2.70 eV (62.3 kcal/mol)....143

Figure 5.6. Appearance curve of K^+ from CID of K^+Glycine. The calculated curve (solid line), fitted from 1.2-2.0 eV, corresponds to n=1.07 and E_0=1.27 eV (29.2 kcal/mol)....144

Figure 5.7. Appearance curve of Na^+ from CID of Na^+Glycine. The calculated curve (solid line), fitted from 1.6-3.4 eV, corresponds to n=1.20 and E_0=1.58 eV (36.3 kcal/mol)....145

Figure 5.8. Appearance curve of Na^+ from CID of Na^+Glycinamide. The calculated curve (solid line), fitted from 2.0-3.5 eV, corresponds to n=1.31 and E_0=1.96 eV (45.1 kcal/mol)....146

Figure 6.1. Front end of apparatus. Electrospray generator, ES, consisting of electrospray capillary with stainless steel tip at high electric potential, generates charged droplets and ultimately gas phase ions....170

Figure 6.2. CID-MS of $(Gly)H^+$ at a collision energy of: (a) 10 eV lab (3.4 eV, CM); (b) 30 eV lab (10.3 eV, CM)....174

Figure 6.3. Appearance curves of $^{+}H_2N{=}CH_2$ (●), $(H_2O)^{+}H_2N{=}CH_2$ (□) and $^{+}H_3N\text{-}CH_2$ (△) from CID of $(Gly)H^{+}$ 175

Figure 6.4. Appearance curve of $^{+}H_2N{=}CH_2$ from CID of $(Gly)H^{+}$. The calculated curve (solid line), fitted from 2.5 to 6.0 eV, corresponds to n=1.82 and E_0=1.93 eV (44.4 kcal/mol)....................179

Figure 6.5. Calculated HF energy (3-21G basis set) of $(Gly)H^{+}$, with the proton located on the hydroxyl group, as a function of the $C\text{-}OH_2$ bond length....................182

Figure 6.6. Calculated HF energy (3-21G basis set) of $(GlyNH_2)H^{+}$, with the proton located on the amide nitrogen, as a function of the $OC\text{-}NH_3$ bond length....................188

Figure 6.7. Appearance curve of $^{+}H_2N{=}CH_2$ from CID of $(GlyNH_2)H^{+}$. The calculated curve (solid line), fitted from 2.5 to 5.0 eV, corresponds to n=1.65 and E_0=1.95 eV (44.9 kcal/mol)....................190

Figure 6.8. CID-MS of $(GlyNHCH_3)H^{+}$ at a collision energy of 20 eV lab (6.2 eV, CM)....................192

Figure 6.9. Appearance curves of $^+H_2N{=}CH_2$ (●) and $^+H_3NCH_3$ (△) from CID of $(GlyNHCH_3)H^+$ 193

Figure 6.10. Appearance curves of $^+H_2N{=}CH_2$ (○) and $(Gly)H^+$ (□) from CID of $(Gly\text{-}Gly)H^+$ 199

Figure 6.11. Appearance curves of the $\mathbf{b}_2$ (●), $\mathbf{a}_2$ (▲), $\mathbf{y}_1$ (□) and $\mathbf{a}_1$ (○) fragment ions from CID of $(Gly\text{-}GlyNH_2)H^+$ 201

Figure 6.12. Appearance curves of the $\mathbf{b}_2$ (●), $\mathbf{y}_2$ (○), $\mathbf{a}_2$ (▲), $\mathbf{a}_1$ (□)and $\mathbf{y}_1$ (△) fragment ions from CID of $(Gly\text{-}Gly\text{-}Gly)H^+$ 205

Figure 6.13. Appearance curves of the $\mathbf{b}_2$ (●), $\mathbf{y}_2$ (■), $\mathbf{a}_2$ (□), $\mathbf{b}_3$ (▲), $\mathbf{y}_3$ (+), $\mathbf{a}_1$ (△)and $\mathbf{y}_1$ (○) fragment ions from CID of $(Gly\text{-}Gly\text{-}Gly\text{-}Gly)H^+$ 207

Chapter 1

Introduction

a. Electrospray-mass spectrometry: a brief overview.

The development of electrospray ionization (ES) as a source of gas phase ions has revolutionized the field of mass spectrometry (MS), particularly in the analysis of non-volatile compounds such as biomolecules. The potential of ES as an ion source for mass spectrometry was first proposed by Dole[1] in 1968; however, it was not until the pioneering work of Yamashita and Fenn[2] in 1984 that the true potential was first demonstrated. At approximately the same time, Aleksandrov and coworkers[3] in the Soviet Union reported the successful interfacing of liquid chromatography and MS using ES. Since then there has been an explosive growth in the use of ES-MS in many areas of chemistry and biochemistry.

The ES technique, for which a brief description is given in the following section, operates at atmospheric pressure and allows for the transfer of ions present in solution to the gas phase. In principle, any ion which exists in solution can be converted to the gas phase. Whether a particular ion is detected mass spectrometrically, however, will depend on its stability in the gas phase. ES is a "soft" ionization technique which means that gas phase ions are not formed in highly vibrationally excited states and are therefore not prone to unimolecular dissociation prior to mass analysis. As a result, ES mass spectra are generally quite "clean", with minimal fragment ions present. Another important feature of ES is that ions which are multiply charged in solution are readily converted to multiply charged gas phase ions. This "multiple charge" capability has important consequences in the analysis of biomolecules, *vide infra*. Although other ionization techniques capable of generating multiply charged gas phase ions exist[4], ES is certainly unique in the ease with which these ions are formed as well as the wide applicability of the technique.

Since the main requirement for a compound to be amenable to ES is that it exist as a stable ion in solution, ES can be used to generate a wide variety of gas phase ions, many of which are difficult to generate by other ionization techniques. Ions which can be produced by ES include alkali metal ions (Li^+, Na^+, K^+, Cs^+, Rb^+); alkaline earth (Mg^{2+}, Ca^{2+}, Sr^{2+}, Ba^{2+}) and transition metal ion-complexes involving a variety of ligands ranging from simple solvent molecules[5,6] (MeOH, H_2O, CH_3CN) to large organic molecules including biomolecules[7,8]; solvated anions of inorganic acids[9] (SO_4^{2-}, HPO_4^{2-}) and singly and multiply protonated organic bases such as peptides and proteins[10] and deprotonated organic acids such as nucleic acids and oligonucleotides[11].

To date, the most important applications of ES-MS has been in the analysis of biological compounds. Large biomolecules (> 10 kDa), such as proteins and oligonucleotides, are generally multiply charged in solution owing to multiple acidic or basic functional groups. With ES, some or all of the charges may be retained into the gas phase; this effectively reduces the mass to charge ratio (m/z) of these ions down to a range that can be handled by most mass spectrometers. As a result, it is possible to determine accurate molecular weights for these large ions[12]. ES, in conjunction with tandem mass spectrometry (MS/MS), has also been used to study the primary structure of biomolecules. To date the most succesful application has been in the elucidation of the amino acid sequence of protonated peptides[13]. There is also considerable interest in the potential of ES-MS to study the higher order structure of biomolecules. Due to the softness of the ES process, non-covalent interactions present in biomolecules in the solution phase may be preserved in the gas phase. Numerous investigation have been undertaken to determine to what extent structural features in the gas phase reflect solution structure[14]. To date, the experimental evidence is non-conclusive, but extensive research continues in this exciting area.

ES-MS has also gained a foothold in the area of inorganic and organometallic chemistry. Prior to the development of ES, it was difficult if not impossible to generate many of these inorganic ion complexes in the gas phase due to their very low volatility. ES circumvents this problem and ES-MS is becoming an important tool for monitoring inorganic solution chemistry[15].

b. The electrospray process

A simplified illustration of the ES process is shown in Figure 1.1. In order to carry out ES-MS, an ionic solution containing the analyte of interest is delivered to a small bore metal capillary (typically < 200 μm i.d.) to which a potential of several kV is applied relative to a counter electrode, located several cm away. Generally, this counter electrode will be the sampling plate of the mass spectrometer, containing a small orifice (100 μm for the present work) through which the ions are sampled into vacuum and mass analyzed. Under the influence of the electric field at the capillary tip, positive ions (for the case where a positive potential is applied) at the liquid surface are drawn towards the counter electrode.

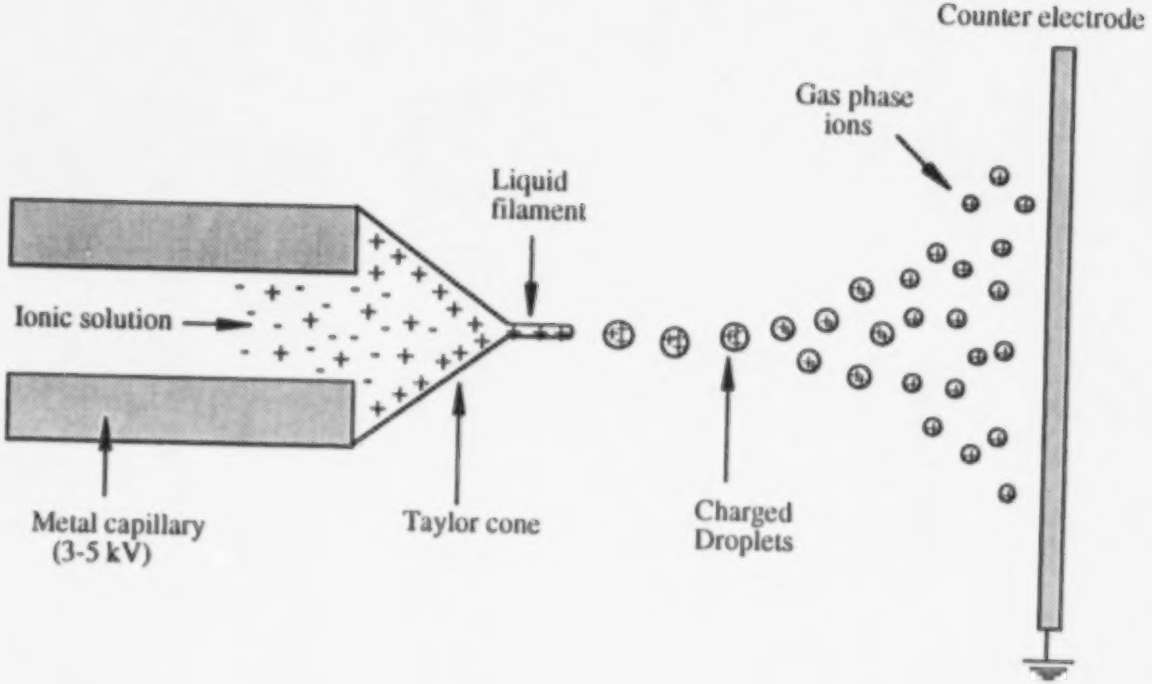
Counter electrode
Gas phase ions
Liquid filament
Ionic solution
Metal capillary (3-5 kV)
Taylor cone
Charged Droplets

Figure 1.1 Illustration of the electrospray process.

This destabilizes the liquid surface which is drawn out in the shape of a cone, referred to as a Taylor cone. At sufficiently high electric fields, a thin filament of liquid is emitted from the tip of the cone and subsequently breaks up into small positively charged droplets. As the droplets drift towards the counter electrode they lose solvent molecules through evaporation. This increases the charge to mass ratio of the droplets which eventually become unstable and undergo fission, producing smaller charged droplets of varying size. This process repeats itself several times until solvated gas phase ions are formed. The exact mechanism by which gas phase ion formation occurs is still being debated. Dole[1] first proposed a mechanism whereby the solvent evaporation-fission process repeats itself until some of the droplets contain a single ion; further solvent evaporation leads to the gas phase ion. This is referred to as the *charged residue model*. Iribarne and Thomson[16] envisioned an alternative mechanism whereby ion evaporation directly from the droplet surface is possible for very small charged droplets, with diameters of a few nm.

c. The present work

Although most of the interest in ES-MS has focussed on analytical applications, this ion source also provides a unique opportunity to study the gas phase chemistry and thermochemistry of previously inaccessible ions, especially the multiply charged and biological ions. Such studies are of great interest from a fundamental standpoint as well as for practical reasons, since a better understanding of the processes occurring in the gas phase, which is an important aspect of the ES process, can only be beneficial in the continuing development of ES-MS as an analytical tool.

Investigations into the gas phase chemistry of ES-ions, as a field of research, has not progressed as rapidly as the advances in applications, mainly to due to the fact that many of the mass spectrometric techniques traditionally used in such measurements (*e.g.* pulsed high pressure mass spectrometers, PHPMS, and flow tube-mass spectrometry apparatus) were not designed to sample ions from atmospheric pressure and instrumental modifications are required in order to accommodate the ES ion source. Such modifications are not always practical and as a result it is desirable to develop new instrumentation and experimental approaches to carry out these investigations.

The objective of the present work was to develop novel ion sampling and experimental strategies which, used in conjunction with a SCIEX TAGA 6000E triple quadrupole mass spectrometer capable of sampling ions from atmospheric pressure, allow for the gas phase chemistry and thermochemistry of ES-ions to be investigated. The main focus of this work deals with the interaction between a variety of singly and doubly charged ES ions ($M^{z+/-}$) and neutral molecules or ligands (L) in the formation of ion-molecule complexes or clusters, as illustrated by eq. 1.1.

$$M^{z+/-}L_{n-1} + L = M^{z+/-}L_n \qquad (1.1)$$

The thermochemistry for ion-molecule clustering or association reactions (*i.e.* eq. 1.1) provides important insight into the nature of ionic solvation, helping to bridge the gap between chemistry in the gas and condensed phase. The bulk of the thermochemical data available in the literature[17] on these clustering reactions was obtained using the equilibrium method[18]. This technique involves determining the equilibrium constant ($K_{n-1,n}$) for eq. 1.1 at a known partial pressure of ligand, P_L, by measuring the intensities of the reactant ($I_{(M^{z+/-}L_{n-1})}$) and product ions ($I_{(M^{z+/-}L_n)}$) mass spectrometrically.

$$K_{n-1,n} = \frac{I_{M^{z+/-}L_n}}{I_{M^{z+/-}L_{n-1}} \times P_L} \qquad (1.2)$$

The free energy change ($\Delta G^o_{n-1,n}$) for the reaction follows directly from the equilibrium constant (1.3):

$$-\Delta G^o_{n-1,n} = RT\ln K_{n-1,n} \qquad (1.3)$$

The enthalpy ($\Delta H^o_{n-1,n}$) and consequently the entropy change ($\Delta S^o_{n-1,n}$) can be evaluated from the temperature dependence of $K_{n-1,n}$, using the van't Hoff equation (1.4). According to the integrated form of eq. 1.4 (see 1.5), a plot of $\ln K_{n-1,n}$ versus 1/T (referred to as a van't Hoff plot) should yield a straight line with a slope equal to $-\Delta H^o/R$.

$$(\partial \ln K / \partial T)_p = \Delta H^o / RT^2 \qquad (1.4)$$

$$\ln K = -\Delta H^o / RT + \text{constant} \qquad (1.5)$$

The measurement of ion-molecule clustering equilibria was initiated in this laboratory over thirty years ago and continues to be an active area of research. Therefore, it should not be surprising that we were interested in extending these studies to include the wide variety of ions which have only become accessible with the development of ES. In this laboratory, the equilibria measurements have traditionally been carried out using pulsed high pressure mass spectrometers[19]. With these instruments, the gas phase ions are generated inside an equilibration reaction chamber, maintained at a pressure of a few Torr, by electron impact, chemical ionization or, in the case of metal ions, by thermionic emissions. These instruments were not designed to sample ions from atmospheric pressure and therefore cannot be used to study ES-generated ions without extensive modification of the reaction chamber and pumping system. On the other hand, mass spectrometers, such as our triple quadrupole, capable of sampling ions from pressures up to ~1 atm would seem ideally suited to carry out equilibria measurements involving ES ions. Unfortunately, as explained in Chapter 2, it is difficult to obtain accurate mass spectrometric determinations of ion intensity ratios at high pressures due to condensation reactions occurring during sampling[20]. It is, therefore, more desirable to sample ions at lower pressures, in the Torr range. In order to accommodate the high pressure requirement of the ES ion source and the lower pressure requirements for ion intensity ratio measurements, we have developed a novel ion sampling approach whereby the gas phase ions are transferred from atmospheric pressure to an interface, maintained at a pressure of ~10 Torr, where they are allowed to react with a neutral clustering reagent at a known partial pressure and then sampled by the mass spectrometer.

The design and operation of this interface, or low pressure ion source as it is referred to in our laboratory, and the first experimental results obtained with it are described in Chapter 2. This apparatus operates at a single temperature (293 K) and can be used to measure clustering free energies near room temperature. Preliminary measurements, involving the clustering of Na^+, H_3O^+ and n-$C_3H_7NH_3^+$ with H_2O and K^+ and $(CH_3)_4N^+$ with CH_3COCH_3, designed to verify the reliability of the results obtained with this apparatus, were found to be in good agreement with previous measurements reported in the literature[17]. New measurements are reported for the hydration free energies of a variety of protonated organic molecules, including singly and doubly protonated diaminoalkanes: $H_2N(CH_2)_pNH_3^+$ (p=2-10, 12) and $^+H_3N(CH_2)_pNH_3^+$ (p=7,8,10,12); and some protonated amino acids and small peptides: Gly_kH^+ (k=1-4), $LysH^+$, Gly-$LysH^+$ and Lys-Tyr-$LysH_2^{2+}$. The hydration of protonated ions, such as n-$C_3H_7NH_3^+$, involves the formation of an ionic hydrogen bond between the oxygen of the water and one of the acidic hydrogens on the nitrogen (*i.e.* $C_3H_7H_2NH^+$---OH_2). The strength of the bonding, which involves primarily ion-dipole and ion-induced dipole interactions, is sensitive to the positive charge on the amino hydrogen. Therefore, the magnitude of the hydration free energies will reflect the extent of charge localization at the site of protonation. Intramolecular interactions which tend to delocalize (stabilize) the charge will result in weaker hydrogen bonding to the water and consequently lower hydration free energies ($-\Delta G^o$). For example, the hydration energies ($-\Delta G^o_{0,1}$) of singly protonated diaminoalkanes, which are known to undergo proton induced cyclization such that the charge is stabilized by both amino groups[21], are found to be ~3 kcal/mol lower than for the monoalkylamines with similar carbon chain length. The addition of a second proton to the diaminoalkanes, which introduces coulombic repulsion between the charge sites and greater charge localization on the amino hydrogens, results in higher free energies ($-\Delta G^o$) compared to the monoalkylamines. Therefore, in addition to providing valuable thermochemical data, the hydration free energies can also be used to study substituent effects and indicate the presence of intramolecular interactions. The sequential hydration energies of the protonated peptides are the first experimentally determined values to be reported and represent another step towards a more complete understanding of the role of solvent in structure and reactivity of biomolecules. In addition, these results should be useful in the development of theoretical models for the hydration of protonated proteins.

In Chapter 3, the investigation into the hydration free energies of ES-ions is extended to include the singly and doubly charged anions of some oxo acids of C, N, S, P, Cl and I. Reported are the hydration free energies of some fifty-five anions. As with the protonated ions, hydration of these anions, XO^{z-}, involves the formation of an ionic hydrogen bond. In this case, the bonding is between one of the water's hydrogen atoms and an oxygen on the acid, *i.e.* XO^----HOH. The magnitude of the hydration free energies is expected to reflect the degree of charge localization on the oxygen atom. An approximately linear relationship was found between the $-\Delta G^o_{0,1}$ values obtained for the singly charged anions, XO^-, and the gas phase acidities reported in the literature for the corresponding acids, XOH. This relationship allows for previously undetermined gas phase acidities to be estimated based on the measured $-\Delta G^o_{0,1}$ values.

While the clustering free energies ($-\Delta G^o$), such as the hydration energies reported in Chapters 2 and 3, provide important and useful thermochemical information on ion-molecule clustering reactions, we were also interested in being able to measure the enthalpy ($-\Delta H^o$) and entropy ($-\Delta S^o$) changes for these reactions. As mentioned earlier, $-\Delta H^o_{n-1,n}$ can be evaluated from the temperature dependence of the equilibrium constant, $K_{n-1,n}$. In order to carry out these temperature studies a modified version of the low pressure source, with a temperature range of 273 to 473 K, was developed. In Chapter 4, the design of this apparatus, along with the first experimental data, are discussed. Using this apparatus the hydration free energies, enthalpies and entropies ($-\Delta G^o_{n-1,n}$, $-\Delta H^o_{n-1,n}$, $-\Delta S^o_{n-1,n}$ where n=1,2) have been determined for the diprotonated diaminoalkanes, $^+H_3N\text{-}(CH_2)_p\text{-}NH_3^+$ where p=5-10, 12, and the doubly charged bis-trimethylammonium alkanes, $^+(CH_3)_3N\text{-}(CH_2)_p\text{-}N(CH_3)_3^+$ where p= 2-4. In the case of the diaminoalkanes, it is found that $-\Delta H^o_{0,1} \approx -\Delta H^o_{1,2}$ indicating that the water molecules add to alternate charge sites and that they do not significantly reduce the coulombic repulsion experienced by the charge sites. A tentative linear relationship is proposed between the hydration free energies, $-\Delta G^o_{0,1}$, determined for the diprotonated diaminoalkanes ($B_2H_2^{2+}$) and the second gas phase basicity of the singly charge diamine (B_2H^+). Using this relationship, the second gas phase basicities of the diaminoalkanes are predicted based on the measured hydration energies.

The equilibrium method has provided and will continue to provide important thermochemical data on the interaction between gas phase ions and neutral molecules, however, the applicability of this technique is limited by two experimental requirements, the first being that the ligand is sufficiently volatile that it can be introduced into the gas phase at known partial pressures. Obviously, non-volatile compounds such as biomolecules are not suitable ligands. Secondly, the experimental conditions must be such that the ion-molecule equilibrium is established within the lifetime of the ions inside the reaction chamber (~ 0.1 ms in our apparatus). Ion-molecule complexes involving strong bonding interactions (> 40 kcal/mol) require temperatures in excess of 700 K in order to achieve equilibrium within the time scale of the experiment. Accurate equilibria determinations at such high temperatures are difficult to achieve.

For ion-molecule complexes which are not amenable to the equilibrium method it is desirable to have an alternative method for measuring the ion-ligand bond energies. The collision-induced dissociation (CID) threshold method is one such technique and has been successfully applied to measurement of ion-ligand binding energies for a wide variety of complexes[22,23], although until now it has not been used to study ES-ions. This method involves the sequential isolation of the precursor ion, for example an ion-ligand complex (ML^+), in the first stage of mass analysis followed by excitation of the ion via energetic collisions with a non-reactive neutral such as argon (Ar), see eq. 1.6. If sufficient internal energy is deposited in the ion such that it can overcome the M-L bond energy, it will undergo unimolecular dissociation producing the ion (M^+) and the neutral ligand (L), eq. 1.7. The ion intensity of M^+ is monitored as a function of kinetic (collision) energy using a second stage of mass analysis to yield the appearance curve. The ion-ligand binding energy, which is assumed to be equal to the activation energy barrier to dissociation (*i.e.* no reverse activation energy), corresponds to the minimum energy or threshold energy required to initiate the reaction and can be determined from the appearance curve.

$$ML^+ \xrightarrow{Ar} ML^{+*} \qquad (1.6)$$

$$ML^{+*} \longrightarrow M^+ + L \qquad (1.7)$$

Using the CID threshold method, the ion-ligand binding energies of the Na^+ and K^+ complexes of a series of amides: CH_3CONH_2, $CH_3CONH(CH_3)$, $CH_3CON(CH_3)_2$, $H_2NCH_2CONH_2$, $H_2NCO(CH_2)_2CONH_2$; as well as glycine, H_2NCH_2COOH, and glycylglycine, $H_2NCH_2CONHCH_2COOH$, were determined and the results are presented in Chapter 5. These ligands are relatively non-volatile and the binding energies are quite high, especially in the case of the sodium ion (> 35 kcal/mol) and therefore not well suited to the equilibrium method. The alkali metal ions interact primarily with the carbonyl oxygens of the amides and peptides. The bonding is electrostatic in nature and is sensitive to substituent effects, which affect the dipole moment of the carbonyl group, as well as to intramolecular interactions where a second functional group (CO or NH_2) assists in the stabilization of the charge. These binding energies are of interest in attempts to theoretically model the interaction between the metal ions and ion channel peptides, such as gramicidin S[24]. These interactions are believed to involve mainly carbonyl oxygens on the peptide backbone[25].

Although our initial interest in the CID threshold method was as an alternative to the equilibrium method for studying non-covalent interactions, we realized that this technique could also be used to probe the dissociation energetics involving the cleavage of covalent bonds of some interesting systems, such as protonated peptides. As discussed earlier, CID-MS has become an established method for sequencing protonated peptides. At low collision energies (<100 eV), protonated peptides dissociate primarily along the peptide backbone and the CID spectrum is generally characterized by three types of fragment ions: immonium ions or **a** ions ($^{+}$RHN=CHR'), acylium or **b** ions (H(-HNCHRCO-)$_n^{+}$) and protonated amino acids or peptides which are referred to as **y** ions[26]. Sequence information is obtained based on the mass difference of successive fragment ions of the same type, which corresponds to mass of the residue by which they differ. As a result, the amount of sequence information obtained from CID-MS depends directly on the type of fragment ions that are generated. Somewhat surprisingly, there is very little known about the actual mechanistic details of the various dissociation processes. This lack of mechanistic information is due in large part to the scarcity of reliable energetics for the dissociation reactions. In an attempt to address this deficiency, we have undertaken a systematic investigation of the dissociation energetics of protonated glycine, H_2NCH_2COOH, the amino amides, H_2NCH_2COX where X=NH_2, $NHCH_3$ and $NHCH_2COOH$, and some small peptides, $H_2NCH_2CONHCH_2COX$ where X=NH_2 and $NHCH_2COOH$. From the appearance curves obtained for the **a**, **b** and **y** type fragment ions, the reaction activation energies were evaluated. Combining the energetic data with *ab initio* calculations, as well as kinetic energy release measurements reported from other laboratories[27], reaction mechanisms are proposed. The results of this study are presented in Chapter 6.

References

1. Dole, M.; Mack, L.L.; Hines, R.L.; Mobley, R.C.; Ferguson, L.D.; Alice, M.B. *J. Chem. Phys.* **1968**, *49*, 2240.
2. Yamashita, M.; Fenn, J.B. *J. Phys. Chem.* **1984**, *88*, 4451; *ibid* 4671.
3. Aleksandrov, M.L.; Gall, L.N.; Krasnov, V.N.; Nikolaev, V.I.; Parlenko, V.A. *Dokl. Akad. Nauk. SSSR* **1984**, *277*, 379.
4. Veckey, K. *Mass Spectrom. Reviews* **1995**, *14*, 195.
5. Blades, A.T.; Jayaweera, P.; Ikonomou, M.G.; Kebarle, P. *J. Chem. Phys.* **1990**, *92*, 5900.
6. Stewart, I.I. Doctoral Thesis *Speciation by Electrospray Mass Spectrometry* University of Alberta, 1996.
7. Hu, P.; Loo, J.A. *J. Am. Chem. Soc.* **1995**, *117*, 11314.
8. Gross, D.S.; Williams, E.R. *J. Am. Chem. Soc.* **1996**, *118*, 202.
9. Blades, A.T.; Kebarle, P. *J. Am. Chem. Soc.* **1994**, *116*, 10761.
10. Bruins, A.P.; Covey, T.R.; Henion, J.D. *Anal. Chem.* **1987**, *59*, 2642.
11. Little, D.P.; Thannhauser, J.W.; McLafferty, F.W. *Proc. Natl. Acad. Sci. USA* **1995**, *92*, 2318.
12. Smith, R.D.; Loo, J.A.; Edmonds, C.G.; Barinaga, C.J.; Udseth, H.R. *Anal. Chem.* **1990**, *62*, 882.
13. Smith, R.D.; Loo, J.A.; Barinaga, C.J.; Edmonds, C.G.; Udseth, H.R. *J. Am. Soc. Mass Spectrom.* **1990**, *1*, 53.
14. Smith, D.L.; Zhang, Z. *Mass Spectrom. Reviews* **1994**, *13*, 411.
15. Colton, R.; D'Agostino, A.; Traeger, J.C. *Mass Spectrom. Reviews* **1995**, *14*, 79.

16. Iribarne, J.V.; Thomson, B.A. *J. Chem. Phys.* **1976**, *64,* 2287; Thomson, B.A.; Iribarne, J.V. *J. Chem. Phys.* **1979**, *71,* 4451.

17. Keesee, R.G.; Castleman, A.W. Jr. *J. Phys. Chem. Ref. Data* **1986**, *15,* 1011.

18. Kebarle, P. *Ann. Rev. Phys. Chem.* **1977**, *28,* 445.

19. Kebarle, P. Pulsed Electron High Pressure Mass Spectrometry in *Techniques for the Study of Ion-Molecule Reactions* , Farrar, J.M.; Saunders, W.H.Jr., Eds. Wiley Interscience, New York, **1988**, Ch. 5.

20. Zook, D.R.; Grimsrud, E.P. *J. Phys. Chem.* **1988**, *92,* 6374.

21. Yamdagni, R.; Kebarle, P. *J. Am. Chem. Soc.* **1973**, *95,* 3504.

22. Armentrout, P.B. Thermochemical Measurements by Guided Ion Beam Mass Spectrometry in *Advances in Gas Phase Ion Chemistry* Adams, N.; Babcock, L.M., Eds. JAI Press Inc. Greenwich CT, **1992**, vol 1, p 83.

23. Sunderlin, L.S.; Wang, D.; Squires, R.R. *J. Am. Chem. Soc.* **1993**, *115,* 12060.

24. Roux, B.; Karplus, M.J. *J. Comp. Chem.* **1995**, *16,* 690.

25. Jordan, P.C. *J. Phys. Chem.* **1987**, *91,* 6582.

26. Hunt, D.F.; Yates, J.R.III; Shabanowitz, J.; Winston, S.; Hauser, C.R. *Proc. Natl. Acad. Sci. USA* **1986**, *83,* 6233.

27. Yalcin, T.; Khouw, C.; Csizmadia, I.G.; Peterson, M.R.; Harrision, A.G. *J. Am. Soc. Mass Spectrom.* **1995**, *6,* 1164; Beranova, S.; Cai, J.; Wesdemiotis, C. *J. Am. Chem. Soc.* **1995**, *117,* 9492.

Chapter 2

Ions Produced by Electrospray.
Hydration of Protonated Amines, Diamines and Some Small Peptides*.

Introduction

Electrospray (ES)[1] is a method with which ions present in solution can be transferred to the gas phase. With ES it is possible to obtain many gas phase ions, such as doubly and triply charged transition metal and alkaline earth ion-ligand complexes,[2] multiply protonated peptides and proteins,[3] doubly charged[4] anions like SO_4^{2-} and HPO_4^{2-} and multiply deprotonated nucleic acids[5] which are of paramount importance in solution chemistry and biochemistry, but which could not be obtained in the gas phase prior to the development of ES.

We have been engaged for many years in measurements of ion-molecule equilibria in the gas phase[6] using a pulsed electron high pressure ion source mass spectrometer (PHPMS).[7] This method has led to measurements from this and other laboratories which have become a major source of gas phase ion thermochemistry.[8] It has been our aim for some years to expand the ion equilibrium method so as to include ions produced by ES.

---

* A version of this chapter has been published: Klassen, J.S.; Blades, A.T.; Kebarle, P. *J. Phys. Chem.* **1995**, *99*, 15509.

The major difficulty with ES is the high pressure, ~1 atm, at which the ions are generated and the presence of solvent vapour. The high pressure is necessary in order to suppress corona discharges initiated by the capillary tip. For the same reason the choice of ambient gas used is restricted. The ambient gas should contain an electron capturing species such as O_2 for discharge suppression. Therefore, air is well-suited but pure gases like the noble gases or N_2 cannot be used.[9,10] Accurate mass spectrometric determinations of ion equilibria at high pressures such as 1 atm are difficult because processes occurring at the orifice and the interface leading to the vacuum of the mass spectrometer can cause severe distortions of the ion ratios which are determined with the mass spectrometer.[11,12]

Pressures in the Torr range as used in the previous ion equilibria determinations[6,7] are desirable and an ion-molecule reaction chamber operating in that pressure range to which ES ions from 1 atm were transferred via a capillary was described recently.[13] This design was not successful for equilibria measurements because the capillary was coaxial with the ion sampling orifice leading to the mass spectrometer. Gas, originally at 1 atm, expanding out of a capillary into a low pressure region forms a supersonic jet which preserves its integrity over a considerable distance.[14] It was found that the neutral reagent gas concentration in the gas surrounding the ions was difficult to control under these conditions. In the present, successful design the direction of the jet is at right angles to the axis of the orifice and the ions are drifted out of the jet and into the reactant gas mixture by means of an applied electric field.

A brief description of the apparatus and first results reporting the hydration equilibria of doubly protonated alkyldiamines,

$NH_3^+(CH_2)_kNH_3^+$, was given in a recent note.[15] The present work provides a more complete description of the apparatus and a documentation of the method. Equilibria determinations with the present method, which are found in agreement with previous measurements involving conventional pulsed high pressure ion sources, are also reported. Finally, new hydration equilibria measurements are described for singly protonated alkylamines, alkyldiamines, and some small singly and doubly protonated peptides.

It is shown that the magnitudes of the hydration energies obtained can provide structural information for the protonated peptides. For example, singly protonated peptides may be cyclized because the protonated amino group forms a strong intramolecular hydrogen bond to a basic group, such as a carbonyl or an amino group, present in the peptide. The formation of such internal hydrogen bonds is of special interest in attempts to understand the mechanism of fragmentation of protonated peptides which, for the purposes of peptide sequencing, are exposed to collision-induced decomposition (CID) in tandem mass spectrometers (vide infra).

The equilibrium reaction chamber and mass spectrometer described here can also be used with ions created at atmospheric pressure by an electric discharge *i.e.* atmospheric pressure ionization (API). Use of the API mode broadens the range of ions that can be studied.

Experimental

a. Apparatus

The electrospray generator and the ion source-reaction chamber are shown in Figure 2.1, while the mounting of the ion source and the front end of the mass spectrometer are shown in Figure 2.2.

The solution to be electrosprayed was passed through the electrospray capillary (ESC) by means of a motor driven syringe. The spray containing the ions was sucked in by the pressure reducing capillary (PRC) leading to the forechamber (FCH) of the ion source. The exit tip of the PRC directs the gas jet in a direction parallel to the bottom of the forechamber, which we call the interface plate (IN). An orifice of 4 mm diameter in the interface plate connects the forechamber to the reaction chamber (RCH). The ions in the jet escaping from the pressure reducing capillary are deflected out of the jet toward the 4 mm orifice and into the reaction chamber by means of an electric field applied across the forechamber. A weak field was also applied across the reaction chamber. At the bottom of the reaction chamber a small orifice, 100 μm diameter, allows some gas and ions to leak into the vacuum of the mass spectrometer. The pumping lead out of the forechamber (FCH) leads through a control valve to a forepump. The valve was adjusted to obtain a given constant pressure, generally 10 Torr, in the forechamber and the reaction chamber. The pressure in FCH and RCH was measured by means of a capacitance pressure sensor attached to the pumping lead (PL) near the forechamber. A reagent gas mixture (RG) consisting of pure nitrogen (10 Torr) as carrier and thermal bath gas, and the reagent L (1-80 mTorr) was passed in slow flow through the reaction chamber. The measured flow rates when fore and reaction chamber were at 10 Torr were typically: 750 ml/min through

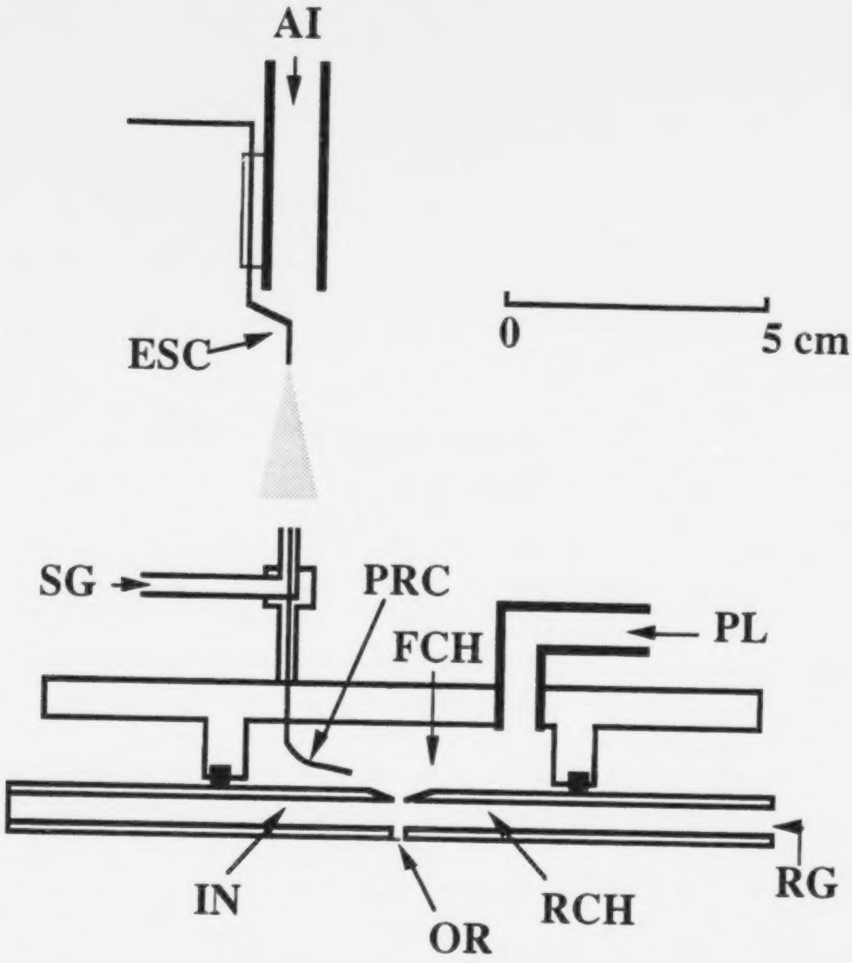

Figure 2.1 Electrospray Generator and Ion Source: ESC, electrospray capillary (4 kV). AI, pipe providing dry air at ~60 L/min. PRC, Pressure reduction capillary (165 V) sucks in gas and ions from electrospray and transfers it to forechamber FCH (165 V). FCH is maintained at 10 Torr by pumping lead PL. IN, interface plate (110 V) separates FCH from reaction chamber, RCH. Reagent gas mixture, RG, flows through reaction chamber and into FCH. Bottom plate of RCH carries an orifice, OR, of 100 µm diameter (100 V) leading to vacuum of mass spectrometer. Ions deflected by electric field out of jet leaving capillary PRC, drift to reaction chamber where ion-molecule equilibria establish. Flow of source gas, SG, 2 L/min of the same composition as the reagent gas, brings composition of gas entering PRC close to that of the reagent gas. Metal tube carrying SG is at at 700 V. All potentials in volts for operation with positive ions.The approximate shape of the plume that exits the electrospray capillary, ESC, is indicated with small dots. This plume consists of small charged droplets, solvent vapor and gas phase ions generated from the droplets. The dotted plume at the exit of the pressure reduction capillary indicates the jet, consisting predominantly of source gas, SG, and gas phase ions. The gas phase ions are deflected out of the jet towards the bottom of the forechamber, FCH, by the applied electric field.

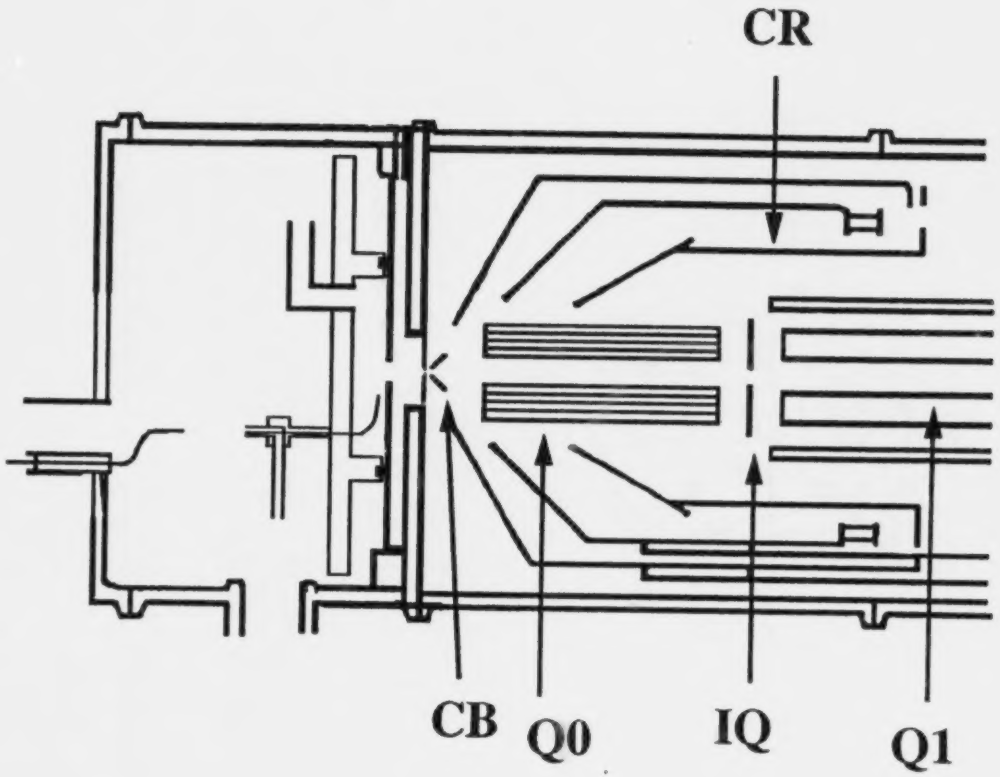

Figure 2.2 Electrospray ion source and front end of triple quadrupole mass spectrometer: CB, skimmer electrode (~100 V). Q_0 Brubacker lens *i.e.* AC only quadrupole constructed of 1 mm rod (~100 V), IQ interquad electrode (~100 V), Q_1 first quadrupole, CR, cryosurfaces of cryopump.

pressure reduction capillary; 90 ml/min reagent gas mixture into reaction chamber; 2 ml/min out of 100 μm orifice and into vacuum of mass spectrometer. All flow rates refer to gas at 700 Torr pressure. The flow rates are such that only a few percent of the reagent gas escapes through the orifice to the vacuum. The rest flows through the interface plate orifice into the forechamber and from there into the forepump line.

The temperature of the gas and ions escaping through the orifice into the vacuum was assumed to be the same as the temperature of the bottom wall of RCH near the orifice. This temperature was determined by a thermocouple which was in firm contact with the wall near the orifice (OR).

The present reaction chamber was operated only at room temperature in an air-conditioned room. It is very desirable to extend the temperature range of the measurements. An ion source reaction chamber similar in design to that shown in Figure 2.1 but with block heaters and cooling channels, which can be operated above and below room temperature has been constructed and equilibrium measurements in agreement with previous work[6,8] were obtained recently. We will report on equilibrium measurements, obtained with this apparatus, in the near future.

The capillary (PRC) was of stainless steel, 0.7 mm o.d., 0.4 mm i.d. and 5 cm long. It was silver soldered into 1.5 mm o.d. tubing for rigidity. The capillary exit was ~3 mm above the interface plate (IN) and 1 cm from the axis of the orifice in IN, leading to the reaction chamber. The width of the forechamber (FCH) was 9 mm while that of RCH was 5 mm.

The solution flow rate through the electrospray capillary (ESC) was 1.5-2 μL/min and the ESC tip was 2-3 cm away from the PRC tip (Figure 2.1). It was found most convenient to use methanol as solvent. The desired ions M^{z+} or BH^+ were obtained by adding 10^{-4} mol/L of the salts $M^{z+}(X)_y$ to the solvent. The methanol vapour entering FCH could be reduced to negligible amounts by using two stages of vapour purging. The first stage is at the ESC, where a fast stream of dry air, ~60 L/min (see Figure 2.1, 2.2), was applied. The second stage was at the entrance tip of the PRC where a stream of reagent gas mixture, ~2 L/min, was used in a counter current to the electrospray plume. The charged droplets and ions were drifted through the counter current to the PRC tip by the low potential of PRC (Figure 2.1). The effectiveness of both of these purging stages could be easily demonstrated. When the reagent gas was L = H_2O at low partial pressures (~1 mTorr), the ions observed in the absence of the purging gas flows were $M^+(CH_3OH)_x(H_2O)_y$ where $x > y$. In the presence of the purging gas this reversed to $x << y$.

Clusters containing mostly methanol, *i.e.* $x >> y$, are expected to be formed from the charged droplets. The exchange of methanol for water in the space between the ESC and PRC tips is facilitated not only by the removal of the methanol and supply of water vapour but also by the collisional activation of the ions by the electric field which is present in this space.

The forechamber construction and the dimensions of the PRC shown in Figure 2.1 are somewhat different from those of the first version of the apparatus reported earlier.[15] The ion intensities observed with the present source were higher by a factor of ~5. We attribute the higher intensity mainly to the shorter capillary length, 5 cm vs 10 cm used in the previous work,[15,16] and the shorter distance, 3 mm present source vs 5 mm previous source,[15] between the PRC tip and the interface plate. Duplicate equilibria determinations with the two sources led to very close results, vide infra.

The mass spectrometer used (see Figure 2.2) is a Sciex TAGA 6000E triple quadrupole,[17] whose front end was modified as detailed in Figure 2.1 and discussion above. The gas escaping from the orifice (OR) expands and is pumped by the cryosurfaces (CR, Figure 2.2) and a second set of cryosurfaces around Q_2, not shown in Figure 2.2.

For the present measurements, where only a single mass filter is required, Q_1 was operated in the ac-only mode and mass analysis was obtained with Q_3. The ions are detected with an ion counting system.

b. Mass Analysis

In normal analytical applications of the mass spectrometer, the offset potentials of the electrode CB and the Brubacker lens (ac-only quadrupole Q_0, constructed of thin, 1 mm diameter rods, so as to achieve high gas conduction), Figure 2.2, are selected lower than that of OR. This leads to maximum sensitivity, but because the gas pressure is relatively high in this region, the accelerated ions are activated by collisions and weakly bonded complexes such as ion hydrates can decompose in this region. To remove this problem, all measurements were performed with $V_{OR} = V_{C_B} = V_{Q_0}$. The ions were accelerated only past Q_0, where the pressure is expected to be relatively low ($p \approx 10^{-5}$ Torr).

Quadrupoles are known to have mass dependent transmission. When used at a constant radial dc/ac ratio and constant ion accelerating voltage, ions of higher mass are transmitted with higher resolution and lower efficiency. In the present work, we corrected for this effect by determining the change of ion transmission (ion intensity) as a function of the selected DC/AC ratio for ions of a given m/z value. An example is given in Figure 2.3, where the ion intensity: $(C_4H_9)_4N^+$, m/z = 242, is

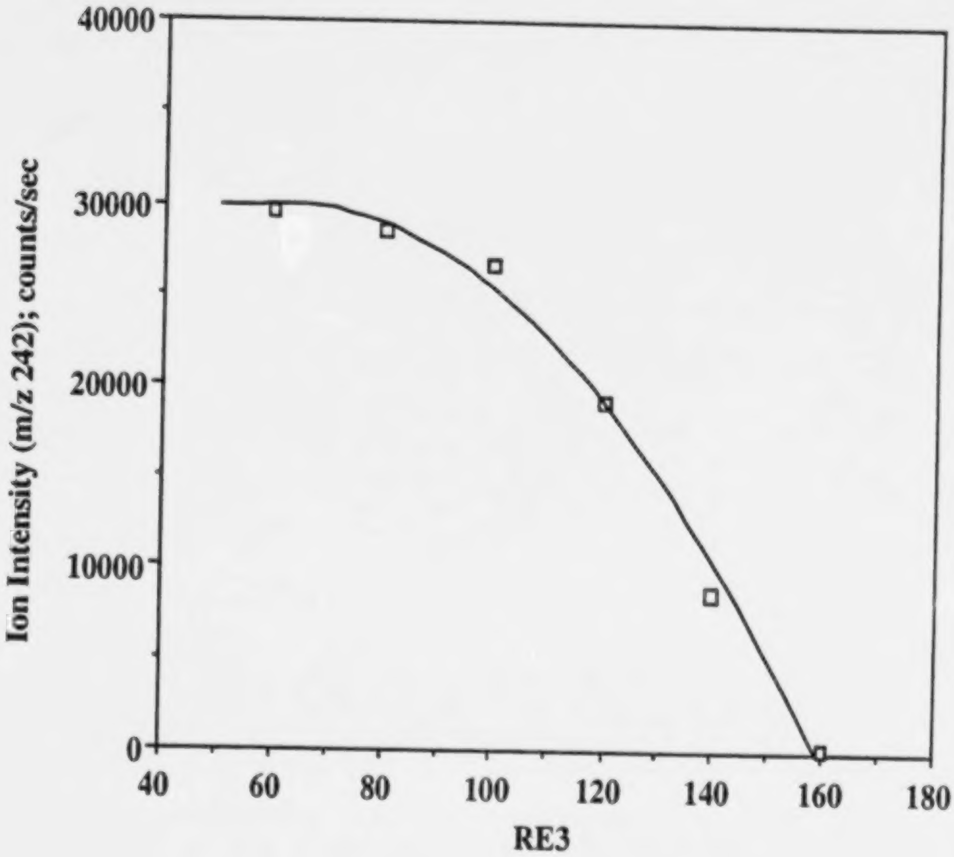

Figure 2.3a Dependence of ion intensity on resolution RE3 setting of mass resolving quadrupole Q3. Ion intensity of ion m/z = 242 $(n\text{-}C_4H_9)_4N^+$, versus RE3 where RE3 $\propto$ AC/DC potentials used in Q3. Acceleration potential of ions: V(OR) - V(Q3) = 10 V.

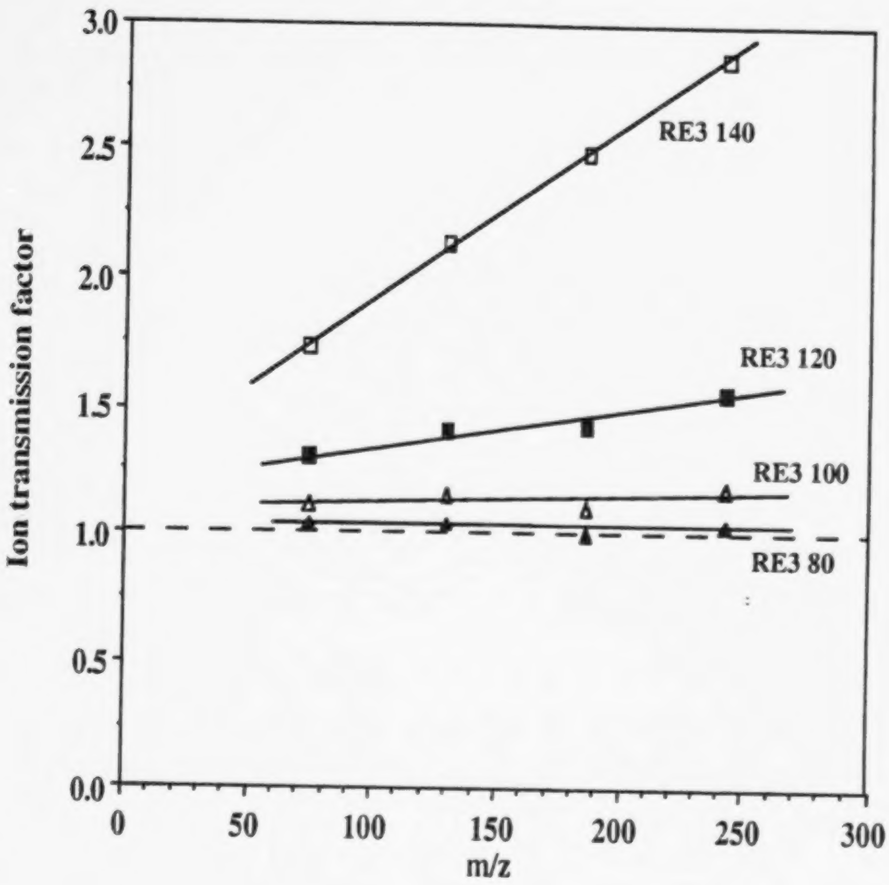

Figure 2.3b Ion transmission correction factors for different resolving powers on Q3 (RE3) versus ion mass to charge ratio.

shown, plotted versus RE3, where RE3 $\propto$ DC/AC voltage in Q_3. The maximum intensity, observed for RE3 < 70, where the peaks are flat topped (trapezoidal), is assumed to represent a region of essentially m/z independent transmission. Curves of this type were obtained with different ions over the complete m/z range (Figure 2.3b). Whenever possible in the actual equilibria measurements the mass spectra were determined at low RE3 (RE3 = 80) such that all ions of interest were near their maximum intensity region. When ions of similar mass were present and a higher resolution, higher RE3, was required the intensities were corrected to the maximum transmission on the basis of curves like that shown in Figure 2.3a but for the corresponding m/z. A plot of these corrections factors, obtained for different RE3 values, versus mass to charge ratio is shown in Figure 2.3b.

A typical mass spectrum from equilibria measurements of protonated diaminopentane, BH^+ and the hydrated ion BH^+H_2O near the flat topped region, RE3 = 100, where only small transmission corrections are required, is shown in Figure 2.4.

c. Conditions in Forechamber and Reaction Chamber

A potential drop of ~55 V between PRC and IN (Figure 2.1) drives the ions into the reaction chamber. This potential was adjusted so as to obtain a near maximum ion intensity. On the other hand, the potential between IN and OR was deliberately selected to be small so as to allow the ions to reach near thermal energies. Generally, that potential drop was 10 V and the distance is 0.5 cm. At 10 Torr this leads to an $E/p \approx 2$ V/(cm Torr). Castleman and coworkers[18] have observed thermal behaviour and measured equilibria at $E/p < 15$ V/(cm Torr). Ion intensity ratios

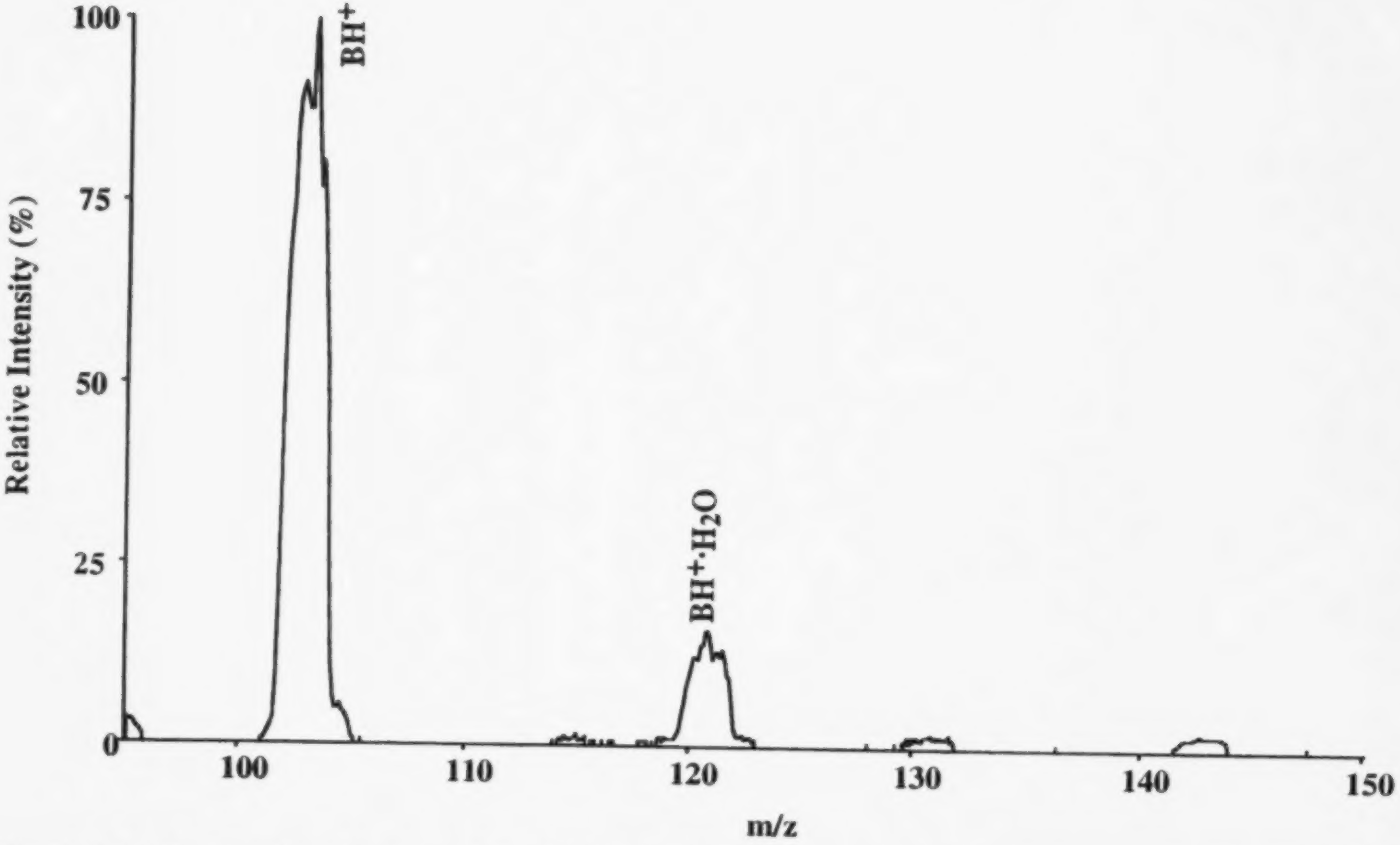

Figure 2.4 Mass spectrum of protonated diamino pentane BH$^+$ and hydrated BH$^+$(H$_2$O) at equilibrium. Ions obtained from a 10^{-4} mol/L solution of diamino pentane 2×10^{-4} mol/L HCl in methanol. Water pressure in RCH 9 mTorr. Relatively low resolution used RE3 = 100 leads to flat topped peaks requiring only small transmission corrections. Total intensity of BH$^+$ and BH$^+$H$_2$O ions ~55000 ions/s.

$BH^+(H_2O)_n/BH^+(H_2O)_{n-1}$ measured in function of the IN-OR potential are shown in Figure 2.5 for B = octylamine and (n/n-1) = (1/0) and (2/1). The ion ratios are found constant as would be expected from thermal ions at equilibrium and Castleman's[18] results. The actual ion intensities, rather than the ratio, are shown in Figure 2.6. These increase with the IN - OR potential, an expected result since the ion transport to the orifice plate is improved by the higher drift field. The potential drop, IN - OR = 10 V, was selected for the equilibria measurements because it leads to a fair intensity while keeping the ions within the thermal range.

The residence time of the ions in the reaction chamber is of interest and can be estimated. If IN - OR = 10 V, at 10 torr N_2 pressure, the drift velocity[19] of an ion with $m/z \approx 50$ is approximately 5000 cm/s and for d = 0.5 cm, this leads to a residence time of 100 µsec. This time should be adequate for the establishment of the equilibria. For room temperature and 10 Torr total pressure, the forward hydration rates are expected[20] to be in the second order region and proceed with rate constants of the Langevin magnitude ($k_f \approx 10^{-9}$ molecules^{-1} cm^3 s^{-1}). At 5 mTorr partial pressure of L = H_2O, one obtains a pseudo first order rate constant of $k_f[H_2O] = 1.5 \times 10^5$ s^{-1} or a reaction lifetime of ~7 µs. These estimates indicate that the residence time in the reaction chamber if long enough for equilibria to establish when the ligand pressure is above a few mTorr.

The ion intensities observed in actual equilibria determinations were in the range of 50000 counts/s for the more intense ions (Figure 2.4). These are very adequate intensities and this suggests that sources with longer reaction chambers which lead to longer ion residence times but lower detected ion intensities are experimentally feasible.

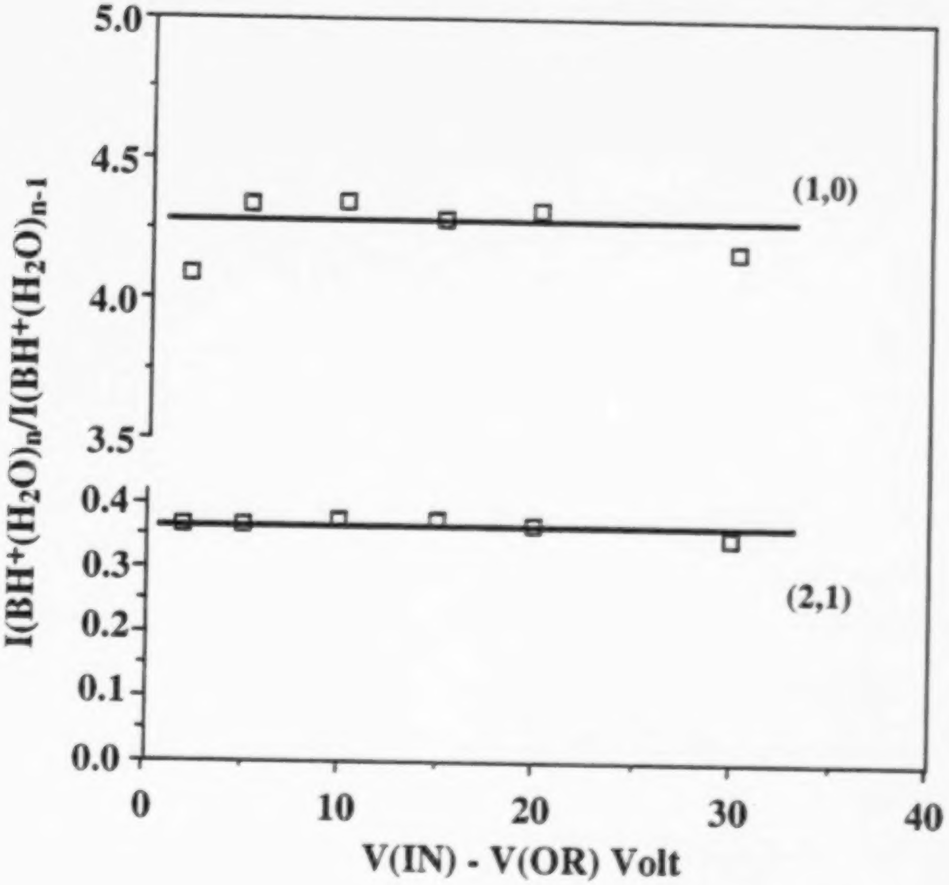

Figure 2.5 Effect of drift potential reaction chamber, RCH, on ion intensity ratios at equilibrium. Ion drift potential V(IN) - V(OR) has no effect on measured ion intensity ratios $BH^+(H_2O)_n$ at equilibrium for V(IN) - V(OR) < 30 V. BH^+ = protonated n-octyl amine. Total ion source pressure 10 Torr. T = 293 K. Numbers above curves give n; the number of H_2O molecules.

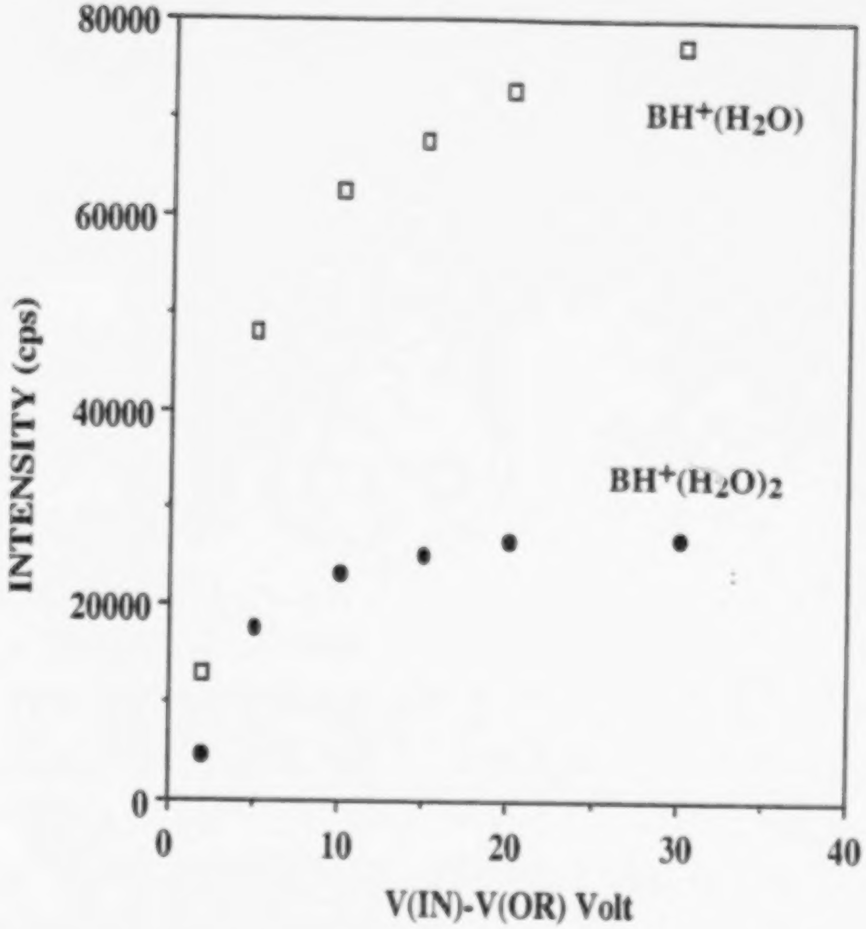

Figure 2.6 Dependence of ion intensities of ions: $BH^+(H_2O)_n$ on drift potential in reaction chamber. The ion intensities decrease as drift potential V(IN) - V(OR) is decreased however ion ratio, shown in Figure 2.5, remains constant.

The gas composition present in the forechamber and the reaction chamber is not exactly identical. The major inflow to the forechamber is through the pressure reduction capillary (PRC), 750 ml/min versus ~90 ml/min reagent gas from the reaction chamber. As mentioned above, the gas through the PRC is purged with reagent gas (Figure 2.1) and therefore is expected to have a composition close to that of the reagent gas. Nevertheless, one might have some concern that the composition might be sufficiently different and that diffusion through the 4 mm orifice connecting the forechamber and reaction chamber might affect the composition of the reaction chamber gas. To demonstrate that this is not the case, equilibria determinations were made for different flow rates of the reagent gas. Increases of the reagent gas flow rate from 90 to 160 ml/min were found to have no effect on the observed ion ratios.

Results and Discussion

a. Equilibria determinations involving systems for which equilibrium data are available in the literature.

Here we give results for a number of systems and compare these with available literature data.

The equilibria studied can be described by the general reaction

$$M^{z+}L_{n-1} + L = M^{z+}L_n \qquad (n-1,n) \qquad (2.1)$$

where L is the ligand or ion solvating agent. In the present work L = H_2O. A few ions were studied also with L = acetone. The equilibrium constant was obtained from

$$K_{n-1,n} = \frac{I_n}{I_{n-1}P_L} \qquad (2.2)$$

where I_n and I_{n-1} are the ion intensities determined with the mass spectrometer under reaction chamber conditions assumed to lead to equilibrium (see Experimental) and P_L is the known pressure of vapor L in the reaction chamber.

According to eq. 2.2, a plot of I_n / I_{n-1} versus P_L should lead to a straight line with slope equal to $K_{n-1,n}$. Shown in Figure 2.7 is the plot for the equilibrium,

$$Na^+(H_2O)_3 + H_2O = Na^+(H_2O)_4 \qquad (2.3)$$

versus the H_2O pressure in the reagent gas at a constant total pressure of 10 Torr. The plot shows excellent linearity and goes through the origin. The correlation coefficient was R = 1.00. Plots of such quality with correlation coefficients better than R = 0.995 were observed in most experiments.

The dependence of the $Na^+(H_2O)_n$ ion intensities on the H_2O pressure is shown in Figure 2.8. The plots in Figure 2.7 and 2.8 are based on the same data set. Of interest is the essentially constant total $Na^+(H_2O)_n$ ion intensity observed in Figure 2.8. In the mass spectra, these ions represent close to 100% of the total ion intensity. Because of conservation of the total number of ions in the reactions, a constant total ion intensity is expected, provided that there is no significant mass dependent discrimination in the transfer of the ions from the reaction chamber to the detector of the mass spectrometer, *i.e.* no mass discrimination not only in the mass analysis stage but also in any other

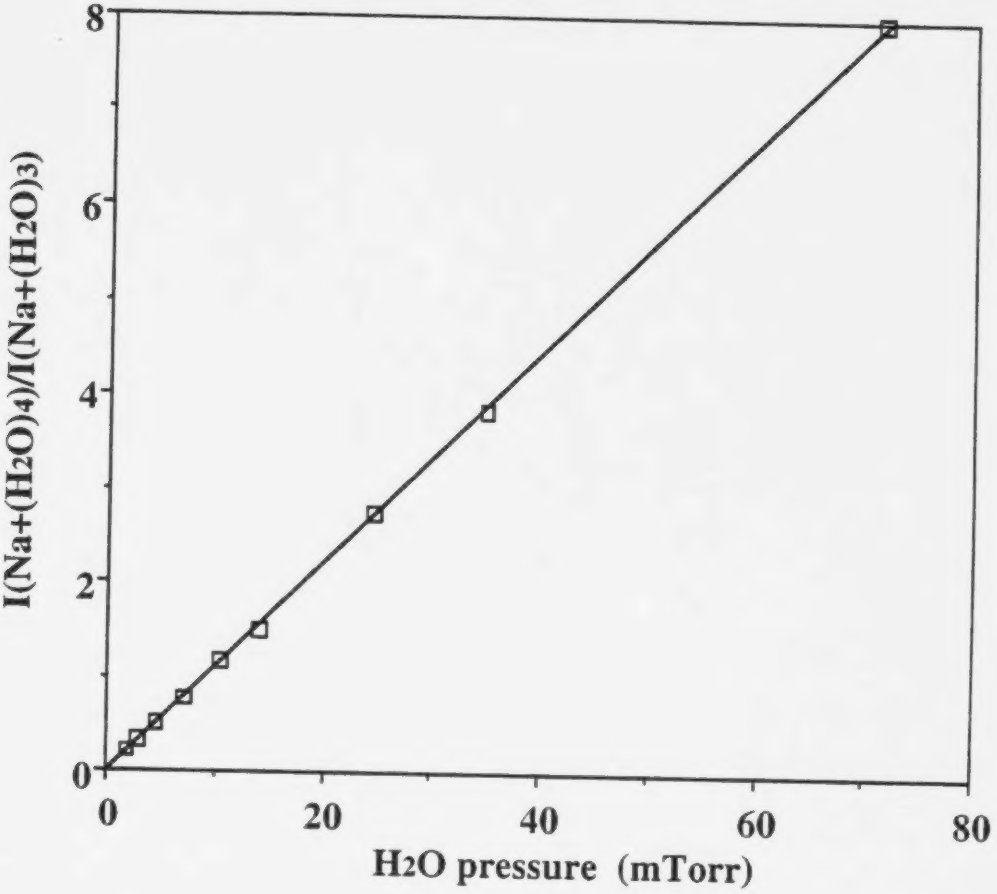

Figure 2.7 Equilibrium ratio plot. Plot of ion intensity ratio $I(Na^+(H_2O)_4)/I(Na^+(H_2O)_3)$ versus H_2O pressure, leads to straight line going through origin as required by equilibrium expression, Eq. 2.2. Slope of line leads to $K_{3,4}$ in $Torr^{-1}$ units. T = 293°K.

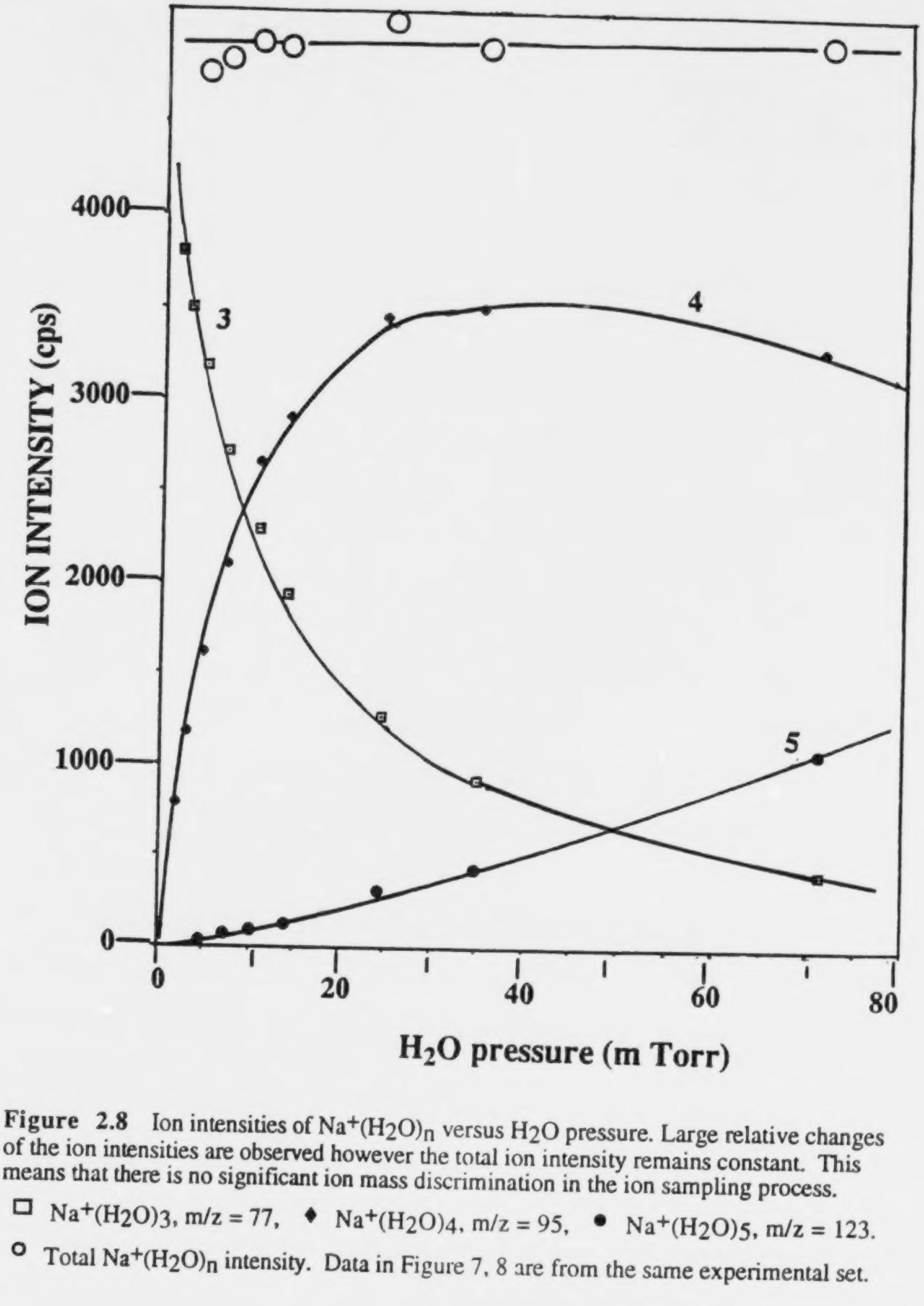

Figure 2.8 Ion intensities of $Na^+(H_2O)_n$ versus H_2O pressure. Large relative changes of the ion intensities are observed however the total ion intensity remains constant. This means that there is no significant ion mass discrimination in the ion sampling process.

□ $Na^+(H_2O)_3$, m/z = 77, ◆ $Na^+(H_2O)_4$, m/z = 95, ● $Na^+(H_2O)_5$, m/z = 123.

○ Total $Na^+(H_2O)_n$ intensity. Data in Figure 7, 8 are from the same experimental set.

stage. The masses of the two major ions, $Na^+(H_2O)_3$, m = 77, and $Na^+(H_2O)_4$, m = 95 do not differ by a large amount and therefore the observed constant total intensity in Figure 2.8 is not a test for the absence of mass discrimination over the complete mass range. However it is a sufficient test when used on every reaction system whose equilibrium is determined and where the ions I_{n-1} and I_n show an appreciable intensity change and make a significant contribution to the total intensity.

The slope in Figure 2.7, when converted to atmosphere^{-1} units, leads to $K_{3,4} = 8.5 \times 10^4$ atm^{-1}. Using the source temperature T = 293°K and the equation

$$\Delta G^\circ = -RT\ell nK \qquad (2.4)$$

one obtains: $\Delta G^\circ_{3,4} = -6.6$ kcal/mol.

The data in Figures 2.7, 2.8 were obtained with our previous ion source.[15] A duplicate determination with the present source led to very similar results: $K_{3,4} = 1.0 \times 10^5$ atm^{-1} and $\Delta G^\circ_{3,4} = -6.7$ kcal/mol. The ion intensities obtained with the present source were considerably higher, a total ion intensity of ~50000 counts/s, versus ~5000 counts/s, with the old source.

Examples of equilibrium plots for the reactions:

$$n\text{–}C_3H_7NH_3^+(H_2O)_{n-1} + H_2O = n\text{–}C_3H_7NH_3^+(H_2O)_n \qquad (2.5)$$

for the (1,2) and (2,3) equilibria are shown in Figure 2.9.

A summary of all measurements involving ions for which independent data in the literature are available, is given in Table 2.1.

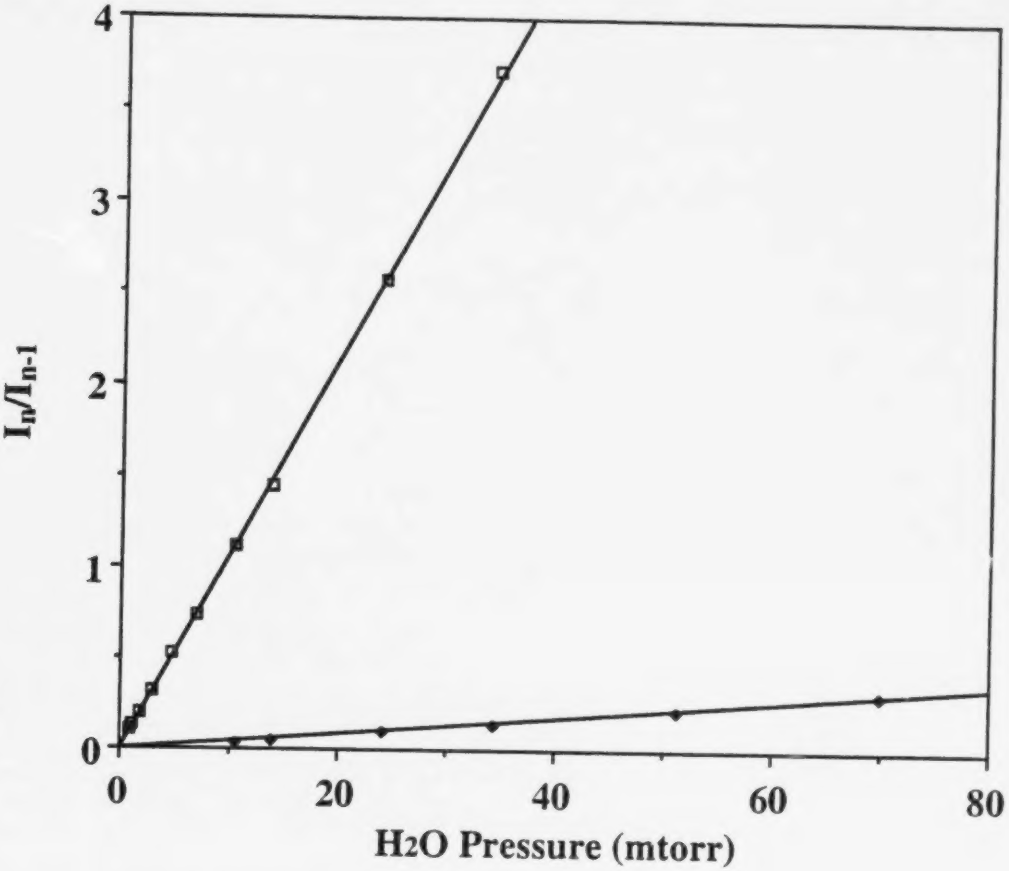

Figure 2.9 Equilibrium ratio plot for BH^+ = protonated n-propylamine.
□ (1,2)-hydration equilibrium, ◆ (2,3)-hydration equilibrium.

Table 2.1. Comparison with Free Energy Data in Literature

Ion	Ligand	(n-1,n)	$-\Delta G^\circ_{n-1,n}$ (kcal/mol)[a]		
H_3O^+	H_2O	(3,4)	5.8	5.8	Lau, (PHPMS)[20]
		(4,5)	4.5	4.3	
Na^+	H_2O	(3,4)	6.6	6.4	Dzidić, (PHPMS)[21]
		(4,5)	4.7	4.0	
$n\text{-}C_3H_7NH_3^+$	H_2O	(1,2)	6.4	5.4	Meot-Ner[22] (PHPMS)
		(2,3)	4.6	3.5	
Mg^{2+}	H_2O	(10,11)	7.2	7.4[b]	Blades, (AP)[2b]
		(11,12)	6.6	7.2	
		(12,13)	6.0	-	
		(13,14)	5.5	-	
		(14,15)	5.2	-	
		(15,16)	4.9	-	
K^+	$(CH_3)_2CO$	(2,3)	9.2	9.2	Sunner, (PHPMS)[23]
		(3,4)	6.0	-	
$(CH_3)_4N^+$	$(CH_3)_2CO$	(0,1)	7.3	7.4	Meot-Ner (PHPMS)[24]
		(1,2)	5.5	4.4	
$(C_2H_5)_4N^+$	$(CH_3)_2CO$	(0,1)	5.4	4.9	

---

[a] Free energy change at 293°K. Standard state 1 atm. Values from the present work in left column. Literature values, right column, were recalculated from 298°K to 293°K, with use of the corresponding entropy change provided in the literature. Because the $-\Delta S^\circ_{n-1,n}$ is within the range: 22-27 cal/(deg mol), the $-\Delta G^\circ$ at 293° is only ~0.1 to 0.2 kcal/degree higher than the $-\Delta G^\circ$ at 298°, for all reactions in the Table. The literature method of measurement is identified as Pulsed Electron High Pressure Mass Spectrometer (PHPMS) and Atmospheric Pressure Sampling (AP).

[b] These determinations[2b], were preliminary results obtained from an ion source at 1 atm and at a single H_2O pressure.

A comparison between the present results and previous measurements with the PHPMS method,[20,21-24] reveals good agreement. The present -ΔG° values are generally higher by 0.1-1.0 kcal/mol. Somewhat better agreement is observed with previous PHPMS determinations from this laboratory such as the hydration of H_3O^+ and Na^+ and interactions of K^+ with acetone than with Meot-Ner's data, n–$C_3H_7NH_3^+$ hydration and tetraalkylamines-acetone.[22,24]

A possible cause for the somewhat higher -ΔG° values in the present work could be the occurrence of ligand addition to the ions in the vacuum region immediately outside the sampling orifice (OR, Figure 2.1). Even though the pressure in the reaction chamber is only 10 Torr, jet formation and a temperature decrease is expected to occur on the vacuum side of the 100 μm orifice. The temperature decrease can drive the ML_n populations to higher n and thus to high $-\Delta G^\circ_{n-1,n}$ values. We have assumed that such a cluster growth does not occur because the time the ions spend in a high gas density low temperature region is very short and the collisions of the ions are predominantly with the buffer gas whose number density is ~100 times higher than that of the gas L. This assumption is supported by the observed linearity of the I_n / I_{n-1} versus ligand pressure plots and the near zero intercept with the y axis. We have not tried to estimate whether the presence of linearity and zero intercept is a sensitive test for the absence of ion cluster growth past the sampling orifice, because of the great complexity of the conditions in the region past the orifice.

Differences of ±0.3 kcal/mol amongst determinations at the same temperature, obtained in different laboratories are quite common,[8b] and the present differences are not out of line with previous work. Therefore, we consider the present data to be of similar quality to previous work.

The literature data for $Mg^{2+}(H_2O)_n$ in Table 2.1 are from our previous determinations[2b] involving ions produced by electrospray but with a different apparatus where the reaction chamber was at 1 atm. In that work only a single partial pressure of ~1 mTorr H_2O was used. Changes of the H_2O pressure were not attempted[2b] because it is difficult to control the partial pressure of H_2O when it is so low while the pressure of the bath gas (N_2) is so high (1 atm). Also jet formation and a large temperature decrease past the orifice are known to occur when the initial pressure is so high. The effects of the temperature decrease could be observed in the mass spectra by the presence of N_2 adducts to the ion hydrates such as $K^+(H_2O)N_2$, $K^+(H_2O)(N_2)_2$ and other such species.[2b] The present equilibrium results for $Mg^{2+}(H_2O)_n$ are considered to be more accurate. Because the H_2O pressure could be changed from 1 to ~80 mTorr, also a much wider (n-1,n) range of the $-\Delta G^\circ_{n-1,n}$ could be obtained.

All ion-ligand species, except $Mg^{2+}(H_2O)_n$, in Table 2.1, can be obtained from ion sources other than electrospray. However, while with electrospray the ion production is very straightforward - the ion should be present in the electrosprayed solution, with the previous methods- a variety of techniques had to be applied. For the alkali ions a special thermoionic source had to be developed.[21] The quaternary alkyl ammonium ions could be obtained in the conventional PHPMS ion source, but their production[24] became possible only after the development of "gas phase synthetic" methods, *i.e.* the alkylation reactions via alkyl chloronium ions.[25]

This comparison illustrates another advantage of electrospray. It is not only the unique route to the biologically important ions and to multiply charged inorganic ion-ligand complexes but it also leads to a very straightforward preparation of many ions which have been produced previously by other methods.

b. Equilibria Determinations involving ions produced by Atmospheric Pressure Ionization API.

The $H_3O^+(H_2O)_n$ equilibrium data given in Table 2.1 were not obtained from electrospray. While these ions can be obtained from electrospray of acidified aqueous solutions, ES using aqueous solutions is less convenient than ES of other solvents such as methanol which have low surface tension.[10]

API, in which ionization is obtained with an electric, corona discharge at atmospheric pressure, produces abundant $H_3O^+(H_2O)_n$ ions in moist air. As is well known, a great variety of ions can be produced by API.[17] In the positive ion mode this includes not only even electron ions obtained by protonation reactions but also odd electron ions obtained by charge exchange. The API mode is easily used with the present apparatus (Figure 2.1). The ES capillary is replaced by a needle which is the positive discharge electrode in the positive ion mode, while the pressure reduction capillary (PRC) is the negative electrode. General conditions used with the API mode are given elsewhere.[17,26] The mass analyzed total ion intensity obtained with API and the present apparatus was considerably higher relative to that observed with electrospray. For example the $H_3O^+H_2O$ ion intensity was ~4 times higher than that of $Na^+(H_2O)_n$ observed with ES. We find the API alternative particularly useful for production of odd electron organic molecular ions which are generally difficult to obtain with ES.

c. Hydration equilibria of protonated alkyl amines, diamines and small peptides.

The hydration free energies of the protonated alkylamines, singly and doubly protonated α,ω-alkyldiamines and a few singly and doubly protonated small peptides obtained in this work are given in Table 2.2.

An illustration of results on which the data are based is given in Figures 2.10 and 2.11. The mass spectrum obtained from an acidified solution of diaminooctane (Figure 2.10) provides very directly information on two important phenomena. The spectrum is dominated by the doubly protonated base BH_2^{2+}. The major hydrate observed is $BH_2^{2+}(H_2O)_4$. Each $-NH_3^+$ group in this ion is solvated on average by two water molecules. On the other hand, the singly protonated base BH^+, which is also observed, is barely hydrated - the major species being the naked BH^+ ion. Evidently, even though the two charges on the BH_2^{2+} are separated by the relatively long distance due to the stretched out $(CH_2)_8$ chain, each charged group exercises a strong substituent effect on the other. This interaction increases the protic character of the $-NH_3^+$ hydrogens and thus also the strength of the H bonding interactions with H_2O molecules. The substituent effect increases rapidly with shortening of the chain, see $\Delta G°$ data in Table 2.2 and discussion in previous work.[15] The hydration of the singly protonated base BH^+ is extremely weak. This is not only because of the missing substituent effect of a positively charged group, but also because this ion can form an intramolecular H-bond to the other neutral amino group, as discussed in greater detail below.

The equilibrium plots shown in Figure 2.11 demonstrate another interesting feature of the hydration of the BH_2^{2+} ions. It is easy to notice that there is a very large drop of the slopes between the (3,4) and (4,5)

Table 2.2. Hydration Free Energies of Some Protonated Alkyl Amines, Alkyl Diamines and Peptides[a]

M^{Z+}	n-1,n	$-\Delta G^\circ_{n-1,n}$	M^{Z+}	n-1,n	$-\Delta G^\circ_{n-1,n}$
$n\text{-}C_3H_7NH_3^+$	1,2	6.4	Gly H^+	0,1	9.7
	2,3	4.6		1,2	7.2
$n\text{-}C_8H_{17}NH_3^+$	0,1	8.5		2,3	5.4
	1,2	6.1	Gly_2 H^+	0,1	8.8
	2,3	4.6		1,2	6.2
$NH_2(CH_2)_2NH_3^+$	0,1	7.8(7.7)[b]	Gly_3 H^+	0,1	6.7
$NH_2(CH_2)_3NH_3^+$	0,1	6.2(5.6)[b]		1,2	5.8
$NH_2(CH_2)_4NH_3^+$	0,1	5.3(5.1)[b]	Gly_4 H^+	0,1	5.8
$NH_2(CH_2)_5NH_3^+$	0,1	5.5	Lys H^+	0,1	5.2
$NH_2(CH_2)_6NH_3^+$	0,1	5.5	$N^{\alpha}CH_3CO$-Lys H^+	0,1	5.8
$NH_2(CH_2)_7NH_3^+$	0,1	5.6	Gly-Lys H^+	0,1	4.9
$NH_2(CH_2)_8NH_3^+$	0,1	5.4	Lys-Tyr-Lys H_2^{2+}	0,1	7.1
$NH_2(CH_2)_{10}NH_3^+$	0,1	5.1		1,2	6.2
$NH_2(CH_2)_{12}NH_3^+$	0,1	4.9		2,3	5.6

Doubly protonated diamines[c]

$[NH_3(CH_2)_kNH_3]^{2+}$	$-\Delta G^\circ_{2,3}$	$-\Delta G^\circ_{3,4}$	$-\Delta G^\circ_{4,5}$	$-\Delta G^\circ_{5,6}$
k = 7	8.0	7.1	5.9	5.3
k = 8	7.7	6.9	5.8	5.2
k = 10	7.4	6.7	5.7	5.1
k = 12	7.1	6.4	5.5	5.0

[a] All ΔG° values are free energy changes in kcal/mol, standard state 1 atm at 293° K.

[b] Literature values Meot-Ner *et al.*[28]

[c] From Klassen *et al*[15]. Present values include a minor correction for the water partial pressure which was redetermined.

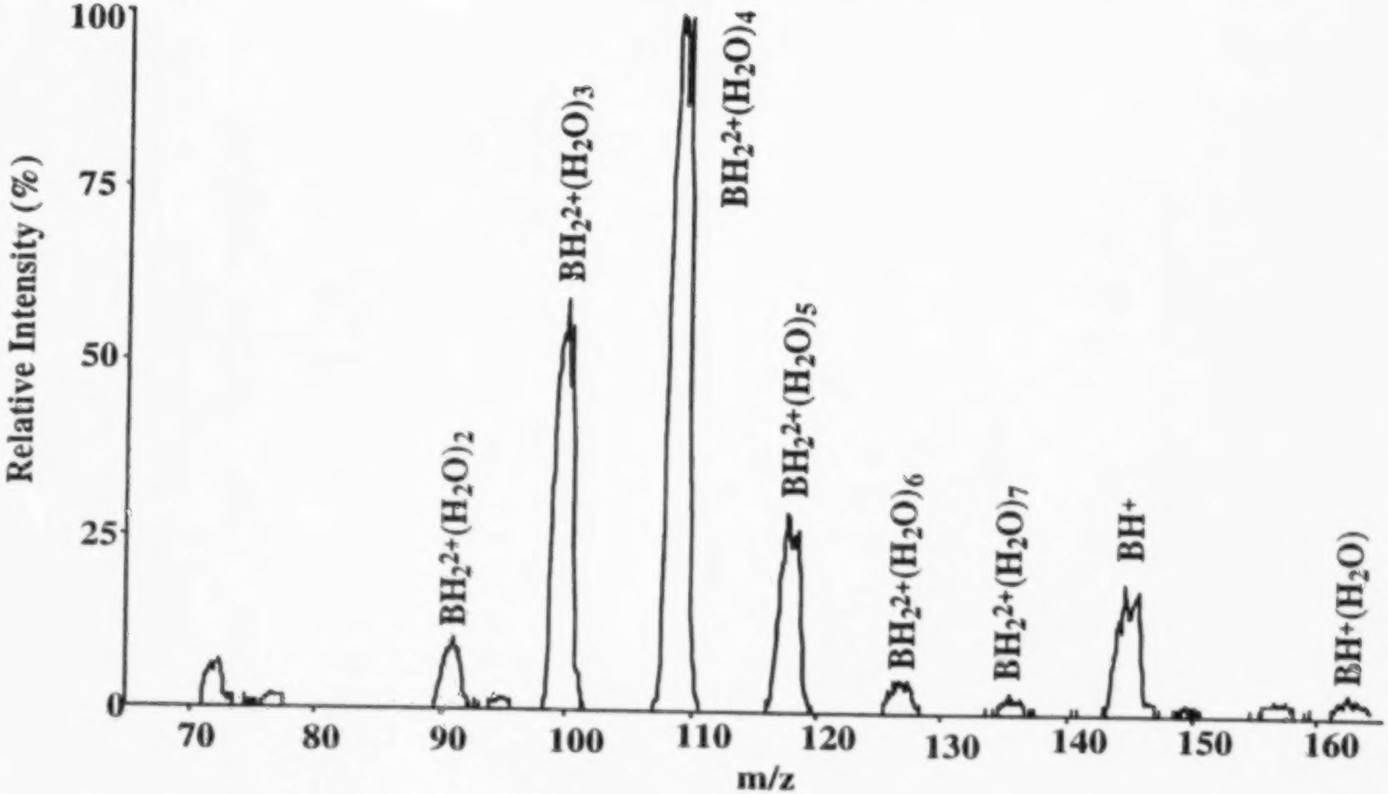

Figure 2.10 Mass spectrum showing hydrates of singly protonated BH^+ and doubly protonated BH_2^{2+} diamino octane. 6.9 mTorr H_2O pressure, T = 293°K. The average hydration n of the diprotonated species is much more than twice that of the mono-protonated amine. This demonstrates the strong influence of the two charge sites on each other in BH_2^{2+}, even when separated by eight CH_2 groups. Relative intensity 100 corresponds to ~46000 ions/s. Resolution of Q_3, RE3 = 100.

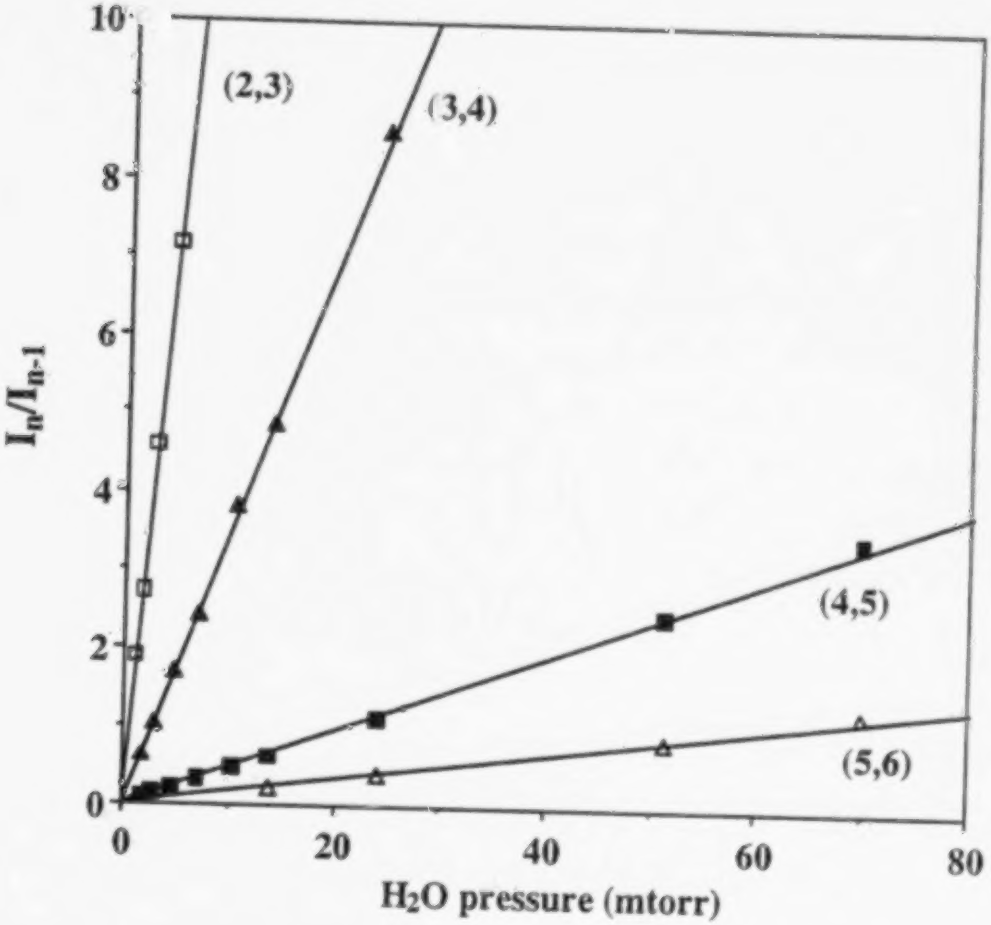

Figure 2.11 Equilibrium ratio plot for diprotonated diaminoheptane hydrates, $BH_2^{2+}(H_2O)_n$. Large relative decrease of slope between (3,4) and (4,5) plots corresponds to large decrease of $-\Delta G^\circ_{4,5}$ on addition of fifth H_2O molecule, see text.

plots. Since the slopes lead to the $\Delta G^{\circ}_{n-1,n}$ values (see Table 2.2) this means that the decrease of the free energy is particularly big between the fourth and fifth water molecule. The same gap is observed for all other diprotonated diamines(Table 2.2). There is a straightforward interpretation for this result. In singly charged ions, such as primary alkylammonium ions there is a gradual decrease of $-\Delta G^{\circ}_{n-1,n}$ as the first shell of 3 H_2O molecules is built up.[27] For the diprotonated diammonium ions, one expects a somewhat different situation. The second water molecule will go to the second charged group and the interaction will be only slightly weaker than that with the first water molecule. The third molecule will have to double up on one of the charged groups and this interaction will be considerably weaker, than the first two. The fourth molecule will double up on the other side which will lead to a slightly weaker interaction. The fifth molecule leads to the first tripling up on one of the charged groups and to a much weaker interaction as observed in the plots of Figure 2.11 and in the corresponding $-\Delta G^{\circ}_{n-1,n}$ values of Table 2.2. It should be noted that the same behaviour is observed for all diprotonated diamines (Table 2.2). Additional discussion concerning the hydration of the BH_2^{2+} species can be found in our previous report.[15]

The hydration of the singly protonated alkylamines and alkyldiamines has been studied before by Meot-Ner and coworkers[22,27,28] with the PHPMS technique. Therefore we will consider here only those aspects of the present findings which are of interest in connection with the hydration of the protonated peptides and the conformations of the protonated peptides.

Meot-Ner's work and the present results (Table 2.2) show that the hydration of the protonated alkylamines is very much stronger than that of the protonated diamines. For example $-\Delta G^\circ_{0,1}$ ($C_8H_{17}NH_3^+$) = 8.5 kcal/mol, while $-\Delta G^\circ_{0,1}$ ($NH_2(CH_2)_8NH_3^+$) = 5.4 kcal/mol (Table 2.2). In the gas phase, the protonated diamines are known[29] to cyclize due to the formation of an intramolecular hydrogen bond, where the $-NH_3^+$ group acts as proton donor and the $-NH_2$ group as acceptor. It is this "internal solvation" of the proton that reduces the exoergicity of the hydration reactions. Data provided by Meot-Ner[28] which compare the exoergicity of the cyclization reaction ($-\Delta G^\circ_{cyl}$) with that of the hydration reaction ($-\Delta G^\circ_{0,1}$) show that there is a good correlation between the two quantities, *i.e.* high cyclization exoergicities lead to low hydration exoergicities. This means that the hydration exoergicities of the protonated peptides can be used to probe for the extent of cyclization due to intramolecular H-bonding.

Three factors determine the cyclization exoergicity[28,29] when an $-NH_3^+$ group is the proton donor: (a) the gas phase basicity of the proton accepting group, where a strong base leads to the formation of a strong bond;[30] (b) ring strain, where strain is reduced with length of the chain; (c) loss of freedom of internal motions where the total loss of freedom increases slowly with the chain length. The first two factors are reflected in the enthalpy, ΔH°_{cyc}, while the last factor is reflected in the entropy, ΔS°_{cyc}.

The most favorable hydrogen bond, $[N—H\cdots N]^+$, geometry is linear and this leads to a large ring strain in the cyclized, $NH_2(CH_2)_2NH_3^+$. The strain decreases for the propane analogue and becomes quite small for all the higher analogues. The cyclization exoergicities,[28,29] $-\Delta G^\circ_{cyc}$: ~4 kcal/mol (C_2), ~10 kcal/mol (C_3), and ~14 kcal/mol (C_4), followed by quite small changes for the higher analogues, reflect largely the change of strain. The hydration exoergicities $-\Delta G^{\circ}_{0,1}$ of the protonated diamines (Table 2.2) which change from 7.8 kcal/mol (C_2) to 6.2 kcal/mol (C_3) to ~5.4 kcal/mol (C_3) and higher analogues, show the expected reverse correlation with the above values.

The protonated peptides have different basic groups which can be involved as proton acceptors in the internal H-bond formation. The strongest of these would be other nitrogen basic groups on the amino acid residues, when such basic residues are present. In the absence of such groups the carbonyl oxygen and the nitrogen at the peptide bond could be involved. The gas phase basicities[8c] of the compounds quoted below provide a guide to the relative strength expected for the different basic groups in the peptides: ethyl amine, 208 kcal/mol; acetamide, 198 kcal/mol, acetic acid, 181 kcal/mol. Ethyl amine would be representative for a basic residue such as the n-butyl amine for lysine. Acetamide represents the carbonyl oxygen at the peptide bond, while acetic acid represents the carbonyl oxygen on the terminal carboxylic group. Direct experimental values for the basicity of the nitrogen at the peptide bond is not available. Theoretical calculations[31] show that it is less basic by several kcal/mol than the adjacent carbonyl oxygen.

The very low hydration exoergicities for Lys H^+ and Gly•Lys H^+ (Table 2.2) are in line with the expected large, $-\Delta G^{\circ}_{cyc}$, exothermicity due to the strongly basic butylamino group on lysine. Also, the butyl group is sufficiently long, so that ring strain in the cyclization is not expected.

Cassady and coworkers[31] have made a detailed study of the protonation of glycine and glycylglycine based on experimental gas phase basicity measurements and ab initio theoretical calculations. The most stable structures for Gly H^+ and Gly_2 H^+ obtained by these authors,[31] are shown below together with the corresponding gas phase basicities (GB).[31-34] The experimentally determined GB[31-34] for Gly_3 and Gly_4 are given also. No calculations were performed[31] and therefore no structural information was provided for these two species.

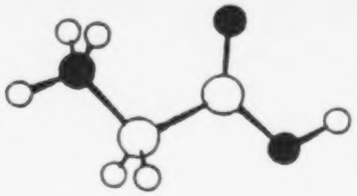

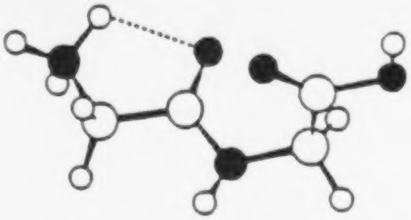

Gly H^+ GB = 202 kcal/mol

Gly$_2$ H^+ GB = 211 kcal/mol

Gly$_3$ H^+ GB = 216 kcal/mol

Gly$_4$ H^+ GB = 221 kcal/mol

Entropy changes were evaluated[31] only for the protonation of Gly and Gly_2: $\Delta S^{\circ}_1 \approx -24$ cal/(deg mol) and $\Delta S^{\circ}_2 \approx -27$ cal/(deg mol). These are typical values for protonation which is not accompanied by cyclization. In the presence of cyclization, the entropy loss is higher by some 15-20 cal/(deg mol).[29]

It is evident from the structures of Gly H^+ and Gly_2 H^+ above, that only very strained H bonds can be formed. For Gly H^+, the H bond would be further weakened by the lower basicity of the carbonyl oxygen, since the carboxylic group is involved. These considerations taken together with the entropy changes, show that there is no internal H-bonding in Gly H^+ and a very weak one in Gly_2 H^+.

The hydration energies $-\Delta G^{\circ}_{0,1}$ (kcal/mol) for the glycine series (Table 2.2) are: Gly H^+, 9.7; Gly_2 H^+, 8.8; Gly_3 H^+, 6.7 and Gly_4 H^+, 5.8. For the protonated alkylamines we used the following $-\Delta G^{\circ}_{1,0}$ values as markers: n-$C_8H_{17}NH_3^+$, 8.5, no internal H bond, no cyclization and $NH_2(CH_2)_5NH_3^+$, 5.5, strong internal H-bond and cyclization. These values should have at least partial validity also for the protonated glycines. On that basis there is essentially no cyclization for Gly H^+ and Gly_2 H^+, definitely some cyclization for Gly_3 H^+ and even stronger cyclization for Gly_4 H^+. The increase of gas phase basicity observed by Cassady *et al* for Gly_3 and Gly_4, see above, should be largely due to stabilization by internal H bonding. For Gly_3 H^+ and Gly_4 H^+ the bonding will be better relative to Gly_2 H^+ because of less ring strain due to formation of larger rings. Thus in Gly_3 H^+, the proton acceptor will be the carbonyl oxygen of the second peptide bond leading to an 8 atom ring, while for Gly_4 H^+ it would be the oxygen of the third peptide bond leading to an 11 atom ring. An increase of stability from Gly_3 H^+ to Gly_4 H^+ could be expected because the peptide chains are considerably more rigid than -CH_2- chains due to restricted rotation around the N-CO bond and steric and polar repulsions between groups on the chain.

The ability of protonated peptides to form internally bonded cyclized structures may be of importance in the decomposition mechanism of collisionally-excited protonated peptides. Collision-induced decomposition (CID) is an important method for mass spectrometric sequencing of protonated peptides.[35] Protonated peptides subjected to low energy collisions (<100 eV) are known to dissociate primarily along the peptide backbone at the peptide bonds. Peptide bond cleavage is believed to be charge directed involving an endothermic proton transfer from the most basic group to the peptide nitrogen. Therefore, in some cases, the decomposition mechanism may be affected by the nature of the intramolecular proton transfer reaction. If the proton transfer occurs via internal H bonding *i.e.* cyclization, fragmentation of peptide bonds to which cyclization is facile will be favored. We have studied recently the energy requirements of such reactions by determining the energy thresholds (appearance energy) of various backbone fragments, in particular the a, b and y ions, with a triple quadrupole mass spectrometer.[36] Studies of $Gly_2 H^+$, $Gly_3 H^+$ and $Gly_4 H^+$ have provided evidence that facile cyclization as determined in the present work, correlates with lower energy thresholds and higher yield for the corresponding backbone fragment ions.[36b]

The hydration energies for the doubly protonated Lys-Tyr-Lys H_2^{2+} can be compared with those for the doubly protonated alkyl diamines, $NH_3^+(CH_2)_kNH_3^+$ (Table 2.2). The hydration energies of the diamines are very much higher. Thus $-\Delta G^\circ_{0,1}$ and $-\Delta G^\circ_{1,2}$ for the diamines were too high and could not be determined at room temperature. Comparing the available values, one finds that $-\Delta G^\circ_{0,1}$ of Lys-Tyr-Lys H_2^{2+} is similar in magnitude to $-\Delta G^\circ_{3,4}$ of the diamines. This result indicates that both protons in the LysTyrLys are dicoordinated. The proton on the N terminal Lys group would be dicoordinated as in Lys H^+, *i.e.* between the N terminal amino group and the amino group of the butyl amine residue. The second proton on the butyl amine residue of the C terminal Lys would have to engage in a weaker interaction with a suitable oxygen base which leads to low ring strain and places it at a maximum distance from the other positive charge.

The present determinations involving protonated peptides provide only a sample of the information that can be obtained with the present apparatus. It is clear that further experiments involving carefully chosen oligopeptides can lead to a systematic build-up of information on the hydration of the protonated peptides and their structures. Such work could be supported also by *ab initio* calculations and molecular modelling based on atom-atom pair potentials.[37]

References

1. Yamashita, M.; Fenn, J.B. *J. Phys. Chem.* **1984**, *88*, 4451. Fenn, J.B.; Mann, M.; Meng, C.K.; Wong, S.F.; Whitehouse, C.M. *Science* **1985**, *246*, 64.
2. (a) Jayaweera, P.; Blades, A.T.; Ikonomou, M.G.; Kebarle, P. *J. Am. Chem. Soc.* **1990**, *112*, 2452-2454. (b) Blades, A.T.; Jayaweera, P.; Ikonomou, M.G.; Kebarle, P. *J. Chem. Phys.* ***1990***, *92*, 2900-2906. (c) Blades, A.T.; Jayaweera, P.; Ikonomou, M.G.; Kebarle, P. *Int. J. Mass Spectrom. Ion Processes* **1990**, *102*, 251-267. (d) Blades, A.T.; Jayaweera, P.; Ikonomou, M.G.; Kebarle, P. *Int. J. Mass Spectrom. Ion Processes* **1990**, *101*, 325-336.
3. Bruins, A.P.; Covey, T.R.; Henion, J.D. *Anal. Chem.* **1987**, *59*, 2642. Covey, T.R.; Bonner, R.F.; Shushan, B.I.; Henion, J.D. *Rapid Commun. Mass Spectrom..* **1988**, *2*, 249. Huang, E.C.; Henion, J.D. *J. Am. Soc. Mass Spectrom.* **1990**, *1*, 158.
4. Blades, A.T.; Kebarle, P. *J. Am. Chem. Soc.* **1994**, *116*, 10761.
5. (a) Limbach, P.A.; Crain, P.F.; McCloskey, J.A. *J. Am. Soc. Mass Spectrom.* **1995**, *6*, 27. (b) Smith, R.D.; Loo, J.A.; Edmonds, C.G.; Barinaga, C.J.; Udseth, H.R. *Anal. Chem.* **1990**, *62*, 882.
6. Kebarle, P. *Annu. Rev. Phys. Chem.* **1977**, *28*, 445.
7. Kebarle, P. in "Techniques for the Study of Ion-Molecule Reactions" Farrar, J.M.; Saunders, W. Jr. John Wiley & Sons Inc. (1988).
8. (a) Lias, S.G.; Bartmess, J.E.; Liebman, J.F.; Holmes, J.L.; Levin, R.D.; Mallard, W.G. Gas Phase Ion and Neutral Thermochemistry. *J. Phys. Chem. Ref. Data* **1988**, 17 Suppl. No. 1. (b) Keesee, R.G.; Castleman, A.W.; *J. Phys. Chem. Ref. Data* **1986**, *15*, 1011. (c)

Lias, S.G.; Liebman, J.F.; Levine, R.D. *J. Phys. Chem. Ref. Data* **1984**, *13*, 695.

9. For a recent discussion of the conditions and mechanism of electrospray mass spectrometry see ref. 10.
10. Kebarle, P.; Tang, L. *Anal. Chem.* **1993**, *65*, 272A.
11. Zook, D.R.; Grimsrud, E.P. *J. Am. Soc. Mass Spectrom..* **1991**, *2*, 232.
12. Zook, D.R.; Grimsrud, E.P. *J. Phys. Chem.* **1988**, *92*, 6374.
13. Ikonomou, M.G.; Kebarle, P. *Int. J. Mass Spectrom. Ion Processes* **1992**, *117*, 283.
14. Miller, D.R. Free Jet Sources. In *Atomic and Molecular Beam Methods*; Scolas, J., Ed.; Oxford University Press: Oxford, 1988, Vol. 1, p. 14.
15. Klassen, J.S.; Blades, A.T.; Kebarle, P. *J. Am. Chem. Soc.* **1994**, *116*, 12075.
16. The capillary length used previously[15] was erroneously reported as 5 cm. It was actually 10 cm.
17. Reid, N.M.; Buckley, J.A.; French, J.B.; Poon, C.C. *Adv. Mass Spectrom. B* **1979**, *8*, 1843.
18. Keesee, R.G.; Lee, N.; Castleman, A.W. Jr., *J. Am. Chem. Soc.* **1979**, *101*, 2599.
19. Lindinger, W.; Albritton, D.L. *J. Chem. Phys.* **1975**, *62*, 3517.
20. Lau, Y.K.; Ikuta, S.; Kebarle, P. *J. Am. Chem. Soc.* **1982**, *104*, 1462.
21. Dzidić, I.; Kebarle, P. *J. Phys. Chem.* **1970**, *7*, 1466.
22. Meot-Ner (Mautner), M. *J. Am. Chem. Soc.* **1984**, *106*, 1265.
23. Sunner, J.; Kebarle, P. *J. Am. Chem. Soc.* **1984**, *106*, 6135.

24. Meot-Ner (Mautner) M.; Deakyne, C.A. *J. Am. Chem. Soc.* **1985**, *107*, 469.

25. Sen-Sharma, D.K.; Kebarle, P. *J. Am. Chem. Soc.* **1982**, *104*, 19.

26. Sunner, J.; Ikonomou, M.G.; Kebarle, P. *Anal. Chem.* **1988**, *60*, 1308.

27. Meot-Ner (Mautner), M. *J. Am. Chem. Soc.* **1984**, *106*, 1265.

28. Meot-Ner (Mautner), M.; Hamlet, P.; Hunter, E.P.; Field, F.H. *J. Am. Chem. Soc.* **1980**, *102*, 6393.

29. Yamdagni, R.; Kebarle, P. *J. Am. Chem. Soc.* **1973**, *95*, 3504.

30. Davidson, W.R.; Sunner, J.; Kebarle, P. *J. Am. Chem. Soc.* **1979**, *101*, 1675.

31. Zhang, K.; Zimmerman, D.M.; Chung-Phillips, A.; Cassady, C.J. *J. Am. Chem. Soc.* **1993**, *115*, 10812.

32. Cassady *et al*[31] determined experimentally proton transfer free energy changes which were converted to absolute GB values by anchoring to data obtained by Meot-Ner *et al*[33]. These provide GB values which are ~4 kcal/mol higher than those from the Lias *et al*[8c] compilation. Recent work by McMahon[34] has shown that the GB values of Lias are to be preferred in the GB region of interest here. Therefore we are quoting the Cassady values reduced by 4 kcal/mol.

33. Meot-Ner (Mautner), M.; Sieck, W.L. *J. Am. Chem. Soc.* **1991**, *113*, 4448.

34. Szulejko, J.E.; McMahon, T.B. *J. Am. Chem. Soc.* **1993**, *115*, 7839.

35. (a) Johnson, R.S.; Martin, S.A.; Biemann, K. *Int. J. Mass Spectrom. Ion Processes* **1988**, *86*, 137. (b) Hunt, D.F.; Yates, J.R. III; Shabanowitz, J.; Winston, S.; Hauer, C.R. *Proc. Natl. Acad. Sci. U.S.A.* **1986**, *83*, 6233.

36. (a) Anderson, S.G.; Blades, A.T.; Klassen, J.S.; Kebarle, P. *Int. J. Mass Spectrom. Ion Processes* **1995**, *141*, 217 (b) Klassen, J.S.; Kebarle, P. "Energy Thresholds for the Collision Induced Decomposition of Some Small Protonated Peptides," to be submitted to *J. Phys. Chem.*

37. (a) Fraga, S.; San Fabian, E.Y.; Thornton, S.; Singh, B. *J. Molecular Recognition* **1990**, *3*, 25. (b) Karplus, P.A.; Gao, J.; Kuczera, K.; Fidor, B.; Karplus, M. *Science* **1989**, 244, 1069.

Chapter 3

Free Energies of Hydration in the Gas Phase of the Anions of Some Oxo Acids of C, N, S, P, Cl, I.*

Introduction

Determinations of gas phase equilibria involving singly charged ions and solvent molecules such as H_2O (see eq. 3.1), or other ligands, were initiated some 30 years ago.[1,2]

$$A^-(H_2O)_{n-1} + H_2O = A^-(H_2O)_n \qquad (n\text{-}1,n) \quad (3.1)$$

The sequential bond free energies, $\Delta G^\circ_{n-1,n}$, and enthalpies, $\Delta H^\circ_{n-1,n}$, resulting from such equilibrium measurements have provided a wealth of data[2,3] on ion-solvent and ion-ligand interactions for positive M^+ and negative A^- ions.

Many ions of great interest in condensed phase chemistry and biochemistry could not be produced in the gas phase by the conventional methods.[1-3] For example, negative ions A^- are obtained by deprotonation of AH in the gas phase but this method requires that the AH compounds be sufficiently volatile. Multiply charged ion-ligand L complexes such as $M^{2+}L_n$ and $A^{2-}L_n$ are also very difficult, if not impossible, to produce in the gas phase by conventional methods.

---

* A version of this chapter has been published: Blades, A.T.; Klassen, J.S.; Kebarle, P. *J. Am. Chem. Soc.* **1995**, *117*, 10563.

Electrospray mass spectrometry (ESMS) developed by John Fenn and coworkers[4] is a method with which electrolyte ions present in solution can be transferred to the gas phase.[5] With ES it is possible to obtain gas phase singly or multiply charged ion-ligand complexes,[6] multiply protonated peptides and proteins,[7] doubly charged anions[8] such as SO_4^{2-} and HPO_4^{2-} and multiply deprotonated nucleic acids.[9] While the major impact of ESMS is in bioanalytical mass spectrometry, the method can be also of great value for physicochemical measurements.

Recently, we described[10,11] an ion source-reaction chamber with which ion-molecule equilibria involving ES produced ions can be determined. The first experiments[10,11], discussed in Chapter 2, involved positive ions. The present work provides data from our first equilibrium determinations involving negative ions.

Free energy values, $\Delta G^{\circ}_{n-1,n}$, for the hydration equilibria, eq. 3.1, involving some 40 singly charged anions A^-, and 15 doubly charged anions A^{2-} were obtained in the present work. The acids from which the anions formally derive are oxo acids of carbon, nitrogen, phosphorus, sulfur, chlorine, and iodine. In spite of the great variety of anions, a systemization and rationalization of the results can be achieved for both the singly and doubly charged anions, as will be shown in the Discussion.

Experimental

A detailed account of the apparatus and method was given elsewhere.[11] Here we provide only a brief description of the essential features. The electrospray generator and the ion source-reaction chamber are shown in Figure 3.1. The solution consisting of methanol solvent and 10^{-4} mol/liter of the sodium or potassium salt; MA or M_2A, of a

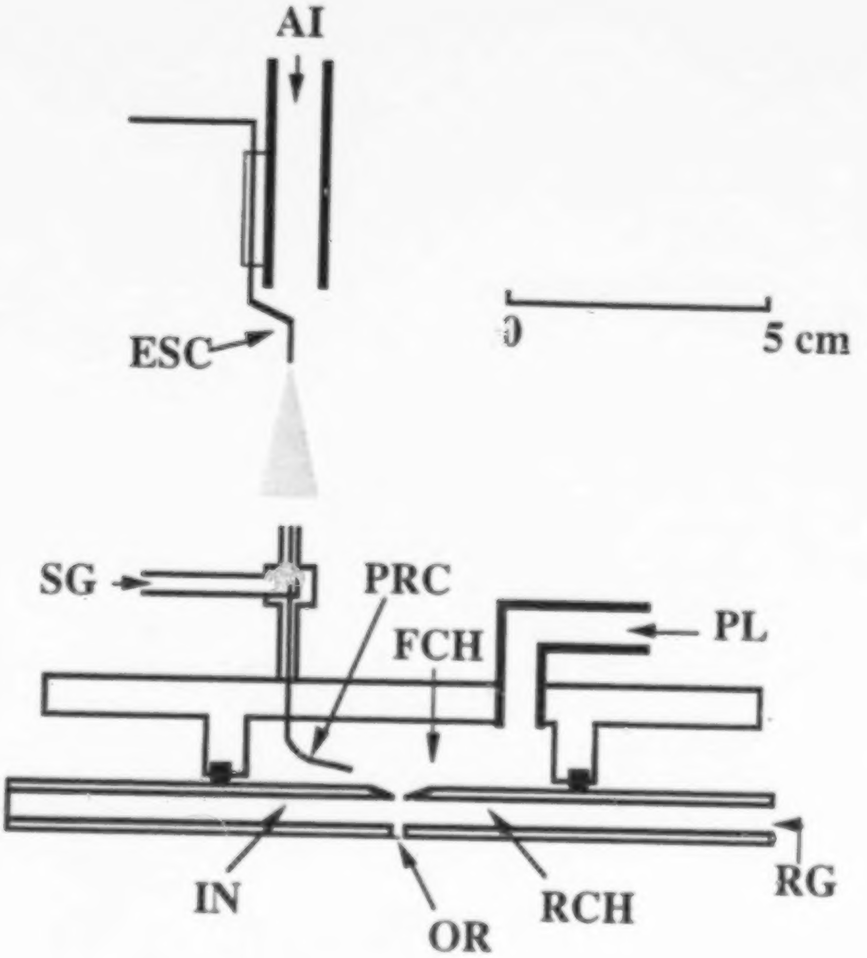

Figure 3.1 Electrospray Generator and Ion Source: ESC, electrospray capillary (4 kV). AI, pipe providing dry air at ~60 L/min. PRC, Pressure reduction capillary (165 V) sucks in gas and ions from electrospray and transfers it to forechamber FCH (165 V). FCH is maintained at 10 Torr by pumping lead PL. IN, interface plate (110 V) separates FCH from reaction chamber, RCH. Reagent gas mixture, RG, flows through reaction chamber and into FCH. Bottom plate of RCH carries an orifice, OR, of 100 µm diameter (100 V) leading to vacuum of mass spectrometer. Ions deflected by electric field out of jet leaving capillary PRC, drift to reaction chamber where ion-molecule equilibria establish. Flow of source gas, SG, 2 L/min of the same composition as the reagent gas, brings composition of gas entering PRC close to that of the reagent gas. Metal tube carrying SG is at at 700 V. All potentials in volts for operation with positive ions.The approximate shape of the plume that exits the electrospray capillary, ESC, is indicated with small dots. This plume consists of small charged droplets, solvent vapor and gas phase ions generated from the droplets. The dotted plume at the exit of the pressure reduction capillary indicates the jet, consisting predominantly of source gas, SG, and gas phase ions. The gas phase ions are deflected out of the jet towards the bottom of the forechamber, FCH, by the applied electric field.

monobasic or dibasic anion is passed in slow flow, ~2 μL/min, through the electrospray capillary, ESC. The tip of the ESC, 0.7 mm o.d., 0.4 mm i.d., is of stainless steel and is at a high negative potential. A fine spray of small droplets, which are negatively charged due to an excess of negative electrolyte ions in them, is emitted from the capillary tip into the ambient air. Solvent evaporation from the droplets leads to droplet shrinkage and an increase of the charge to surface area ratio of the droplets. This destabilizes the droplets and leads to droplet fissions. Repeated fissions ultimately lead to gas phase ions.[5]

The spray containing the ions is sucked into the forechamber of the ion source, FCH, via the pressure reducing capillary, PRC. The forechamber, FCH, and the reaction chamber, RCH, are maintained at 10 torr by outflow through pumping lead, PL. A gas jet containing the ions escapes from the capillary PRC. The ions are deflected out of the jet by an electric field applied between the forechamber, FCH, and the top plate, IN, of the reaction chamber, RCH. Some of the deflected ions drift into RCH through a 4 mm diameter orifice in IN. A reagent gas mixture consisting of 10 torr N_2 bath gas and vapor L = H_2O at a known partial pressure, generally between 1-70 m torr, flows slowly through RCH, enters FCH, and is pumped out. The ions entering RCH are drifted across RCH towards the sampling orifice OR (100 μm) by a very weak electric field. The drift velocities are very low and the internal energy of the ions remains thermal.[11] The ions react with the water molecules and reach equilibrium within their residence time of ~100 μs in RCH.[11] Ions escaping through the orifice OR into the vacuum are detected with a quadrupole mass spectrometer.

Typical electrode potentials used, were: ESC -4.5 kV, SG exit tube -500 V, PRC and top of FCH -42 V, IN -17 V, OR plate -3 V, first electrode in vacuum, not shown in Figure 3.1, -0.5 V.

The equilibrium constants are determined from the mass spectrometrically measured intensities of the ions $A^-(H_2O)_n$ and $A^-(H_2O)_{n-1}$, whose ratio, I_n/I_{n-1}, is taken to be equal to the ion concentration ratio in RCH at equilibrium so that eq. 3.2 can be applied.

$$K_{n-1,n} = \frac{I_n}{I_{n-1}\ P_{H_2O}} \qquad (3.2)$$

Results and Discussion

a. Ion Abundances and $K_{n-1,n}$ Determinations in some Typical Experiments.

A mass spectrum giving the ion abundances at different mass to charge, m/z, ratios is shown in Figure 3.2. It was obtained from electrospray of a 5×10^{-5} mol/L solution of disodium suberate in methanol. The reagent gas used in the reaction chamber was 12 torr N_2 and 5 m torr H_2O. The suberate dianion, $CO_2^-(CH_2)_6CO_2^-$ under these conditions is observed as the $Sub^{2-}(H_2O)_n$ where the n = 3 hydrate is the most abundant. The singly charged Sub^- which is also observed under the same conditions is essentially completely unhydrated. The methyl ester of the carbonic acid anion $MeOCO_2^-$ is often observed in electrospray with methanol as solvent.[8] The $MeOCO_2^-$ is much more strongly hydrated than the singly charged Sub^-. The very different strength of hydration for Sub^{2-}, Sub^- and $MeOCO_2^-$ observed in Figure 3.2 represents

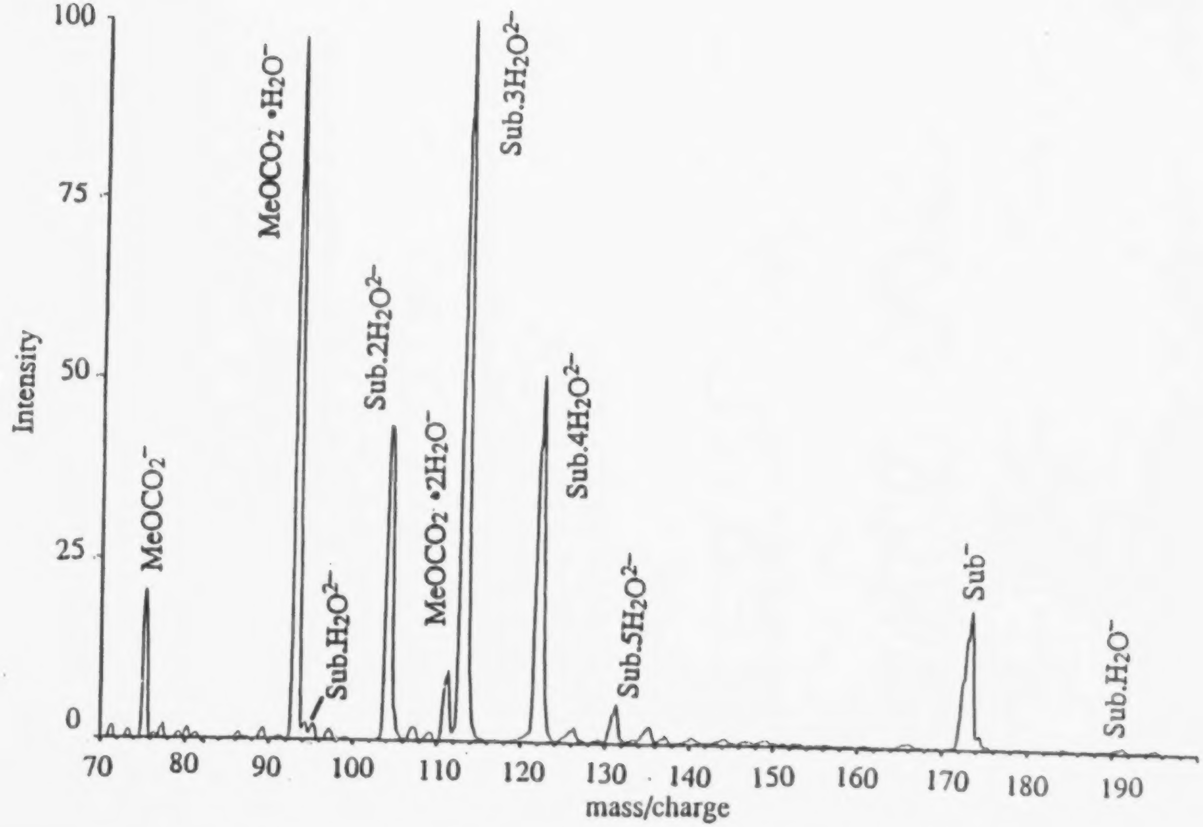

Figure 3.2 Ion intensities observed from a solution of $Na_2CO_2(CH_2)_6CO_2$, disodium suberate. Both the doubly, Sub^{2-}, and singly Sub^- charged ions are observed. A pressure of 7 mTorr in the reaction chamber, RCH, Figure 3.1, leads to the observed hydration of Sub^{2-} and Sub^-. The methoxycarbonate ion $MeOCO_2^-$ is due to a sodium bicarbonate impurity. This singly charged ion is much more strongly hydrated than Sub^-.

three different types of hydration interactions explored via the equilibrium determinations in the present work.

The dependence of the ion hydrate intensities on the partial pressure of H_2O is illustrated in Figure 3.3 for the nitrate ion NO_3^-. These data were obtained from determinations of the hydrate intensities at eight different H_2O partial pressures. The intensities shown in Figure 3.3 were used for the evaluation of the intensity ratio, I_n/I_{n-1}, plots, Figure 3.4. The ion intensities observed in Figure 3.3 are quite high except for the $NO_3^-(H_2O)_3$ ion. For a H_2O pressure of 7 mTorr, this ion had an intensity of only 20 counts/s. Intensities at this and higher levels can be measured quite accurately by time averaging and therefore all three equilibrium constants $K_{0,1}$, $K_{1,2}$ and $K_{2,3}$ could be determined from the data obtained. The total $NO_3^-(H_2O)_n$ ion intensity is also shown in Figure 3.3. Ideally, this intensity should have remained constant. A decrease with H_2O pressure is observed but the decrease is small.

The equilibrium constant plots, on the basis of eq. 3.2, are shown in Figure 3.4. Good linear plots are observed for all three equilibria. In general, good straight line plots going through the origin were observed in all measurements.

b. Hydration of Singly Charged Anions

The hydration free energies $\Delta G^\circ_{n-1,n}$ for singly charged anions A^- are summarized in Table 3.1. Section (a) provides the data for the bicarbonate anion and a variety of carboxylic acids RCO_2^- while section (b) deals with anions of some oxo acids of the N, P, S, Cl, and I atoms. The range of (n-1,n) values provided for a given anion was dependent on the equilibria which could be determined at the experimental temperature

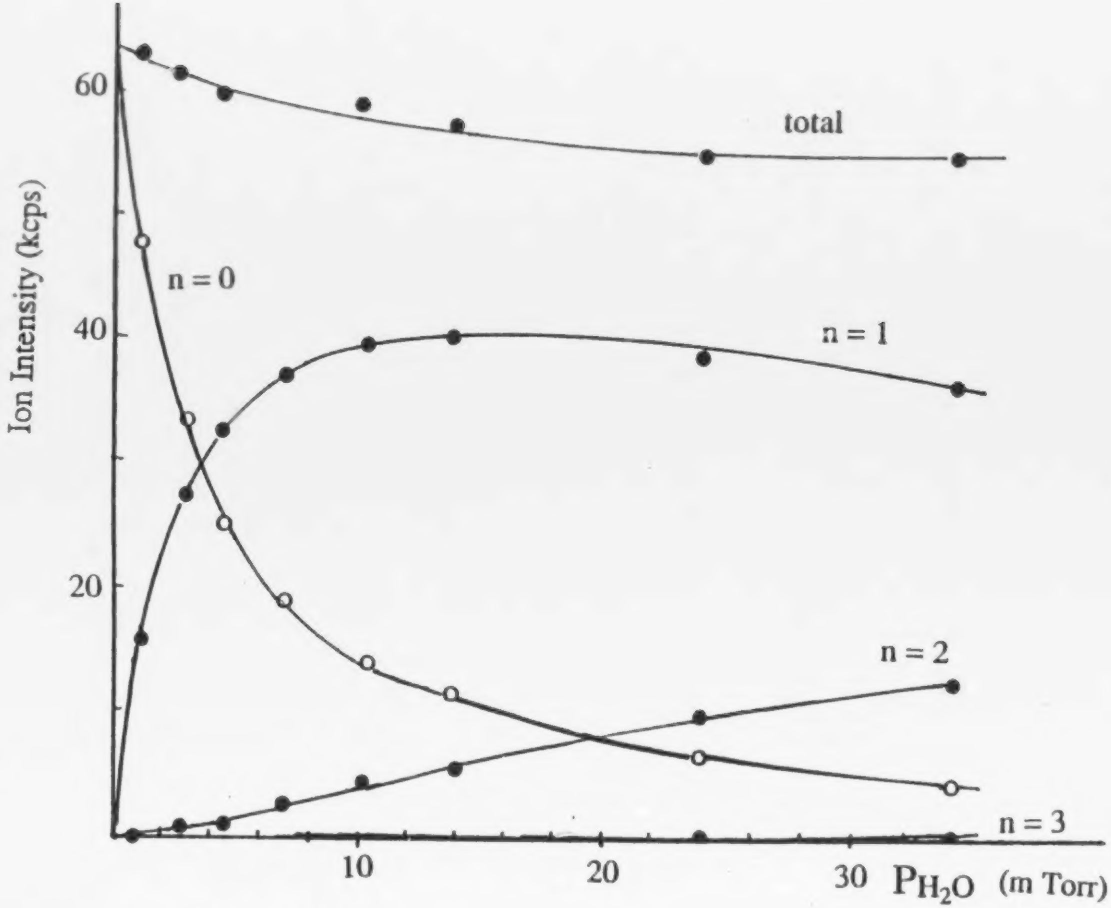

Figure 3.3 Ion intensities for NO_3^- $(H_2O)_n$ ions determined at different constant H_2O pressures in the reaction chamber. Actually observed ion intensities in kilocounts per second (kcps) are given, see vertical axis. The total intensity, which is approximately constant with H_2O pressure, is also given.

Table 3.1. Free Energies of Hydration of Anions A^- and of Acid Dissociation, $AH = A^- + H^+$.

a. Carboxylates, RCO_2^-

ion	$-\Delta G^\circ_{n-1,n}$(kcal/mol) [a]			ΔG°_{ac}(kcal/mol) [b]
n-1, n	0,1	1,2	2,3	
$CH_3CO_2^-$	9.4	6.8	5.2	341.5
	(9.75) [d]			
$C_2H_5CO_2^-$	9.3	6.6	5.1	340.3
HCO_2^-	9.2	6.8	5.1	338.2
$CH_3OCH_2CO_2^-$	8.6	6.1	4.8	-
$HOCO_2^-$	(8.50) [e]	(6.2) [e]	(4.6) [e]	(334.0) [c]
$CH_3OCO_2^-$	8.3	6.1	4.6	(331.8) [c]
$CH_2FCO_2^-$	8.3	5.9	4.6	331.0
$C_6H_5CO_2^-$	8.1	5.7	4.5	331.7
$CH_2ClCO_2^-$	7.7	-	-	328.8
$CH_3CHOHCO_2^-$	7.7	5.3	-	(326.6) [c]
$CHF_2CO_2^-$	7.5	5.3	-	323.5
$CH_2ICO_2^-$	7.2	5.3	4.3	(322.6) [c]
$CH_2CNCO_2^-$	7.1	5.2	-	323.7
$CHCl_2CO_2^-$	6.8	4.9	-	321.9
$CF_3CO_2^-$	6.8	4.7	-	316.3
$CCl_3CO_2^-$	5.8	-	-	(309.6)[c]

b. Anions of some oxo acids of N, P, S, Cl, I.

ion	$-\Delta G^{\circ}_{n-1,n}$(kcal/mol) [a]			ΔG°_{ac}(kcal/mol) [b]
n-1, n	0,1	1,2	2,3	
NO_2^-	~8.5	6.00	4.5	332.3±4.5 [g]
	(8.0-8.4) [f]			
NO_3^-	7.1	5.2	3.9	318.18 [g,h]
	(6.7-7.1) [f]			
$H_2PO_2^-$	8.4	6.4	4.7	-
$(HO)HPO_2^-$	7.8	6.6	5.2	-
$(HO)_2PO_2^-$	7.6	6.1	4.8	-
	(7.5) [m]	(5.8) [m]		
PO_3^-	(6.27) [ℓ]	(4.90) [ℓ]	-	303.8 [k]
	(6.20) [m]	(4.00) [m]	-	
$CH_3SO_3^-$	6.9	5.4	4.4	315.00 [i]
$C_7H_{15}SO_3^-$	6.3	5.0	-	-
$C_6H_5SO_3^-$	5.9	4.4	-	-
$C_2H_5OSO_3^-$	5.8	4.6	-	-
$HOSO_3^-$	5.9	4.7	-	302.6 [k]
	(6.0) [n]			
$CF_3SO_3^-$	4.6	3.8		299 [k], 299.5 [i]
ClO_2^-	9.0	6.1	4.8	-
ClO_3^-	6.2	4.7	-	-
ClO_4^-	4.8	-	-	-
BrO_3^-	6.5	5.0	-	-
IO_3^-	6.4	5.0	4.2	-
IO_4^-	4.3	-	-	-

Footnotes:

(a) Free energy change in kcal/mol, standard state 1 atm. for hydration equilibria (n-1,n): $A^-(H_2O)_{n-1} + H_2O = A^-(H_2O)_n$ at 293° K determination from this laboratory. Literature values in brackets.

(b) Free energy change for reaction: $HA = H^+ + A^-$ in kcal/mol. Standard state 1 atm. 298° K. Unless otherwise indicated values given are from Cunningham and Kebarle[20] or Caldwell, Renneboog, Kebarle.[21]

(c) Estimated acidity value value based on relationship with $\Delta G^\circ_{0,1}$, see Figure 3.5.

(d) Meot-Ner.[12]

(e) Castleman.[13]

(f) Castleman.[3]

(g) Lias.[25]

(h) Fehsenfeld.[14]

(i) Taft.[22]

(k) Viggiano.[23]

(ℓ) Castleman.[15]

(m) Houk.[16]

(n) Fehsenfeld.[17]

$T = 293^\circ$ K and the range of H_2O pressures, ~1 to 70 mTorr, which led to good linear plots, see preceding section and Figures 3.3, 3.4.

Previous determinations in the literature,[3,12-17] mostly of $\Delta G^o_{0,1}$, with which the present results can be compared are available only for a few of the anions ($CH_3CO_2^-$, NO_2^-, NO_3^-, $H_2PO_4^-$, $HOSO_3^-$), see Table 3.1. In general, the present results do not differ by more than 0.3 kcal/mol from the literature results, and this may be considered as very good agreement. The literature data quoted for all anions except $H_2PO_4^-$ are experimental results. The $\Delta G^o_{0,1}$ and $\Delta G^\circ_{1,2}$ given for $H_2PO_4^-$ are based on recent high level ab initio calculations by Houk and coworkers.[16] These authors do not list directly the above values since their calculations were made for a different purpose, however total energies and entropies provided for the reactants of eq. 3.1 allow an evaluation of the free energies quoted in Table 3.1.

The anions listed in Table 3.1 represent a wide range of chemical types and a concise examination of the relationship between the observed energies and the chemical properties of the anions appears challenging. Fortunately this is possible on the basis of a correlation between the hydration energy $\Delta G^o_{0,1}$ and the Arrhenius gas phase basicity of A^-. Previous experimental determinations[18,19] have shown that the bond strength in hydrogen bonded complexes, $XH{-}{-}{-}A^-$, increases with the gas phase acidity of XH and the gas phase basicity of A^-. The special case presented here, where XH = HOH and A^- is changed, was examined earlier[18b] for only a few anions (OH^-, F^-, Cl^-, Br^-, I^-, NO_2^-, NO_3^-) and a fair linear correlation was obtained.

A plot of the present hydration energies $\Delta G^o_{0,1}$ versus the corresponding gas phase acidities of AH is shown in Figure 3.5. The gas

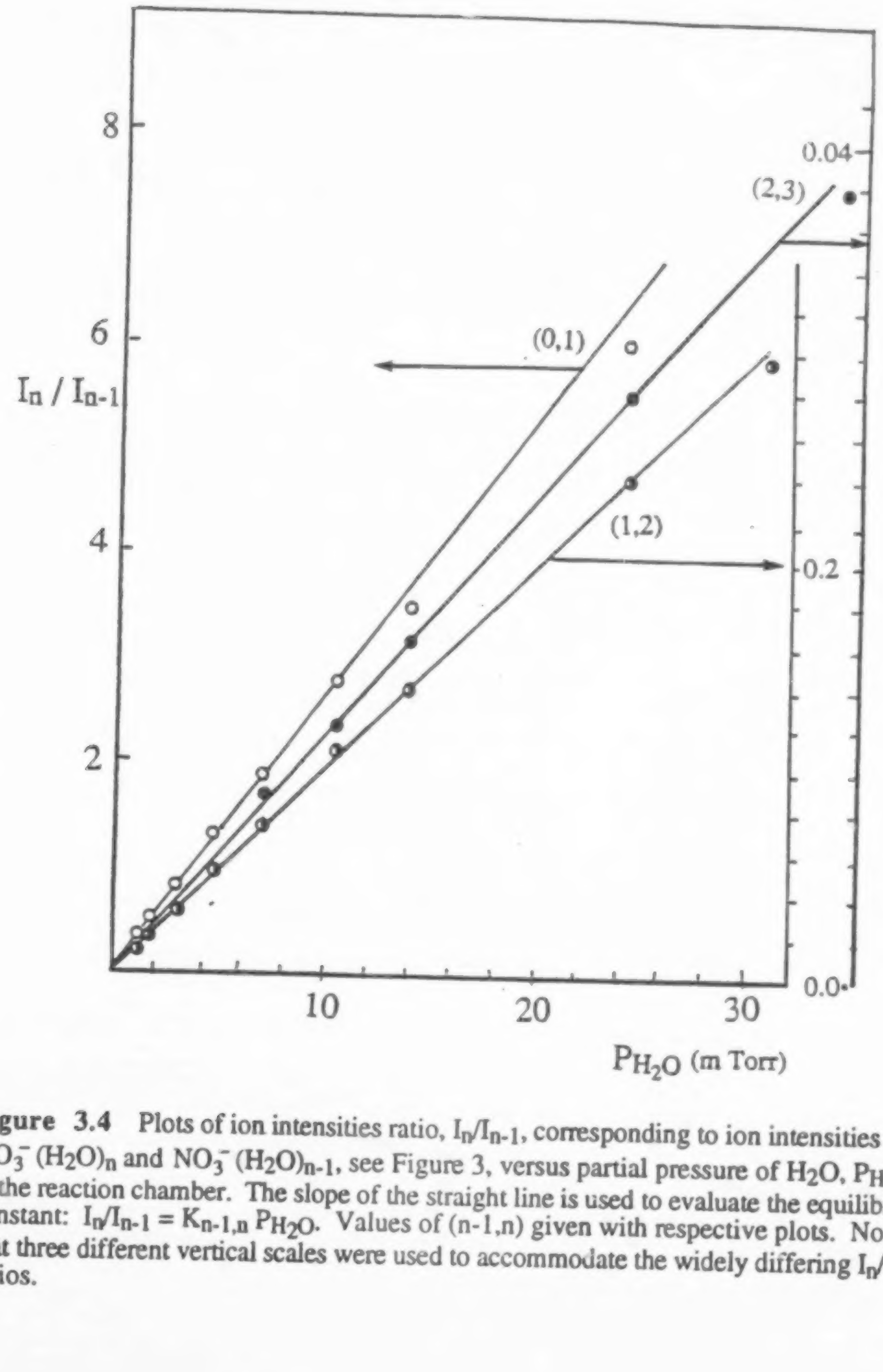

Figure 3.4 Plots of ion intensities ratio, I_n/I_{n-1}, corresponding to ion intensities $NO_3^-(H_2O)_n$ and $NO_3^-(H_2O)_{n-1}$, see Figure 3, versus partial pressure of H_2O, P_{H_2O}, in the reaction chamber. The slope of the straight line is used to evaluate the equilibrium constant: $I_n/I_{n-1} = K_{n-1,n} P_{H_2O}$. Values of (n-1,n) given with respective plots. Note that three different vertical scales were used to accommodate the widely differing I_n/I_{n-1} ratios.

phase acidity, $\Delta G^{\circ}_{ac}(AH)$, is generally defined as the free energy for the gas phase reaction.

$$AH = A^- + H^+ \qquad \Delta G^{\circ}_{ac}(AH) \qquad (3.3)$$

The gas phase acidity of AH corresponds to the gas phase basicity of A^-, $GB(A^-)$. The gas phase acidities of a large number of acids have been determined on the basis of proton transfer equilibrium measurements. The acidity values used for Figure 3.5 and also quoted in Table 3.1 are mostly due to three interconnected acidity scale determinations[20-22] based on equilibrium measurements.

A fair linear relationship is observed in Figure 3.5. The carboxylic acids as a group provide a significantly better fit to the straight line.

A positive correlation between $-\Delta G^{o}_{0,1}(A^-)$ and $\Delta G^{\circ}_{ac}(AH)$ is expected because both energies should decrease as the electronic stabilization of A^- increases. Thus, changes in the anion that introduce electron withdrawing groups, which delocalize the charge and stabilize it, will weaken the hydrogen bond of the anion with HOH ($\Delta G^{o}_{0,1}$) since the bond is largely due to electrostatic forces. Changes in $\Delta G^{\circ}_{ac}(AH)$ can be examined on the basis of the corresponding gas phase acidity enthalpy, $\Delta H^{\circ}_{ac}(AH)$, which can be thermochemically decomposed into three

$$\Delta H^{\circ}_{ac} = D(A\text{-}H) + IP(H) - EA(A) \qquad (3.4)$$

terms, the bond energy, the ionization energy of the hydrogen atom and the electron affinity of A. The acidity is determined by: $IP(H) = 313.6$ kcal/mol, which is constant, the bond energy $\sim D(O\text{-}H) \approx 105$ kcal/mol which is approximately constant[24,25] for oxygen acids, and the electron affinity EA, which undergoes the largest change (~70-120 kcal/mol) for the series represented in Figure 3.5. Charge delocalization in the anion is expected to be the major factor determining the magnitude of the EA values of the oxygen acids.

The observed slope in Figure 3.5 should correspond approximately to

$$d(\Delta G_{0,1}(A^-)) \,/\, d(EA(A)) \approx \text{slope} \;=\; -0.11 \qquad (3.5)$$

In other words, a change in the nature of A which leads to increased stabilization of A^- leads to an increase of the electron affinity EA(A) which is 9 times larger than the corresponding decrease of the hydrogen bond energy, HOH–A^-.

Because of the approximate correlation observed in Figure 3.5, much of the discussion of acidity changes with the nature of AH, which is available in the literature,[20-22] and references therein, applies also to the changes of the hydration free energies observed here.

The relationship in Figure 3.5 observed for the carboxylic acid group is good enough to provide estimates for gas phase acidities that have not been determined so far. These are given in Table 3.1, see values for ΔG°_{ac} which are shown in brackets.

Of special interest are the predicted acidity values for carbonic acid $(HO)_2CO$, and its methyl ester, $(CH_3O)(HO)CO$. The acidities of these compounds cannot be measured by proton transfer equilibria because the acids are unstable in the gas phase. The two acids are predicted to be more acidic than acetic and formic acid. This result is reasonable. One may view the anions $CH_3CO_2^-$ and $HOCO_2^-$ as belonging to the same acid

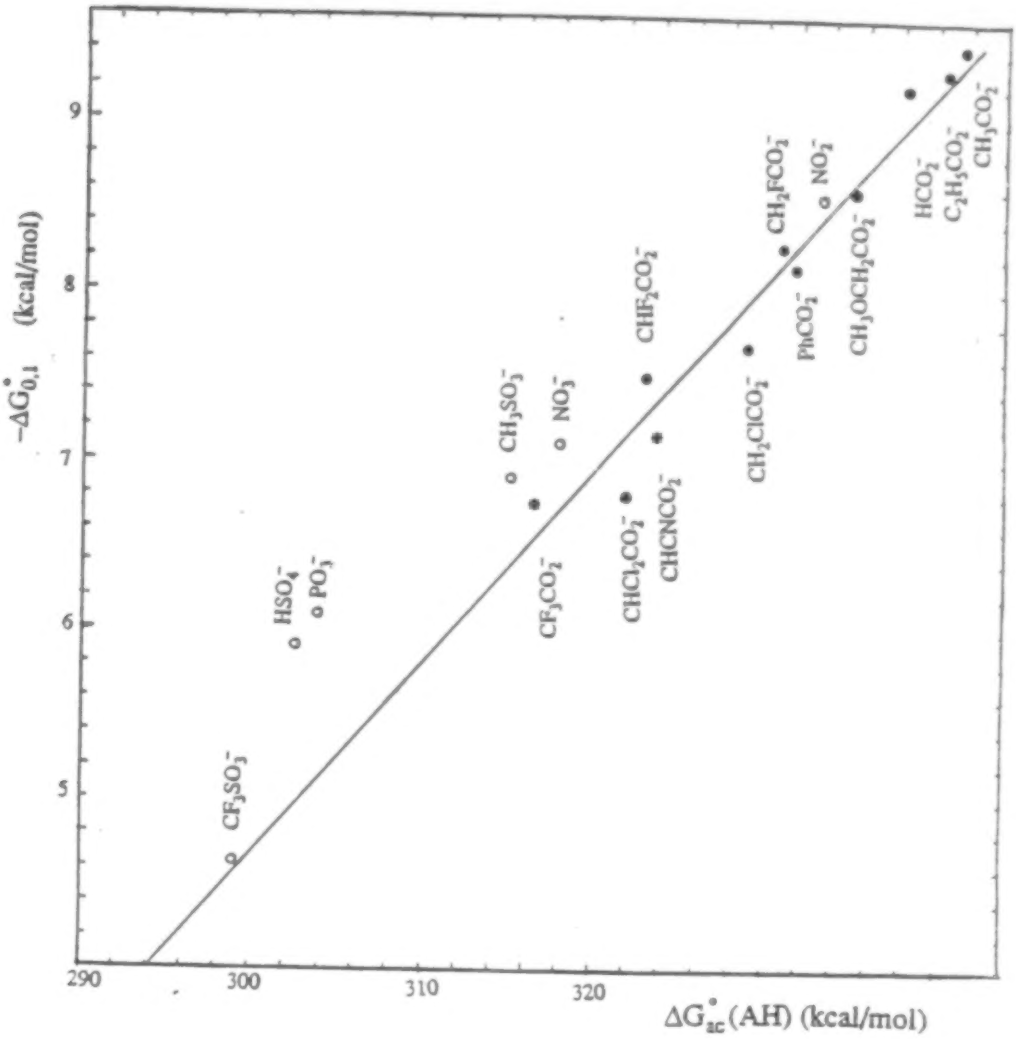

Figure 3.5 Plot of the hydration free energies for A^-, $-\Delta G^\circ_{0,1}$, corresponding to the reaction $A^- + H_2O = A^-(H_2O)$ versus gas phase acidity of AH, ΔG°_{ac} (AH), corresponding to the free energy of the reaction: $HA = H^+ + A^-$. An approximately linear relationship is observed. Carboxylic acids, Table 1a, which are more numerous and essentially define the straight line are shown with filled circles.

group but with two different substituents, CH_3 and OH. One expects the electron withdrawing inductive and field effect of OH to lead to an increased stabilization of the $HOCO_2^-$ anion relative to the $CH_3CO_2^-$ anion. The field and inductive effect of OH directly substituted to the carboxylic group should be big, however this effect is counteracted by the π electron donor ability of OH so that the total acidifying effect is moderate.

Some anions, such as $CHCl_2CO_2^-$, show large deviations from the straight line plot in Figure 3.5. If one assumes that this is due to experimental error in the $\Delta G^o_{0,1}$ determination, a fit to the line would indicate a 0.36 kcal/mol error, while if the error is assigned to the ΔG°_{ac} it would be ~3 kcal/mol. Both errors appear somewhat larger than the expected uncertainty of the determinations. The error in the acidities[20-22] is generally less than 1 kcal/mol while the relative $\Delta G^o_{0,1}$ values error is probably less than 0.3 kcal/mol. At present, it is not clear whether the observed large deviations are due to accidental, larger experimental errors or due to a special intrinsic difference in the energies of acid dissociation and anion hydration.

The trichloroacetate anion has the lowest $-\Delta G^o_{0,1}$ value among the carboxylates shown in Table 3.1. The value is lower by ~ 1 kcal/mol than the result for trifluoroacetate and this indicates that trichloroacetic acid is considerably more acidic than the trifluoro compound. Previous acidity determinations for the di and monosubstituted acids[20,21] also have shown that the chlorosubstituted acids have higher gas phase acidities than the fluoro substituted analogues.

The correlation between acidities and hydration energies, Figure 3.5, is less good when oxo anions other than the carboxy anions are included.

One might consider that this could be due to significantly different structures of the anion hydrates for the oxoanions of C, N, P, S etc. However, theoretical calculations for the *mono* hydrates of HCO_2^-,[26] NO_3^-,[27] (PO_3^-),[16,28] and $(H_2PO_4^-)$[16] predict the same doubly hydrogen-bonded structure. The structure is illustrated below for $NO_3^-H_2O$, based on Schaefer's[27] calculations, see structure **1**. The singly hydrogen-bonded structure, **2**, is less stable by ~2.2 kcal/mol.[27] Similar stability differences between the structures **1** and **2** are present for the other anions,[16,26-28] and this means that differences of the H bonded structures are not likely to be responsible for relative scatter in the correlation, Figure 3.5. However, more subtle differences may be present. In a discussion of the bonding of H_2O to (PO_3^-), Schaefer *et al*[28] point out that changes in the bond distances of (PO_3^-), namely a shortening

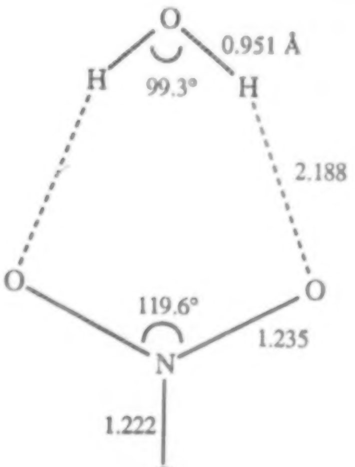

1

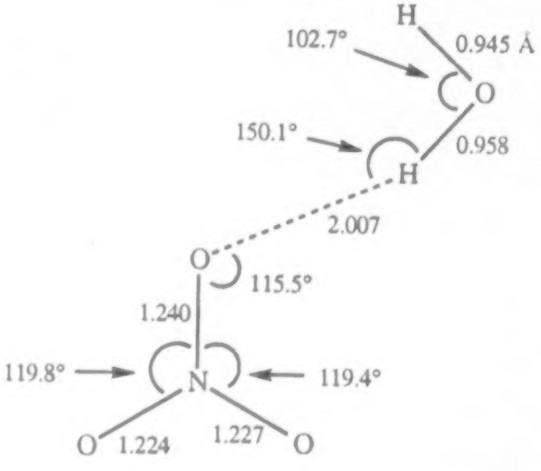

2

of the P–O bond not participating in the hydrogen bonding by ~0.008 Å on hydrate formation, structure **1**, relative to the bond length in the free

(PO_3^-) and a lengthening of the two P–O bonds by 0.003 Å, indicates an increased contribution of the Lewis-type structure **3** in the hydrate relative to that in the free (PO_3^-). Electronic charge redistributions of this type favouring the doubly hydrogen-bonded structure, **3**, can occur to different degrees for the NO_3^-, (PO_3^-), $(H_2PO_4^-)$ and RSO_4^- anions but not for the carboxylic acids which have only two oxygens. It is possible that such electronic differences are responsible for deviations from the correlation in Figure 3.5 where the nitrate, phosphate and sulfate hydration energies are seen generally to be relatively larger than predicted by the straight line correlation which is based mostly on the carboxylic acids.

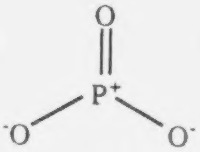

3

The importance of the above argument is obscured somewhat when the comparison is made at a free energy, ΔG°, level. Normal frequencies evaluated for $NO_3^-H_2O$, structures **1** and **2** are available[27] and the entropy difference between the two structures can be evaluated. The looser structure **2** has a more favorable entropy and when the TΔS° term is included, one finds that the $\Delta G^o_{0,1}$ values for the formation of the two structures are essentially the same. Thus, even at room temperature a multiplicity of structures contribute to the stability of the hydrates and the situation becomes less tractable.

A comparison of the $-\Delta G^o_{0,1}$ for the sulfonates, Table 3.1b, with that for the carboxylates Table 3.1a, shows that the substituent effects are quite similar. The carboxylate energies decrease in the substituent order $CH_3 < C_2H_5 < CH_3O < C_6H_5 \ll CF_3$ while for the sulfonates one observes $CH_3 < C_2H_5 < C_2H_5O \approx C_6H_5 \ll CF_3$. The relative changes for the sulfonates are somewhat smaller corresponding to the smaller absolute magnitude of the $-\Delta G^o_{0,1}$ values for these ions.

An examination of the data for all oxo anions in Table 3.1a,b reveals that the factors leading to stabilization of the oxo- anions and to a decrease of $-\Delta G^o_{0,1}$ and also presumably ΔG°_{ac}, can be expressed by a few simple rules: (a) the number of equivalent oxygens over which the negative charge is localized, (b) the presence of electron withdrawing substituents, (c) the nature and particularly the size of the central atom. The rules will be illustrated by a few examples.

The oxo anions of phosphorus show the following hydration energies (kcal/mol):

$-\Delta G^o_{0,1}$: 8.4 7.9 7.6 6.2

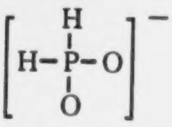

$\left[\mathrm{H{-}\overset{H}{\underset{O}{P}}{-}O}\right]^-$

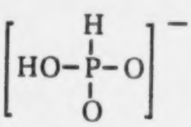

$\left[\mathrm{HO{-}\overset{H}{\underset{O}{P}}{-}O}\right]^-$

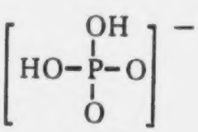

$\left[\mathrm{HO{-}\overset{OH}{\underset{O}{P}}{-}O}\right]^-$

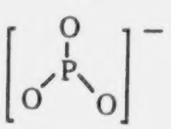

The most stabilized anion is (PO_3^-) which has three equivalent charge delocalizing oxygens. The other three anions have only two such oxygens. The stability differences for these three anions are due to the electron withdrawing substituent effect of the OH group. The stability increases as the number of OH substituents increases from zero to two.

The rule concerning the number of equivalent charge carrying oxygens is followed also by the three groups: NO_2^-, NO_3^-; ClO_2^-, ClO_3^-, ClO_4^- and IO_3^-, IO_4^-, see Table 3.1a,b.

When comparing anions with equal number of equivalent charge bearing oxygens and similar substituents but different central atoms such as, $C \lessdot N < P \lessdot S \lessdot Cl < I$, one finds that the stability of the anion increases in the above order which is not an order of changing electronegativity but an order of increasing size. Most clear cut examples of this effect are the observed increases of $-\Delta G^{o}_{0,1}$ in the order: $NO_3^- <$ (PO_3^-) and $ClO_4^- < IO_4^-$. On the basis of Table 3.1a,b and the relationship Figure 3.5, one expects HIO_4 to be the strongest gas phase acid of all oxo acids whose anions were studied in the present work.

The role of the central atom and its electronic structure could be far more complex. The simple correlation with the size of the atom is a consequence of the dominance of electrostatic effects for the gas phase anions. Large central atoms put the charge bearing oxygens at largest distances from each other. Large atoms are also more polarizable and this could lead to additional stabilization.

c. Hydration of Singly Charged Anions of Dicarboxylic Acids

The hydration free energies for singly charged anions of dicarboxylic acids are summarized in Table 3.2. Two classes of compounds were examined, the alkanedioic acids, $HOCO\text{-}(CH_2)_k\text{-}COOH$, and the unsaturated systems; 1,2- and 1,4-benzenedicarboxylic acids, and *cis* and *trans* butenedioic acids.

The hydration free energies for the singly charged dicarboxylates with longer alkane links $(CH_2)_k$ where $k \geqslant 3$, are found to be quite similar, $-\Delta G^{o}_{0,1} \approx 5.3 \pm 0.3$. This value is much lower than the hydration energies of alkylcarboxylates such as propionic acid ($-\Delta G^{o}_{0,1} = 9.3$ kcal/mol) Table 3.1a. The low values for the dicarboxylates are due to the

Table 3.2. Hydration Free Energies of Singly Charged Anions of Dicarboxylic Acids [a].

ion	$-\Delta G^{\circ}_{0,1}$	$-\Delta G^{\circ}_{1,2}$
$CO_2HCO_2^-$	6.3	-
$CO_2HCH_2CO_2^-$	5.3	4.0
$CO_2H(CH_2)_2CO_2^-$	5.4	~4.0
$CH_3OCO(CH_2)_2CO_2^-$	8.4	6.1
$CO_2H(CH_2)_3CO_2^-$	5.5	~4.2
$CO_2H(CH_2)_4CO_2^-$	5.7	4.4
$CO_2H(CH_2)_5CO_2^-$	5.5	-
$CO_2H(CH_2)_6CO_2^-$	5.4	-
$CO_2H(CH_2)_7CO_2^-$	5.3	-
$CO_2H(CH_2)_8CO_2^-$	5.0	-
1,2 $CO_2HC_6H_4CO_2^-$	4.7	-
1,4 $CO_2HC_6H_4CO_2^-$	7.4	-
cis-$CO_2HC_2H_2CO_2^-$	5.0	-
trans-$CO_2C_2H_2CO_2^-$	7.3	5.2

a. All values in kcal/mol. Standard state 1 atmosphere, 293° K.

formation of an internal strong hydrogen bond by cyclization of the anion as illustrated below. The hydrogen bond stabilizes the anion and reduces the hydration exothermicity. Cyclization with formation of an internal strong hydrogen bond has been shown to occur[29,30] for other bifunctional systems such as the protonated alkane diamines $H_2N-(CH_2)_kNH_3^+$. The evidence was based on the observations[29,30] that on protonation these systems led to high exothermicities (high $-\Delta H^\circ$ values) and considerable losses of entropy (high $-\Delta S$ values) which were consistent with bond formation and loss of freedom due to the cyclization. It was found[29] that the rings became strained for $NH_2(CH_2)_kNH_3^+$, with $k < 3$. Thus the cyclization exoergicity, $-\Delta G^\circ_{cyc}$, for $NH_2CH_2CH_2NH_3^+$ was found to be only ~4 kcal/mol while that for the higher analogues, up to k = 6, was ~12 kcal/mol.[29,30] The hydration of the cyclized diamines has also been studied[11,30] and the exothermicity was found to be low, as expected for an internally hydrogen bonded system.

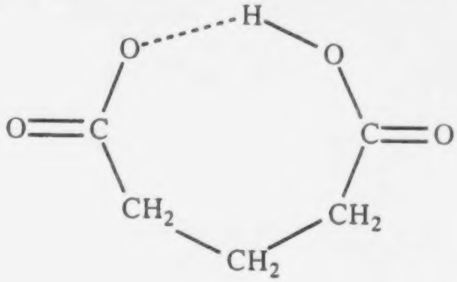

A comparison of the $\Delta G^o_{0,1}$ values for the hydration of the alkane dicarboxylates and the previous results for the diamines from this laboratory[11] is shown in Figure 3.6. The cyclized dicarboxy compound forms a ring that contains two more chain participating atoms, than the diamine with the same number of CH_2 groups. Therefore, the hydration energies for the diamines with k CH_2 groups were plotted at the same x

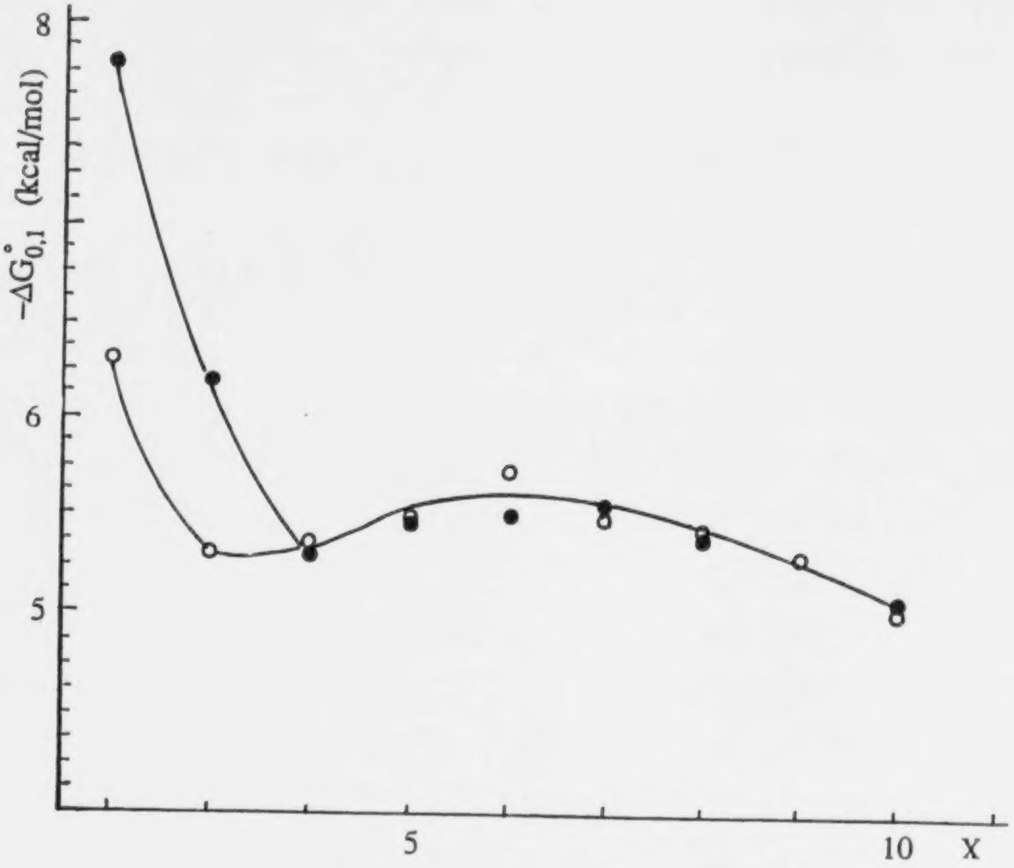

Figure 3.6 Plot of hydration free energies, $\Delta G^{\circ}_{0,1}$, for the dicarboxylates, $CO_2H(CH_2)_kCO_2^-$, ○, also shown are $\Delta G^{\circ}_{0,1}$ for protonated diamines, $NH_2(CH_2)_kNH_3^+$, ●. Both types of compounds have low $-\Delta G^{\circ}_{0,1}$ values which are due to stabilization of the anions by an internal hydrogen bond which leads to cyclization. The horizontal scale x has been adjusted, x = k (amines); x = k + 2 (carboxylates) in order to compare cyclic structure with equal number of atoms in ring. Large increases of $-\Delta G^{\circ}_{0,1}$ for the $x \leqslant 3$ are due to ring strain which reduces the stabilization of the anion.

value on the horizontal axis as the hydration energies of the dicarboxylates with k-2 CH_2 groups. See below comparison of structures for x = 2. A close correspondence between the two plots is observed for the fairly flat

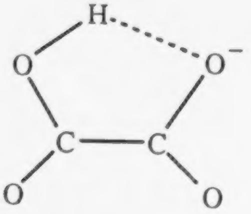

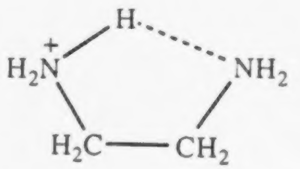

region above x = 3, while a sharp increase occurs below x = 3. This increase reflects the decreased stabilization of the anion because of weakening of the internal hydrogen bond due to strain in the ring.

The increase observed for the diamine system is considerably larger. Thus $-\Delta G^o_{0,1} = 7.8$ kcal/mol for the protonated diamino ethane and only 6.3 kcal/mol for the oxalate ion. This difference probably reflects a larger weakening of the internal hydrogen bond of the diamine relative to the oxalate ion. However also important is the expected low hydration energy of the oxalate ion due to: (a) a larger charge delocalization on the anionic carboxylic group (CO_2^-) relative to NH_3^+ and (b) the stabilizing electron withdrawing substituent effect of the neighboring COOH group at the oxalate anion, see structures above. A measure for the significance of factor (a) can be obtained by the difference between the hydration energies for $CH_3NH_3^+$ ($-\Delta G^o_{0,1} \approx 11$ kcal/mol)[3] and HCO_2^- ($-\Delta G^o_{0,1} \approx 9$ kcal/mol, Table 3.1a). The stabilizing substituent effect of the COOH group in the oxalate anion is indicated by the observed difference between the hydration energies, Table 3.1a, between the acetate ($-\Delta G^o_{0,1} = 9.4$ kcal/mol) and the cyanoacetate anion ($-\Delta G^o_{0,1} = 7.1$ kcal/mol). The electron withdrawing effects of CN and CO_2H are known to be of similar magnitude.[22b]

The flat region of the plot for x > 3 shows a low broad maximum centred at x = 6. This is observed for both the amino and carboxy systems. The height of the maximum is small and within experimental error, but the feature is probably not an experimental artifact.

The four unsaturated dicarboxylic acids, *cis* and *trans* $HCO_2C_2H_2CO_2H$ and 1,2 and 1,4 $HCO_2C_6H_4CO_2H$, lead to anions whose structures are much more rigid than those of the alkane dicarboxylates. This makes their free energies of hydration of special interest. The $-\Delta G^{o}_{0,1}$ for the *cis* and *trans* dicarboxyethylene are given below.

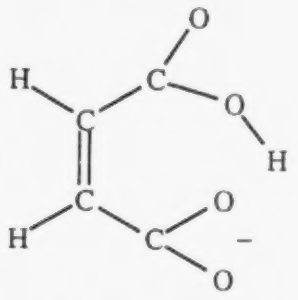

$-\Delta G^{o}_{0,1} = 5.0$ kcal/mol

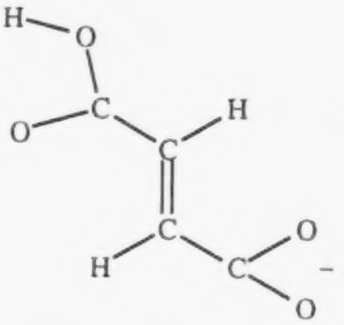

$-\Delta G^{o}_{0,1} = 7.3$ kcal/mol

The energy value for the trans isomer is similar to values observed for anions stabilized by electron withdrawing substituents, see for example difluoroacetate (7.5 kcal/mol). The trans anion is stabilized by both the vinyl group[32] and the COOH substituent. The much lower value for the *cis* isomer indicates additional stabilization of the anion by internal hydrogen bond formation. Space filling models of the maleate anion indicate that the carboxylic groups are very crowded. The anion is not planar because the carboxylic groups have rotated around the C-C bonds to release strain. The internal H bond in this ion is probably more strained than the bond in the much less rigid $CO_2H(CH_2)_2CO_2^-$ anion.

The hydration free energies for the 1,4 and 1,2 benzene dicarboxylates, Table 3.2, are similar to those discussed above and the effects for these compounds are also expected to be similar. These data provide a confirmation for the consistency of the experimental results.

d. Hydration Energies of Doubly Charged Anions

The hydration energies of doubly charged anions determined in this work are given in Table 3.3. The values obtained are also shown in Figure 3.7, where the $\Delta G^{\circ}_{n-1,n}$ are plotted versus n. The data are based on those equilibrium constants $K_{n-1,n}$ which could be determined at room temperature when the H_2O partial pressure was in the range 1 to ~50 mTorr. For very strongly hydrating species only the higher n-1,n equilibria were observed, while the determinations for a more weakly hydrating species could be obtained at lower n-1,n including (0,1) for the weakest hydrating species. Examination of the plots for the individual anions from left to right, *i.e.* from low to high n reveals at a glance the order of increasing hydration strength: 1,5-naphthalene disulfonate, tetrathionate $O_3S\text{-}S\text{-}S\text{-}SO_3^{2-}$, persulfate, $O_3S\text{-}O\text{-}OSO_3^{2-}$, 1,2-ethane disulfonate $SO_3CH_2CH_2SO_3^{2-}$, alkane dicarboxylates $CO_2(CH_2)_kCO_2^{2-}$ k = 4 to k = 8, dithionate, $O_3S\text{-}SO_3^{2-}$, thiosulfate $SO_3\text{-}S^{2-}$, selenate SeO_4^{2-}, sulfate SO_4^{2-}-.

The slope for each plot shows an increase as n is decreased. The values of n at which rapid increases of the slope occur, follow the same order as above. Thus, the rapid increase occurs at n ≈ 1 for 1,5-naphthalene disulphonate and at n ≈ 6 for the sulfate anion.

Table 3.3 Hydration free energies of doubly charged anions [a].

a. Doubly charged ions of dicarboxylic acids.

ion	$-\Delta G^\circ_{2,3}$	$-\Delta G^\circ_{3,4}$	$-\Delta G^\circ_{4,5}$	$-\Delta G^\circ_{5,6}$
$CO_2(CH_2)_4CO_2^{2-}$	8.4	7.5	6.4	5.8
$CO_2(CH_2)_5CO_2^{2-}$	8.0	7.2	6.2	5.5
$CO_2(CH_2)_6CO_2^{2-}$	7.8	7.1	6.1	5.5
$CO_2(CH_2)_7CO_2^{2-}$	7.6	6.9	5.9	5.2
$CO_2(CH_2)_8CO_2^{2-}$	7.4	6.7	5.8	5.1
1,4 $CO_2C_6H_4CO_2^{2-}$	8.4	7.3	6.3	5.9

b. Doubly charged anions of some oxo acids of sulphur and selenium.

ion	(n-1,n) and $-\Delta G^\circ_{n-1,n}$ (kcal/mol)											
Sulfate SO_4^{2-}	(5,6)	8.5	(6,7)	7.5	(7,8)	6.7	(8,9)	6.0	(9,10)	5.5	(10,11)	5.0
Selenate SeO_4^{2-}	(5,6)	8.0	(6,7)	7.0	(7,8)	6.3	(8,9)	5.6				
Thiosulphate $S_2O_3^{2-}$	(4,5)	8.3	(5,6)	7.3	(6,7)	6.5	(7,8)	5.9	(8,9)	5.3	(9,10)	4.7
Dithionate $O_3SSO_3^{2-}$	(2,3)	9.4	(3,4)	8.0	(4,5)	7.1	(5,6)	6.3	(6,7)	5.6	(7,8)	5.1
Ethane disulfonate $SO_3C_2H_4SO_3^{2-}$	(1,2)	8.7	(2,3)	7.5	(3,4)	6.6	(4,5)	597	(5,6)	5.3		
Persulfate $O_3SOOSO_3^{2-}$	(1,2)	8.5	(2,3)	7.5	(3,4)	6.7	(4,5)	5.9	(5,6)	5.4		
Tetrathionate $O_3SSSSO_3^{2-}$	(0,1)	9.1	(1,2)	7.8	(2,3)	6.7	(3,4)	6.1	(4,5)	5.4		
1,5 naphthalene disulfonate	(0,1)	7.8	(1,2)	7.0	(2,3)	6.3	(3,4)	5.5				

(a) All values in kcal/mol. Standard state 1 atm, 293° K.

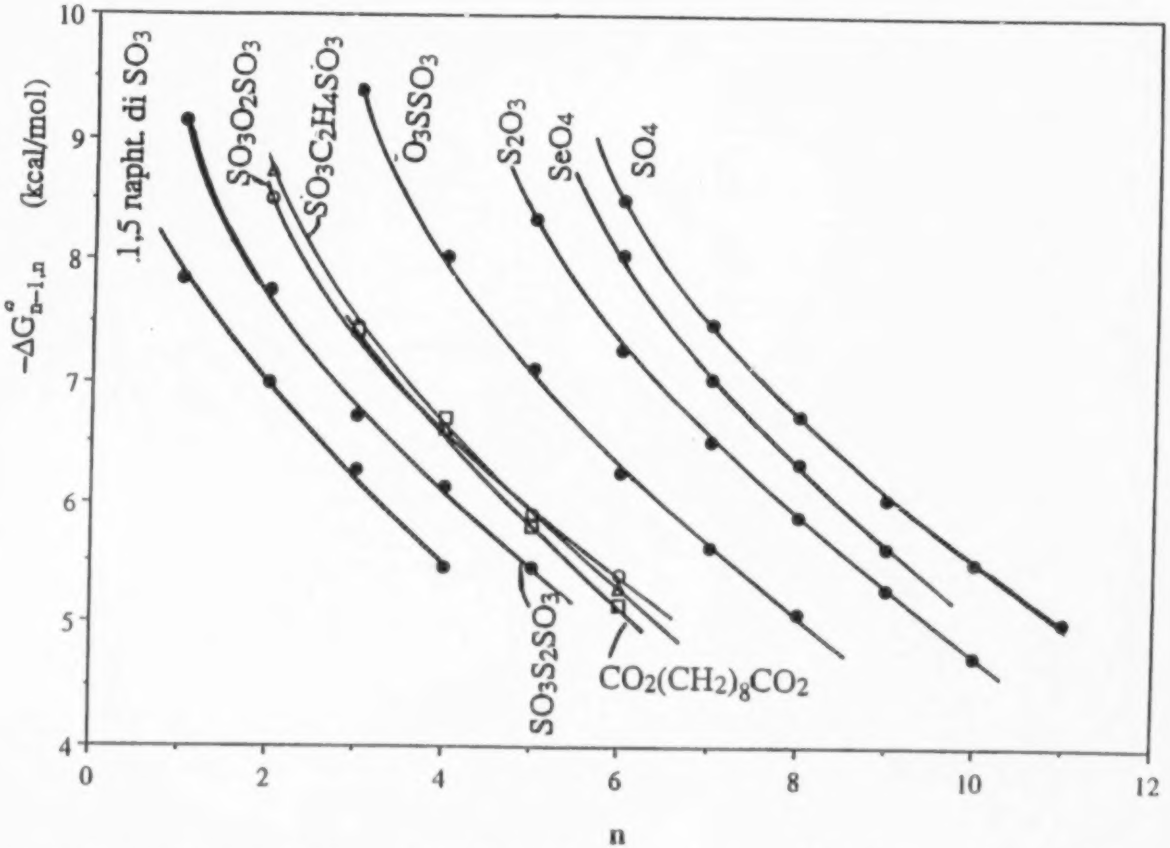

Figure 3.7 Hydration free energies $\Delta G^{\circ}_{n-1,n}$ for several doubly charged anions. Hydration exothermicity increases in the order: 1,5 di SO_3 naphthalene^{2-}, $SO_3S_2SO_3^{2-}$, $SO_3O_2SO_3^{2-}$, $SO_3C_2H_4SO_3^{2-}$, $CO_2(CH_2)_8CO_2^{2-}$, $SO_3SO_3^{2-}$, $S_2O_3^{2-}$ (thiosulfate), SeO_4^{2-}, SO_4^{2-}. These results reflect the stabilization on the anions with increasing distance between the two charged groups.

The order observed in the plots is easily rationalized. First we shall consider the cases where two functional groups are present leading to two distinct charge centres. The doubly charged anions like SeO_4^{2-}, $S_2O_3^{2-}$ (thiosulfate) and SO_4^{2-} could then be considered as special cases where the distance between the two charge centres is very small. Two major factors determine the observed order of hydration energies: (a) The distance between the two charged groups. This most important factor is a consequence of the intense coulombic repulsion between the two charges which is present in the gas phase. (b) The charge delocalization within the functional group, *i.e.* $-SO_3^- > -CO_2^-$. The order of stabilization by charge delocalization was examined in the preceding section dealing with monobasic group anions. It was established that the stabilization increases with the number of equivalent oxygens over which the charge is delocalized and with the size of the central atom. A large central atom leads to stabilization because it increases the distance between the negative oxygens.

Examples illustrating (a) and (b) will be given: (a) The importance of distance between the charges is most clearly demonstrated by the observed increase of hydration exothermicities of the dicarboxylates $CO_2(CH_2)_kCO_2^{2-}$ with decreasing k. This series will be examined later in greater detail. However the increase in the order: $SO_3S_2SO_3^{2-}$, $SO_3O_2SO_3^{2-}$, $SO_3CH_2CH_2SO_3^{2-}$, $O_3S\text{-}SO_3^{2-}$ is also mainly determined by the decreasing distance between the two charged $-SO_3^-$ groups.

(b) The effect of the nature of the charge delocalization within each functional group is well illustrated by the observed substantial increase of hydration energy from $SO_3CH_2CH_2SO_3^{2-}$ to $CO_2CH_2CH_2CO_2^{2-}$. The results in Figure 3.7 show that the hydration energies of the dicarboxylates become the same as that for the ethane disulfonate only after the carboxylate chain increases to k = 8, an impressive difference.

A third factor due to the stabilizing effect of charge delocalization from the functional group to the moiety connecting the two groups might be expected also. Different moieties connecting two charged groups separated by the same distance could be expected to lead to differing hydration energies due to the differential stabilization that might be provided by these moieties.

Clear cut evidence for such an effect does seem to be available in the present results. This can be shown by considering one example: a comparison of the hydration of: $1,4\text{-}CO_2C_6H_4CO_2^{2-}$ ($-\Delta G^{\circ}_{2,3} = 8.4$ kcal/mol) and $CO_2(CH_2)_4CO_2^{2-}$ ($-\Delta G^{\circ}_{2,3} = 8.4$ kcal/mol) whose structures are shown below.

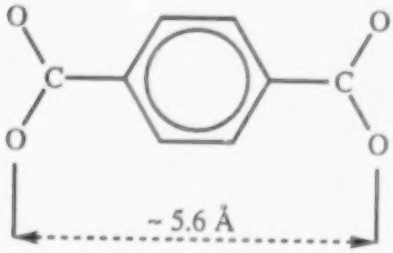

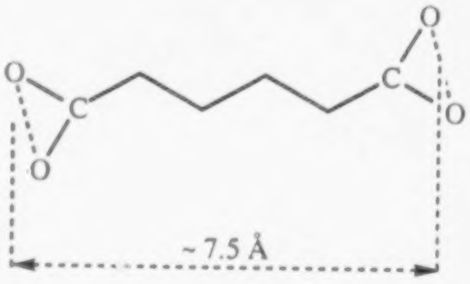

Also shown are the estimated (33) distances between the two charge centres. An estimate of the increase of $-\Delta G^{\circ}_{2,3}$ for a hypothetical alkanedioate dianion with a charge separation equal to that of the benzenedicarboxylate dianion, 5.6 A, can be obtained from an extrapolation of the $-\Delta G^{\circ}_{2,3}$ data for these acids as a function of k and thus the separation (34). The estimated increase is 0.8 kcal/mol., giving a $-\Delta G^{\circ}_{2,3} = 8.4 + 0.8 = 9.2$ kcal/mol. The 0.8 kcal/mol between this value and the 8.4 kcal/mol for 1,4-benzenedicarboxylate dianion is attributed to a larger stabilization of this anion relative to the alkanedioate of the same charge separation due to the delocalization and polarization of the electrons in the aryl moiety. Although this dianion has two distinct charge centres, the charges are not totally isolated. Hydration of one charge centre causes a redistribution of the π electrons resulting in a partial stabilization of the second charge centre. The $-\Delta G^{o}_{0,1}$ value would be a more sensitive probe of this stabilization and these values will be available when equilibrium measurements are extended to higher temperatures.

The plots of the $\Delta G^{\circ}_{n-1,n}$ values in Figure 3.7 are fitted to smooth curves. Actually, discontinuous changes of the values as a function of n can be expected since the stabilities of the hydrates depends on the specific structures of the individual hydrates. The fact that the data can be approximately fitted to smooth curves indicates that specific structural features do not have a large effect on the hydration energies. A more detailed examination of the energy values for the alkane dicarboxylates shows that some structural effects can be found.

A plot of the $\Delta G^{\circ}_{n-1,n}$ of the dicarboxylates $CO_2(CH_2)_kCO_2^{2-}$ is shown in Figure 3.8. In each plot the $\Delta G^{\circ}_{n-1,n}$ at constant n are plotted against the value of k. Comparing the four plots one finds that the energy difference between them does not decrease regularly as n is increased. The observed difference: $(-\Delta G^{\circ}_{2,3}) - (-\Delta G^{\circ}_{3,4}) = \Delta\Delta G^{\circ}_{4} \approx 0.8$ kcal/mol is smaller than $\Delta\Delta G^{\circ}_{5} \approx 1.0$ kcal/mol which is followed by the smallest $\Delta\Delta G^{\circ}_{6} \approx 0.6$ kcal/mol. A similar pattern was observed in earlier work[10,11] for the hydration of the doubly charged diamines, $NH_3^+(CH_2)_kNH_3^+$. The cause should be the same. When two separated charge centres are present, successive incoming water molecules will alternate between the two centres, the first going to either charge centre, the second to the other.

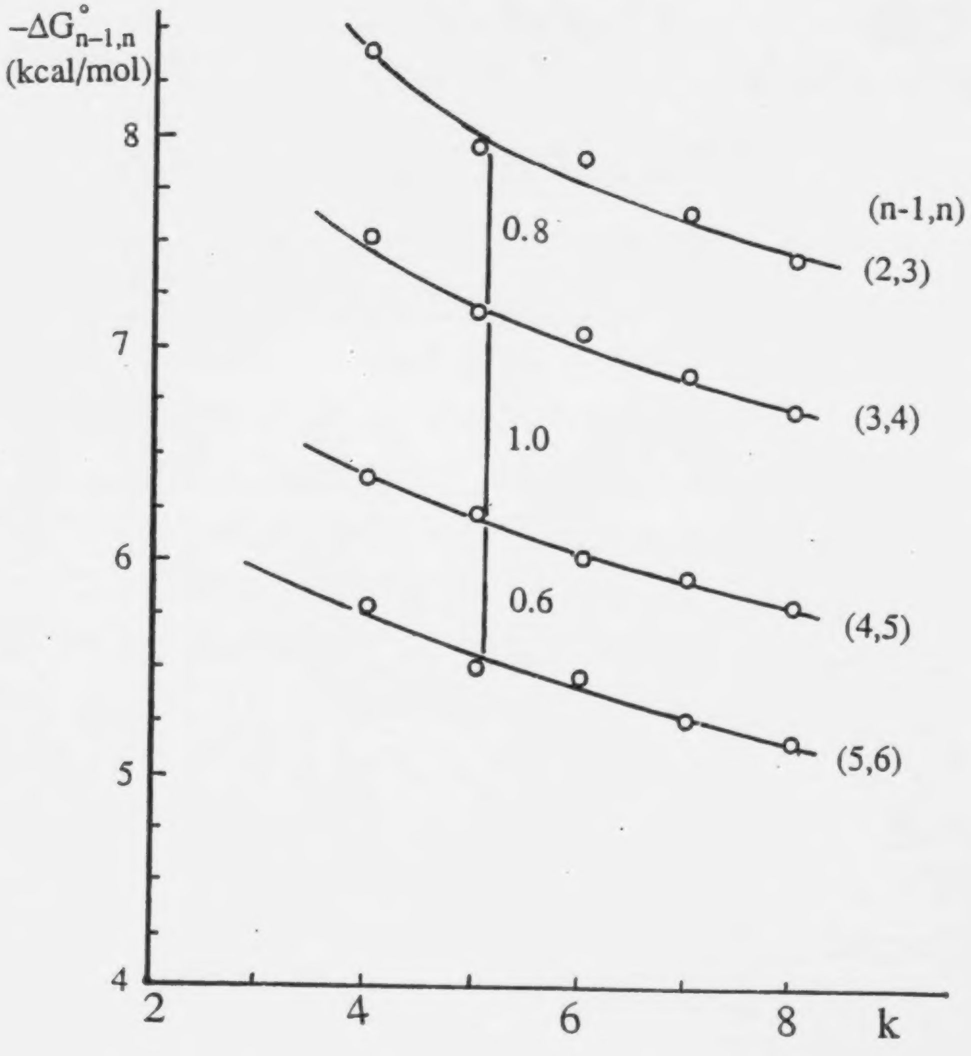

Figure 3.8 Hydration free energies $-\Delta G^{\circ}_{n-1,n}$ for doubly charged dicarboxylates, $CO_2(CH_2)_kCO_2^{2-}$, with increasing chain length

The third molecule will have to double up with one of the water molecules. Such doubling up leads to a larger drop of hydration energy. The fourth molecule will double up on the other charge centre and the $\Delta\Delta G_4^\circ$ will be relatively low. The fifth water molecule will have to triple up leading to a relatively large $\Delta\Delta G_5^\circ$ while the sixth molecule also tripling up will lead to a relatively low $\Delta\Delta G_6^\circ$, as observed in Figure 3.8. Ions without a distinct separation of charges, such as SO_4^{2-}, SeO_4^{2-}, etc., Table 3.3b, do not follow the same pattern, showing constantly decreasing $\Delta\Delta G$ values.

e. Enthalpy Changes and Temperature Dependence of Equilibria

The present apparatus operates only at room temperature and therefore the results provide only equilibrium constants and free energy changes at ~300° K. Approximate $\Delta H_{n-1,n}^\circ$ values can be obtained for the singly charged, not cyclized ions from the present $\Delta G_{n-1,n}^\circ$ by subtracting 7 kcal/mol from the $\Delta G_{n-1,n}^\circ$ value. The ΔS value for the n-1,n reactions is often ~24 cal/degree mol[3] and this leads to a $T\Delta S$ term of ~7 kcal/mol. For the doubly charged ions the loss of freedom will be larger and a value of -8 or -9 kcal/mol might be more appropriate.

A variable temperature ion source using the same design as shown in Figure 3.1 which will lead to equilibrium determinations over a wide temperature range and to ΔH° and ΔS° determinations has just been developed and put into operation.

References

1. Hogg, A.M.; Haynes, R.N.; Kebarle, P. *J. Am. Chem. Soc.* **1966**, *88*, 28.
2. Kebarle, P. *Annu. Rev. Phys. Chem.* **1977**, *28*, 455.
3. Keesee, R.G.; Castleman, A.W. *J. Phys. Chem. Ref. Data* **1986**, *15*, 1011.
4. Yamashita, M.; Fenn, J.B. *J. Phys. Chem.* **1984**, *88*, 4451. Fenn, J.B.; Mann, M.; Meng, C.K.; Wong, S.F.; Whitehouse, C.M. *Science* **1985**, *246*, 64.
5. Kebarle, P.; Tang, L. *Anal. Chem.* **1993**, *65*, 272A.
6. Blades, A.T.; Jayaweera, P.; Ikonomou, M.G.; Kebarle, P. *J. Chem. Phys.* **1990**, *92*, 2900. Blades, A.T.; Jayaweera, P.; Ikonomou, M.G.; Kebarle, P. *Int. J. Mass Spectrom. Ion Processes* **1990**, *102*, 251.
7. Bruins, A.P.; Covey, T.R.; Henion, J.D. *Anal. Chem.* **1987**, *59*, 2642.
8. Blades, A.T.; Kebarle, P. *J. Am. Chem. Soc.* **1994**, *116*, 10761.
9. (a) Limbach, P.A.; Crain, P.F.; McCloskey, J.A. *J. Am. Soc. Mass Spectrom.* **1995**, *6*, 27. (b) Smith, R.D.; Lou, J.A.; Edmonds, C.G.; Barinaga, C.J.; Udseth, H.R. *Anal. Chem.* **1990**, *62*, 882.
10. Klassen, J.S.; Blades, A.T.; Kebarle, P. *J. Am. Chem. Soc.* **1994**, *116*, 12075.
11. Klassen, J.S.; Blades, A.T.; Kebarle, P. *J. Phys. Chem*, **1995**, *99*, 15509.
12. Meot-Ner, (Mautner) M. *J. Am. Chem. Soc.* **1988**, *110*, 3854. Payzant, J.D.; Yamdagni, R.; Kebarle, P. *Can. J. Chem.* **1971**, *49*, 3308.

13. Keesee, R.G.; Lee, N.; Castleman Jr., A.W. *J. Am. Chem. Soc.* **1979**, *101*, 2599.

14. Davidson, J.A.; Fehsenfeld, F.C.; Howard, C.J. *Int. J. Chem. Kinet.* **1977**, *9*, 17.

15. Keesee, R.G.; Castleman, Jr., A.W. *J. Am. Chem. Soc.* **1989**, *111*, 9015.

16. Wu, Y.D., Houk, K.N. *J. Am. Chem. Soc.* **1993**, *115*, 11997.

17. Bohringer, H.; Fakey, D.W.; Fehsenfeld, F.C.; Ferguson, E.E. J. Chem. Phys. **1984**, *81*, 2805.

18. (a) Yamdagni, R.; Kebarle, P. *J. Am. Chem. Soc.* **1971**, *93*, 7139. (b) Payzant, J.D.; Yamdagni, R.; Kebarle, P. *Can. J. Chem.* **1971**, *49*, 3308. (c) Cumming, J.B.; French, M.A.; Kebarle, P. *J. Am. Chem. Soc.* **1977**, *99*, 6999. (d) Caldwell, G.; Kebarle, P. *Can. J. Chem.* **1985**, *63*, 1399. (e) Paul, G.J.C.; Kebarle, P. *Can. J. Chem.* **1990**, *68*, 2070.

19. (a) Larson, J.W.; McMahon, T.B. *J. Phys. Chem.* **1984**, *88*, 1083. (b) Larson, J.W.; McMahon, T.B. *Inorg. Chem.* **1984**, *23*, 2029. (c) Larson, J.W.; McMahon, T.B. *J. Am. Chem. Soc*, **1984**, *106*, 517.

20. Cumming, J.B.; Kebarle, P. *Can. J. Chem.* **1978**, *56*, 1.

21. Caldwell, G.; Renneboog, R.; Kebarle, P. *Can. J. Chem.* **1989**, *67*, 611.

22. Koppel, I.A.; Taft, R.W. Anvia, F.; Zhu, S.Z.; Hu, L.Q.; Sung, K.S.; DesMarteau, D.D.; Yagupolskii, L.M.; Yagupolskii, Y.L.; Vlasor, V.M.; Notario, R.; Maria, P.C. *J. Am. Chem. Soc.* **1994**, *116*, 3047. Taft, R.W.; Topsom, R.D. *Prog. Phys. Org. Chem.* **1987**, *16*. 1..

23. Viggiano, A.A.; Henchman, M.J.; Dale, F.; Deakyne, C.A.; Paulson, J.F. *J. Am. Chem. Soc.* **1992**, *114*, 4299.
24. Reliable values for the bond dissociation energies D(A-H) of oxy acids are scarce. For some approximate values see listings for A^- in ref. 25. Viggiano *et al*[23] provide a table of approximate electron affinities and bond energies for some oxo acids. These authors see a trend for the sulphonic acids, XSO_3H ($X = HO, F, CF_3$), where both EA and D(A-H) increase, but EA increases approximately 3 times faster.
25. Lias, S.G.; Bartmes, J.E.; Liebman, J.F.; Holmes, J.L.; Levin, R.D.; Mallard, W.G. *J. Phys. Chem. Ref. Data* **1988**, *17*, supplement No. 1.
26. Gao, J.; Garner, D.S.; Jorgensen, W.L. *J. Am. Chem. Soc.* **1986**, *108*, 4784.
27. Shen, M.; Xie, Y.; Schaefer, H.F. *J. Chem. Phys.* **1990**, *93*, 3379.
28. Ma, B.; Xie, Y.; Shen, M.; Schaefer, H.F. *J. Am. Chem. Soc.* **1993**, *115*, 1943.
29. Yamdagni, R.; Kebarle, P. *J. Am. Chem. Soc.* **1973**, *95*, 3504.
30. Meot-Ner, (Mautner) M.; Hamlet, P.; Hunter, E.P.; Field, F.H. *J. Am. Chem. Soc.* **1980**, *102*, 6393.
31. The monocarboxylic acid, CH_2CHCO_2H is more acidic by some 1 kcal/mol than formic acid.[32]
32. Graul, S.T.; Schnute, M.E.; Squires, R.R. *J. Mass Spectrom. and Ion Proc.* **1990**, *96*, 181.
33. Estimate of distances based on $\mathrm{C}\overset{\cdots}{-}\mathrm{C}$ aromatic 1.399 Å., $\mathrm{C}-\mathrm{CO_2}$ 1.5 Å., $\mathrm{C}\overset{\cdots}{-}\mathrm{O}$ 1.4 Å ; $\mathrm{C}-\mathrm{C}$ 1.54 Å.

34. The estimate was obtained by extrapolating the $-\Delta G^{\circ}_{2,3}$ value to k = 2 using $\Delta G^{\circ}_{2,3}$ values for k = 4 and 6. This led to $\Delta G^{\circ}_{2,3}$ (k = 4) - $\Delta G^{\circ}_{2,3}$ (k = 2) ≈ 1 kcal/mol. This difference was then divided by the distance difference for k = 2 to k = 4 (~2.5 Å) and multiplied by the 1.9 Å difference between the hexanedioate and 1,4-benzenedicarboxylate charge centres.

Chapter 4

Determination of ion-solvent equilibria in the gas phase. Hydration of di-protonated diamines and bis-trimethylammonium alkanes.*

Introduction

Determinations of gas-phase equilibria involving singly charged ions and solvent molecules such as H_2O (see eq. 4.1, z=1) or other ligands, were initiated some 30 years ago.[1,2] The sequential free energies, $\Delta G^o_{n-1,n}$, enthalpies, $\Delta H^o_{n-1,n}$ and entropies, $\Delta S^o_{n-1,n}$, resulting from these measurements have provided a wealth of data[2,3] on ion-solvent and ion-ligand interactions for positive and negative ions.

$$M^{z+/-}(H_2O)_{n-1} + H_2O = M^{z+/-}(H_2O)_n \qquad (n-1,n) \qquad (4.1)$$

Many ions of great interest in condensed phase chemistry and biochemistry could not be produced in the gas phase by conventional methods.[1-3] Electrospray mass spectrometry (ESMS)[4] is a method whereby electrolyte ions present in solution can be transferred to the gas phase.[5] With ES it is possible to obtain in the gas phase multiply charged ion-ligand complexes,[6] multiply protonated peptides and proteins[7] and

---

*A version of this chapter has been submitted for publication: Blades, A.T.; Klassen, J.S.; Kebarle, P. *J. Am. Chem. Soc.*

multiply deprotonated nucleic acids.[9] Most of these ions could not be obtained in the gas phase by conventional methods.[2]

In Chapter 2 and elsewhere we described[10] an ion source reaction chamber with which ion-molecule equilibria involving ES produced ions could be determined. This reaction chamber could only be operated at a single temperature, T= 293 K, such that only free energy changes, $\Delta G^{o}_{n-1,n}$, could be obtained.[10-13] In the present work we describe briefly a variable temperature source with which $\Delta H^{o}_{n-1,n}$ and $\Delta S^{o}_{n-1,n}$ values can also be obtained. The first results obtained with this apparatus are a study of the hydration of diprotonated diamines $H_3N(CH_2)_pNH_3{}^{2+}$ and the doubly charged $(CH_3)_3N(CH_2)_pN(CH_3)_3{}^{2+}$ methyl ammonium ions.

The results obtained for the above diammonium ion provide a good illustration of the changes in the interactions with water when the length of the alkyl chain $(CH_2)_p$ is decreased and the two charged centres come closer to each other. The charged groups selected in the two compound series: $-NH_3{}^+$ and $-N(CH_3)_3{}^+$ represent two extremes, *i.e.* a strongly hydrogen bonding and a very weakly hydrogen bonding species, and the results obtained for these contrasting compounds are of additional interest.

Experimental

The variable temperature ion source is shown in Figure 4.1. It is of very similar design to the room temperature source described previously[10] (see Chapters 2 and 3), except for the following changes. The forechamber, FC, and the reaction chamber, RC, are now housed in a solid cylindrical copper block, CB. The copper block has four wells for

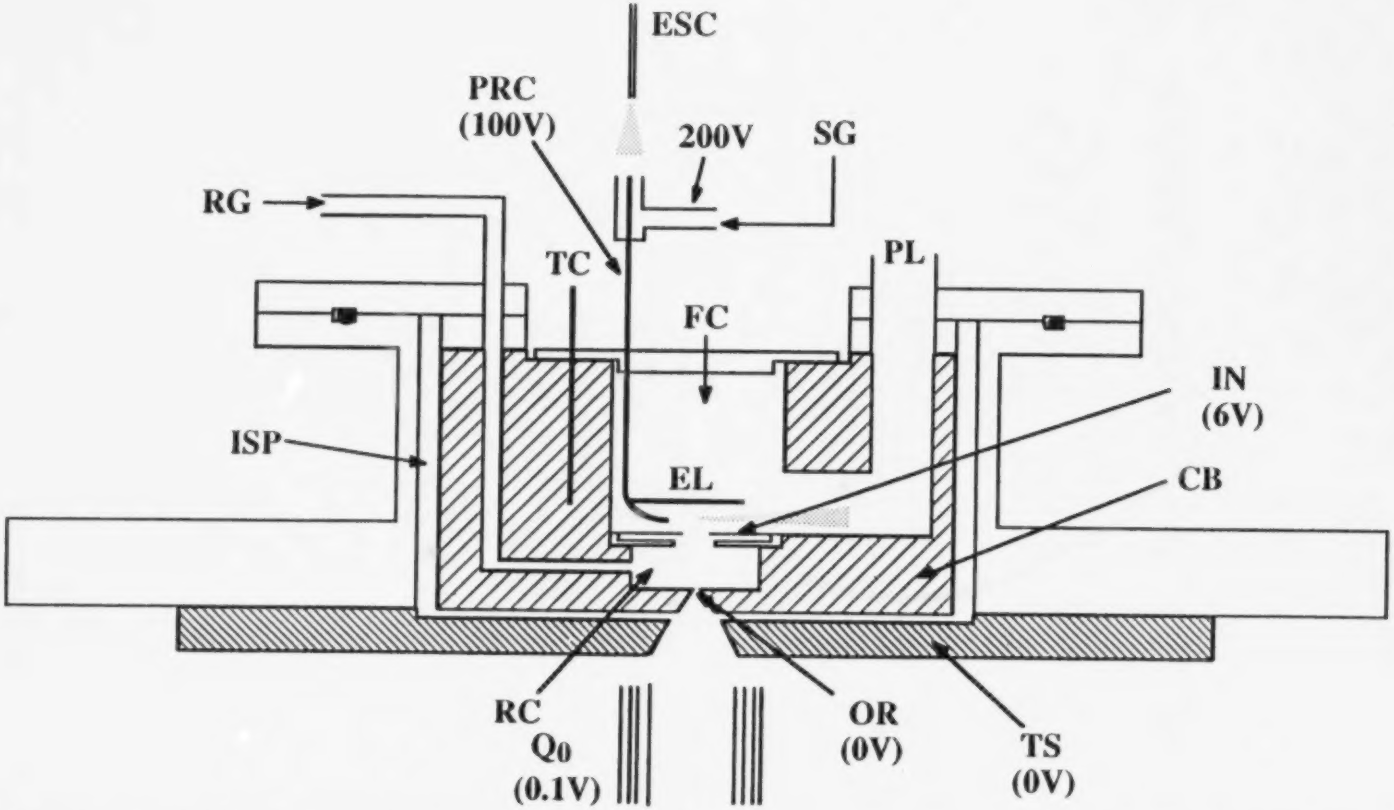

Figure 4.1. Ion source for determining ion-molecule equilibria involving electrospray generated ions. ESC, electrospray capillary. SG pipe and sleeve through which N_2 gas is supplied which reduces inflow of solvent vapour into pressure reducing capillary CAP. Forechamber FC at 10 torr, EL electrode attached to PRC. CB copper block housing of FC and reaction chamber RC. Thermocouple TC. Evacuated space for thermal insulation ISP. Interface IN with 4 mm orifice. Supply of reagent gas RG to reaction chamber. PL pumping lead. TS thermal shield; reduces radiative heating of cryopump surfaces of vacuum chamber. Q_0 AC only Brubacker lens. Q_0 is followed the triple quadrupole assembly Q_1, Q_2, Q_3, not shown in this Figure.

cartridge heaters (wells not shown in the Figure) and a narrow well for the thermocouple TC with which the temperature was measured.

The ion source operates on the same principles as the previous source.[10] The electrospray generating capillary, ESC, produces a fine spray of very small charged droplets The evaporation of solvent from the droplets leads ultimately to the formation of gas phase ions.[4,5] This stage occurs at atmospheric pressure. Some of the ions and surrounding gases are drawn into the pressure reducing capillary, PRC, which leads to the forechamber, FC. Inside FC the ions drift towards the reaction chamber, RC, under the influence of an electric field imposed between the electrode, EL (which is connected to PRC), and the interface plate IN. Some ions enter RC through a 3 mm orifice in IN. Reagent gas, consisting of nitrogen at 10 torr and water vapour at 1-80 m-torr, is supplied to the reaction chamber via the channel RG. The pressure in RC and FC is maintained at the desired magnitude (10 torr) by the pumping lead, PL. Ion hydration equilibria establish in RC, through which the ions drift at near thermal velocities. The ions in RC are then sampled through the orifice, OR, and into a vacuum chamber which houses the triple quadrupole mass spectrometer.

The present reaction chamber was somewhat longer, 8 mm, compared to 5 mm with the previous design,[10] and the potential drop between IN and OR was smaller, 6 V versus 10 V. Other typical potentials used with the present apparatus were: SG=200V; PRC=EL=100V; IN=6V; CB=OR=0V; Q_0=-0.1V. The design of the ion source was much simplified by choosing ground potential for CB and OR, which could be directly silver soldered to the flange which is bolted to the vacuum housing. Mass resolution was obtained with the third quadrupole

Q_3, which was operated at an offset potential of -10V. Corrections for the mass dependent transmission of the quadrupole were made with a procedure detailed in the previous work.[11]

The solution flow rate through the electrospray capillary was 1-2 µL/min with methanol as the solvent. The ammonium ions were obtained from the ammonium salts, either the chlorides or iodides, at $\sim 10^{-4}$ molar concentrations.

Results and Discussion

a. Determination of the Equilibrium Constants and ΔG^o, ΔH^o, ΔS^o values. Comparison with some data from the literature

The equilibrium constants $K_{n-1,n}$, see eq 4.1, were obtained from the ion intensities I_n and I_{n-1} of the corresponding hydrates, determined at a known partial pressure of water vapour p_{H_2O}. Plots of the intensity ratio, I_n/I_{n-1}, versus p_{H_2O} are shown in Figure 4.2 for the n-propyl and n-hexylammonium ions. Good straight lines passing through the origin are observed. According to eq. 4.2,

$$K_{n-1,n} = I_n/I_{n-1}p_{H_2O} \qquad (4.2)$$

the slope of the straight line should be equal to the equlibrium constant $K_{n-1,n}$.

Equilibrium constants determined at different temperatures are then used in van't Hoff plots to obtain $\Delta H^o_{n-1,n}$ and $\Delta S^o_{n-1,n}$, while the free energy can be obtained at any temperature from, $-\Delta G^o_{n-1,n} = RT\ell nK_{n-1,n}$. van't Hoff plots for the n-propyl and n-hexyl ammonium ions as well as the α,ω hexane diammonium ion are given in Figure 4.3. These plots illustrate very directly the stronger hydration present for the doubly

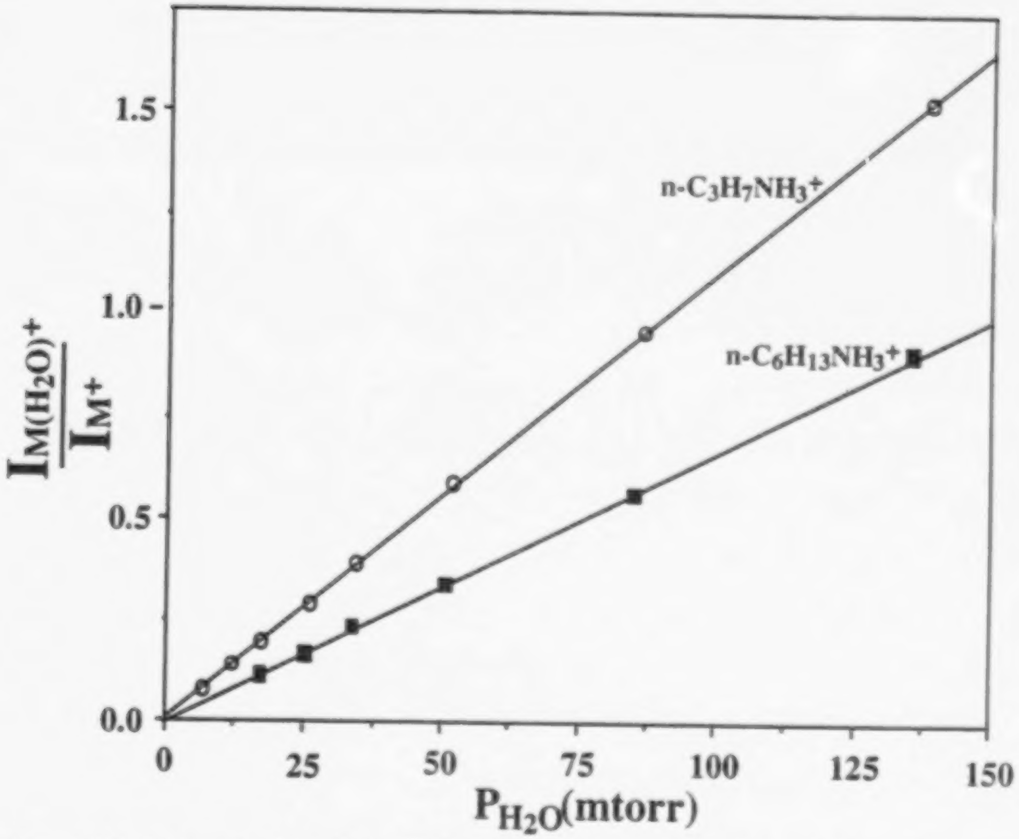

Figure 4.2. Determination of equilibrium constants: Plot of ion intensity ratio $I_{M(H_2O)^+}/I_{M^+}$ for hydration equilibrium: $M^+ + H_2O = M(H_2O)^+$, (0,1), versus P_{H_2O}, pressure of water vapour in ion source reaction chamber, at a temperature T = 382 K for M^+ = n-$C_3H_7NH_3^+$ and M^+ = n-$C_6H_{13}NH_3^+$. Slope of straight lines observed corresponds to equilibrium constant $K_{0,1}$. The equilibrium expression eq. 2 requires also that the straight line goes through the origin, as is the case in the present plots.

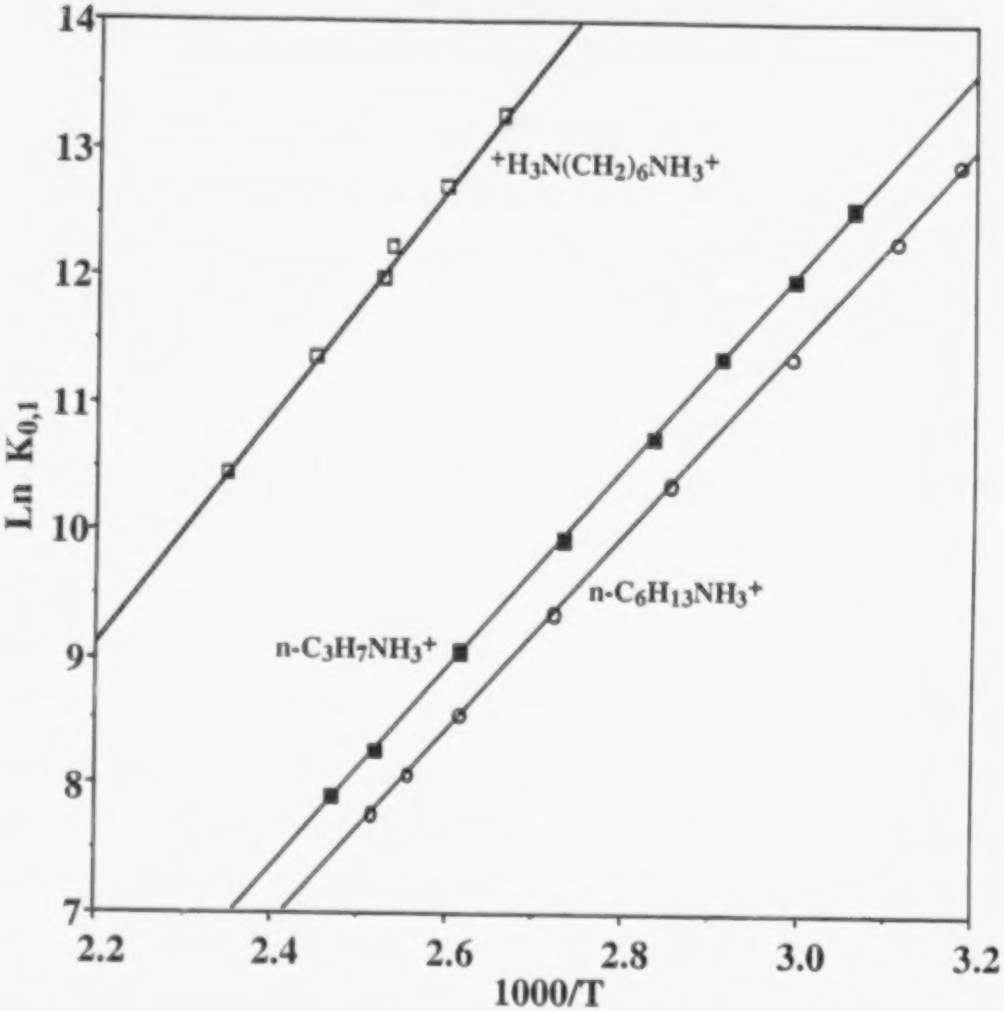

Figure 4.3. van't Hoff plots of ln $K_{0,1}$ vs reciprocal absolute temperature for hydration of n-$C_3H_7NH_3^+$, n-$C_6H_{13}NH_3^+$, and $NH_3(CH_2)_6NH_3^{2+}$. The much stronger hydration of the doubly charged ion is indicated by the much larger equilibrium constant values $K_{0,1}$ which corresponds to a larger exoergicity $-\Delta G^{\circ}_{0,1} = RT\ln K_{0,1}$ and by the steeper slope of the straight line obtained, which corresponds to a larger exothermicity, $-\Delta H^{\circ}_{0,1}$.

charged ion. Thus, the (0,1) line for the doubly charged ion is very much higher, which signals a much higher exoergicity, and the slope of the line is steeper, which signals a higher exothermicity.

van't Hoff plots for the sequential hydration of the α, ω dodecane diammonium ion are shown in Figure 4.4. These (n-1,n) plots show a very interesting pattern with n which will be examined further in the discussion. The van't Hoff plots for the (0,1) hydration of the doubly protonated $H_3N(CH_2)_pNH_3{}^{2+}$ with increasing value of p are given in Figure 4.5 and the same type of plots but for $(CH_3)_3N(CH_2)_pN(CH_3)_3{}^{2+}$ are given in Figure 4.6. The ΔH^o, ΔG^o and ΔS^o values resulting from these plots are summarized in Table 4.1-4.3

Table 4.1 gives data for which previous determinations have been reported in the literature. The data from the present work for the sodium and potassium ions, given in Table 4.1, were obtained from van't Hoff plots but these plots are not shown. Comparison of the present values with the literature results[14-16] shows agreement within 1 kcal/mole for the ΔH^o and ΔG^o values and 2 cal/deg mol for the ΔS^o results, which is as good as can be expected considering previously observed consistency within ion-equilibria determinations.[17,18]

b. Sequential hydration of a doubly protonated diamine

The van't Hoff plots for the sequential hydration of $H_3N(CH_2)_{12}NH_3{}^{2+}$ are shown in Figure 4.4, and the resulting thermodynamic data are given in Table 4.2. The $\Delta H^o_{n-1,n}$ values follow an interesting pattern: $\Delta H^o_{0,1} = \Delta H^o_{1,2} = 15.7$ kcal/mol, then a drop in exothermicity occurs, $\Delta H^o_{2,3} = \Delta H^o_{3,4} = 13.5$ kcal/mol. This pattern is very different from the gradual decrease of $\Delta H^o_{n-1,n}$ with increase of n observed

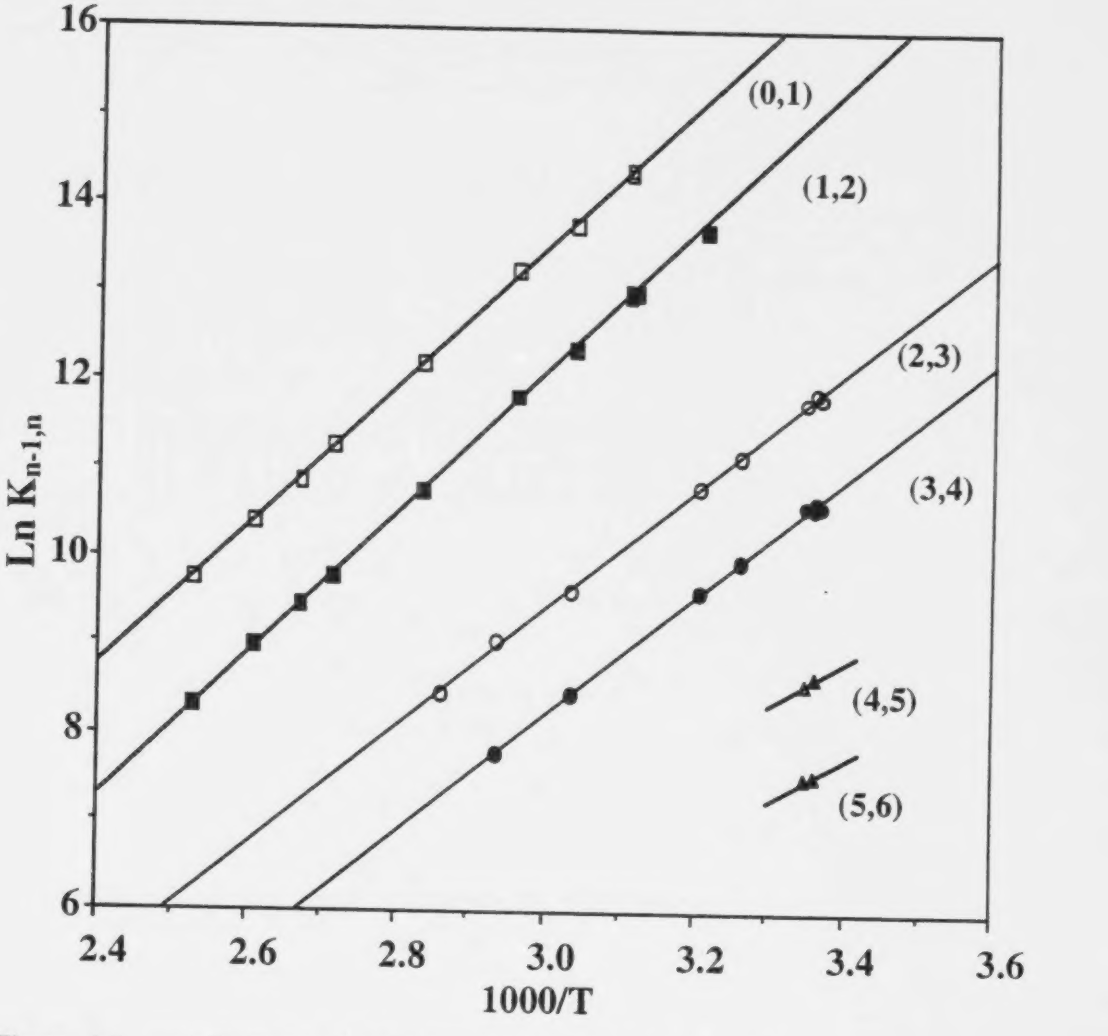

Figure 4.4. van't Hoff plots for the sequential hydration (n-1,n) of $NH_3(CH_2)_{12}NH_3^{2+}$. Determinations for (n-1,n) = 4,5 and 5,6 could be obtained only at the lowest temperature i.e. T = 298 K.

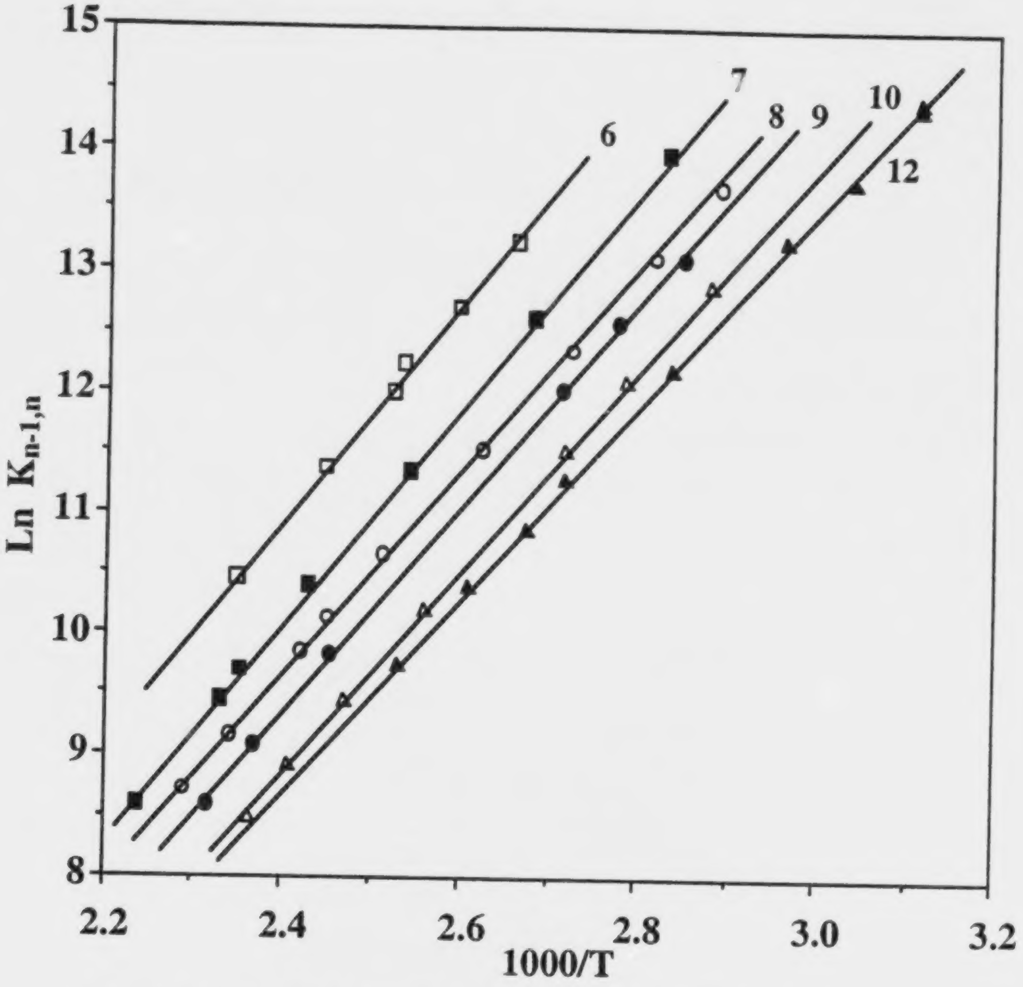

Figure 4.5. van't Hoff plots for the monohydration (0,1) of several diprotonated diamines $NH_3(CH_2)_pNH_3^{2+}$. Value of p is shown beside each plot.

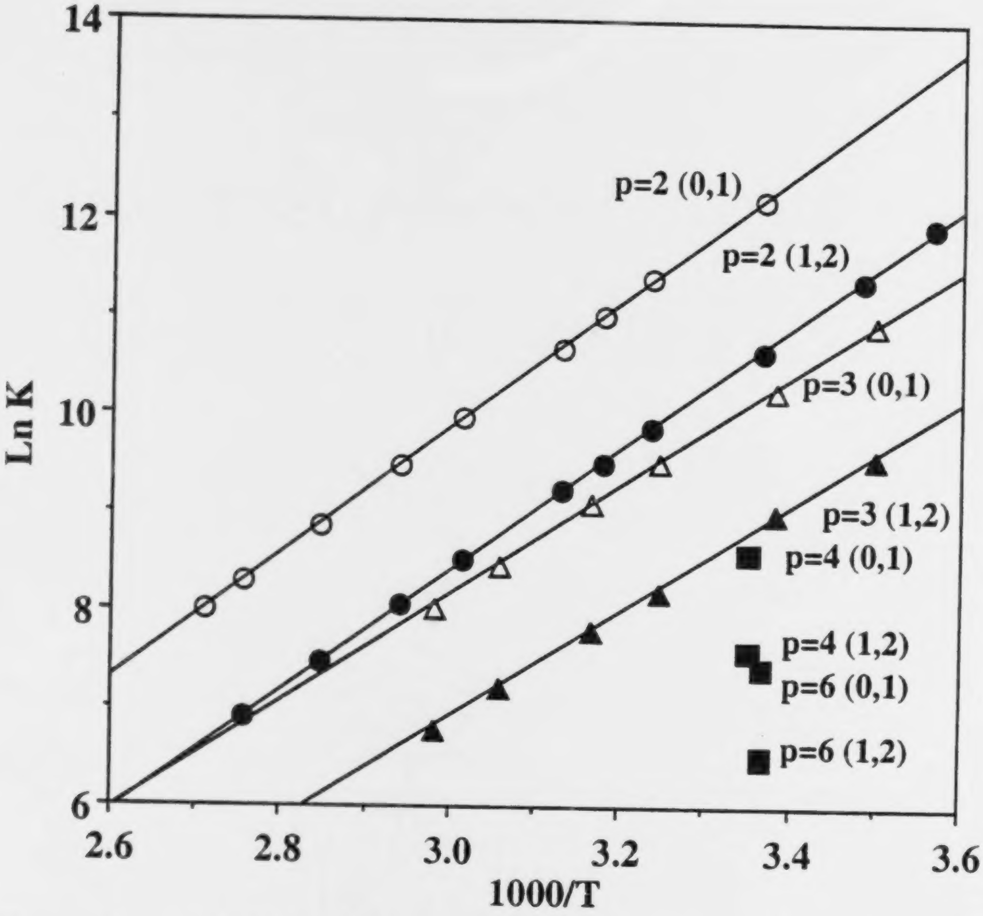

Figure 4.6. van't Hoff plots for the (0,1) and (1,2) hydration of $(CH_3)_3N(CH_2)_p$-$N(CH_3)_3^{2+}$. Values of p are given beside each plot. The hydration of the ions with $p > 3$ was weak at temperatures above T = 298 K and equilibrium constant determinations for these compounds could be obtained only for the lowest temperature, T = 298 K.

Table 4.1. Hydration Energies of Some Singly Charged Ions.

Ion	(n-1,n)	$-\Delta G^{o}_{298}$	$-\Delta H^{o}$	$-\Delta S^{o}$
		kcal/mol	kcal/mol	cal/deg mol
Na^+	(2,3)	9.5	16.1	22.0
		(9.3)[a]	(15.8)[a]	(21.9)[a]
		(8.7)[b]	(14.9)[b]	(20.8)[b]
	(3,4)	6.1	12.7	22.0
		(6.3)[a]	(13.0)[a]	(22.5)[a]
		(5.5)[b]	(12.6)[b]	(23.7)[b]
K^+	(2,3)	6.3	13.0	22.5
		(6.3)[a]	(13.2)[a]	(23.0)[a]
$n\text{-}C_3H_7NH_3^+$	(0,1)	8.8	15.6	22.8
		(8.7)[c]	(15.1)[c]	(21.5)[c]
$n\text{-}C_6H_{13}NH_3^+$	(0,1)	8.4	15.2	22.8
$(CH_3)_4N^+$	(0,1)[a]	(2.6)[d]	(9.0)[d]	(21.5)[d]

(a) Dzidic Kebarle;[14] (b) Tang, Lian, Castleman;[18] (c) Meot-Ner (Mautner)[16a]
(d) Meot-Ner & Deakyne[16b]

Table 4.2 Sequential hydration of $H_3N(CH_2)_{12}NH_3^{2+}$.

n-1,n	$-\Delta G^o_{298}$ kcal/mol	$-\Delta H^o$ kcal/mol	$-\Delta S^o$ cal/deg mol
0,1	9.7	15.7	20.1
1,2	8.8	15.7	23.2
2,3	7.0	13.4	21.5
3,4	6.3	13.6	24.5
4,5	5.1	-	-
5,6	4.4	-	-

Table 4.3 Hydration of α, ω di-ammonium alkanes and di-methylammonium alkanes

	$-\Delta G^{o}_{298}$		$-\Delta H^{o}$		$-\Delta S^{o}$	
	(kcal/mol)		(kcal/mol)		cal/degree·mol	
p	(0,1)	(1,2)	(0,1)	(1,2)	(0,1)	(1,2)
			$H_3N(CH_2)_pNH_3^{2+}$			
12	9.7	8.8	15.7	15.7	20.1	23.2
10	10.3	9.3	16.8	16.8	22.8	25.2
9	10.3	9.3	16.5	16.3	20.8	23.4
8	10.5	9.7	16.9	16.8	21.5	23.8
7	11.1	9.8	17.8	17.2	22.6	23.7
6	11.5	10.4	17.8	17.3	21.0	23.1
5	(12.2)[a]	(11.3)[a]	(18.6)[a]	(18.4)[a]	(21.5)[a]	(23.9)[a]
			$(CH_3)_3N(CH_2)_pN(CH_3)_3^{2+}$			
6	4.4	~3.8	–	–	–	–
5						
4	5.1	4.5	(10.0)[b]	–	(16.5)[b]	–
3	6.1	5.0	11.0	10.7	16.5	19.0
2	7.0	6.4	12.7	12.2	19.3	19.8

(a) Due to low yield of doubly protonated, p=5, ion obtained with electrospray, measurements of equilibria at only one temperature were feasible. These led to $\Delta G^{o}_{0,1} = 10.1$ kcal/mol and $\Delta G^{o}_{1,2} = 8.9$ kcal/mol at T = 398K. The values given in the table were obtained by assuming $\Delta S^{o}_{0,1} = 21.5$ cal/deg mol and $\Delta S^{o}_{1,2} = 23.9$ cal/deg mol. These values correspond to averages obtained for the longer chain length (p>5) diammonium ion. (b) $-\Delta H^{o}$ was obtained assuming $\Delta S^{o}_{0,1} = 16.5$ cal/deg mol.

for singly charged ions.[17,18] This difference is easily understood. Since the charges in the diammonium ion are separated, the strongest interactions occur when the sequential water molecules go to different charged sites. Furthermore, because in the dodecane the two charged sites are very widely separated, the interaction of the second water molecule with the second site is essentially identical to the first with the first site.

The hydration of alternate charged sites by sequentially added water molecules is also fully in accord with the observed $\Delta S^o_{n-1,n}$ changes, Table 4.2. Thus, the observed values:

$$\Delta\Delta S^o_{0,2} = \Delta S^o_{0,1} - \Delta S^o_{1,2} = 3.1 \text{ cal/degree.mol}$$

$$\Delta\Delta S^o_{2,4} = \Delta S^o_{2,3} - \Delta S^o_{3,4} = 3.0 \text{ cal/degree.mol}$$

can be predicted by considering the expected symmetry number ratios for the forward and reverse rates k_f/k_r, of the given (n-1,n) equilibrium. This procedure is detailed in Scheme 4.1 shown below for the 0,1 and 1,2 equilibria.

Scheme 4.1 Evaluation of ΔS^o_{sym} for Hydration of:

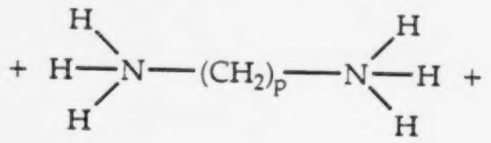

Equilibrium $K = \frac{k_f}{k_r}$

Symmetry factors $\frac{\sigma_f}{\sigma_r}$

n-1,n	S_f/S_r	ΔS^o_{sym}	$\Delta\Delta S^o_{sym}$
0,1	6/1	$R\ell n6/1$	$R\ell n\left(\frac{6/1}{3/2}\right)=R\ell n4=2.75$
1,2	3/2	$R\ell n3/2$	

The ratio of 6/1 for the (0,1) equilibrium comes about from the six equivalent hydrogen bonding positions on the diammonium ion for an incoming water molecule in the forward process and a single water molecule available to leave the monohydrate of the diammonium ion in the reverse. In deducing the ratio 3/2 for the (1,2) equilibrium one takes into account that only 3 hydrogen bonding positions (those on the second charged site) are available for the second incoming water molecule, while two equivalent water molecules can leave the dihydrate of the ion in the reverse reaction. We assume that only three hydrogen bonding positions and not five, are available for the second incoming molecule because the other two positions on the already singly occupied ammonium site form significantly weaker bonds. The energy difference can be estimated to be ~2.2 kcal/mol, on the basis of the difference between $\Delta H^o_{0,1} = \Delta H^o_{1,2} =$ -15.7 kcal/mol and $\Delta H^o_{2,3} = \Delta H^o_{3,4} =$ -13.5 kcal/mol, see Table 4.2. An energy difference of 2.2 kcal/mol is sufficient to "shut down" the singly occupied site; the maximum $T\Delta S$ term contribution favouring this site will be only ~0.55 kcal/mol (evaluated from: $\Delta S = R\ell n\ 5/2$ and $T \approx 300$ K and assuming all hydrogens are equivalent).

The value for $\Delta\Delta S^o_{2,4} = R\ell n\,(4/1)$, was obtained in an analogous manner from the symmetry number ratios: 4/2 and 2/4 for the (2,3) and (3,4) equilibria. An entropy change due to symmetry numbers of $\Delta\Delta S^o_{4,6} = R\ell n\,(4/1) = 2.75$ cal/degree.mol can be deduced also. Only single temperature determinations at 298 K were obtained for the (4,5) and (5,6) equilibria, see Table 4.2 and Figure 4.4. However because the $\Delta H^o_{4,5}$ and $\Delta H^o_{5,6}$ are expected to be the same, the $\Delta\Delta G^o_{4,6}$ can be used to obtain the entropy change and this procedure leads to $\Delta\Delta S^o_{4,6} \approx 2.3$

cal/degree.mol in fairly good agreement with the symmetry predicted value of 2.75 cal/degree.mol.

c. Changes of hydration thermochemistry with distance between the charged substituents, $H_3N(CH_2)_pNH_3^{2+}$

The ΔG^o, ΔH^o and ΔS^o values obtained from hydration equilibria determinations (0,1) and (1,2) involving the diammonium ions $H_3N(CH_2)_pNH_3^{2+}$ are given in Table 4.3 for p=5-10, 12. A plot of the enthalpy changes in $\Delta H^o_{0,1}$, as a function of the chain length p is given in Figure 4.7. The $-\Delta H^o_{0,1}$ values are seen to increase gradually as p decreases. The change, which initially is quite slow, is followed by more rapid increase at p=6 and 5. A very rapid increase is expected at still lower p values. Unfortunately, measurements of equilibria were possible only for p>4, because the intensity of doubly protonated ions obtained with p<5 with electrospray, was too low.[19]

The increase of the hydration exothermicity with decreasing separation of the two charged centres is easily understood. The presence of a positively charged substituent exerts a coulombic repulsion on the three protic hydrogens of the other $-NH_3^+$ group which increases their protic character. Better hydrogen bonding with water is expected when the hydrogens involved have a higher partial positive charge.[20,21]

For the dodecane diammonium ion we found that the $\Delta H^o_{0,1}$ and $\Delta H^o_{1,2}$ values are essentially the same, see Section b. This result was attributed to the very large distance between the charged groups for this system, p=12 . One expects that as p decreases the $-\Delta H^o_{0,1}$ will become larger than $-\Delta H^o_{1,2}$, because the hydration of the first functional group induces a small shift of the positive charge on this group away from the

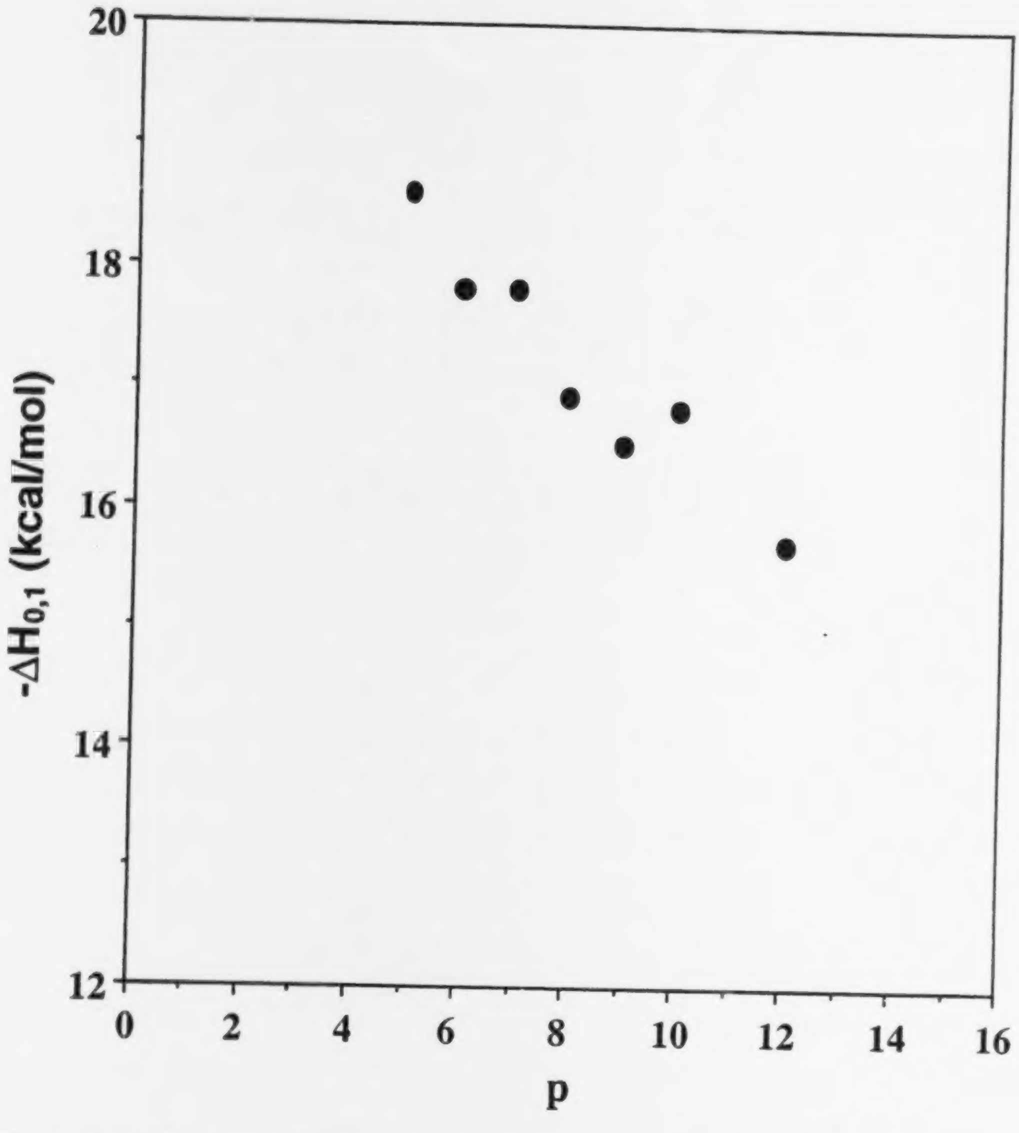

Figure 4.7. Enthalpy change, $-\Delta H^{\circ}_{0,1}$ for monohydration of $H_3N(CH_2)_pNH_3^{2+}$ as a function of chain length, p.

nitrogen atom towards the H atom that interacts with the water molecule. This shift has a very small effect when p is large but should become noticable for low p. The data for $\Delta H^o_{0,1}$ and $\Delta H^o_{1,2}$ given in Table 4.3 show that the two values remain approximately the same down to p=7. For p=6 and p=5 there is an indication of a change in the direction $-\Delta H^o_{0,1} > -\Delta H^o_{1,2}$, however the difference observed is small ~0.3 kcal/mol and essentially within the experimental error.

The coulombic repulsion between the two charged $-NH_3^+$ substituents has also a strong effect on the gas phase acidity of the doubly protonated diamines. Recent *ab initio* calculations by Gronert[20] for the $H_3N(CH_2)_7NH_3^{2+}$ (= HB_2H^{2+}), provide a gas phase acidity for HB_2H^{2+} of 181.6 kcal/mol. This value can be converted to a gas phase basicity (GB), $GB(B_2H^+) \approx 174$ kcal/mol, by subtracting the entropy term ($T\Delta S = 7.8$ kcal/mol, T=298 K) for the free proton. The GB for the singly protonated diamine is some 36 kcal/mol lower than that of the neutral diamine B_2. The B_2H^+ was assumed[20] to be in the same extended (noncyclised) structure as the HB_2H^{2+}.

In previous work[21,22] involving measurements of the hydration of singly protonated monobasic nitrogen and oxygen bases it was established that an approximately linear relationship exists between the gas phase basicity of the base B, GB(B), and the hydration energy of BH^+, $-\Delta G^o_{0,1}$ (BH^+). High GB(B)'s, *i.e.* relatively weak BH^+ acids, where the charge is well stabilized lead to low hydration exoergicities, $-\Delta G^o_{0,1}$. A very similar dependence was found also for the enthalpy change counterparts, *i.e.* the proton affinity PA(B) and $-\Delta H^o_{0,1}$ (BH^+). The relationship is illustrated by the plot shown in Figure 4.8 for the alkylammonium ions, BH^+; a fair straight line relationship is indicated by these data. We were

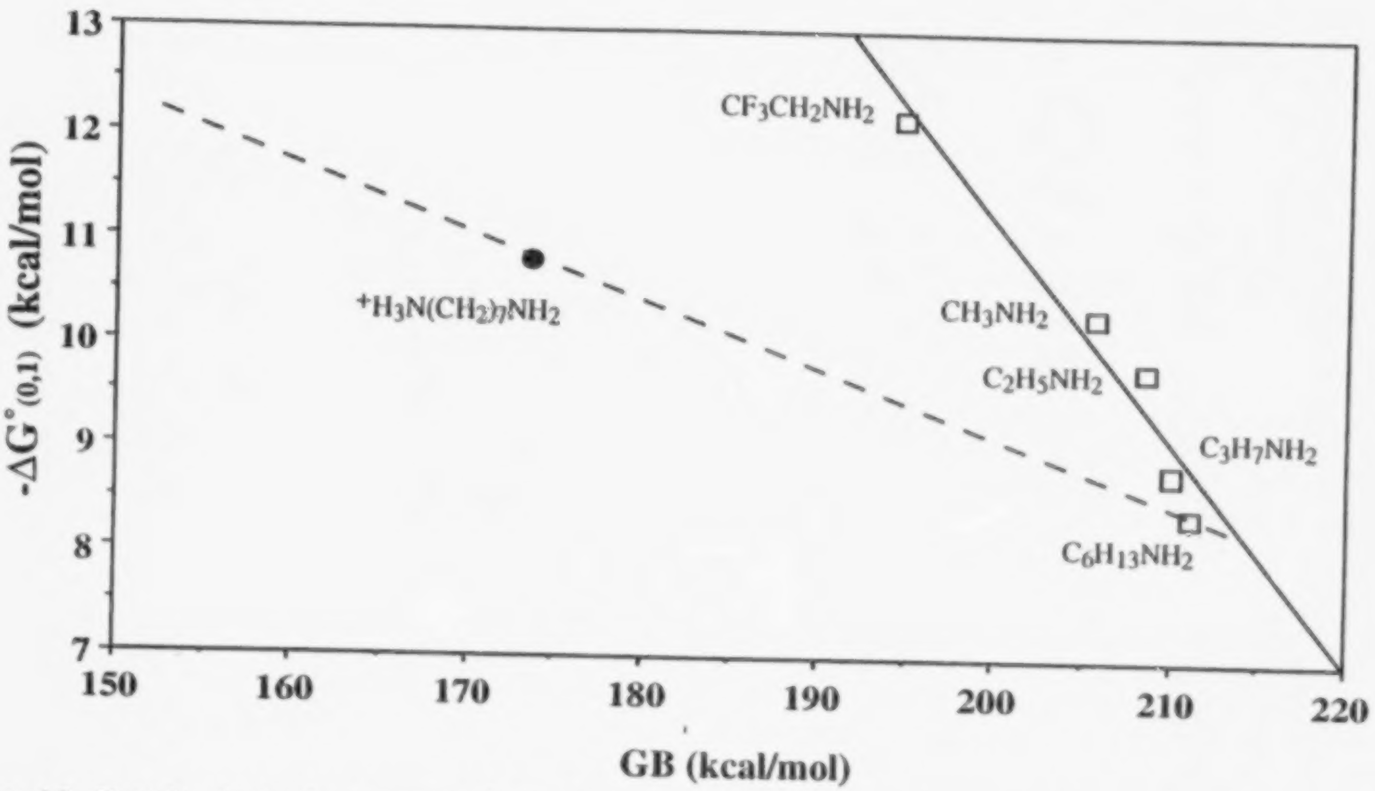

Figure 4.8. Plot of hydration free energy $\Delta G^\circ_{0,1}$ for singly protonated alkyl amines BH^+ versus the gas phase basicity, GB (B), corresponding to free energy change for reaction: $BH^+ = B + H^+$. The bases B used are identified in the figure. Also shown in the hydration energy of $H_3N(CH_2)_7NH_3^{2+}$ plotted versus the gas phase basicity $GB(H_2N(CH_2)_7NH_3^+)$ obtained by Gronert.[20] The diprotonated ion clearly does not fit the linear relationship observed for the singly protonated bases. GB (B) values from Lias et al[25], Hydration free energies of BH^+: n-$C_3H_7NH_3^+$ and n-$C_6H_{13}NH_3^+$, present work; $CH_3NH_3^+$, $C_2H_5NH_3^+$ and $CF_3CH_2NH_3^+$ from Meot-Ner.[16a]

interested in examining whether the di-protonated diamines would fit on the same line. The single point available is for the p=7 di-ammonium ion, $H_2N(CH_2)_7NH_3^+$, for which, as mentioned above, a theoretically evaluated proton affinity for was obtained by Gronert.[20] As evident from Figure 4.8, the diprotonated diamine does not at all fall on the line obtained with the singly protonated amines. In hindsight, this large deviation is not unexpected considering the large difference between a charged and a neutral substituent. The coulombic repulsion present when the substituent is charged leads to an extension of the N–H$^+$ bond which increases the strength of the hydrogen bond with the water molecule. However, only a small part of the coulombic energy is used in that process since significant charge delocalization occurs over the charge site. On the other hand, when the proton is completely removed, the total coulombic energy is used to reduce the gas phase basicity. Therefore, the decrease of the gas phase basicity by the coulombic repulsion is expected to be much larger than the increase of the hydrogen bond energy. The direction of the deviation of the di-protonated diamine from the correlation for the singly charged amines, Figure 4.8, conforms to the above conclusion; the actual gas phase basicity, 174 kcal/mol, is very much lower than the GB value ~202 kcal/mol predicted by the correlation for a neutral base that has the same hydration value,$-\Delta G^o_{0,1}$ = 11.1 kcal/mol, as the protonated diamine base. Actually, the value predicted by the correlation may be expected[23] to be closer to the apparent gas phase basicity of B_2H^+, $GB^{app}(B_2H^+)$, as determined by kinetic bracketing proton transfer measurements[20,24]. Gronert's[22] calculations lead to a $GB^{app}(B_2H^+)$ ~192 kcal/mol, compared with the correlation value of ~202 kcal/mol.

Now while the correlation between $-\Delta G^{o}_{0,1}$ (HB_2H^{2+}) and $GB(B_2H^+)$ differs from that observed for the monoalkylamines, a linear relationship is still expected, albeit with a smaller negative slope. This inverse relationship is reasonable since GB is expected to decrease linearly with increasing coulombic repulsion between the charge sites, while the hydration energy should increase proportionately with coulombic repulsion. From this relationship it should be possible to determine the gas phase basicities of the B_2H^+ ion (in extended conformation) based on the measured hydration energies. Unfortunately, only a single GB is available for the B_2H^+ ions, that of $H_2N(CH_2)_7NH_3^+$. Nevertheless, a tentative relationship (shown by the dashed line in Figure 4.8) is proposed based on the experimentally determined GB of n-hexylamine, which should be a reasonable approximation for the case where the amino groups on the diamine are remote from one another such that the effect of the coulombic repulsion is negligeable. Using this plot, the GB's of the B_2H^+ ions were evaluated based on the measured $-\Delta G^{o}_{0,1}$ values: (p=5) GB=158, (p=6) 169, (p=8) 185, (p=9, 10) 187 and (p=12) 197 kcal/mol (note that the $-\Delta G^{o}_{0,1}$ values for the diamines were reduced by 0.4 kcal/mol to account for the effect of the charge site multiplicity (symmetry effect) which is not present in n-hexylamine) . Work is currently underway in this laboratory to evaluate theoretically the GB's of the B_2H^+ ions in order to compare them with these predicted values.

d. Hydration Energies of $(CH_3)_3N(CH_2)_pN(CH_3)_3^{2+}$ ions

The energies for the (0,1) and (1,2) hydration of the bis-trimethylammonium ions are given in Table 4.3. Determinations of the hydration enthalpies for p>3, where the hydration interaction becomes quite weak, require equilibration temperatures well below room temperature. These are as yet not accessible with the present ion source. Therefore, only the -ΔG^o values for p=4 and 6 could be determined. Due to the low stability of the hydrates, van't Hoff plots for p = 3 and 2 could be obtained only over a narrower temperature range. Therefore, the resulting ΔH^o and ΔS^o data are expected to be of lower accuracy than the data for the ammonium ions.

The hydration energies for the doubly charged methylammonium compounds are seen to be much lower than for the ammonium analogues, see Table 4.3 and Figure 4.9. For example, $-\Delta G^o_{0,1}$ = 11.5 kcal/mol for $H_3N(CH_2)_6NH_3^{2+}$ but only 4.4 kcal/mol for $(CH_3)_3N(CH_2)_6N(CH_3)_3^{2+}$. The major reason for this difference is the much poorer H bonding ability of the CH_3 relative to the NH_3 hydrogens. This is due to the lower electronegativity of the N relative to the C atom and for the charged substituents, the longer distance between the N atom and the CH_3 hydrogens. Similar differences in the hydration energies are observed also for the singly charged ions, see Table 4.1, where $-\Delta G^o_{0,1}$ = 8.8 kcal/mol for n-$C_3H_7NH_3^+$ and only 2.6 kcal/mol for $N(CH_3)_4^+$.[13b]

The bonding of water and other ligands to singly charged quaternary alkyl ammonium ions has been studied by Meot-Ner and Deakyne[13b] by experimental and theoretical methods. The theoretical calculations have shown that the most stable geometry is obtained when the oxygen atom of the water molecule interacts with three C-H hydrogens and when each of these hydrogens come from a different methyl group. The interaction with the three hydrogens from the different methyl groups is ~6 kcal/mol more stable than the interaction of

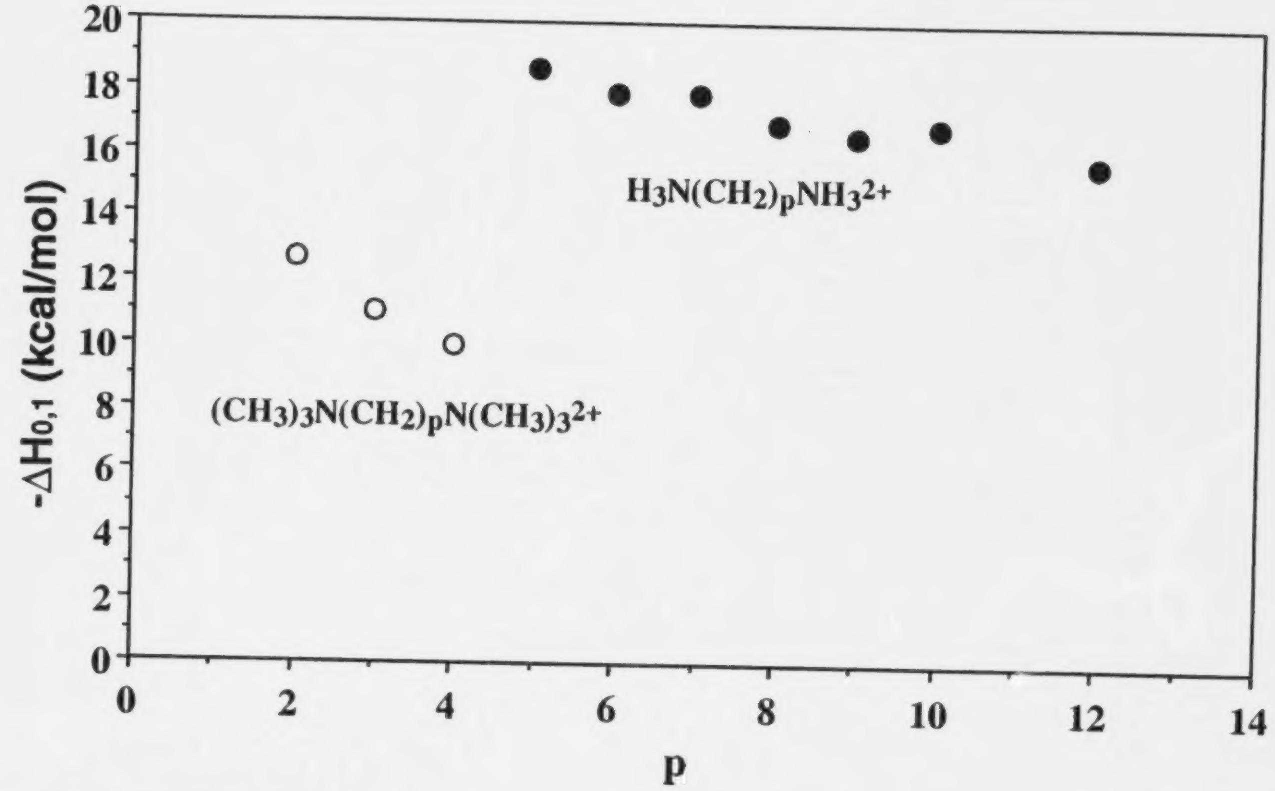

Figure 4.9. Comparison of enthalpy change for monohydration of $H_3N(CH_2)_pNH_3^{2+}$ and $(CH_3)_3N(CH_2)_pN(CH_3)_3^{2+}$ ions. The $\Delta H^{\circ}_{0,1}$ value for the methyl ammonium ion p = 3 was estimated from $\Delta G^{\circ}_{0,1}$ for this compound, see Table 4.3.

the oxygen with three hydrogens from the same methyl group (data for $N(CH_3)_4^+$).[13b] Another interesting result was the finding that the second water molecule in a dihydrate interacts preferentially with a hydrogen atom on the first water molecule and that this interaction is equivalent in magnitude to the interaction between the first H_2O and three methyl hydrogens.

The observations of Meot-Ner and Deakyne can be used to predict expected entropy changes for the hydration of the $(CH_3)_3N(CH_2)_pN(CH_3)^{2+}$ ions. For p = 2, an entropy change, $\Delta\Delta S^o_{0,2}$ = 2.5 cal/(deg mol) is obtained from the data in Table 4.3. Proceeding as in Section C, one can evaluate $\Delta\Delta S^o$ values on the basis of symmetry number changes. Assuming that the first H_2O molecule goes to the one charged site forming the stable three methyl hydrogens complex and the second H_2O does the same at the other charged site, a $\Delta\Delta S^o_{0,2}$ = Rln 4 = 2.75 cal/(deg·mol) is predicted. This agrees well with the experimentally determined value, supporting the notion that the two waters add on different ends of the ion. For p=3, the situation is very different with $\Delta\Delta S^o_{0,2}$ = 0.5 cal/(deg mol). The lower value for p=3 compared with p=2 may be due to experimental error, partly because the van't Hoff plots, as already mentioned, were obtained over a narrow temperature range. However, it is also possible that the small $\Delta\Delta S^o_{0,2}$ is a consequence of the second H_2O preferrentially binding to the first H_2O[13b]. If this occurs then the $\Delta\Delta S^o_{0,2}$ is no longer expected to be equal to 2.75 cal/deg mol. The actual value will reflect true differences in entropy associated with the addtion of the first and second H_2O molecules. Clearly, better data are required to prove that the difference in $\Delta\Delta S^o_{0,2}$ for p=2 and 3 reflects differences in bonding of the two H_2O's. Such accuracy is within the capability of the method and we hope to demonstrate this in future work. The present results provide an illustration that the thermochemical data can lead to useful insights into the structures of the hydrates of multiply charged ions.

References

1. Hogg, A.M.; Haynes, R.N.; Kebarle, P. *J. Am. Chem. Soc.* **1966**, *88*, 28.
2. Kebarle, P. *Annu. Rev. Phys. Chem.* **1977**, *28*, 455.
3. Keesee, R.G.; Castleman, A.W. *J. Phys. Chem. Ref. Data* **1986**, *15*, 1011.
4. Yamashita, M.; Fenn, J.B. *J. Phys. Chem.* **1984**, *88*, 4451. Fenn, J.B.; Mann, M.; Meng, C.K.; Wong, S.F.; Whitehouse, C.M. *Science* **1985**, *246*, 64.
5. Kebarle, P.; Tang, L. *Anal. Chem.* **1993**, *65*, 272A.
6. Blades, A.T.; Jayaweera, P.; Ikonomou, M.G.; Kebarle, P. *J. Chem. Phys.* **1990**, *92*, 2900. Blades, A.T.; Jayaweera, M.G.; Kebarle, P. *J. Chem. Phys.* **1990**, *102*, 251.
7. Bruins, A.P.; Covey, T.R.; Henion, J.D. *Anal. Chem.* **1987**, *59*, 2642.
8. Blades, A.T.; Kebarle, P. *J. Am. Chem. Soc.* **1994**, *116*, 10761.
9. Limbach, P.A.; Crain, P.F.; McCloskey, J.A. *J. Am. Soc. Mass Spectrom.* **1995**, *6*, 27. Smith, R.D.; Lou, J.A.; Edonds, C.G.; Barinaga, C.J.; Udseth, H.R. *Anal. Chem.* **1990**, *62*, 882.
10. Klassen, J.S.; Blades, A.T.; Kebarle, P. *J. Am. Chem. Soc.* **1994**, *116*, 12075.
11. Klassen, J.S.; Blades, A.T.; Kebarle, P. *J. Am. Chem. Soc.* **1995**, *99*, 15509.
12. Blades, A.T.; Klassen, J.S.; Kebarle, P. *J. Am. Chem. Soc.* **1995**, *117*, 10563.
13. Blades, A.T.; Ho, Y.; Kebarle, P. *J. Phys. Chem.* **1996**, *100*, 2443.
14. Dzidic, I.; Kebarle, P. *J. Phys. Chem.* **1970**, *7*, 1466.

15. Tang, I.N.; Lian, M.S.; Castleman, A.W., Jr. *J. Chem. Phys.* **1976**, *65*, 4022.

16. a) Meot-Ner (Mautner), M. *J. Am. Chem. Soc.* **1984**, *106*, 1265.
    b) Meot-Ner (Mautner), M.; Deakyne, C.A. *J. Am. Chem. Soc.* **1985**, *107*, 469.

17. Kebarle, P. *Annu. Rev. Phys. Chem.* **1977**, *28*, 445.

18. Keesee, R.G.; Castleman, A.W., *J. Phys. Chem. Ref. Data* **1986**, *15*, 1011.

19. For p>6 the intensities of the doubly protonated ions were very much higher than those of the singly protonated species. However the intensity of the singly protonated ion became dominant for p<6 and the doubly protonated species disappeared for p<4. With electrospray, multiply protonated ions which are known to be present in the solution may not be observed in the gas phase when the sites of protonation are quite close to each other. The proton loss occurs in the transition from solution to gas phase as the ion is desolvated.

20. Gronert, S. *J. Am. Chem. Soc.* **1996**, *118*, 3525.

21. Davidson, W.R.; Sunner, J.; Kebarle, P. *J. Am. Chem. Soc.* **1979**, *101*, 1675.

22. Lau, Y.K.; Kebarle, P. *Can. J. Chem.* **1981**, *59*, 151.

23. The "expected" closer correspondence with the apparent gas phase basicity follows from an inspection of a reaction coordinate for the proton transfer reaction, see for example Figure 4.1, 4.2 in Gronert[20].

24. Gross, D.S.; Rodriguez-Cruz, S.E.; Bock, S.; Williams, E.R. *J. Phys. Chem.* **1995**, *99*, 4034.

25. Lias, S.G.; Bartmess, J.E.; Liebman, J.L.; Levine, R.D. *J. Phys. Chem. Ref. Data* **1984**, *13*, 695.

Chapter 5

Reaction Enthalpies for: $M^+L = M^+ + L$ where $M^+(Na^+,K^+)$ and L (acetamide, N-methylacetamide, N,N-dimethylacetamide, glycine and glycylglycine) from Determinations of the Collision-Induced Dissociation Thresholds.*

Introduction

The bond enthalpies corresponding to reaction 5.1 where $M^+ = Na^+$,

$$ML^+ = M^+ + L \qquad (5.1)$$

K^+ and $L = CH_3NHCOCH_3$ are of special interest because of attempts to understand the microscopic factors controlling the passage of these ions through transmembrane channels such as the gramicidin channel. The permeation of the ion through the channel involves partial dehydration of the ion, where the endoergicity of the dehydration is offset by attractive interactions of the ion with polar groups in the channel.[1] The ion-channel interactions are believed to involve mainly the carbonyl oxygens of the peptide backbone.[2-4]

Theoretical investigations of the Monte Carlo and Molecular Dynamics techniques rely on the development of realistic pair potential functions representing the microscopic interactions. For ion-solvent molecule interactions, such as ion-water molecule interactions the pair potential functions were developed on the basis of ab initio calculations of the ion-molecule interactions.[5] Of considerable help to this approach were the experimentally determined free energy, ΔG_1°, enthalpy, ΔH_1° and entropy, ΔS_1° changes obtained from ion-solvent molecule equilibria observed by mass spectrometric techniques.[6] These experimental data helped establish the quality of the basis set and electron correlation required in order to obtain values[5] in agreement with experiment.

---

* A version of this chapter has been published: Klassen, J.S.; Anderson, S.G.; Blades, A.T.; Kebarle, P. *J. Phys. Chem.* **1996**, *100*, 14218.

The interactions of the ions with peptides such as the transmembrane channels are also amenable to this approach but in this case, rather than the actual peptide, a model compound such as methylacetamide is used to obtain information on the dominant interactions.[7] Previous experimental ion-equilibria determinations are available only for K^+ and dimethylacetamide.[8] It is therefore desirable to extend the equilibria determinations, which lead to the bond enthalpy and free energy changes ΔH_1° and ΔG_1°, to N-methylacetamide, acetamide and Na^+ ions.

The previous determinations[8] were obtained with alkali ions produced in the gas phase by thermionic emission of the ions from a heated metal filament painted with the alkali ion salts.[9,10] This apparatus was dismantled several years ago. Recently, the electrospray (ES) method with which ions present in a solution can be tranferred into the gas phase and subjected to mass spectrometric detection, was developed by Fenn and coworkers.[11] Electrospray affords the production not only of ions such as Na^+ and K^+ and other singly charged ions but also that of doubly and triply charged transition metal and alkaline earth ion-ligand complexes[12], multiply protonated peptides and proteins,[13] doubly charged anions[14] like SO_4^{2-}, HPO_4^{2-} and multiply deprotonated nucleic acids.[15] The latter are also of paramount importance in solution chemistry and biochemistry but could not be obtained in the gas phase prior to the development of ES.

ES generates ions in ambient gas at ~1 atmosphere and the determination of ion concentrations with a mass spectrometer in gas at such high pressure is difficult. A successful design where the gas is transferred to a reaction chamber at 5-10 torr pressure, where the ion-molecule equilibria establish, was described recently[16] and is also discussed in Chapter 2.

The ion-equilibrium method is not well suited for determinations where the bond enthalpies are high, *i.e.* greater than ~40 kcal/mol, because of the very high temperatures required for the equilibrium to establish. However, many ion-ligand complexes can have such high bond enthalpies particularly when multiply charged ions are involved.[17] Therefore, it is very desirable to have a method with which the bond energies of strongly bonded ion-ligand complexes, produced by electrospray, can be determined.

Determination of the threshold of the product ion, M^+, where the reactant ion, ML^+, is accelerated to known kinetic energies, experiences a collision with a noble gas atom and undergoes dissociation, is a method with which bond enthalpies, e.g., ΔH_1° values can be determined. This collision-induced dissociation (CID) threshold method [18,19] is applicable also when high bond energies are involved. The present work describes some of the first results with this method as applied to ions generated by ES. The determinations for M^+ (Na^+, K^+) and L (acetamide, AA; N-methyl acetamide, MAA; and N,N-dimethyl acetamide, DMA) are described in subsequent sections.

Determinations for K^+ and L = acetone and dimethyl sulfoxide were also made for the purpose of comparing the CID threshold data with available previous determinations based on ion-equilibria. Determinations involving Na^+ and K^+ and L = glycine, glycinamide, succinamide and the dipeptide glycylglycine were also made. The last three ligands may lead to bi- and tridentate complexes and provide an interesting extension of the CID threshold results.

Mass spectral analysis of electrospray produced ions from aqueous and methanol solutions containing low concentrations of peptides or proteins and Na^+ ions due to the presence of electrolytes $Na^+ + X^-$ in the solutions has shown[11] that the peptides and proteins form sodium ion adducts. Multiple sodium ion addition occurs with polypeptide and protein molecules. The number of sodium ions increases with the number of the peptide units in the molecule.[11] The sodium ions evidently form complexes with polar regions of the peptides although the complexation may be largely occurring as a consequence of the ion transfer from solution to the gas phase. Therefore, data on the bonding forces between alkali ions and peptides or models of peptides, such as described in this work, are of interest also from the standpoint of electrospray mass spectrometry and the mechanism of electrospray mass spectrometry. One should not fail to notice that there are certain analogies between the transfer of sodium and potassium ions from solution to the transmembrane channels and the transfer from solution to the gas phase when the solution contains peptides or proteins.

Experimental and Curve Fitting Procedure

a. Apparatus and Conditions

As mentioned in the Introduction, with Electrospray one obtains gas phase ions in ambient gas at one atmosphere pressure. The transfer of these ions to the vacuum of the mass spectrometer used for the CID studies presents some special challenges because the accelerated ions entering the collision cell must have a known internal energy distribution, preferably a Maxwell Boltzmann distribution at a known temperature. Furthermore, the translational kinetic energy of the ions must be well defined and have a narrow distribution. The present measurements were performed with a modified triple quadrupole mass spectrometer.[20] A detailed account which described how and to what extent the above challenges could be met, is given elsewhere.[20] Here, we give only a brief description of the apparatus and conditions of the present measurements.

The mass spectrometer used was a SCIEX Trace Atmospheric Gas Analyzer 6000 E, triple quadrupole mass spectrometer.[21] The front end was modified as shown in Figure 5.1. There are four sections:

(1) The electrospray generator, ES, which produces charged droplets and ultimately gas phase ions from an electrolyte solution which flows through the ES capillary.

Solutions of electrolytes NaCl or KCl at 10^{-4} mol/L in methanol and the ligand L at 10^{-3} mol/L were used to generate the ions NaL^+ and KL^+.

(2) The low pressure ion source, LPS, is maintained at 10 torr by means of a pump. Atmospheric pressure gas containing ES produced ions is admitted through the sampling capillary CAP. The clustered ions such as M^+L_n or $M^+L_n(H_2O)_x$ entering the chamber can be partially declustered to a given desired species such as M^+L, by applying a high ion drift field between the tip of CAP and the bottom plate IN of the low pressure source LPS.

(3) The ion thermalization chamber IT is at the same pressure as the

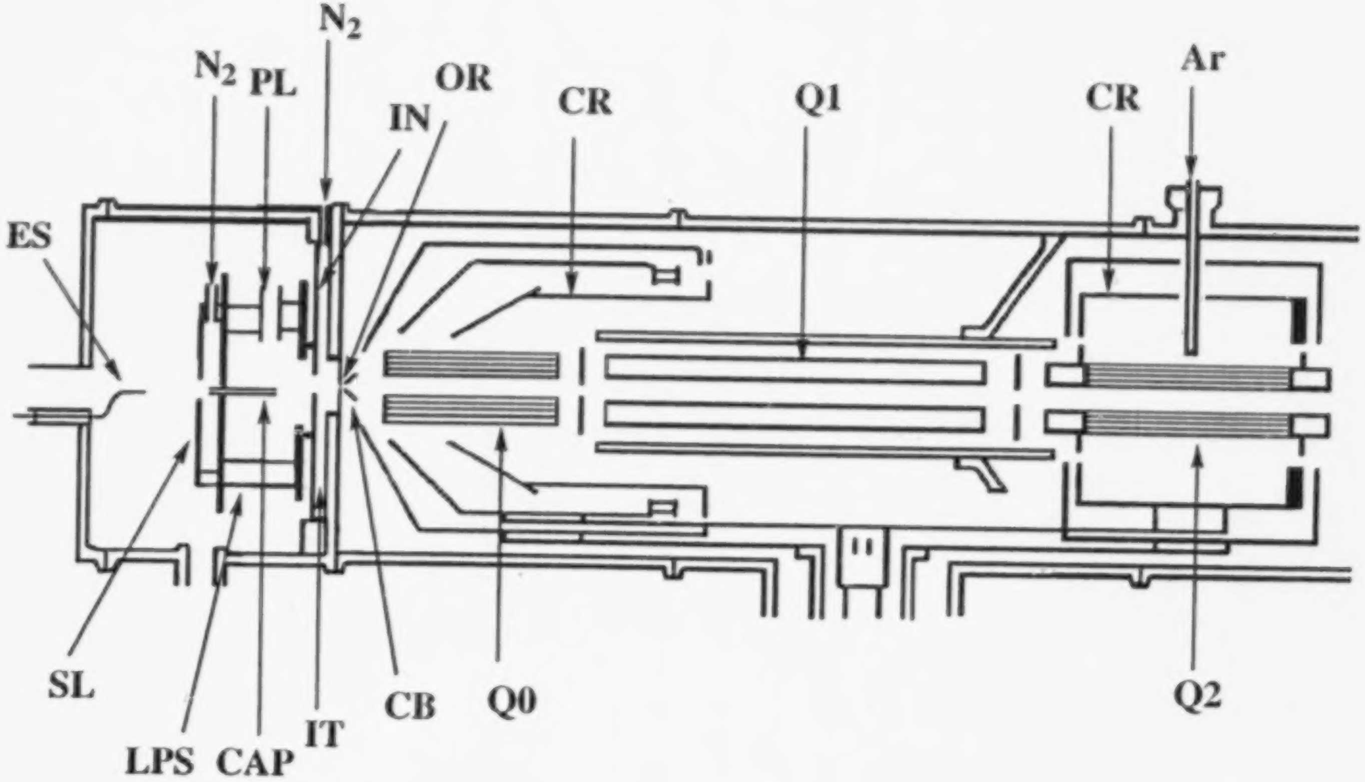

Figure 5.1 Front end of Apparatus. Electrospray generator, ES, consisting of electrospray capillary with stainless steel tip at high electric potential, generates charged droplets and ultimately gas phase ions. ES is partially surrounded by glass tube providing flow of dry air. Capillary, CAP, transfers gas and ions from 1 atm to a low pressure ion source LPS maintained at 10 torr. Ions can be partially declustered by applying a high drift field between CAP and interface plate IN. Ions are allowed to thermalize in low drift field, 10 torr pressure, ion thermalization chamber IT. Orifice OR, 100 um diameter leads to vacuum. First electrode and skimmer, CB. RF only ion guide quadrupole Qo. First quadrupole Q1. Cryosurfaces CR for cryopumping.

low pressure source. The ion drift field between IN and the orifice OR is low, E/p < 6 Volt/(cm torr), so that thermalization of the ions can occur in this region.[20]

(4) The triple quadrupole mass spectrometer with which ions entering the cryopumped vacuum region are subjected to mass analysis and CID. Precursor ions selected by Q_1 are accelerated to the RF only collision cell Q_2 where product ions are created by collisions with Ar gas. A given product ion is mass selected with Q_3 and detected with an ion counting system.

It was shown[20] that the precursor and product -ion kinetic energy profiles are independent of the potential difference CAP-IN used for the declustering of ions in the low pressure ion source LPS. The profiles were also independent of the potential drop between IN and OR when E/p < 6 volt/(cm torr). This is consistent with the assumed ion thermalization in the IT chamber.

It was found[20] that the kinetic energy profiles of the precursor ions are somewhat broadened, *i.e.* develop a tail towards higher kinetic energies. The broadening increased with the magnitude of the radial DC field in the first quadrupole Q_1. Collisions of the parent ions with neutral gas molecules of the gas jet present in Q_1, were assumed to be responsible for the broadening.[20] The broadening was reduced by working at low radial DC fields, *i.e.* low mass resolution in Q_1. It was found, in the present work, that the broadening could be further reduced by selecting a specific offset potential for the Q_1 quadrupole, *i.e.* by controlling the axial kinetic energy of the precursor ions entering Q_1. For an ion of mass to charge ratio, m/z = 110, the selected kinetic energy was typically 12 eV. The selected energy decreased as m/z decreased. The exact cause for the observed behaviour is under investigation.

It was also established[20] that collisions of the ions with gas molecules in the front end space between the electrodes OR, CB, Q_0 lead to kinetic energy broadening. This broadening was eliminated by setting equal potentials to OR, CB, Q_0. While the mass analyzed parent ion intensity is reduced under these conditions, the signals obtained, ~20000 ions/sec, are sufficient for the threshold measurements.

The collision gas argon was at a pressure of ~0.1 m torr (collision cell length 8 cm). At such a pressure single collisions are dominant and the contribution of double collisions to the foot of the threshold curve are negligible. This was verified by making threshold measurements at decreasing pressures and observing that the E_o value obtained increased by less than 0.02 eV for a decrease of the pressure from 0.2 to 0.1 m torr.[20]

b. Determination of threshold energies E_o.

Determinations of the energy thresholds E_o were obtained by fitting the product ion energy profiles with the CRUNCH program developed by Armentrout and coworkers.[18,22] The fitting procedure is based on the equation:

$$\sigma = \sigma_o \sum_i g_i (E + E_i + E_{rot} - E_o)^n / E \qquad (5.2)$$

where σ is the cross section, which is proportional to the observed product ion intensity at single collision conditions. E is the kinetic energy in the centre of mass frame. E_i is the internal vibrational energy of the precursor ion whose relative abundance at a given temperature is g_i, where $\sum_i g_i = 1$. E_o is the threshold energy, corresponding to the energy required for the dissociation reaction, *i.e.* eq. 5.1 in the present work , at 0°K.

The fitting procedure based on eq. 5.2 treats n and E_o as variable parameters which are determined through the best fit. The vibrational energies E_i are calculated from the frequencies of the normal vibrations of the precursor ion. The frequencies are generally obtained from quantum chemical calculations.

An important feature underlying eq. 5.2 is the assumption that due to the relatively long residence time of the excited ions in Q_2, dissociation at the threshold involves the process where the internal energy of the products is close to 0°K, *i.e.* essentially all the internal energy of the precursor ion is used up in the dissociation at the observed threshold.

The observed precursor ion kinetic energy profiles were fitted to a Gaussian distribution and the zero centre of mass kinetic energy was taken at the maximum of the Gaussian curve.

Results and Discussion

a. Results: Evaluation of the Threshold Energies. Effect of Kinetic Shift.

Threshold curves for the product ions Na^+ and K^+ from the dissociation of the sodium and potassium complexes M^+L are shown in Figures 5.2-5.8. The values of the exponents n and the E_o values obtained by fitting the data to the expression, eq. 5.2, are given in the Figures and Table 5.1. The vibrational frequencies for the M^+L complexes required for the evaluation of the internal energies E_i, see eq. 5.2, were obtained with *ab initio* calculations (3-21 G basis set) for $Na^+CH_3CONH_2$ and CH_3CONH_2 and the semiempirical MNDO for the other reactants). The frequencies used are given in Table 5.2. A temperature of 298K was assumed for the precursor ions.

Illustrations of alternate fitting results are given in Figure 5.2. The

Table 5.1 Energies for reaction: $M^+L = M^+ + L$ from CID threshold determinations.[a]

$M^+ = K^+$	$E^b_{o(OK)}$	ΔH°_{298} [b]	ΔH°_{298} [c]	ΔH°_{298} [d]	ΔH°_{298} lit.
Me_2CO	24.2	24.4	24.4	24.4	26.0[e]
Me_2SO	31.3	31.6	30.2	31.1	35±3[e]
$HCONMe_2$	32.0	32.0	27.1	29.5	31.0[e]
$MeCONH_2$	29.7	29.6	29.6	29.7	(26.2)[f]
MeCONHMe	32.3	31.9	28.3	30.4	(24.8)[f]
$MeCONMe_2$	32.9	32.2	25.5	29.0	31[e]
H_2NCH_2COOH	29.2	30.1	29.4	30.0	-
$M^+ = Na^+$					
$MeCONH_2$	34.3	34.7	34.7	34.7	(36.0)[g]
MeCONHMe	38.9	39.0	33.7	35.7	(38.4)[g]
$MeCONMe_2$	46.9	46.7	35.2	37.5	-
H_2NCH_2COOH	36.3	37.5	35.7	36.6	(38.5)[h]
$H_2NCH_2CONH_2$	45.1	45.1	39.5	41.4	-
$(H_2NCOCH_2)_2$	62.3	61.8	41.5	44.5	-
$H_2NCH_2CONHCH_2COOH$	64.6	64.7	40.1	42.9	-

[a] All energies in kcal/mol.

[b] Without correction for kinetic shift, E_o internal energy change, ΔH° enthalpy change for reaction eq. 5.1.

[c] With correction kinetic shift, two lowest frequencies, 30 cm^{-1}, for both K^+ and Na^+ complexes.

[d] With correction for kinetic shift, two lowest frequencies, 10 cm^{-1}, for Na^+ complexes and 5 cm^{-1} for K^+ complexes. This set is considered to be the best.

[e] Experimental determinations based on ion-molecule equilibria, Sunner et al.[8]

[f] Theoretical calculations, HF/6-31G, combined with a semiempirical correction. Roux and Karplus.[7]

[g] Theoretical calculations, HF/6-31G*, combined with a semiempirical correction. Roux and Karplus.[7]

[h] Theoretical calculations, 6-31+G(2d)MP2, Jensen.[28]

Table 5.2. Vibrational Frequencies.[a]

Acetone[b]	K$^+$Acetone[b]	DMSO[b]	K$^+$DMSO[b]	DMF[c]	K$^+$DMF[c]
	37		71		36
	69		81		45
	90		155		59
86	150	148	187	82	80
160	186	179	191	105	117
406	425	220	263	149	182
549	556	238	280	247	277
553	561	304	315	335	341
806	819	633	644	435	437
981	991	700	700	649	654
1019	1015	712	881	1024	1032
1201	1203	1027	1040	1036	1036
1257	1261	1061	1080	1160	1156
1315	1337	1104	1121	1166	1160
1553	1561	1155	1161	1169	1175
1562	1573	1493	1499	1190	1189
1627	1617	1520	1527	1404	1403
1630	1622	1610	1604	1426	1426
1638	1625	1623	1618	1431	1427
1662	1655	1628	1618	1432	1428
1940	1891	1643	1634	1433	1431
3199	3204	3239	3243	1520	1511
3206	3212	3240	3243	1527	1524
3249	3258	3342	3350	1540	1537
3258	3267	3342	3351	1567	1588
3306	3307	3345	3353	2083	2043
3307	3308	3347	3355	3215	3230
				3217	3231
				3236	3249
				3247	3254
				3267	3271
				3308	3318
				3325	3327

Table 5.2. Continued

AA[b]	K+AA[c]	Na+AA[b]	MAA[b]	K+MAA[c]	Na+MAA[c]
	44	92		29	55
	57	103		43	55
	67	124		57	101
147	142	328	108	103	111
451	360	489	137	131	133
530	417	591	194	173	174
590	448	609	308	302	304
596	583	710	457	423	457
735	616	849	619	156	159
874	1032	902	672	617	621
1090	1077	1128	682	651	652
1193	1099	1207	930	999	1000
1247	1220	1258	1051	1085	1085
1442	1425	1530	1190	1098	1098
1556	1436	1571	1192	1172	1170
1637	1483	1628	1262	1234	1233
1658	1542	1650	1289	1311	1308
1814	1804	1806	1380	1421	1421
1917	2056	1846	1554	1424	1422
3208	3268	3215	1596	1425	1423
3263	3276	3276	1630	1438	1436
3337	3346	3327	1658	1472	1476
3784	3608	3748	1663	1492	1482
3910	3630	3866	1686	1530	1530
			1708	1702	1707
			1895	2053	2040
			3198	3229	3233
			3205	3257	3259
			3248	3269	3269
			3262	3278	3279
			3322	3328	3328
			3344	3349	3349
			3807	3575	3568

Table 5.2. Continued

DMA^d	K$^+$DMA^d	Na$^+$DMA^d	Glycine^c	K$^+$ Glycine^c	Na$^+$ Glycine^c
	25	40		23	39
	35	45		53	59
	47	80		57	84
108	103	111	65	65	103
108	103	111	162	232	218
137	131	133	295	300	307
194	173	174	427	426	459
194	173	174	476	498	533
308	302	304	590	589	592
457	423	457	741	739	674
619	156	159	991	987	988
672	617	321	1000	1003	1002
682	651	352	1118	1148	1169
930	999	1000	1214	1213	1222
1051	1085	1085	1302	1310	1322
1051	1085	1085	1363	1363	1367
1190	1098	1098	1417	1390	1387
1192	1172	1170	1462	1456	1429
1262	1234	1233	1474	1471	1477
1289	1311	1308	1596	1609	1619
1289	1311	1308	1810	1810	1805
1380	1421	1421	2109	2084	2074
1554	1425	1422	3192	3195	3206
1554	1424	1422	3279	3255	3272
1596	1425	1423	3536	3538	3534
1630	1438	1436	3587	3581	3585
1658	1472	1436	3953	3974	3930
1663	1492	1476			
1663	1492	1476			
1686	1530	1482			
1686	1530	1530			
1708	1702	1707			
1895	2053	2040			
3198	3229	3233			
3205	3229	3259			
3248	3257	3269			
3198	3257	3233			
3205	3269	3259			
3248	3269	3269			
3262	3278	3279			
3322	3328	3328			
3807	3575	3568			

Table 5.2. Continued

Glycinamide^c	Na$^+$Glycinamide^c	Succinamide^c	Na$^+$Succinamide^c	Gly$_2$	Na$^+$Gly$_2$^{e}
	50		31		39
	73		49		42
	94		69		63
54	103	18	77	35	72
227	193	36	100	42	92
294	291	167	103	56	96
372	410	235	220	99	98
431	441	267	275	167	157
567	498	321	380	226	221
689	577	414	390	287	248
783	742	433	429	324	365
987	977	490	451	454	399
989	991	501	501	485	486
1128	1123	529	518	510	528
1214	1190	540	582	540	549
1262	1228	589	589	588	604
1298	1316	596	694	612	624
1359	1364	740	755	638	660
1457	1453	922	901	703	766
1466	1471	935	939	917	872
1513	1553	1048	1058	953	943
1812	1808	1065	1067	1006	962
1813	1811	1143	1168	1039	1030
2098	2045	1181	1196	1070	1055
3206	3200	1194	1216	1161	1164
3272	3266	1208	1231	1195	1199
3551	3547	1246	1264	1256	1272
3579	3593	1366	1404	1315	1313
3594	3613	1379	1415	1339	1336
3606	3627	1398	1458	1345	1349
		1404	1466	1381	1356
		1561	1538	1408	1418
		1564	1546	1431	1434
		1704	1806	1455	1442
		1705	1809	1474	1472
		1985	2054	1547	1575
		2000	2071	1644	1657
		3015	3222	1724	1722
		3019	3236	2001	1961
		3081	3293	2081	2062
		3093	3303	2952	2944
		3487	3592	2958	2980
		3524	3607	3024	3013
		3542	3635	3028	3038
		3546	3636	3416	3384
				3437	3441
				3475	3446
				3481	3486

Footnote to Table 5.2:

[a] The vibrational frequencies (in cm^{-1}) of the ligand and ion-ligand complexes were obtained by evaluating the hessian of the corresponding optimized geometries using the GAMESS program. Only frequencies below 1000 cm^{-1} are significant in the fitting procedure, see eq. 5.2, and in the calculation of the internal energies needed in eq. 5.3. Furthermore, the fitting procedure and internal energy calculations are not sensitive to the values of the frequencies and errors of 20% are expected to have only a small effect on the energy determinations.

[b] The vibrational frequencies were obtained from HF calculations done using a 3-21G basis set.

[c] The vibrational frequencies were obtained from semi-empirical calculations (MNDO).

[d] The frequencies for $CH_3CON(CH_3)_2$ (DMA), $K^+CH_3ON(CH_3)_2$ K^+DMA) and $Na^+CH_3CON(CH_3)_2$ (Na^+DMA) were estimated by comparing the calculated frequencies for CH_3CONH_2 (AA) and $CH_3CONHCH_3$ (MAA) and the corresponding metal ion complexes.

[e] The frequencies for $H_2NCH_2CONHCH_2COOH$ (Gly_2) and Na^+Gly_2 were obtained from semi-empirical calculations (AMI).

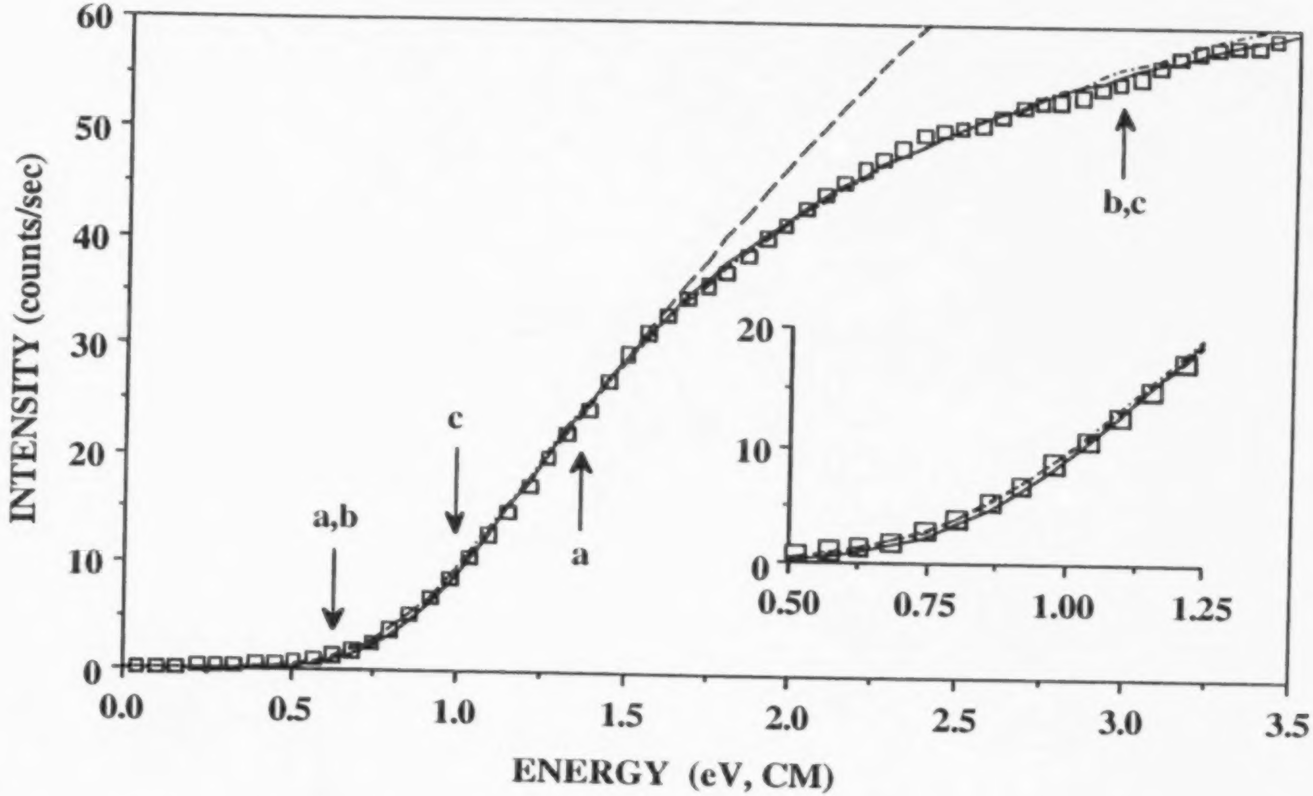

Figure 5.2 Appearance curve of K^+ from CID of K^+Acetone. Also shown are three calculated cross section curves (**a-c**), obtained by fitting the cross section model, eq. 5.2, to different portions of the appearance curve. Curve **a** (--), fitted from 0.6-1.4 eV, corresponds to n=1.46 and E_0=0.99 eV (22.8 kcal/mol). Curve **b** (---), fitted from 0.6-3.0 eV, corresponds to n=1.05 and E_0=1.09 eV (25.1 kcal/mol). Curve **c** (—), fitted from 1.0-3.0 eV, corrsponds to n=1.00 and E_0=1.11 eV (25.5 kcal/mol). Expanded scale used for insert at lower right in Figure provides a better view of the three curve fits at the threshold.

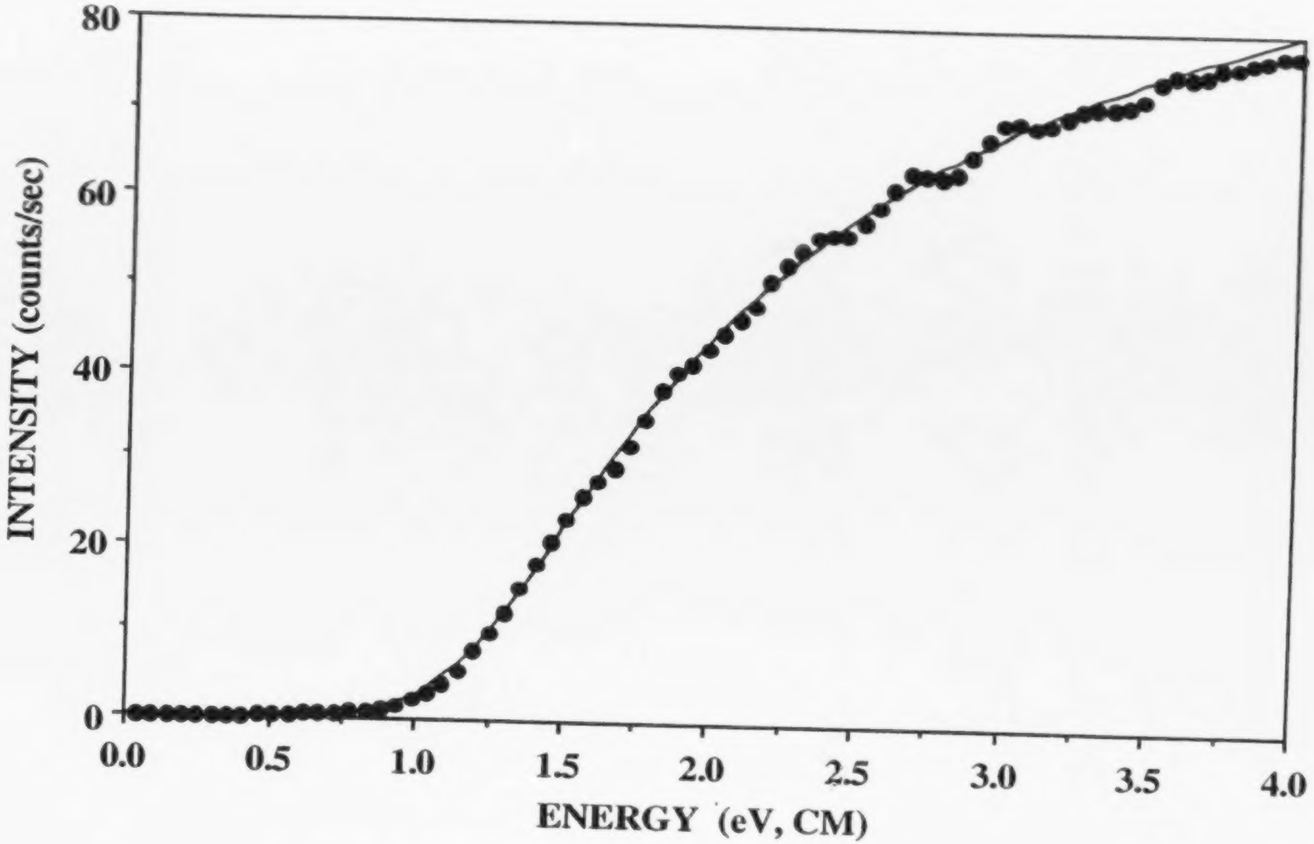

Figure 5.3 Appearance curve of K^+ from CID of K^+N-Methylacetamide. The calculated curve (solid line), fitted from 1.1-2.5 eV, corresponds to n=1.02 and E_0=1.40 eV (32.2 kcal/mol). Cross section model, eq. 5.2.

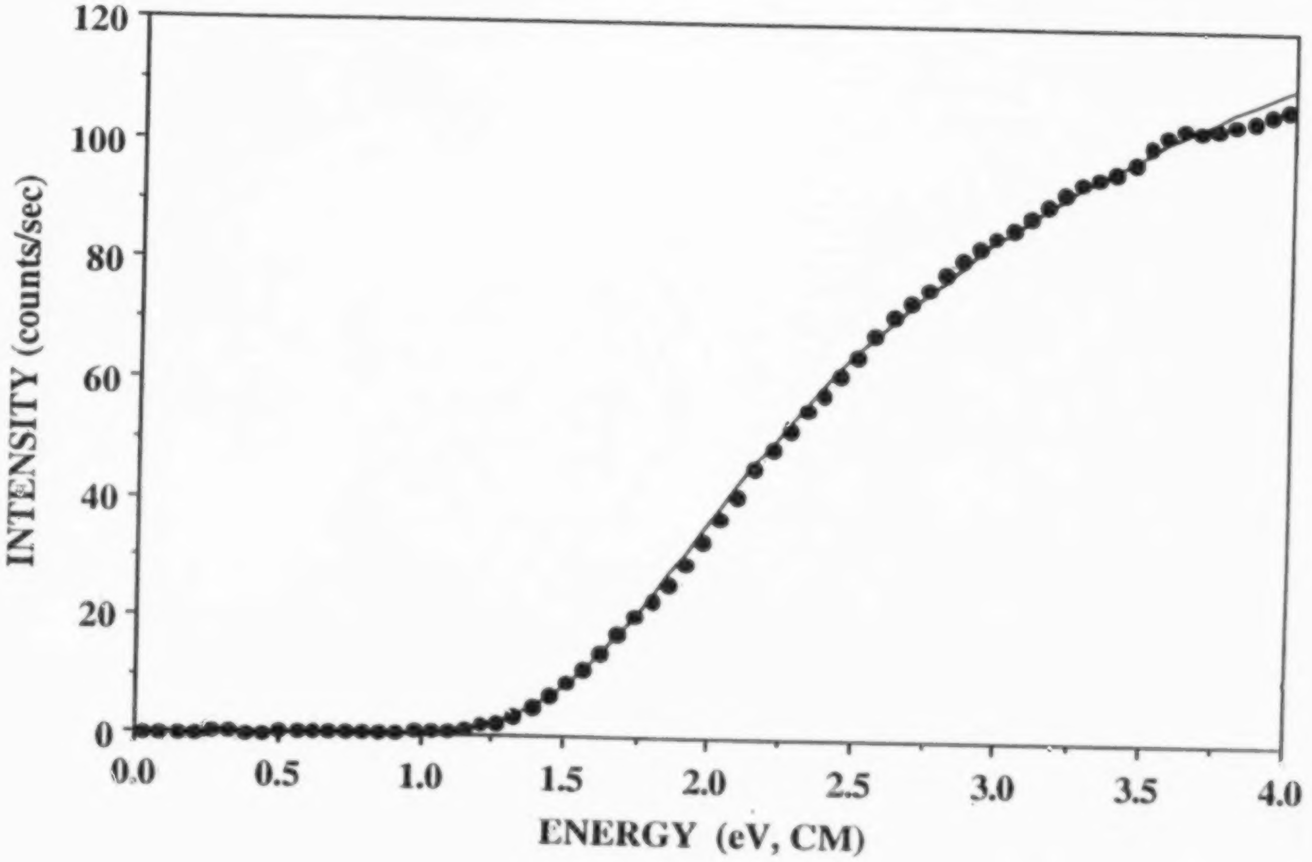

Figure 5.4 Appearance curve of Na^+ from CID of Na^+N-Methylacetamide. The calculated curve (solid line), fitted from 1.4-4.0 eV, corresponds to n=1.25 and E_0=1.69 eV (38.9 kcal/mol). Cross section model, eq. 5.2.

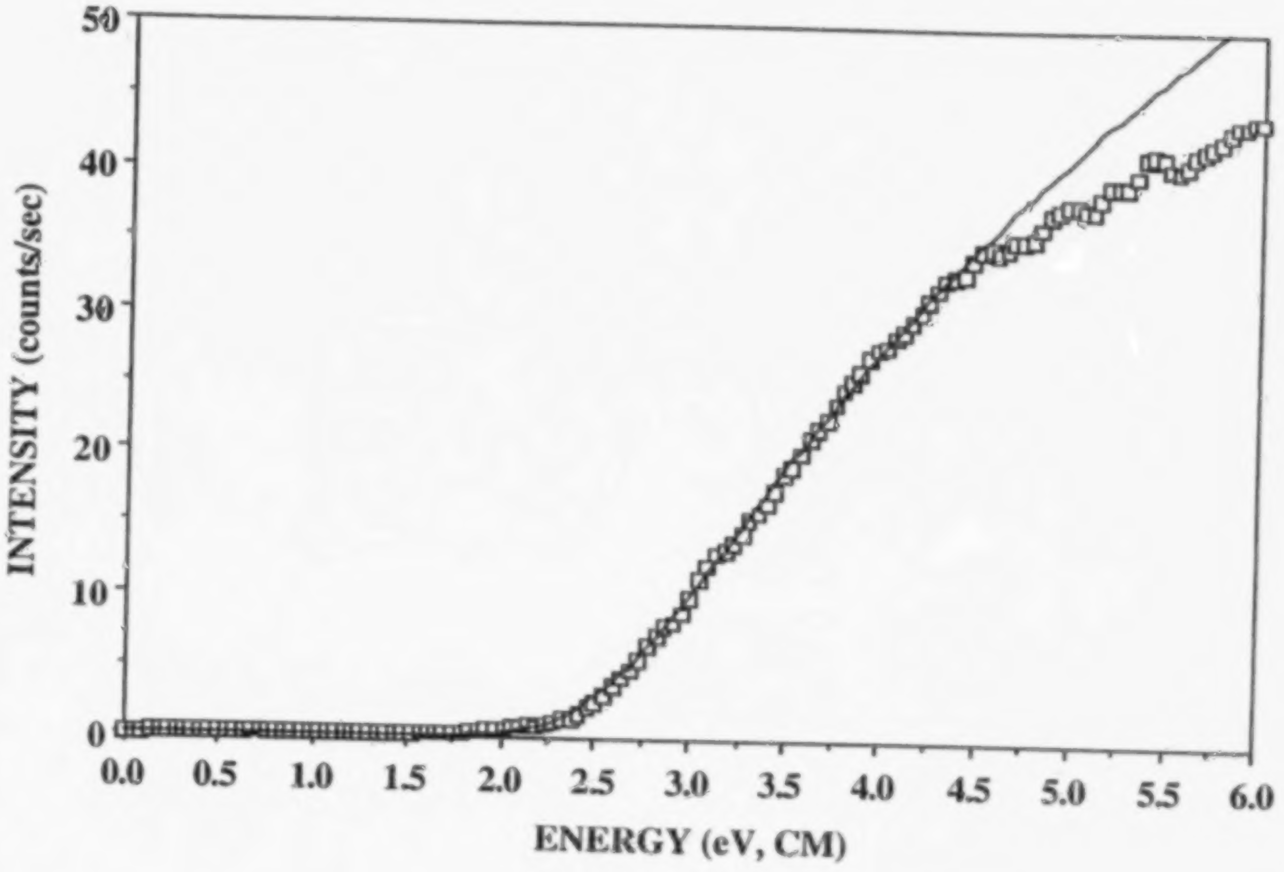

Figure 5.5 Appearance curve of Na^+ from CID of Na^+Succinamide. The calculated curve (solid line), fitted from 2.8-4.5 eV, corresponds to n=1.25 and E_0=2.70 eV (62.3 kcal/mol). Cross section model, eq. 5.2.

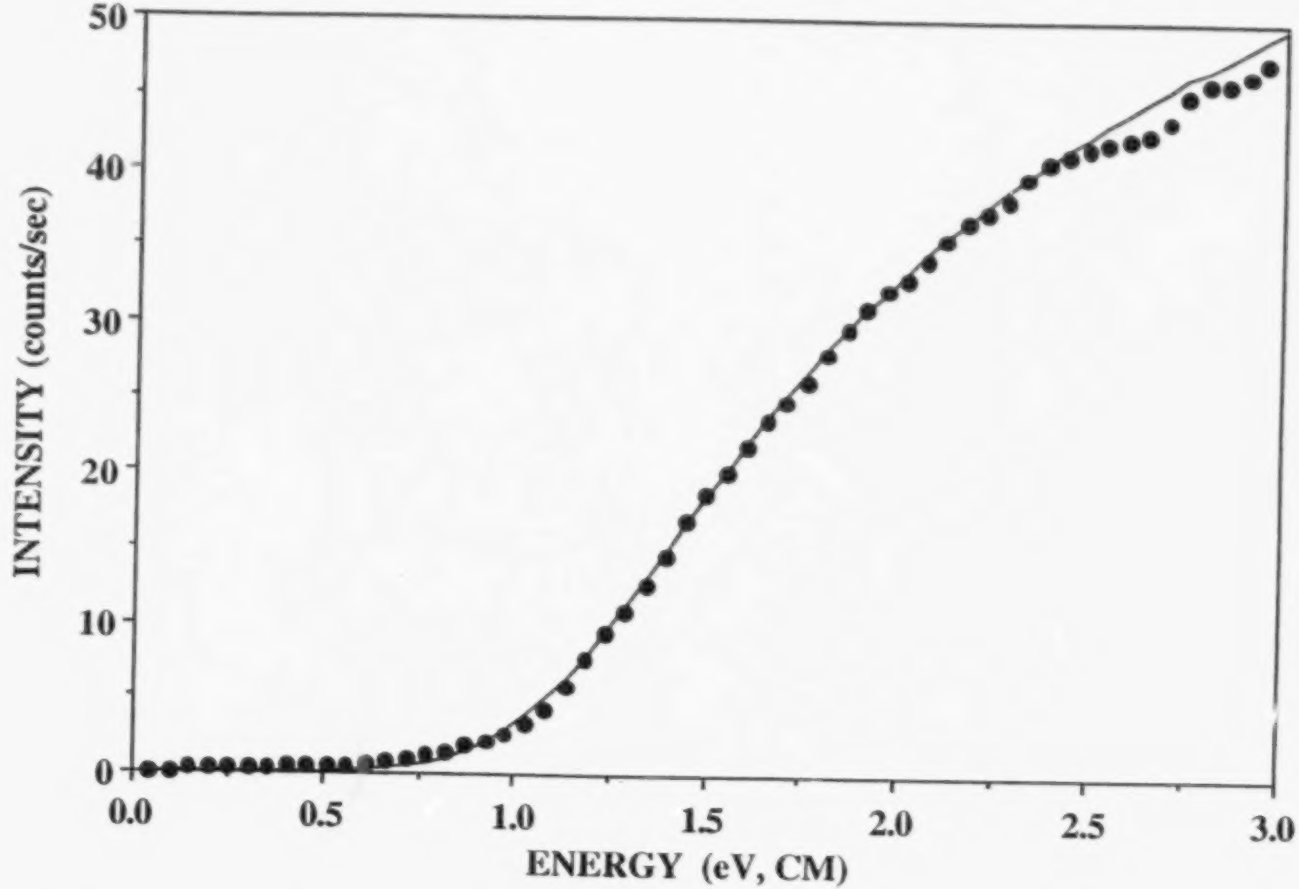

Figure 5.6 Appearance curve of K^+ from CID of K^+Glycine. The calculated curve (solid line), fitted from 1.2-2.0 eV, corresponds to n=1.07 and E_0=1.27 eV (29.2 kcal/mol). Cross section model, eq. 5.2.

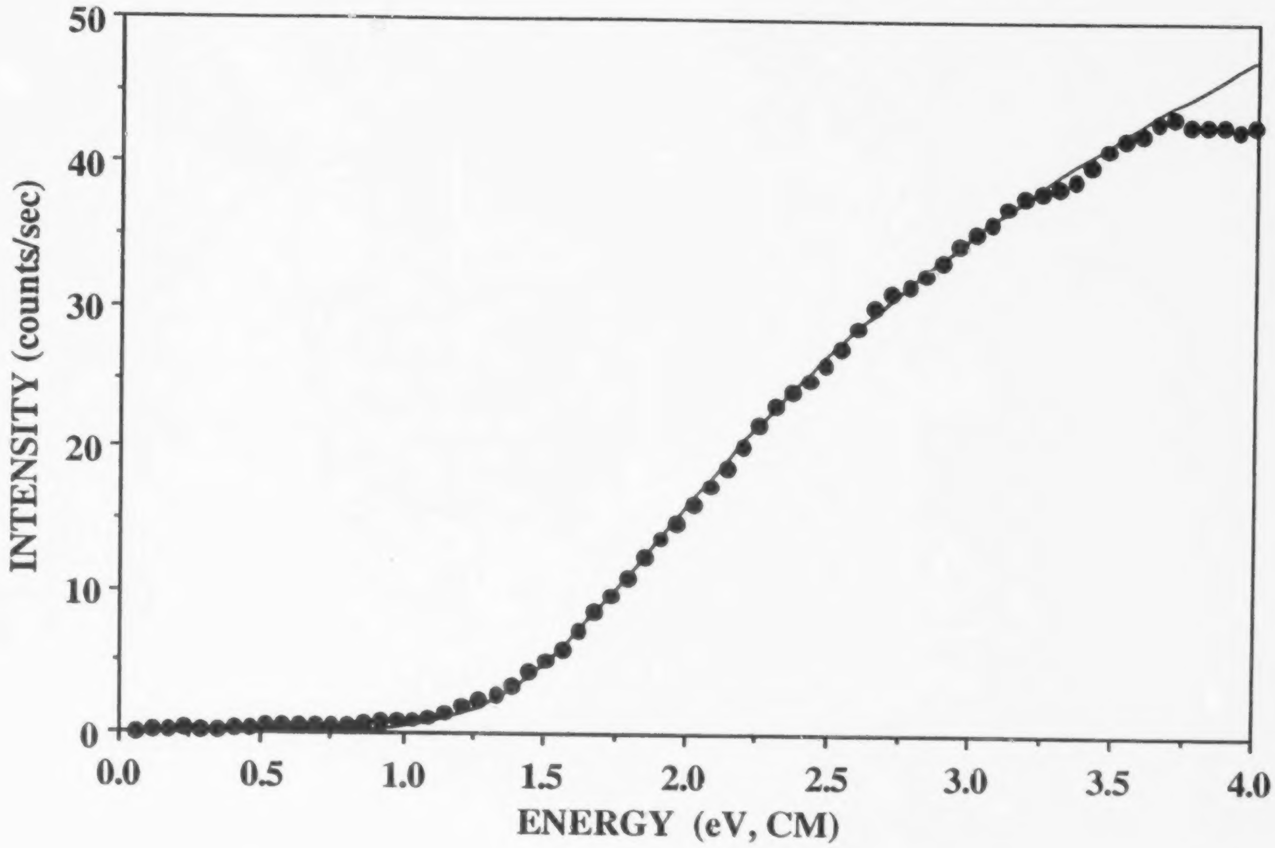

Figure 5.7 Appearance curve of Na^+ from CID of Na^+Glycine. The calculated curve (solid line), fitted from 1.6-3.4 eV, corresponds to $n=1.20$ and $E_0=1.58$ eV (36.3 kcal/mol). Cross section model, eq. 5.2.

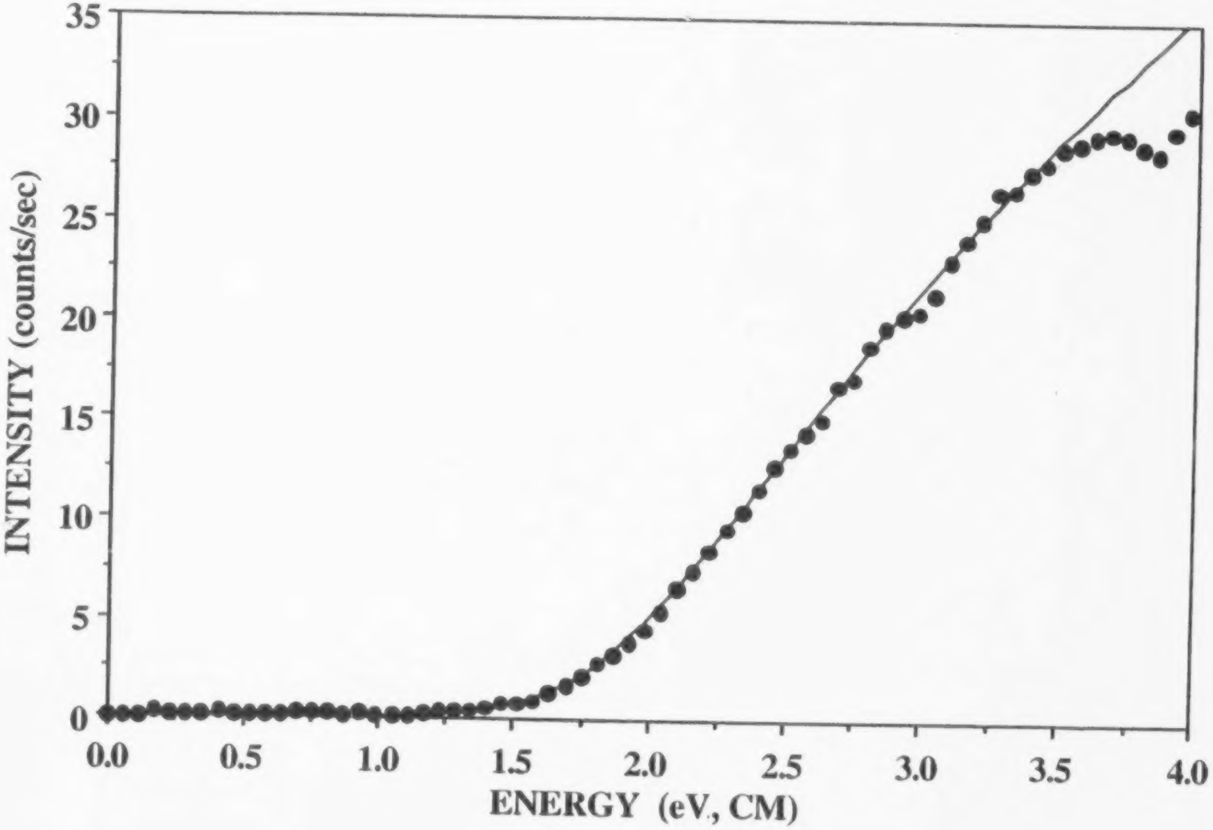

Figure 5.8 Appearance curve of Na^+ from CID of Na^+Glycinamide. The calculated curve (solid line), fitted from 2.0-3.5 eV, corresponds to $n=1.31$ and $E_0=1.96$ eV (45.1 kcal/mol). Cross section model, eq. 5.2.

different values of n and E_o for K^+(Acetone) given in the Figure result from different choices of the range of points, at the foot of the threshold and near the maximum of the cross section, which were included in the fit.

In general, we have excluded the experimental points of very low intensity at the very end of the foot because, these probably originate from precursor ions of higher than thermal energies.[20] The very small difference observed between the E_o values obtained for the fits b and c, E_o (b) = 1.09 eV, E_o (c) = 1.11 eV which differ by points excluded at the foot, provide assurance that points of very low intensity at the foot can be excluded. The relatively close values for the fits a and b, E_o (a) = 0.99 eV,. E_o (b) = 1.09 eV demonstrate that inclusion of experimental points past the steeply rising portion of the curve does not affect the E_o values very significantly. Thus, while there is a certain arbitrary element in the choice of the fit, the E_o values agree within ~0.1 eV. The E_o values quoted in Table 5.1 correspond to the averages between two or three of the fits, considered as best. We assign an error of ±0.1 eV to these results.

We have included the thermal rotational energy of the precursor ion, $E_{rot} = 3/2\ RT$, see eq. 5.2, in our curve fitting procedure. Armentrout et al[24] who fit the threshold curves right to the very bottom of the threshold, do include this term. Squires et al[19] who omit points from the bottom *i.e.* the foot of the curve, which are presumed to be due to above thermal ions, do not include the rotational energy, making the assumption that the rotational energy will affect only the bottom of the curve *i.e.* the portion that is omitted from the fit. Since in our experiments we also don't fit the foot of the curve, following Squires et al, we should have omitted the rotational energy. However, the transition states involved in the present work, *vide infra*, are expected to have two very large moments of inertia, and since the angular momentum quantum number is conserved, a decrease of rotational energy for these rotations is expected and this energy will be converted into internal energy, on formation of the transition state. Therefore, these two rotational energy terms (2 x 1/2 RT) should be included in the fit. For simplicity, we have included 3/2 RT.

The E_O values, which correspond to the dissociation energy at 0°K, were converted to enthalpy changes at T = 298°K, with use of eq. 5.3, (Armentrout[22]).

$$\Delta H^\circ = E_O - E_{vib}(ML^+) + E_{vib}(L) + 5/2\ RT \qquad (5.3)$$

Eq. 5.3 is based on a thermodynamic cycle for the enthalpy change, ΔH°, of reaction 5.1 between 0°K and T°K. The required vibrational thermal energies $E_{vib}(ML^+)$ and $E_{vib}(L)$ were evaluated from the corresponding vibrational frequencies which are given in Table 5.2. Due to cancellation of heat capacity terms in the cycle, the values of E_O at 0°K and ΔH° at 298K turn out to be very similar.

The fits of the experimental profiles with eq. 5.2 are based on the assumption that the energized reactant ions, whose total energy is equal or larger than E_O, will decompose within the residence time t of the ion before entering the mass analyzer Q3. For the present apparatus, t is estimated to be between 30 and 40 μs and complete dissociation within that time, for ions with energies just above E_O can be expected only for relatively small polyatomic ions. Ions with many internal degrees of freedom will attain the required dissociation rate only at internal energies which are somewhat higher than E_O. This "kinetic shift",[23] if not taken into account, will lead to E_O values that are too high.

Armentrout et al[24] have developed a method with which the kinetic shift can be taken into account in the curve fitting procedure. This fitting procedure includes only to the fraction of the precursor ions which decompose during the residence time t. This fraction is given by, 1-exp(-kt), where k is the rate constant for the decomposition. k can be evaluated with the RRKM formalism.[25] k is a function of the internal energy of the ion and the threshold energy E_o *i.e.* $k(E+E_i-\Delta E-E_o)$ where E is the kinetic energy in the centre of mass frame, E_i is the internal energy of the ion prior to the collision and ΔE is the centre of mass kinetic energy which was not converted into internal energy of the ion. The dependence of ΔE on the centre of mass energy, E, was obtained[24] on the basis of an assumed relationship, since an accurate theoretical expression for that dependence is not available.

For the evaluation of k with RRKM one needs to know the vibrational frequencies of the transition states occurring in reactions eq. 5.1. These were estimated as follows. Examination of the frequencies of the M^+L species in Table 5.2 shows that these contain three lowest frequencies which are associated with motions of M^+ relative to L, while the rest of the frequencies are all quite close to those of L. Since the transition state for the dissociation is a "late" transition state which resembles the separated M^+ and L, its frequencies can be obtained by dropping one of the three low frequencies of M^+L and reducing the remaining two to low values. Energy changes, based on fits of the experimental threshold curves obtained with this procedure are given in Table 5.1.

The energy values obtained with the correction for the kinetic shift are dependent on the choice of the value of the two lowest frequencies of the transition state. Two sets of kinetic shift corrected ΔH° values are given in Table 5.1. The first set uses 30 cm^{-1} for all K^+ and Na^+ complexes. This frequency was based on the choice of 25 cm^{-1} made by Wenthold and Squires in a study of the CID of chlorophenyl radical anions[26] leading to Cl^- as product ion where a late transition state is also expected to occur. The authors[26] made the choice of 25 cm^{-1} on the basis of literature data for experimentally measured $\Delta S^\ddagger$ values of similar reactions.

There are significant differences between the chloride dissociation and the dissociation of the alkali ion-ligand complexes. The ion-dipole and induced dipole interaction which dominate the bonding in the alkali complexes involve weaker but longer range forces. Furthermore, the bonding modes involving the alkali ion and the ligand have lower frequencies due to the less directional character of the electrostatic, relative to the covalent bond. At the large distances between the ligand and the alkali ion expected for the transition state, the frequencies associated with the bonding should be considerably lower than is the case for the chlorophenyl anion transition state.

To obtain frequencies for a looser transition state, the following procedure was used. ab-initio calculations at the 3-21 G level of the energies and frequencies of the complex, $Na^+.CH_3CONH_2$ were performed for different ion-oxygen atom distances extending from the equilibrium distance (2Å) to a maximum distance of 14Å. For this distance, the bond energy of the complex had reduced to ~2% of the equilibrium distance energy. At this distance, the average of the two lowest frequencies, which did not correspond to the reaction coordinate, was ~10 cm^{-1}. Assuming that the contribution of the rotational barrier to the transition state energy is very small, such that the transition state occurs very near to the complete dissociation, the value of 10 cm^{-1} can be adopted for the two lowest transition state frequencies. For the K^+ complex, the frequencies should be somewhat lower and a value of 5 cm^{-1} was chosen. ΔH° values obtained with these frequencies for all the Na^+ complexes and K^+ complexes are given in Table 5.1, see second last column, $\Delta H^{\circ d}$.

The entropy change associated with the formation of the transition state at 1000 K, $\Delta S^\ddagger_{1000}$, is often quoted[26] and used as a measure of the "looseness" of the transition state, where a loose transition state is assumed to have a value, $\Delta S^\ddagger_{1000} > 0$. The vibrational frequencies used for the transition state of $Na^+.CH_3CONH_2$, lead to a $\Delta S^\ddagger_{vib} \approx 3.7$ cal/(degree.mol). The transition state has two moments of inertia which are much larger than those for the precursor ion and this rotational change leads to $\Delta S^\ddagger_{rot} \approx 5$ cal/(deg mol), for a total of $\Delta S^\ddagger_{1000} = 8.7$ cal/(deg mol). This value corresponds to a very loose transition state and appears appropriate for the electrostatically long range bonding prevailing in the present ion-ligand complexes.

Comparison of the ΔH° data without and with kinetic shift correction, Table 5.1, provides an illustration for the magnitudes of the corrections. The corrections for small ligands, Me_2CO, Me_2SO, $MeCONH_2$ are small, *i.e.* less than 1 kcal/mol and the exact value of the frequencies used is not important. Larger corrections are required for the bigger and the more strongly bonded ligands. Succinamide $(H_2NCOCH_2)_2$ is an extreme case where the strong bonding and the large size of the ligand require a correction which is: 15-20 kcal/mol. Due to the uncertainty of the choice for the transition state frequencies, the ΔH data for this compound might be in error by as much as ±5 kcal/mol.

The choice of the two lowest frequencies for the Na^+ complexes (10 cm^{-1}) and K^+ complexes (5 cm^{-1}), although justified to a certain extent in the discussion above, is also a semiempirical choice. As will be seen in the next section, these values lead to the closest agreement with available ΔH° data in the literature.

A somewhat different procedure was used in a very recent CID threshold study of $Li^+(CH_3OCH_3)_x$ complexes, by Armentrout and coworkers.[27] These authors also used the frequencies of the complex as the starting point for the transition state frequencies. For x=1, they dropped the frequency which corresponded to the reaction coordinate and divided the two other lowest frequencies by 2 and by 10 obtaining thus two sets of frequencies. The two threshold values obtained with these two choices were considered as the limits of the true value.

The quadrupole collision cell used in the present work has some drawbacks relative to the octapole cell used by Armentrout and coworkers.[18] These have been discussed.[18] The major advantage of the octapole is the type of energy well that it produces. The AC potential well in the octapole increases very slowly, inverse sixth power, with radial distance R, from the octapole axis, while in the quadrupole, this field increases much faster, with the inverse square power of R. The flat bottom of the octapole well, leads to a lesser pick up of kinetic energy in the radial direction by ions which are off centre from the multipole axis. Part of the tailing towards low energies observed in the threshold curves Figure 5.2-8 is undoubtedly due to pick up of such kinetic energy in the quadrupole cell Q_2. However, the tailing is small and can be avoided by omitting points at very low energies, see Figure 5.2-3 and Discussion. Evidence that the tailing due to excess internal energy in the precursor ions is small is provided by a comparison of the theoretical fit based on eq. 5.2 and the experimental points, see Figures 2-7. The experimental points at the very onset coincide quite closely with the theoretical fit. While the accuracy achieved with the quadrupole trap is lower than that obtained with the apparatus of Armentrout,[18] the main uncertainty in the data obtained for the measurements which involve larger molecules is not the energy spread but the modelling of the kinetic shift.

Squires and his coworkers[19] who have used a triple quadrupole for threshold measurements for many years have shown that such an apparatus can provide many measurements of great interest, with sufficient accuracy. The present apparatus allows threshold measurements involving a large variety of ions that at present can be obtained only by electrospray. We believe this capability justifies its use even at the cost of some reduced accuracy of the measurements.

b. Comparison of threshold based energies with literature data. Types of bonding present in the complexes

The ΔH^{o}_{298} data obtained from the CID thresholds, discussed in the preceding section, can be compared with previous determinations in the literature.[7,8,28] Previous determinations are available from ion equilibria studies[8] for complexes of potassium with acetone, dimethyl sulfoxide, dimethylformamide and dimethylacetamide, see Table 5.1. There is relatively good agreement between the equilibrium derived ΔH° values and the present CID results, particularly so with the set shown in the second last column, $\Delta H^{\circ d}$, which we consider as the best values and which were obtained with the low frequency choice for the transition states. These CID vlaues are found to be ~1.5 kcal/mol lower than the equilibrium data. Only for dimethylsulfoxide is there a larger difference of ~4 kcal/mol. However, the error limits given for the dimethylsulfoxide equilibrium determination[8] are quite high ±3 kcal/mol. Examination of the original data[8] indicates that the slope of the van't Hoff plot was based on experimental points covering a narrow temperature range. In such cases, the ΔH_1^o values obtained are less certain than the ΔG° values at the experimental temperature. The experimental points[8] are also compatible with a lower ΔH_1^o and a lower ΔS_1^o value. A lower ΔH_1^o value is also suggested by a correlation with lithium ion affinities determined by Taft and coworkers.[29,30] A plot of the Li^+ affinities[29] versus ΔH_1^o values involving K^+ complexes determined by ion equilibria,[8-10] leads to a fairly good correlation. This correlation indicates for L=Me_2SO a value of $\Delta H_1^o \approx 31$ kcal/mol, while the value $\Delta H_1^o = 35$ kcal/mol lies outside the curve. We conclude that the CID threshold result of 31.1 kcal/mol is to be preferred over the equilibrium value.[8]

Energy values from theoretical calculations, HF/6-31G, obtained by Roux and Karplus[7] are available for K^+ and L=acetamide (26.2 kcal/mol) and N-methylacetamide (24.8 kcal/mol). Both of these values are lower than the threshold results (29.7 kcal/mol and 30.4 kcal/mol). However the authors[7] were primarily interested in developing pair potential functions for molecular dynamics simulations and therefore did not refine their ab initio calculations as much as they could have. The values[7] quoted in Table 5.1 are not the actual ab initio results which were considerably higher, but results obtained after a semiempirical correction based on the experimental and theoretical dipole moment.[7] Therefore, we believe that the CID threshold results are to be preferred.

Roux and Karplus[7] have obtained energy values (HF/6-31G*) also for the sodium ion complexes with acetamide (36.0 kcal/mol) and N-methylacetamide (38.4 kcal/mol). Also in this case, the semiempirical correction was applied to obtain the quoted results. These results are somewhat higher than the threshold values of 34.7 and 35.7 kcal/mol. Again, we believe that the threshold results should be preferred.

A theoretical result obtained by Jensen[28] is available for the complex of the sodium ion with glycine (H_2NCH_2COOH). The calculations performed at the MP2/6-31G* and MP2/6-31+G(2d) level predict a complexation energy of 38.5 kcal/mol. A zero point energy correction was not included, but the correction should be small. Also, the conversion from ΔE at 0°K to ΔH° at 298 is expected to be small (~1.2 kcal/mol), see Table 5.1. This theoretical result, which is ~2-3 kcal/mol higher than the threshold result (36.6 kcal/mol) is within the expected combined error limits of the two determinations. Bouchonnet and Hoppilliard[31] have also performed calculations for the Na^+.Glycine complex. These authors carried their calculations only to the MP2/6-31G* level at which they obtained an energy of 45.2 kcal/mol. A very similar result (46.0 kcal/mol) was obtained by Jensen[28] with the same basis set. However, when the calculation was carried to the higher, MP2/6-31G+(2d) level, Jensen obtained the value, 38.5 kcal/mol, which is quoted in Table 5.1 and used in the present discussion.

The structures of the sodium and potassium ion complexes and their relationship to the observed bond energies are of interest and will be discussed in the following text. All ligands in Table 5.1 except dimethylsulfoxide, which will not be discussed, can be considered as substituted carbonyl compounds. Because of the expected dominance of electrostatic interactions and the large bond dipole and polarizability of the carbonyl group, the major contribution to the bonding in the complex should be due to this group. The other polar groups *i.e.* -NH_2, $NHCH_3$, $N(CH_3)_2$ and OH, also make contributions to the bonding as indicated by the observed changes of ΔH_1^o values in Table 5.1.

Acetone may be considered as the simplest of the ligands involved. Unfortunately, recent theoretical results for the structure and energies of the acetone sodium and potassium ion complexes do not seem to be available. Early work[32] for the Na^+ complex predicts that the ion lies on the same axis as the C-O bond, as expected on the basis of electrostatics. The same structure can be expected for the potassium complex.

The bond with acetamide as the ligand, is stronger. An increase from 24.4 kcal/mol (acetone) to 29.7 kcal/mol (acetamide) is observed for the potassium ion complexes, Table 5.1. The theoretical calculations of Roux and Karplus[7] predict a structure in which the Na^+ ion is close to coaxial with the C-O bond. There is a tilt of a few degrees away from the C-O axis, in the plane of the N-C-O atoms as shown in structure I. This tilt approximately aligns the ion with the axis of the molecular dipole of acetamide, which is due to the combined effect of the C-O and the C-N partial charges, the latter being due to the partial electron pair shift from the lone pair of the nitrogen to form a partial C-N π bond.

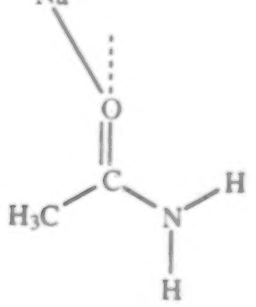

I

Substitution of H with methyl on the nitrogen in acetamide may be expected to strengthen somewhat the interaction with the sodium and potassium ion due to electron donation by the methyl group and to the increased polarizability of the ligand. Lithium ion affinities determined by Taft et al.[29,30] exhibit such increases. Thus, the Li affinity increases by ~3.4 kcal/mol from acetamide to N,N-dimethylacetamide.[29] For Na^+ this value may be expected to become reduced by a factor of ~2/3 on the basis of comparisons between energies of Li^+ and Na^+ complexes.[33] This leads to an expected increase of 2.3 kcal/mol between Na^+ acetamide and Na^+ dimethylacetamide which is close to the observed difference of 2.8 kcal/mol between the corresponding ΔH^{d}_{298} values in Table 5.1. It is important to note that in the absence of a kinetic shift correction, see ΔH^{b}_{298} column, an increase of 12 kcal/mol would have been predicted which is clearly an erroneous result.

Methyl substitution in the potassium acetamide complexes should have a smaller effect roughly 1/2 to 2/3 of the effect expected for sodium because of the increasing remoteness of the methyl groups from the positive charge. On this basis one can expect an increase by ~1.5 kcal/mol for two methyl substitution. The observed ΔH^{d}_{298} values are, 0.7 kcal/mol increase for the first methyl and a decrease of 1.4 kcal/mol for the second methyl. This is probably an erroneous trend but the expected changes are small *i.e.* within the experimental error of ±3 kcal/mol of the threshold determinations.

The threshold energies of the Na^+ or K^+ complexes with acetic acid were not determined. They are expected to be lower than those for acetamide because the more electronegative oxygen atom leads to significantly lower π and σ electron donation from -OH relative to $-NH_2$. The relatively high ΔH_1^o values observed for the complexes of K^+ and Na^+ with the α amino acetic acid (glycine) indicate that the α amino group makes an important contribution to the bonding of the complex and this suggests dicoordination involving the carbonyl and the amino group as shown in structure II.

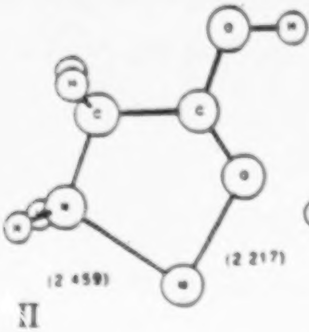

II

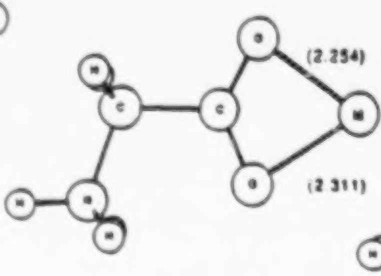

III

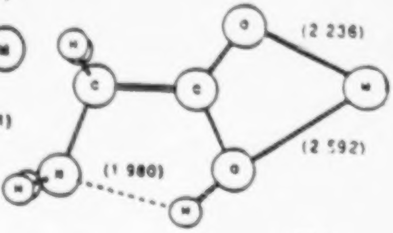

IV

The theoretical calculations for the sodium glycine complex by Jensen[28] at the MP2/6-31G* level predict structure II to be the most stable one. The distances, shown in Å, indicate a stronger bond to the carbonyl oxygen. Two other structures, III and IV, have only slightly lower stabilities. The glycine zwitterion structure III is only 2.2 kcal/mol higher in energy while the related structure IV in which a proton transfer has not occurred but a hydrogen bond interaction is present, is higher by 4.7 kcal/mol.[28] Very similar results were obtained also by Bouchonnet and Hoppilliard.[31] The variety of interactions leading to similar bond energies is interesting. Thus, the lowest energy structures II and III provide information on the interactions of a sodium ion with the N-terminal (structure II) and C-terminal (structure III) of neutral peptides.

The bond energy of the glycinamide complex with sodium was also determined, Table 5.1. The enthalpy change obtained is 41.4 kcal/mol, which is close to 6 kcal/mol higher than the 36.6 kcal/mol value observed for the sodium glycine complex, Table 5.1. As pointed out above, a higher value is expected because the amide NH_2 group is a better π and σ electron donor than the -OH group of glycine.

Threshold based enthalpy changes for the sodium ion complexes with the dipeptide glycylglycine and the diamide of succinic acid (succinamide) were also obtained, Table 5.1. Theoretical calculations for these complexes are not available in the literature. Probable structures for the two complexes are shown below. Structure V for the succinamide is based on an optimized MNDO geometry determination, and structure VI was obtained using the AM1 method.

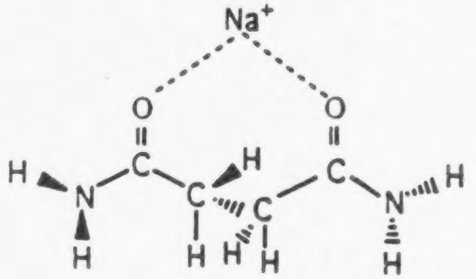

V

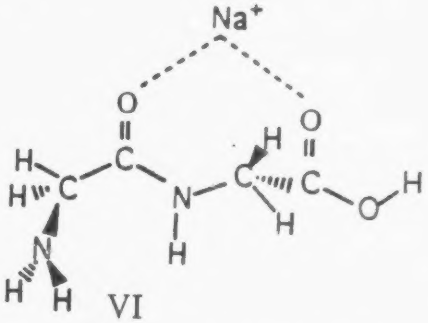

VI

The enthalpy change obtained for dissociation of the succinamide complex is $\Delta H_1^{o\,d}$ = 44.5 kcal/mol, Table 5.1. One can examine whether this value is reasonable. Geometric constraints in structure V hinder the optimum orientation of the two carbonyl groups relative to the Na$^+$ ion. Such an optimum orientation can be achieved by two separate acetamide molecules and the bond energy of such a complex would set the upper limit for the energy of the sodium succinamide complex. Data for the complexation of a second ligand molecule are often available from ion equilibria measuremenets.[8-10,34] Unfortunately, such results are not available for the sodium ion and acetamide. However, data are available for sodium and acetone.[34] These show that the enthalpy required to fully dissociate the two acetone complex equals 1.75 times the entlaphy for the dissociation of the one molecule complex. Applying this factor to sodium and acetamide and using $\Delta H_1^{\circ\, d}$ = 34.7 kcal/mol, one obtains 60.7 kcal/mol as an upper limit for the dissociation of the sodium succinamide complex. The experimental value, $\Delta H_1^{\circ\, d}$ = 44.5 kcal/mol, Table 5.1, equals approximately 75% of the upper limit. The orientation of the two C-O dipoles in structure V is far from optimal and a bond energy that is ~75% of the optimal energy appears quite reasonable.

The structure VI shown for the sodium-glycylglycine complex indicates strong interactions only with the two carbonyl groups. Examination of space models of glycylglycine indicates that an alignment of the three groups: the two carbonyl groups and the terminal amino group, leading to interactions with the sodium as a tridentate complex, cannot be achieved.

The bond energy of complex VI is expected to be fairly close to that of the succinamide complex V *i.e.* 44.5 kcal/mol. A somewhat smaller bond energy is expected for structure VI on the basis that succinamide has two NH_2 groups acting as π and σ electron donors while in glycylglycine there is only one amino group and a weaker donating hydroxy group. The value obtained, $\Delta H_1^{\circ\, d}$ = 42.9 kcal/mol, Table 5.1 is smaller, in agreement with the expected substituent effects.

On the basis of the above considerations, one may conclude that the interactions of a sodium ion with two adjacent carbonyl groups in a polypeptide will be somewhat stronger than those observed for the glycylglycine complex and very close to those for the succinamide complex because in the polypeptide and the succinamide complex stabilization is provided by two amide nitrogens.

Very recent and as yet unpublished work by Beauchamp and coworkers,[36] has provided evidence that the most stable structures of the sodium ion complexes with the tri and higher polyglycines are zwitter ion structures. These are similar to structure III for glycine, but include an additional interaction where the terminal ammonium group is close to and thus stabilizes the negatively charged carboxy group. No results for glycylglycine are available yet.[36] If the zwitter ion is the most stable structure also for glycylglycine, then the arguments given above concerning the agreement between the observed ΔH and expected bonding for structure VI will be invalidated, but only partially. Theoretical calculations[36] for the two structures indicate that the zwitter ion is lower in energy but not by much, see also structures II and III due to Jensen[28] which were very close in energy as discussed above. This "coincidence" of energies would partially validate the discussion of structure VI. The closeness of the ΔH values for the sodium complexes with succinamide where a zwitter ion structure is not expected and glycylglycine also supports this view.

Assuming that the glycylglycine complex has the zwitter ion structure, one might be concerned that structure VI will not provide the correct frequencies for the threshold fitting procedure. However, the frequencies of the zwitter ion structure and structure VI will not be all that different and since the fitting procedure is not very sensitive to the frequencies, the error will be small. Concerning the transition state, the choice of frequencies will be the same for both cases.

One may ask whether the gas phase experiments can be extended to complexes which more closely model the interactions of the sodium and potassium ions in the gramicidin channel. Achieving a close correspondence seems impossible at the present time. However, the gas phase experimental data may provide some limiting complexation energy values. According to 2D NMR evidence[35] and theoretical work,[2-4] the ion-channel interactions are principally due to interactions with four carbonyl oxygens of the peptide backbone and two water molecules which accompany the ion. A crude model for the optimum complexation energy may be provided by the complexation energy of the sodium ion with two suitable dicarbonyl molecules, such as glycylglycinamide (GGAm) and two water molecules, leading to: $Na^+(GGAm)_2(H_2O)_2$. Experimental work presently underway in our laboratory has shown that such a complex can be produced in the gas phase. The dihydration of the complex $Na^+(GGAm)_2$ can be determined by ion equilibria measurements,[16] while the complexation energies of the $Na^+(GGAm)_2$ would be amenable to CID threshold measurements and also ion molecule equilibria, for the addition of the second less strongly bonded GGAm molecule. Determination of the free energy changes rather than only the enthalpy changes will be desirable because the transfer of the sodium ion from an aqueous medium to the transmembrane channel depends on the free energy change.

References

1. Andersen, O.S. *Ann. Rev. Physiol.* **1984**, 46, 531.
2. Pullman, A. *Quat. Rev. Biophys.* **1987**, 20, 173.
3. Jordan, P.C. *J. Phys. Chem.* **1987**, 91, 6582.
4. (a) Roux, B.; Karplus, M. *Biophys. J.* **1991**, 59, 961. (b) *J. Phys. Chem.* **1991**, 95, 4856. (c) *J. Am. Chem. Soc.* **1993**, 115, 3250.
5. Kistenmacher, H.; Popkie, H.; Clementi, E. *J. Chem. Phys.* **1973**, 58, 1689. Chandrasekhar, J.; Spellmeyer, D.C.; Jorgensen, W.L. *J. Am. Chem. Soc.* **1984**, 106, 903.
6. Kebarle, P. *Ann. Rev. Phys. Chem.* **1977**, 28, 445.
7. Roux, B.; Karplus, M. *J. Phys. Chem.* **1991**, 95, 4856. (b) *J. Am. Chem. Soc.* **1993**, 115, 3250. (c) *J. of Computational Chemistry* **1995**, 16, 690.
8. Sunner, J.; Kebarle, P. *J. Am. Chem. Soc.* **1984**, 106, 6135.
9. Dzidic, I.; Kebarle, P. *J. Phys. Chem.* **1970**, 74, 1466.
10. Davidson, W.R.; Kebarle, P. *J. Am. Chem. Soc.* **1976**, 98, 6125.
11. Yamashita, M.; Fenn, J.B. *J. Phys. Chem.* **1984**, 88, 4451. Fenn, J.B.; Mann, M.; Meng, C.K.; Wong, S.F.; Whitehouse, C.M. *Science* **1985**, 246, 64.
12. (a) Jayaweera, P.; Blades, A.T.; Ikonomou, M.G.; Kebarle, P. *J. Am. Chem. Soc.* **1990**, 112, 2452-2454. (b) Blades, A.T.; Jayaweera, P.; Ikonomou, M.G.; Kebarle, P. *J. Chem. Phys.* **1990**, 92, 2900-2906. (c) Blades, A.T.; Jayaweera, P.; Ikonomou, M.G.; Kebarle, P. *Int. J. Mass Spectrom.. Ion Processes* **1990**, 102, 251-267. (d) Blades, A.T., Jayaweera, P.; Ikonomou, M.G.; Kebarle, P. *Int. J. Mass Spectrom.. Ion Processes* **1990**, 101, 325-336.
13. Bruins, A.P.; Covey, T.R.; Henion, J.D. *Anal. Chem.* **1987**, 59,

2642. Covey, T.R.; Bonner, R.F.; Shushan, B.I.; Henion, J.D. *Rapid Commun. Mass Spectrom.* **1988**, 2, 249. Huang, E.C.; Henion, J.D. *J. Am. Soc. Mass Spectrom.* **1990**, 1, 158.

14. Blades, A.T.; Kebarle, P. *J. Am. Chem. Soc.* **1994**, 116, 10761.
15. Smith, R.D.; Loo, J.A.; Edmonds, C.G.; Barinaga, C.J.; Udseth, H.R. *Anal. Chem.* **1990**, 62, 882.
16. Klassen J.; Blades, A.T.; Kebarle, P. *J. Phys. Chem.* **1995**, 99, 15509.
17. Klobukowski, M. *Can. J. Chem.* **1992**, 70, 589.
18. Armentrout, P.B. "Thermochemical Measurements by Guided Ion Beam Mass Spectrometry", in "Advances in Gas Phase Ion Chemistry", **1992**, Vol. 1, p. 83. Adams, N. and Babcock, L.M., Eds., JAI Press Inc., Greenwich, Conn. U.S.A.
19. Sunderlin, L.S.; Wang, D.; Squires, R.R. *J. Am. Chem. Soc.* **1993**, *115*, 12060; Mazinelli, P.J.; Paulino, J.A.; Sunderlin, L.S.; Wenthold, P.G.; Poutsma, J.C.; Squires, R.R. *Int. J. Mass Spectrom.. Ion Processes* **1994**, *130*, 89.
20. Anderson, S.G.; Blades, A.T.; Klassen, J.S.; Kebarle, P. *Int. J. Mass Spectrom.. Ion Processes* **1995**, *141*, 217.
21. Reid, N.M.; Buckley, J.A.; French, J.B.; Poon, C.C. *Adv. Mass Spectrometry B* **1979**, 8, 1843.
22. Dalleska, N.F.; Honma, K.; Armentrout, P.B. *J. Am. Chem. Soc.* **1993**, 115, 12125.
23. Chupka, W.A. *J. Chem. Phys.* **1959**, 30, 191.
24. Loh, S.K.; Hales, D.A.; Lian, L.; Armentrout, P. *J. Chem. Phys.* **1989**, 90, 5466; Hales, D.A.; Lian, L.; Armentrout, P. *Int. J. Mass Spectrom. Ion Processes* **1990**, 102, 269.

25. Robinson, P.J.; Holbrook, K.A. "Unimolecular Reactions", Wiley Interscience, N.Y., 1972.

26. Wenthold, P.G.; Squires, R.R. *J. Am. Chem. Soc.* **1994**, 116, 6401.

27. More, M.B.; Glendening, E.D.; Ray, D.; Feller, D.; Armentrout, P.B. *J. Phys. Chem.* **1996**, 100, 1605.

28. Jensen, F. *J. Am. Chem. Soc.* **1992**, 114, 9533.

29. Taft, R.W.; Anvia, F.; Gal, J.F.; Walsh, S.; Capon, M.; Holmes, M.C.; Hosh, K.; Oloumi, G.; Vasanwala, R.; Yazdani, S. *Pure and Appl. Chem.* **1990**, 62, 17.

30. The Li^+ affinity differences given in ref. 29 correspond to free energy differences *i.e.* changes in the $-\Delta G^\circ_1$ at 298 K for reaction 5.1.

31. Bouchonnet, S.; Hoppilliard, Y. *Organic Mass Spectrom* **1992**, 27, 71.

32. Weller, T.; Lochman, R.; Meiler, W. *J. Molecular Structure* **1982**, 90, 81.

33. Bojesen, G.; Breindahl, T.; Andersen, U.N. *Organic Mass Spectrom.* **1993**, 28, 1448.

34. Guo, B.C.; Conklin, B.J.; Castleman, A.W., Jr. *J. Am. Chem. Soc.* **1989**, 111, 6506.

35. Arseniev, A.S.; Bystrov, V.F.; Ivanov, T.V.; Ovchinmikov, Y.A. *FEBS Lett.* **1985**, *186*, 168.

36. Beauchamp, J.L. private communication.

Chapter 6

Collision-induced dissociation threshold energies of some protonated amino amides and small peptides*

Introduction

Tandem mass spectrometry (MS/MS) has become an important tool for elucidating the amino acid sequence of protonated peptides. The technique involves the sequential isolation of the precursor ion in the first stage of mass analysis, excitation of the ion to induce dissociation, and mass analysis of the resulting fragment ions. Excitation of the precursor ion is most commonly achieved by energetic collisions with a non-reactive gas, such as argon, and is referred to as collision-induced dissociation (CID). At collision energies compatible with a triple quadrupole mass spectrometer (<100 eV), protonated peptides dissociate primarily along the backbone at the amide bonds producing **b** ions which contain the N-terminus and are formally acylium ions, $H(-HNCHRCO-)_n^+$, and **y** ions which contain the C-terminus and correspond to protonated peptides or amino acids[1]. Theoretical results [2] suggest that these reactions are charge directed, involving protonation of the amide nitrogen at the site of cleavage. In a typical CID experiment the average internal energy deposited in the precursor ion is much larger than the dissociation activation energies and, as a result, the primary fragment ions may also dissociate, producing smaller fragment ions.

---

* A version of this chapter has been submitted for publication: Klassen, J.S.; Kebarle, P. *J. Am. Chem. Soc.*

Decomposition of the **b** ions results in the formation of smaller **b** ions as well as immonium ions (**a** ions) which are commonly observed in the low energy CID spectra of peptides [3,4]. Sequence information is obtained from the mass difference of successive fragment ions of the same type (e.g. $\mathbf{b_n}$-$\mathbf{b_{n-1}}$) which corresponds to the mass of the residue by which they differ. The amount of sequence information available from an MS/MS experiment, therefore, depends on the type of fragment ions that are generated and the range of the residues that they span.

Despite the importance and widespread use of CID-MS to sequence peptides, the mechanistic details of the dissociation processes are poorly understood. A better understanding of major dissociation pathways and the effects of primary and higher order structure on these reactions is of interest not only from a fundamental point of view but also for practical reasons, such as for future refinements of CID-MS as a sequencing technique. This lack of mechanistic information is due in large part to the scarcity of experimentally determined dissociation energetics, a deficiency which is currently being addressed by several research groups. Meot-ner and coworkers have recently determined the activation energy for the dissociation of protonated leucine enkaphalin by measuring the temperature dependence for the loss of the peptide ion inside a heated capillary flow reactor interfaced with a mass spectrometer[5]. The flow reactor was operated at a pressure close to 1 atm which allowed for the activation energy to be measured in the high pressure limit. Williams and coworkers are presently investigating a promising new technique to study the temperature dependence of the dissociation kinetics of large biomolecules in which the precursor ions are heated via blackbody infrared radiation inside an ICR cell[6]. For sufficiently large ions the rate of radiative absorption is expected to be much larger than the dissociation rate thereby leading to ions with a Boltzmann distribution of internal energies. With this technique it should be possible to study the molecular interactions present in many biologically-important systems, both covalent and non-covalent in nature.

An on-going area of research in our laboratory involves the development and application of energy-resolved CID-MS[7,8] to measure the dissociation threshold energies of ions generated by electrospray (ES). Our original interest in this technique was as an alternative to the ion-equilibrium method[9] for measuring ion-ligand binding energies for complexes generated by ES[10]. Using the CID threshold method, we have recently measured the sodium and potassium ion affinities of several amide compounds as well as glycine and glycylglycine[11a] (see Chapter 5). In the present work, we use this technique to measure the appearance curves of the dominant low energy CID fragment ions of several protonated amino amides and small peptides. The resulting curves provide not only qualitative insight into the dissociation processes but also energetic data from the threshold energies. Part one of this report deals with the the dissociation of ions with the general structure, $^+H(H_2N\text{-}CH_2\text{-}CO\text{-}X)$, where X=OH, NH_2, NHMe, $NHCH_2COOH$. At low collision energies (< 50 eV lab), these ions dissociate preferentially at the C-X bond, leading to fragment ions which are analogous to $\mathbf{a_1}$ and $\mathbf{y_1}$ ions. Mechanisms are proposed for these reactions and the corresponding threshold energies are reported. Part two examines the dissociation behaviour of the small protonated peptides, Gly-Gly-NH_2, Gly-Gly-Gly and Gly-Gly-Gly-Gly, which contain multiple amide bonds at which cleavage can occur. These results provide some insight into the competitive nature of the dissociation processes and how this can effect the fragment ions which are observed. For reasons described herein, determination of accurate threshold energies becomes more difficult as the size of the ion increases and therefore only upper limits of the threshold energies are reported for these larger systems.

Experimental

a. Apparatus

The present measurements were performed with a modified SCIEX Trace Atmospheric Gas Analyzer (6000E) triple quadrupole mass spectrometer that has been described previously in Chapter 5 and elsewhere[11] and only a brief description is given here. The modified front end of the mass spectrometer is shown in Figure 6.1.

The gas phase ions were generated by electrospraying methanol solutions containing 10^{-3}-10^{-4}M of the peptides and 10^{-4} M HCl. The ions are sampled from atmospheric pressure into the low pressure source (LPS) via a stainless steel capillary (CAP, 200-400 V, 3.5 cm long, 0.33 mm i.d.). The pressure in the LPS is maintained at 10 Torr by means of a pump. Protonated peptides (MH^+) generated by ES are often clustered with water or solvent molecules ($MH^+(H_2O)_n(MeOH)_m$). Some initial declustering of the ions is obtained by flowing dry N_2 (~1 L/min) around the CAP, countercurrent to the ES ions. Additional declustering is achieved by applying a high ion drift field between the tip of the CAP and the bottom plate, IN (110V). A weak drift field ($E/p < 6$ Volt cm^{-1} $torr^{-1}$) between IN and the orifice, OR (100 V), ensures that the ions reach OR with thermal energies. In order to avoid collisional heating during sampling into the mass spectrometer, OR, CB and Q0 were set at equal

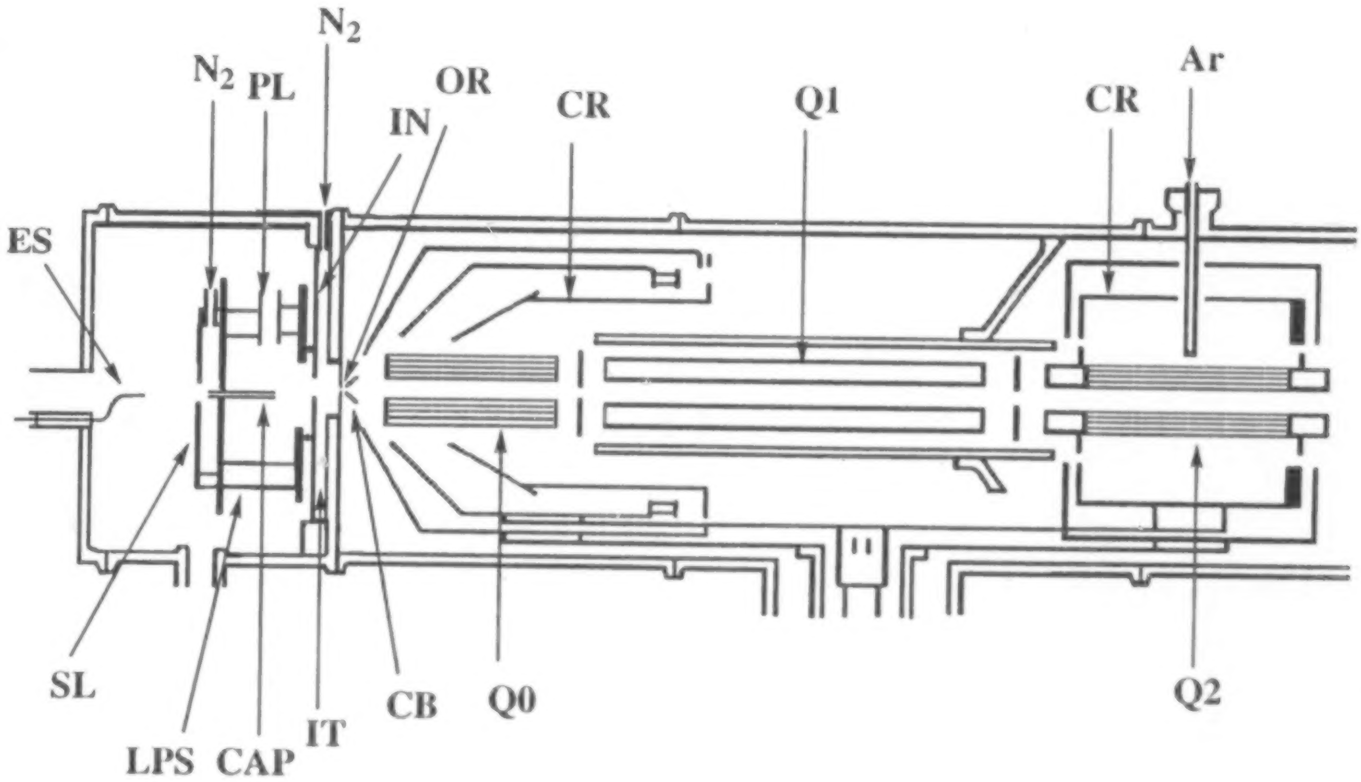

Figure 6.1 Front end of Apparatus. Electrospray generator, ES, consisting of electrospray capillary with stainless steel tip at high electric potential, generates charged droplets and ultimately gas phase ions. ES is partially surrounded by glass tube providing flow of dry air. Capillary, CAP, transfers gas and ions from 1 atm to a low pressure ion source LPS maintained at 10 torr. Ions can be partially declustered by applying a high drift field between CAP and interface plate IN. Ions are allowed to thermalize in low drift field, 10 torr pressure, ion thermalization chamber IT. Orifice OR, 100 um diameter leads to vacuum. First electrode and skimmer, CB. RF only ion guide quadrupole Qo. First quadrupole Q1. Cryosurfaces CR for cryopumping.

potentials (100 V). Precursor ions are mass selected with the first quadrupole (Q1) and introduced into the rf only quadrupole (Q2), which serves as the collision cell, with known nominal kinetic energies. Argon was used as the collision gas and was maintained at a pressure of ≤ 0.05 mtorr (collision cell length 15 cm). We have previously shown that these pressures lead to conditions where single collisions dominate[11b]. The fragment ions are mass analyzed by the third quadrupole (Q3) and detected using an ion counting system.

b. Determination of threshold energies, E_o

The threshold energies, E_o, were obtained by fitting the fragment ion appearance curves with eq. 6.1, using the CRUNCH program developed by Armentrout and coworkers[12],

$$\sigma = \sigma_o \sum g_i (E + E_i - E_o)^n / E \qquad (6.1)$$

where E is the collision energy (in centre of mass frame, CM), E_o is the threshold energy (at 0 K) and E_i is the vibrational energy of a given vibrational state with a relative population given by g_i. The temperature of the precursor ions was assumed to be 298 K. σ_o is a scaling factor and n is a variable parameter; both are optimized during the fitting procedure, along with E_o.

An underlying assumption in eq. 6.1 is that any precursor ion with an internal energy greater than E_o will decompose inside the collision cell (Q2), prior to reaching the mass analyzer (Q3). The residence time (t) in Q2 is estimated to be 30-40 μs. For precursor ions with many degrees of freedom or for reactions with high E_o values, additional internal energy is required to achieve a dissociation rate constant large enough to ensure that fragmentation occurs prior to Q3. This additional energy is referred to as a "kinetic shift" and if not taken into account will lead to E_0 values that are artificially high. A modified version of eq. 6.1 available in the CRUNCH program[13], allows for lifetime effects to be considered explicitly. This is done by calculating the unimolecular rate constants for a given process as a function of internal energy of the precursor ion, according to the RRKM formalism. Based on these rate constants, the probability (P) that a precursor ions with an intial translational energy (E) and internal energy (E_i) will decompose within the given experimental window (t) can be evaluated and eq. 6.1 is scaled accordingly (see eq. 6.2).

$$\sigma = \sigma_0 \sum_i \left[g_i P(E, E_i, t)\,(E + E_i - E_0)^n / E \right] \qquad (6.2)$$

c. Theoretical calculations

The vibrational energy distribution of the precursor ions, required for eqs.6.1 and 6.2, was obtained from calculated normal vibrational modes. Geometry optimization and hessian analysis was carried out using low level *ab initio* or semiempirical methods available in the GAMESS program[14]. Evaluation of the unimolecular dissociation rate constants (RRKM), used in eq. 6.2 to account for lifetime effects, requires the vibrational frequencies of the transition state. Where possible the transition states were modelled theoretically. Details of the methods used to locate the transition states are given in the Results and Discussion section.

Results and Discussion

a. CID of $^{+}H(H_2NCH_2COX)$, where X=OH, NH_2, NHMe and $NHCH_2COOH$.

Due to the wealth of experimental[15,16] and theoretical[17] information available in the literature on the gas phase chemistry of protonated amino acids, protonated glycine was chosen as the starting point for the present study. CID of protonated glycine at a collision energy of 10 eV lab (3.4 eV CM) leads predominantly to the formation of the immonium ion $^{+}H_2N=CH_2$ (m/z 30) with a small amount of the immonium ion-water complex (m/z 48) (Figure 6.2a). These fragment ions have been previously observed in the metastable ion spectrum of FAB-generated protonated glycine[16], wherein the hydrate is observed as the dominant fragment ion. Formation of the immonium ion via the dissociation of protonated amino acids is known to occur with a sizeable kinetic energy release ($T_{1/2}$=0.36-0.39 eV) indicating a reverse activation energy for this reaction[4a]. The kinetic energy release associated with the hydrate is even larger, $T_{1/2}$~0.46 eV[16]. At higher collision energies (> 6 eV (CM)), a new reaction pathway is observed, leading to the formation of a fragment ion at m/z 31 (CH_5N^{+}) (Figure 6.2b). This ion has been observed in high energy CID experiments and has been identified on the basis of MS/MS as the distonic ylide ion ($^{+}H_3N\text{-}CH_2\cdot$)[16]. The appearance curves of the three fragment ions (m/z 30, 31 and 48) are shown in Figure 6.3. The M^{+} ion has also been reported in high energy CID[16]; however, at the mass resolution used in the present work this ion could not be differentiated from the precursor ion (MH^{+}).

Formation of the immonium ion, the dominant fragment ion over the energy range studied, formally involves the loss of CO_2H_2. The most

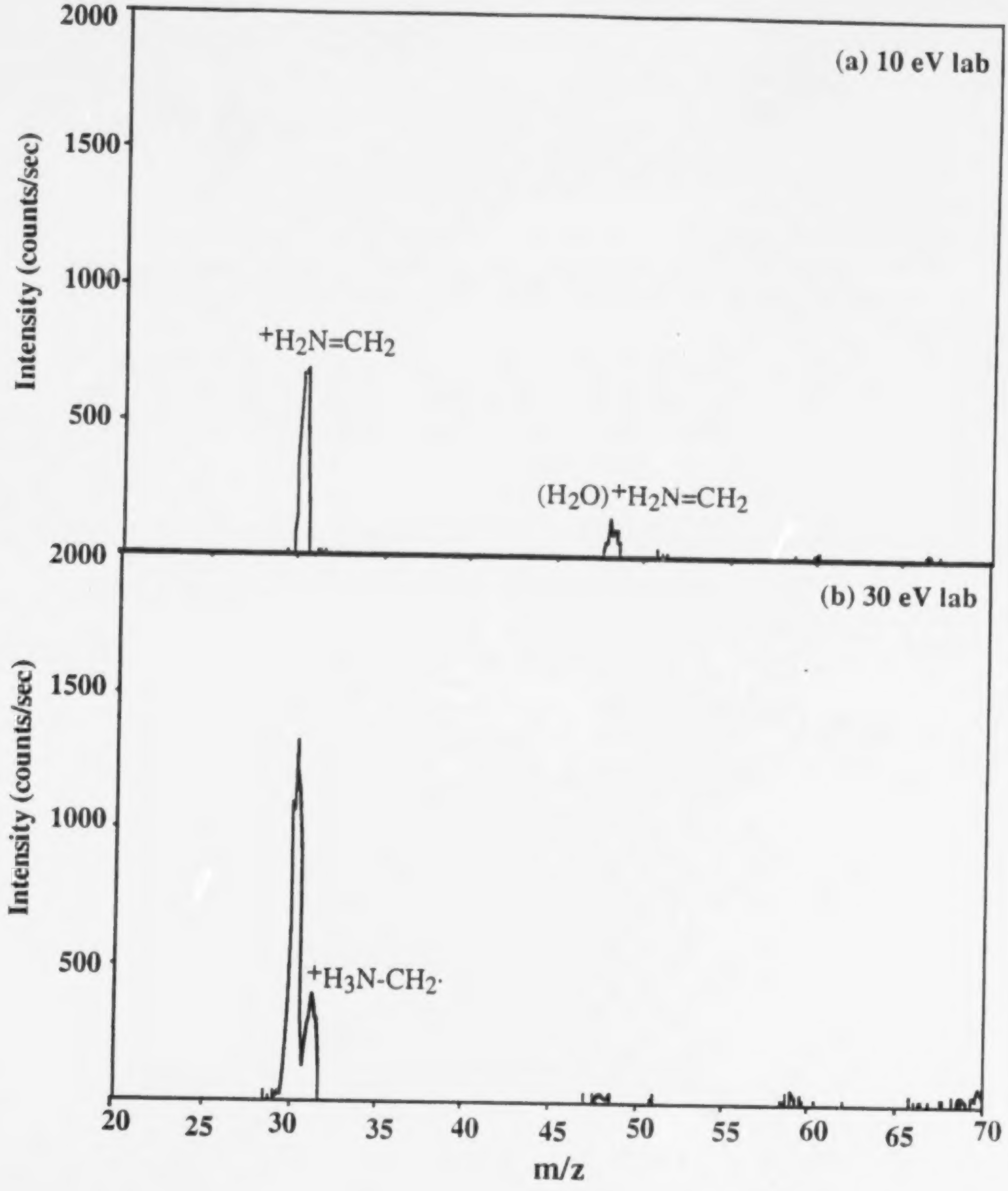

Figure 6.2 CID-MS of $(Gly)H^+$ at a collision energy of: (a) 10 eV lab (3.4 eV, CM); (b) 30 eV lab (10.3 eV, CM).

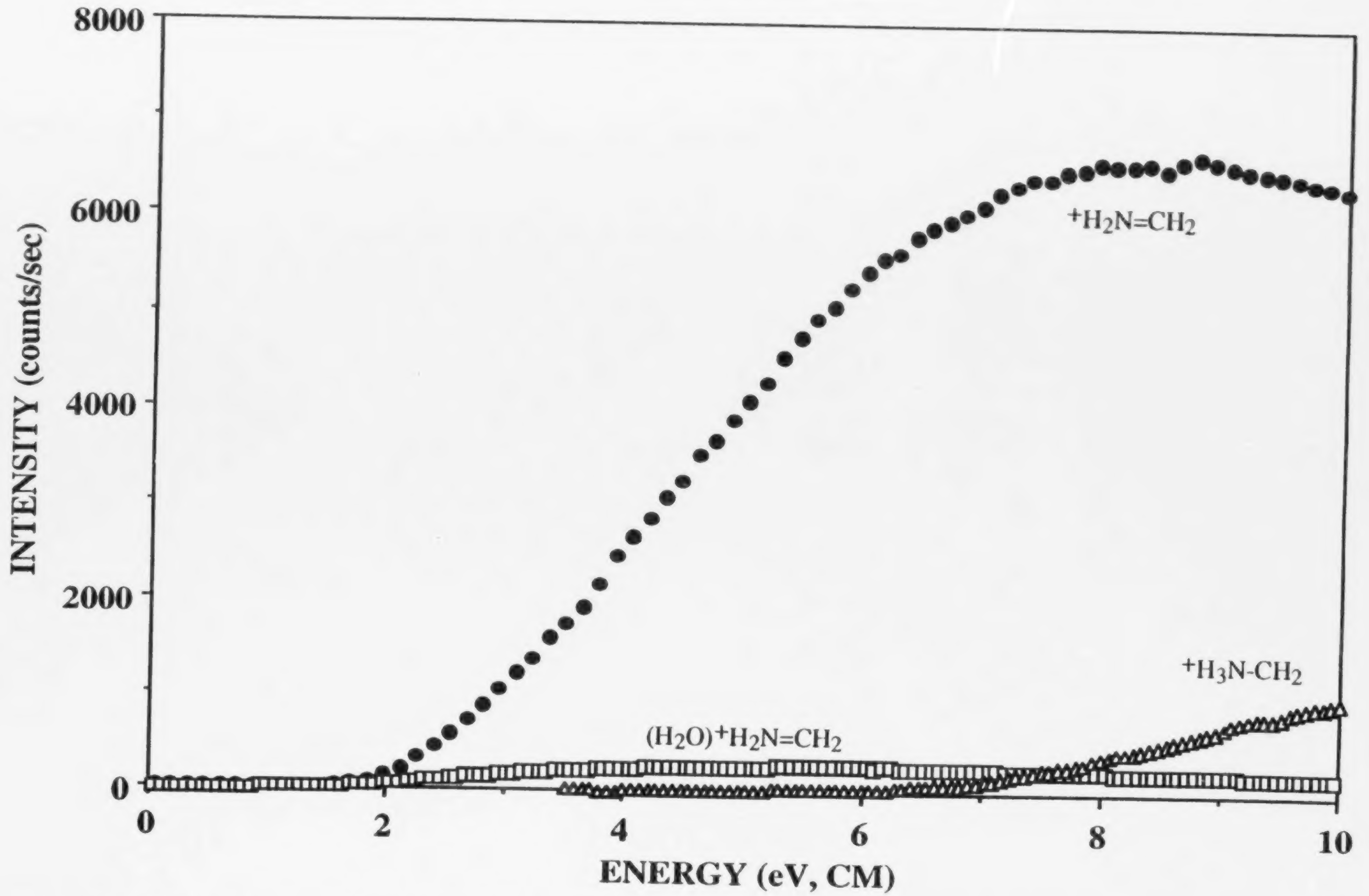

Figure 6.3 Appearance curves of $^+H_2N{=}CH_2$ (●), $(H_2O)^+H_2N{=}CH_2$ (□) and $^+H_3N\text{-}CH_2$ (Δ) from CID of $(Gly)H^+$.

direct route leading to the immonium ion would involve proton tranfer from the amino group to the carbonyl oxygen, followed by heterolytic bond cleavage and loss of the dihydroxycarbene neutral (scheme 6.1, reaction 6.1a). An alternative mechanism, proposed by Tsang and Harrison[15b], proceeds by protonation of the hydroxyl group followed by the sequential loss of H_2O and CO (reaction 6.1b). The acylium ion ($H_2N\text{-}CH_2\text{-}CO^+$) intermediate has not been detected mass spectrometrically and is believed to be unstable with respect to the loss of CO[15b]. Using heats of formation of the precursor ion and the final products taken from the literature, Beranova *et al* have recently evaluated the endothermicities for the formation of the final products in the two reaction pathways[16]. Formation of the immonium ion and dihydroxycarbene neutral (reaction 6.1a) is 64 kcal/mol endothermic, while reaction 6.1b, leading immonium ion plus H_2O and CO, is 33 kcal/mol endothermic. Although no heats of formation are available for the reaction intermediates proposed in scheme 6.1, reasonable estimates are provided by Bouchoux and Hoppilliard who have calculated the relative energies (MP2/6-31G*//3-21G, not including zero point energy corrections) of the isomeric forms of protonated glycine (**Ia**, **b** and **c**)[17a]. Protonation of the amino group (**Ia**) is calculated to be 18 kcal/mol more stable than protonation of the carbonyl oxygen (**Ib**) and 43 kcal/mol more stable than protonation of the hydroxyl group (**Ic**). The calculations also reveal that protonation of the hydroxyl group results in an unusually long $C\text{-}OH_2$ bond (2.1 Å) such that **Ic** resembles an acylium ion-water complex. Based on these calculated values, a lower limit for the energy barrier to reaction 6.1b is 43 kcal/mol and corresponds to proton transfer

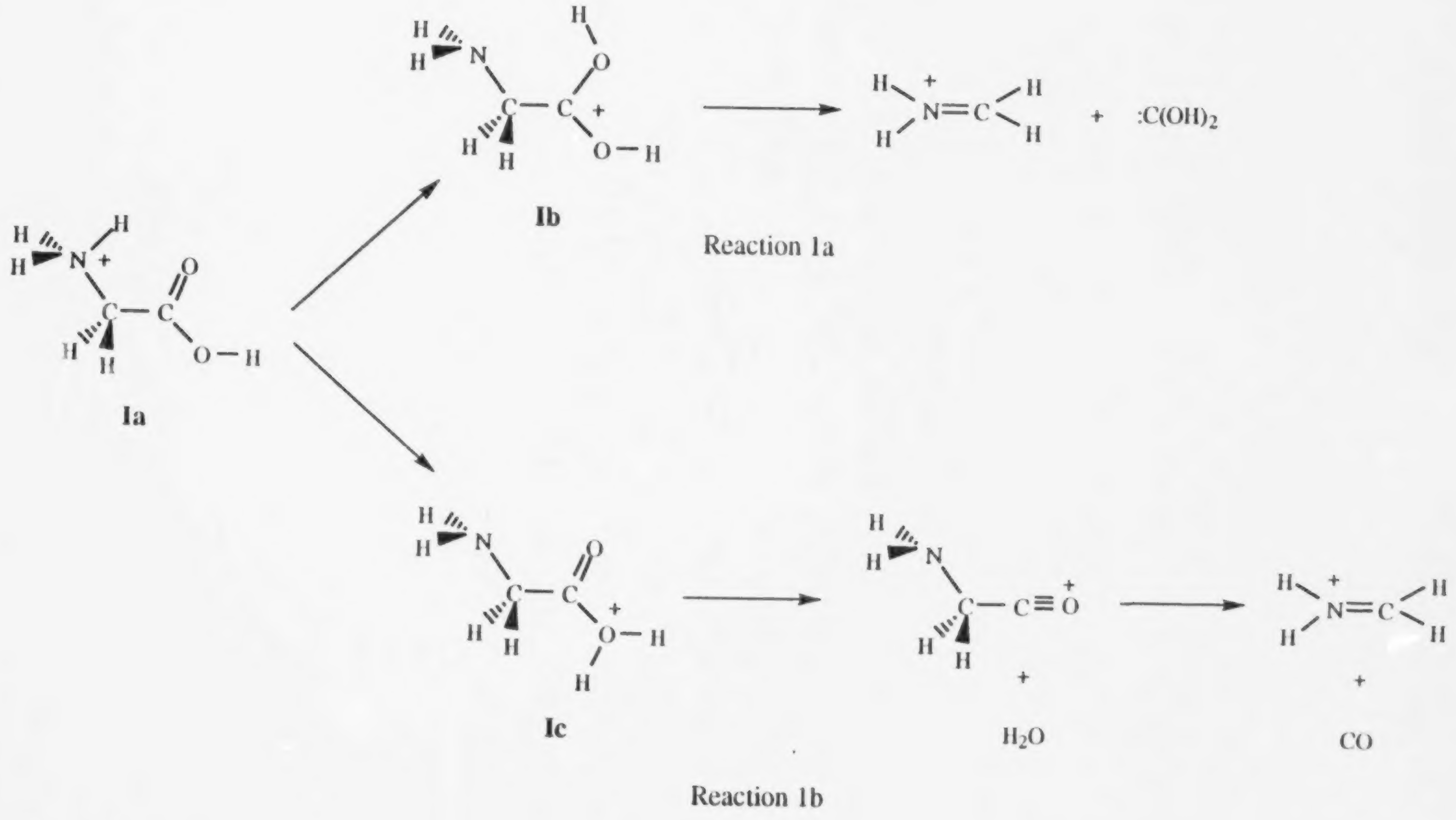
Ia
Ib
Ic
Reaction 1a
Reaction 1b
:C(OH)2
H2O
CO

Scheme 6.1

from the amino group to the hydroxyl group. The final products from this reaction are predicted to lie 10 kcal/mol below **Ib**.

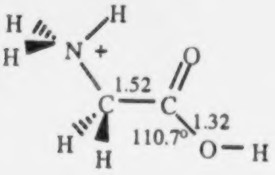

Ia

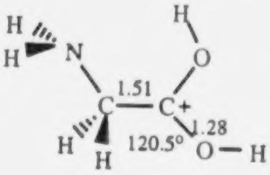

Ib

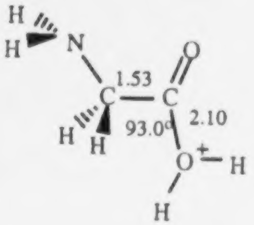

Ic

Fitting the immonium ion appearance curve with eq. 6.1 gives a threshold energy of 44.4 kcal/mol (see Table 6.1). The calculated cross section curve is shown together with the appearance curve in Figure 6.4. The calculated values of E_0 and n are known to be sensitive to the range of experimental points that are considered in the fitting procedure. Normally, several fits are carried out using different portions of the appearance curve, giving a range of threshold energies. The E_0 values reported in Table 6.1 correspond to the average value of several fits. Based on previous results reported in Chapter 5 and elswhere[11], the uncertainty associated with the fitting procedure is ±0.1 eV (2.3 kcal/mol).

As discussed in the Experimental section, the threshold energy obtained with eq. 6.1 assumes that there is no kinetic shift present and therefore can be viewed as an upper limit of the true threshold energy. A more reliable value is obtained when lifetime effects are explicitly considered. In order to evaluate the RRKM rate constants, an estimate of the vibrational frequencies of the transition state is required, which in turn requires some insight into the reaction mechanism. Since the

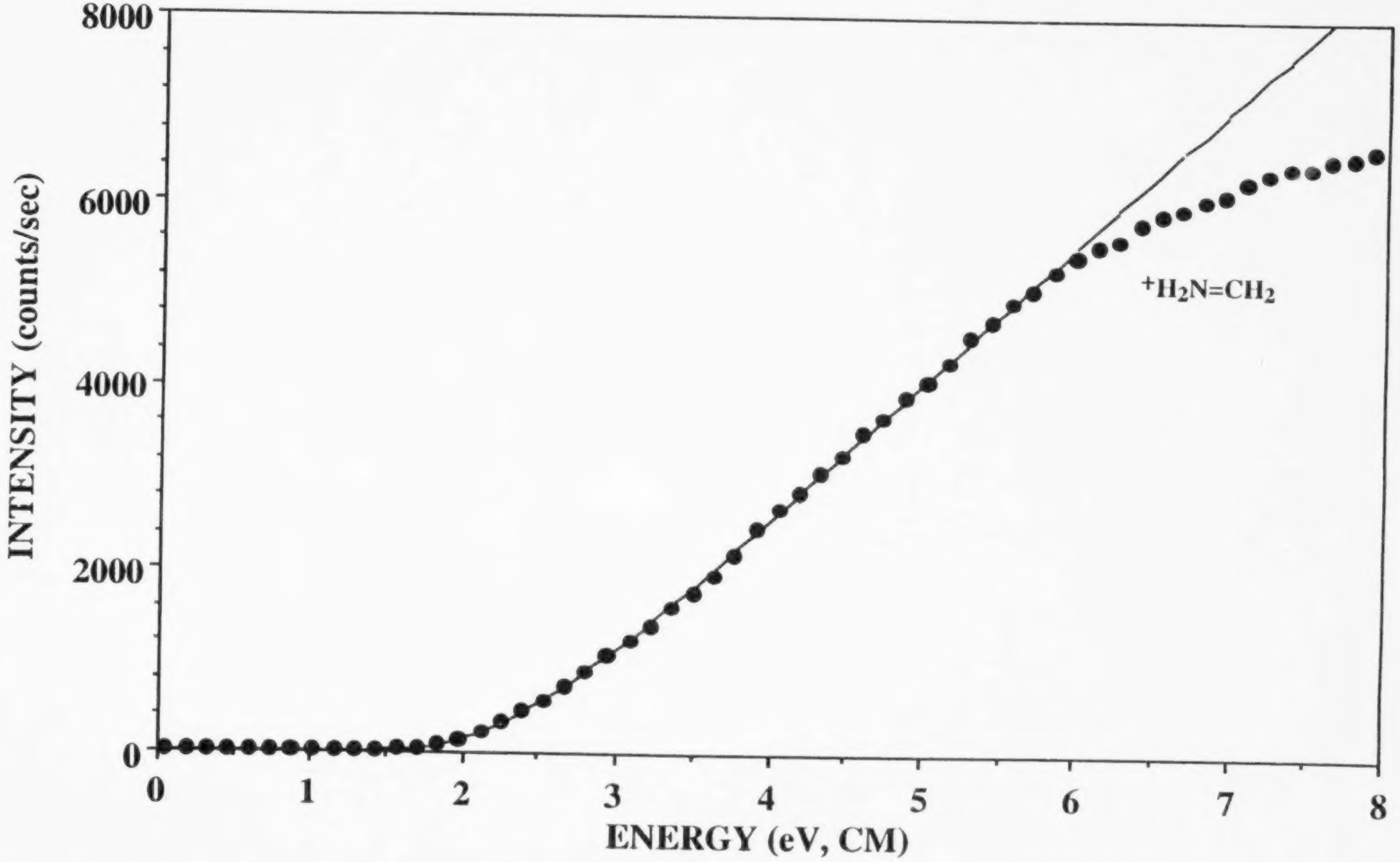

Figure 6.4 Appearance curve of $^{+}H_2N=CH_2$ from CID of $(Gly)H^{+}$. The calculated curve (solid line), fitted from 2.5 to 6.0 eV, corresponds to $n=1.82$ and $E_0=1.93$ eV (44.4 kcal/mol) (eq. 6.1).

Table 6.1. CID threshold energies (E_o)^a.

Precursor Ion (MH$^+$)	Fragment Ion	E_0^{b}	E_0^{c}	$\Delta S^{\ddagger d}$
$^+H_3NCH_2COOH$	$^+H_2N{=}CH_2$ **(a_1)**	43.9	44.4	10.4
$^+H_3NCH_2CONH_2$	$^+H_2N{=}CH_2$ **(a_1)**	44.2	44.9	12.8
$^+H_3NCH_2CONHMe$	$^+H_2N{=}CH_2$ **(a_1)**	49.9	60.0	5.8
"	^+H_3NMe **(y_1)**	$< 49.9^e$	59.8	< 5.8
(Gly-Gly)H$^+$	$^+H_2N{=}CH_2$ **(a_1)**	43.7	64.9	-3.2
"	$^+H_3NCH_2COOH$ **(y_1)**	$< 37.3^e$	54.1	< -3.2
(Gly-Gly-NH$_2$)H$^+$	MH$^+$ - NH_3 **(b_2)**	20.4	21.4	3.8
"	MH$^+$ - ($CO{+}NH_3$) **(a_2)**	-	69.0	-
"	MH$^+$ - GlyNH$_2$ **(y_1)**	-	69.0	-
"	$^+H_2N{=}CH_2$ **(a_1)**	-	82.3	-
(Gly-Gly-Gly)H$^+$	MH$^+$ - Gly **(b_2)**	-	54.5	-
"	(Gly-Gly)H$^+$ **(y_2)**	-	73.1	-
(Gly-Gly-Gly-Gly)H$^+$	MH$^+$ - Gly$_2$ **(b_2)**	-	79^f	-
"	(Gly-Gly)H$^+$ **(y_2)**	-	63^f	-

a. Threshold energies (E_o) in kcal/mol.
b. Threshold energies, obtained using eq. 6.2, include correction for kinetic shift and are considered the most accurate
c. Threshold energies obtained using eq 6.1.
d. $\Delta S^\ddagger$ values are calculated at 1000 K, in units of cal/deg mol.
e. Upper limit for threshold energy obtained using the vibrational frequencies of the transition state of the complementary **a_1** ion.
f. Average internal energy of precursor estimated to be 10.0 kcal/mol.

threshold energy obtained with eq. 6.1 can be considered as an upper limit to the true activation energy, one can rule out any contribution from reaction 6.1a to the immonium ion appearance curve, at least in the onset region. Based on this result, reaction 6.1b was taken as an initial guess of the actual reaction mechanism. The first step in reaction 6.1b involves intramolecular proton transfer between the amino nitrogen and the hydroxyl group, proceeding via a five-membered proton-bridged ring intermediate. The energy barrier for this process is expected to correspond to the thermochemical barrier of 43 kcal/mol. The next step involves the loss of H_2O from **Ic**. This process was modelled with low level *ab initio* calculations (3-21G), see Figure 6.5. Using **Ic** as the starting geometry, the C-OH_2 bond length was systematically increased while the remaining degrees of freedom were optimized. Lengthening the bond leads to a slight increase in energy (relative to **Ic**), reaching a maximum of 1.4 kcal/mol at 2.4 Å (see **Id**)[18]. Increasing the bond length to 2.5 Å (**Ie**) results in a large drop in energy, -14 kcal/mol relative to **Ic**[18]. This drop in energy coincides with the C-C bond increasing from 1.52 to 2.64 Å, indicating that the acylium ion is no longer sufficiently stabilized by the water molecule and that the C-C bond dissociates such that **Ie** resembles a hydrated immonium ion, weakly associated with a CO molecule. Subsequent dissociation of **Ie** into the final products is exothermic. These calculations predict that the energy barrier for the formation of the immonium ion is due almost entirely to the energy barrier to proton transfer to the hydroxyl group and the transition state is expected to resemble **Id**. Using the vibrational frequencies of **Id** (shown in Table 6.2) to represent those of the transition state, a threshold energy of 43.9 kcal/mol is obtained, which is in excellent agreement with the

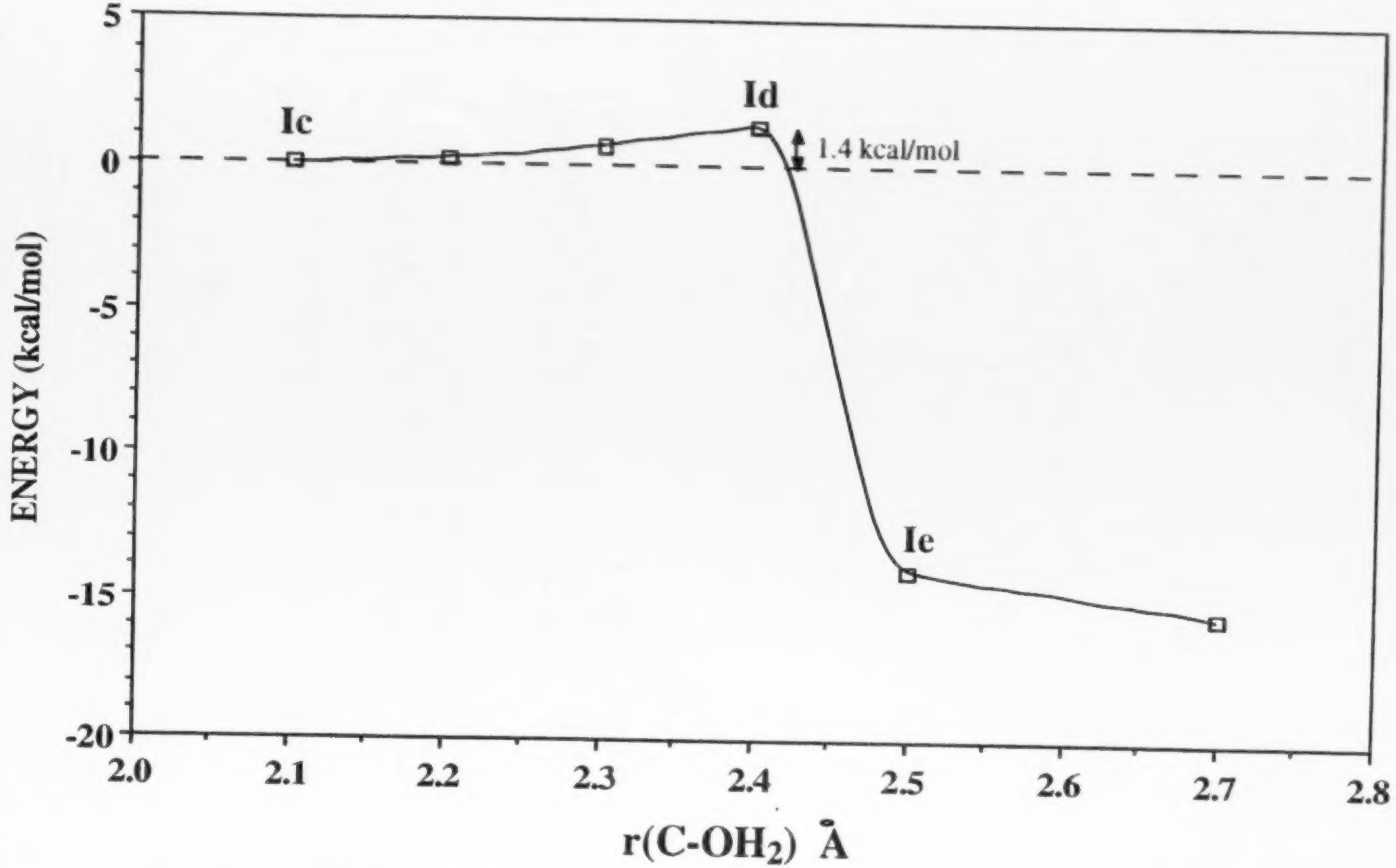

Figure 6.5 Calculated HF energy (3-21G basis set) of (Gly)H$^+$, with the proton located on the hydroxyl group, as a function of the C-OH$_2$ bond length. The energies are scaled relative to the calculated energy of **Ic** which is taken as 0 kcal/mol. The maximum energy (1.4 kcal/mol) occurs at a bond length of 2.4 Å (**Id**).

Table 6.2. Vibrational frequencies (cm^{-1}) of precursor ions and transition states (TS) leading to a given fragment ion.

$(Gly)H^{+a}$ /	TS^{d} ($H_2N=CH_2^+$)	$(GlyNH_2)H^{+a}$ /	TS^{d} ($H_2N=CH_2^+$)	$(GlyNHMe)H^{+b}$ /	TS^{d} ($H_2N=CH_2^+$)
100	-108	106	-135	60	-143
227	107	304	62	70	36
320	121	358	86	79	77
508	176	513	141	154	135
561	206	523	234	237	152
680	373	648	296	392	198
698	388	703	341	432	228
883	463	836	433	497	302
994	468	838	509	585	318
1011	496	1003	546	685	472
1230	626	1014	583	927	500
1235	753	1218	782	956	615
1247	974	1229	961	1100	788
1420	1198	1257	1195	1122	923
1473	1336	1435	1318	1152	1013
1560	1476	1463	1331	1200	1049
1609	1485	1532	1496	1239	1139
1709	1595	1618	1507	1273	1249
1825	1823	1668	1596	1319	1254
1850	1824	1816	1815	1350	1279
1957	2470	1827	1869	1356	1330
3277	3265	1852	1876	1359	1334
3323	3327	1904	2440	1383	1342
3346	3765	3119	3262	1412	1364
3572	3829	3280	3358	1451	1379
3621	3886	3347	3586	1625	1457
3810	3942	3597	3704	1640	1522
		3651	3707	1651	1692
		3738	3777	1655	1712
		3854	3904	2002	2338
				2976	2921
				2998	2987
				3005	2989
				3034	3011
				3088	3094
				3088	3396
				3222	3455
				3332	3482
				3488	3512

(Gly-Gly)H^{+b}	/ TS^d ($H_2N=CH_2^+$)	(Gly_2NH_2)H^{+b}	/ TS^e (b_2)	(Gly-Gly-Gly)H^{+c}	
25	-226	46	-17	24	1716
49	60	69	25	47	1727
73	93	84	97	59	2075
95	96	129	115	63	2086
149	123	226	125	79	2089
238	154	258	179	82	3207
282	207	305	220	92	3218
349	262	356	225	183	3231
412	298	434	266	214	3262
508	326	457	369	260	3277
521	417	493	372	285	3277
538	489	564	407	310	3347
582	516	569	508	327	3378
587	534	600	519	350	3463
652	538	623	577	385	3575
687	622	698	650	417	3582
935	634	764	655	441	3940
946	656	918	711	500	
1031	930	952	801	513	
1059	953	969	941	593	
1122	958	1053	970	620	
1168	1010	1081	1002	630	
1203	1142	1174	1023	673	
1239	1146	1177	1079	681	
1275	1175	1207	1142	750	
1288	1275	1232	1155	948	
1336	1282	1267	1218	958	
1646	1298	1288	1267	980	
1372	1318	1331	1296	1014	
1399	1328	1361	1305	1063	
1421	1345	1382	1317	1096	
1435	1407	1412	1323	1128	
1568	1441	1422	1347	1160	
1623	1469	1581	1408	1193	
1628	1606	1586	1460	1229	
1644	1701	1630	1570	1262	
1648	1711	1636	1716	1286	
2002	2036	1657	1751	1305	
2072	2329	1702	1755	1318	
2956	2890	1953	1757	1386	
2966	2956	2025	2089	1397	
3026	2960	2968	2630	1412	
3028	3030	2984	2959	1419	
3113	3345	3040	2969	1422	
3218	3399	3052	3035	1457	
3325	3452	3101	3406	1464	
3397	3464	3198	3434	1480	
3452	3499	3327	3437	1483	
		3452	3454	1603	
		3468	3478	1672	
				1703	

a. Vibrational frequencies were obtained from HF calculations using a 3-21G basis set.
b. Vibrational frequencies were obtained from semiempirical calculations (AM1).
c. The vibrational frequencies of (Gly-Gly-Gly)H+ were taken from a single local minima obtained from semiempirical calculations (MNDO).
d. The vibrational frequencies of the transition state leading to the immonium ion were obtained from HF calculations (3-21G) for the precursor ions of $GlyH^+$ and $GlyNH_2H^+$ and from semiempirical calculations (AM1) for $GlyNHMeH^+$ and $(Gly\text{-}Gly)H^+$. Negative frequencies correspond to imaginary frequencies.
e. The vibrational frequencies of the transition state leading to the $\mathbf{b_2}$ ion were obtained from semiempirical calculations (AM1).

energy barrier predicted for the reaction proceeding via **Id**. The kinetic shift for this reaction is quite small, 0.5 kcal/mol.

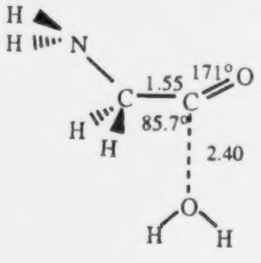

Id

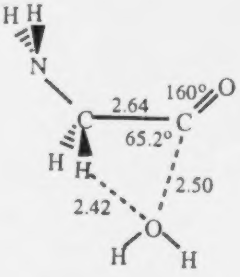

Ie

The appearance of the hydrated immonium ion in the CID spectrum is somewhat surprising based on energetic grounds. Both immonium ion and its hydrate have similar onset energies, suggesting that they are formed from a common intermediate, namely **Id**. However, as discussed above, **Id** lies higher in energy than the products: $^{+}H_2N{=}CH_2$, H_2O and CO. Therefore, in order for the hydrate to remain stable its internal energy must lie below the water-immonium ion binding energy. The large kinetic energy release associated with the formation of this ion suggets that some of the internal energy released during loss of CO is converted to kinetic energy of the resulting fragments, thereby leading to a stable hydrate.

Formation of the immonium ion is an example of a charge directed process, where the proton catalyzes bond dissociation. Charge remote fragmentation processes, in which simple homolytic bond cleavage occurs, require substantially higher internal energies. For example, C-C bond cleavage, which occurs in the formation of the ylide cation ($^{+}H_3N$-CH_2), is expected to have a threshold energy of ~90 kcal/mol (based on the average C-C bond energy). The observed onset energy of the ylide ion in Figure 6.3 is above 6 eV (140 kcal/mol). This onset energy is likely artificially high due to a significant kinetic shift which can be attributed to both to lifetime effects as well as to kinetic suppression of this pathway by the competing reaction leading to the immonium ion.

The CID behaviour of the protonated amino amide, glycinamide (**IIa**), is similar to that observed for glycine. Low collision energies results almost exclusively in the formation of the immonium ion, along with a small amount of the $(^{+}H_2N{=}CH_2)NH_3$ complex. As was the case for the amino acids, a large kinetic energy release, $T_{1/2}$=0.30-0.37 eV, is associated with the immonium ions formed by the decomposition of protonated amino amides[4a]. Formation of the immonium ion likely proceeds by the same mechanism proposed for glycine, namely proton transfer from the amino group to the amide nitrogen followed by the loss of NH_3 and CO:

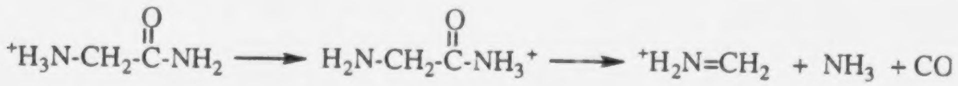

$$^{+}H_3N\text{-}CH_2\text{-}\overset{\overset{\displaystyle O}{\|}}{C}\text{-}NH_2 \longrightarrow H_2N\text{-}CH_2\text{-}\overset{\overset{\displaystyle O}{\|}}{C}\text{-}NH_3^{+} \longrightarrow {}^{+}H_2N{=}CH_2 + NH_3 + CO$$

Based on the relative energies of **IIa** and **IIb**, calculated at the 3-21G level, the energy barrier to proton transfer from the amino group to the amide nitrogen is ~22 kcal/mol[19]. Protonation of the amide nitrogen results in lengthening of the C(O)-N bond, from 1.32 to 1.54 Å, indicating that the bond is weakened but still retains most of its covalent character. In order to estimate the transition state structure, the loss of NH_3 from **IIb** was modelled using the same approach described for glycine, see Figure 6.6. The calculated energy (relative to **IIb**) is found to increase with increasing $C\text{-}NH_3$ bond length, reaching a maximum of

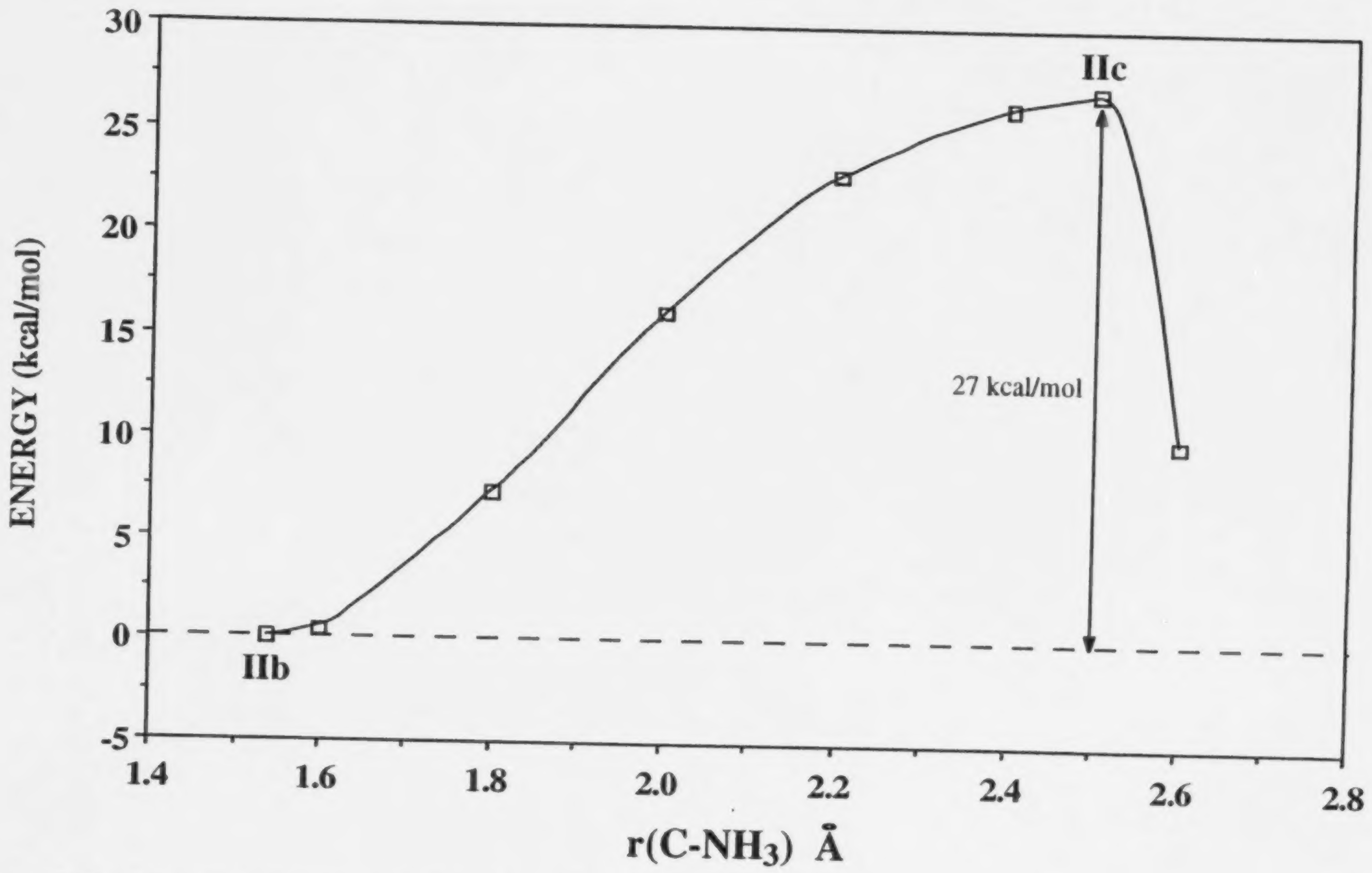

Figure 6.6 Calculated HF energy (3-21G basis set) of $(GlyNH_2)H^+$, with the proton located on the amide nitrogen, as a function of the OC-NH_3 bond length. The energies are scaled relative to the calculated energy of **IIb** which is taken as 0 kcal/mol. The maximum energy (27.0 kcal/mol) occurs at a bond length of 2.5 Å (**IIc**).

27 kcal/mol at a bond length of 2.5 Å (**IIc**)[19]. The energy at larger distances is found to decrease rapidly, coinciding with the loss of CO.

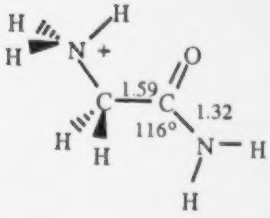

IIa

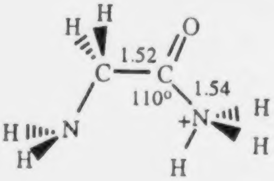

IIb

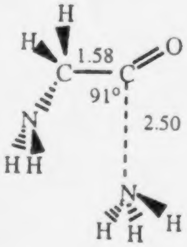

IIc

Using the vibrational frequencies of **IIa** and **IIc** (see Table 6.2) to represent the precursor ion and transition state, a threshold energy of 44.2 kcal/mol is obtained (eq.6.2, see Figure 6.7). The kinetic shift for this reaction is 0.7 kcal/mol. It is interesting that the immonium ion threshold energy is the same, within experimental error, as that determined with glycine as the precursor ion, despite large differences in the endothermicities for the two reaction steps. The proton transfer step is ~21 kcal/mol more endothermic in the case of glycine owing to the lower proton affinity of the hydroxyl group compared with that of the amide nitrogen which is a better lone pair donor. For the second step, which involves cleavage of the C-XH+ bond, the difference in endothermicity is exactly opposite. In the case of glycinamide, this involves cleavage of a covalent bond, whereas for glycine the bonding is non-covalent and requires substantially less energy. As a result, the threshold energy of the immonium ion is relatively insensitive to the nature of X. This is further supported by similar threshold energies obtained when X is NHMe and $NHCH_2COOH$ (see Table 6.1).

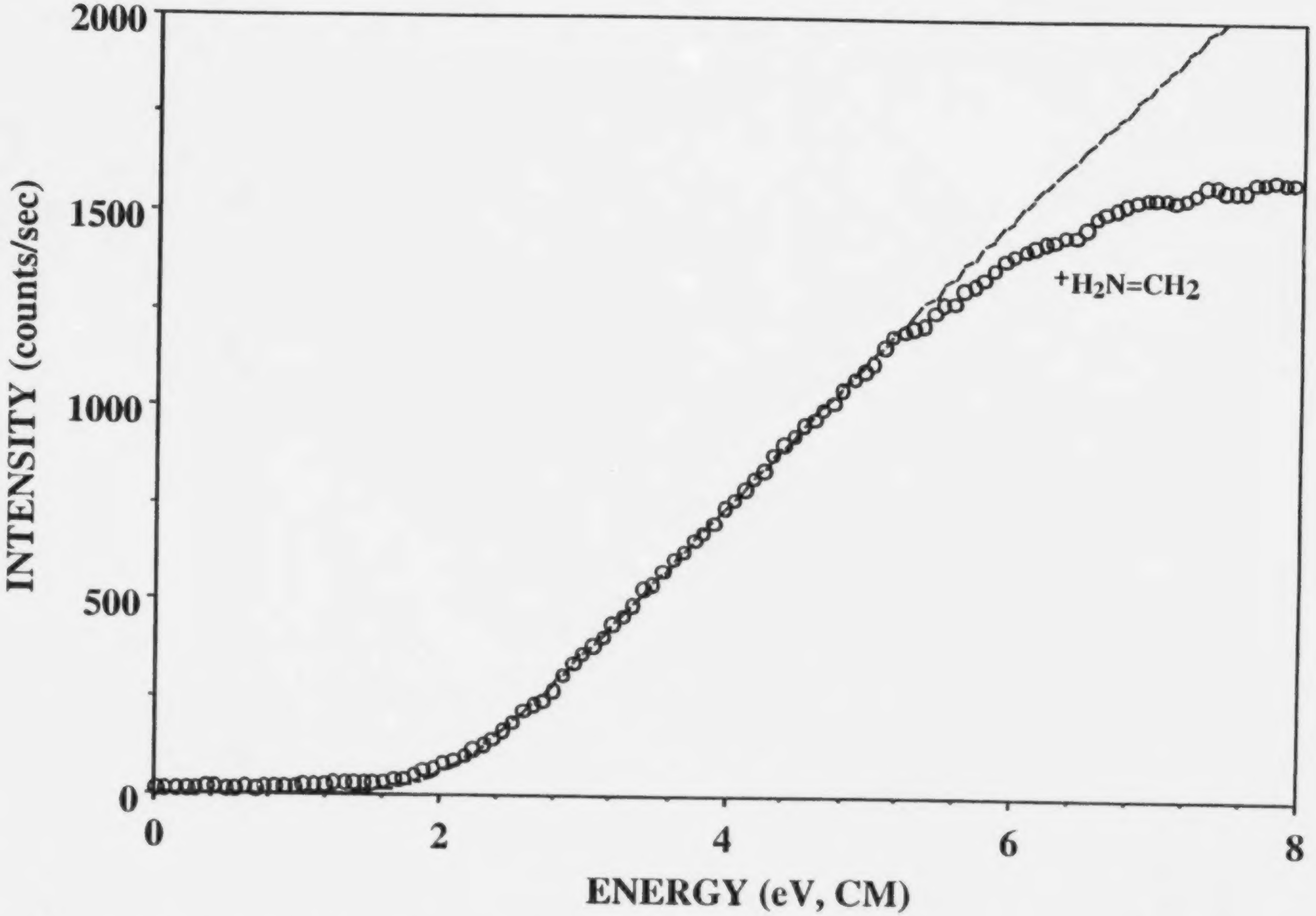

Figure 6.7 Appearance curve of $^+H_2N=CH_2$ from CID of $(GlyNH_2)H^+$. The calculated curve (solid line), fitted from 2.5 to 5.0 eV, corresponds to n=1.65 and E_0=1.95 eV (44.9 kcal/mol) (eq. 6.1).

CID of protonated methylglycinamide (**IIIa**) is interesting in that it is leads to the immonium ion as well as protonated methylamine, $^{+}H_3NCH_3$, at low collision energies (Figure 6.8). Formation of $^{+}H_3NCH_3$, which is analogous to a $\mathbf{y_1}$ ion, involves the transfer of both a proton and a hydrogen atom to the amide nitrogen. Based on CID experiments carried out on (Phe-Phe-Phe(d_5)+D)$^+$, Mueller et al[20] concluded that the transferred hydrogen associated with the formation of the **y** ions originates from the nitrogen atoms on the N-terminal side of the cleavage site. Additional insight into this reaction has been obtained from neutralization-reionization mass spectrometry experiments, carried out by Cordero and co-workers[21], which identified the neutral that is lost in the formation of the $\mathbf{y_1}$ ion from (Ala-Ala)H$^+$ as the cyclic aziridinone molecule. This same neutral is expected in the formation of the $^{+}H_3NMe$ ion:

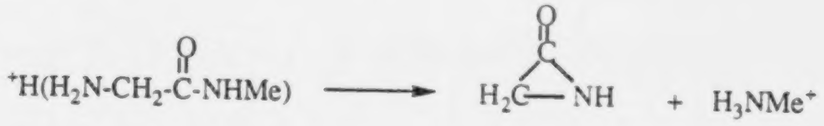

The appearance curves for the immonium ion and H_3NMe^+ are shown in Figure 6.9. The two ions appear to have very similar onset energies, although the immonium ion exhibits a reaction cross section that rises much more rapidly with energy. This type of behaviour suggests that the reaction leading to the immonium ion passes through a much looser transition state compared with H_3NMe^+. The geometry and corresponding vibrational frequencies of **IIIa** were evaluated from semiemprical calculations (AM1). Using eq. 6.1 to fit the appearance curves, the immonium ion and protonated methylamine are found to have

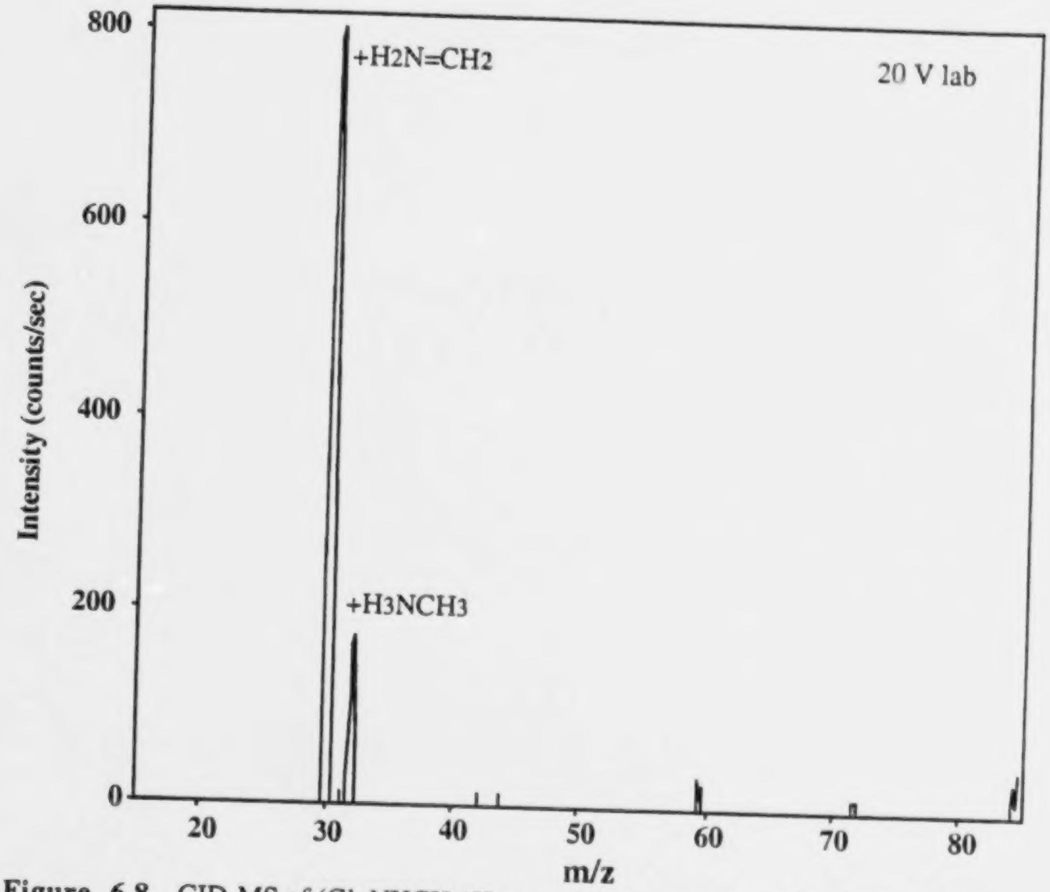

Figure 6.8 CID-MS of (GlyNHCH$_3$)H+ at a collision energy of 20 eV lab (6.2 eV, CM).

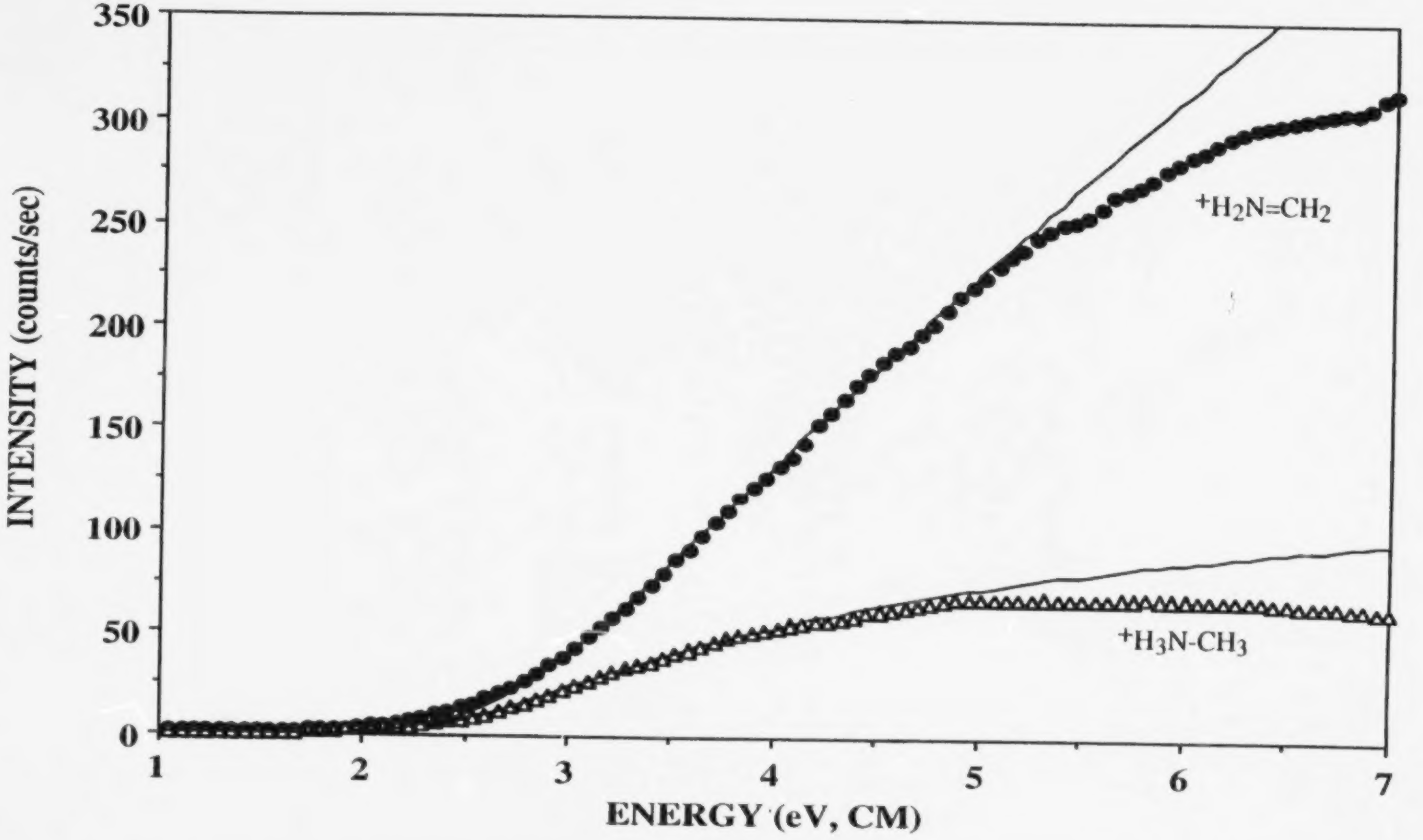

Figure 6.9 Appearance curves of $^+H_2N{=}CH_2$ (●) and $^+H_3NCH_3$ (Δ) from CID of $(GlyNHCH_3)H^+$. The calculated curves (solid lines), fitted from 3.0 to 5.0 eV for $^+H_2N{=}CH_2$ and 2.5 to 3.5 for $^+H_3NCH_3$, correspond to n=1.54 and E_o=2.61 eV (60.0 kcal/mol) and n=1.07 and E_o=2.60 (59.8 kcal/mol) respectively (eq. 6.1).

similar threshold energies, 60.0 and 59.8 kcal/mol respectively. The kinetic shifts for these two reactions are expected to be somewhat larger than observed for glycine and glycinamide due to the extra degrees of freedom. It is important to note that the presence of competing pathways may adversely affect the accuracy of the reported threshold energies. This is especially true when one reaction kinetically suppresses another in the threshold region thereby leading to a kinetic shift and an artificially high threshold energy for the slower process. In the present case, the immonium ion does exhibit a much larger reaction cross section, however, both ions have very similar onset energies and therefore, we do not anticipate any additional kinetic shift associated with kinetic suppression.

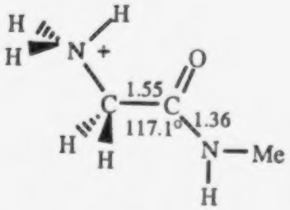

IIIa

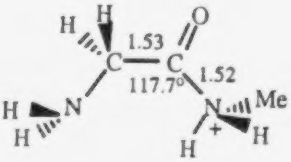

IIIb

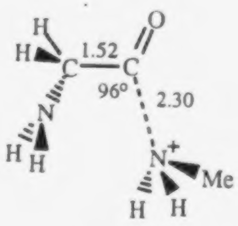

IIIc

The transition state leading to the immonium is expected to be similar to that determined for glycinamide. The geometry of the transition state (**IIIc**) was obtained from semiempirical calculations (AM1) used to model the loss of H_2NMe from **IIIb**[22], as previously described. Using the calculated frequencies of **IIIc**, a threshold energy of 49.9 kcal/mol is obtained. This value agrees reasonably well with the threshold energy measured for glycinamide and is consistent with both reactions occuring via the same type of mechanism. The degree to which the kinetic shift is sensitive to the number of degrees of freedom can be seen by comparing the results obtained for glycinamide and methylglycinamide. Replacing a hydrogen with a methyl group causes the kinetic shift to increase from 0.7 to 10.1 kcal/mol. As discussed in our earlier paper[11], we have found that kinetic shift is also very sensitive to the magnitude of the transition state frequencies, in particular the low energy frequencies ($< 200\ \mathrm{cm}^{-1}$). Due to the general uncertainty associated with the calculated transition state geometries and more importantly the frequencies, it is difficult to assess the error limits of the threshold energies for reactions which exhibit large kinetic shifts.

To our knowledge, no detailed evaluation of the mechanism leading to the $\mathbf{y_1}$ ion has been reported. In the absence of a more detailed analysis, we propose the mechanism shown in scheme 6.2. As with the immonium ion, the first step in the reaction is expected to involve proton transfer from the amino group (**IIIa**) to the amide nitrogen (**IIIb**). If aziridinone is in fact formed as the neutral formed in this reaction, it implies that the cyclization process involving the amino nitrogen and the carbonyl carbon occurs prior to complete dissociation of the $C\text{-}NH_2Me^+$ bond such that the loss of CO does not occur. This rearrangement process, which likely involves a tight four membered ring type intermediate (**IIId**), leads ultimately to the proton bound dimer (**IIIe**), see scheme 6.2. The proton bound dimer can then dissociate, giving protonated methylamine or conceivably, at higher energy, protonated aziridinone. Calculations from this laboratory indicate that protonated aziridinone is unstable and undergoes ring opening, resulting in the loss of CO to give the immonium ion. It is unlikely however, that this process contributes significantly to the formation of the immonium ion compared

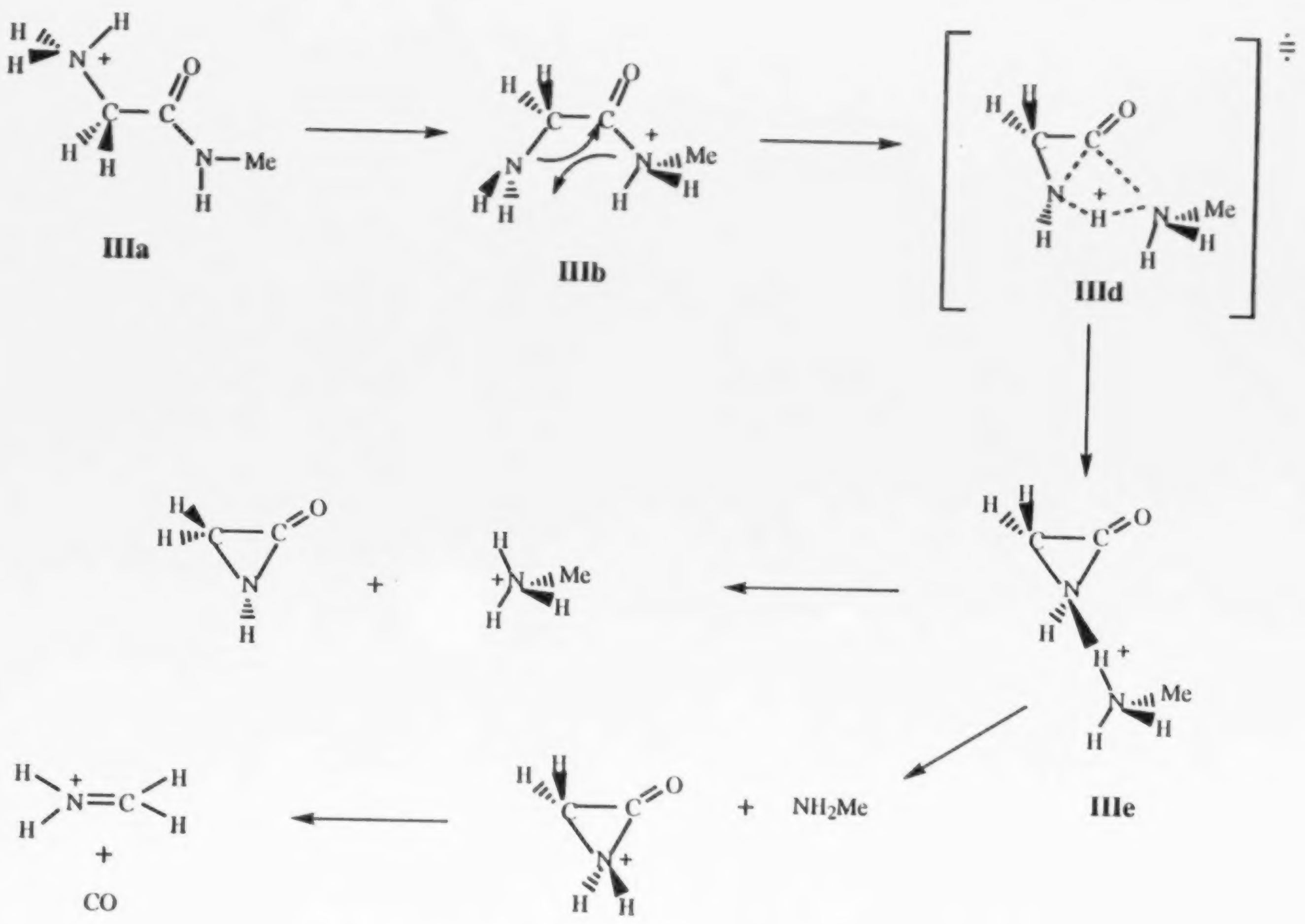
IIIa
IIIb
IIId
IIIe
+
NH2Me
CO

Scheme 6.2

with the much faster pathway which proceeds via **IIIc** . As discussed earlier, the smaller reaction cross section for protonated methylamine compared to the immonium ion indicates that this reaction proceeds through a tighter transition state then the immonium ion (i.e. has a smaller $\Delta S^{\ddagger}$). The $\Delta S^{\ddagger}$ associated with the dissociation of the dimer (**IIIe**) is estimated to lie between 13 and 24 cal/deg mol.[23] , which is larger than $\Delta S^{\ddagger}$ calculated for the immonium ion, 5.8 cal/deg mol. This suggests that the maximum energy barrier leading to ^+H_3NMe corresponds to the rearrangement step, passing through **IIId**, shown in scheme 6.2. No detailed search for the transition state has been carried out and therefore no vibrational frequencies are available for evaluation of the kinetic shift. Instead, an upper limit to the threshold energy, 49.9 kcal/mol, was obtained by fitting the experimental data using the vibrational frequencies of **IIIc**. The true $\Delta S^{\ddagger}$ for this reaction, which is smaller than that corresponding to **IIIc**, will result in a lower threshold energy.

At this point it is reasonable to ask why the $\mathbf{y_1}$ type ion is observed for protonated methylglycinamide but not for glycinamide, since these two precursor ions differ only by a methyl group. In the proposed transition state ring closure, to give the aziridinone neutral, occurs in a concerted fashion with proton transfer to XH, leading ultimately to the protonated species XH_2^+. If the energy barrier for this process does in fact correspond to the overall activation energy, then it seems reasonable that the stability of the transition state and hence the magnitude of the activation energy will be affected by the gas phase basicity (GB) of XH. Since the GB of methylamine is 10 kcal/mol higher than that of NH_3[24], one can conclude that the activation energy for methylglycinamide will be lower than for glycinamide. The fact that the NH_4^+ ion is not observed at all in the CID spectrum of glycinamide, even at high collision energies where this process should be energetically accessible, suggests that this process is kinetically supressed by the much faster reaction leading to the immonium ion.

CID of the protonated dipeptide, glycylglycine (Gly-Gly), which for the purpose of the present discussion can also be viewed as a substituted glycinamide, results exclusively in the formation of the $\mathbf{y_1}$ (protonated glycine) and $\mathbf{a_1}$ (immonium ion) fragment ions at energies less than 50 eV(lab). From the appearance curves, shown in Figure 6.10, it can be seen that the $\mathbf{y_1}$ ion has the lower onset energy, but that at higher energies the $\mathbf{a_1}$ ion becomes the dominant fragment ion. HF calculations (6-31G*) carried out by Cassady et al[25] predict that the most stable form of protonated glycylglycine involves protonation at the terminal amino nitrogen (**IVa**); protonation of the amide nitrogen (**IVb**) was found to be 18 kcal/mol less stable.

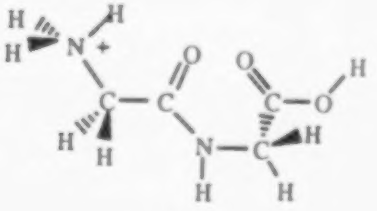

IVa

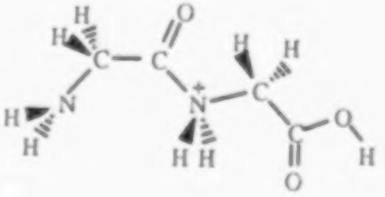

IVb

AM1 calculations were used to locate the $\mathbf{a_1}$ transition state and to evaluate the corresponding vibrational frequencies. At this level of calculation, the transition state is predicted to lie 17 kcal/mol higher in energy than the amide protonated form of the dipeptide (**IVb**). From the

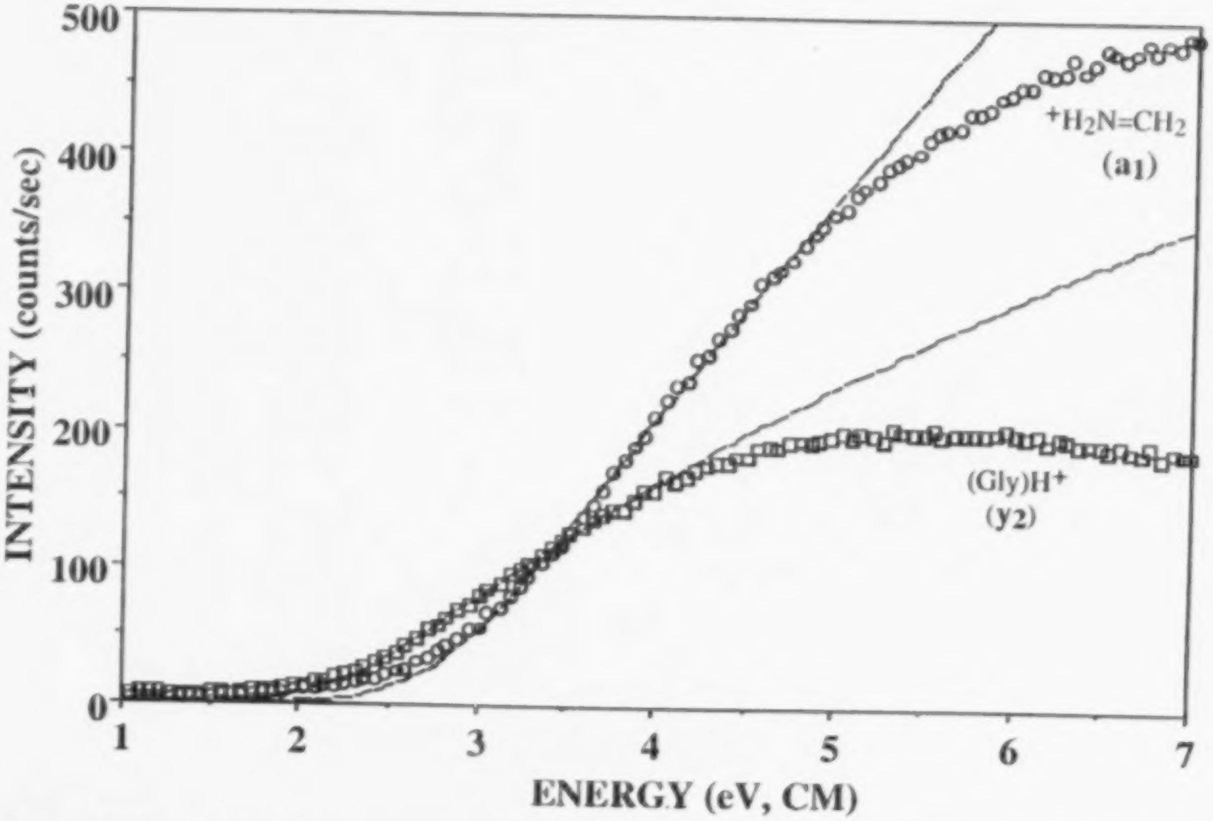

Figure 6.10 Appearance curves of $^+H_2N=CH_2$ (○) and (Gly)H$^+$ (□) from CID of (Gly-Gly)H$^+$.The calculated curves (solid lines), fitted from 3.0 to 5.0 eV for $^+H_2N=CH_2$ and 2.5 to 3.5 for (Gly)H$^+$, correspond to n=1.78 and E_0=1.87 eV (43.0 kcal/mol) and n=1.58 and E_0=1.62 (37.3 kcal/mol) respectively (eq. 6.2).

appearance curve a threshold energy of 43.7 kcal/mol is obtained for the $\mathbf{a_1}$ ion. This value is in good agreement with the $\mathbf{a_1}$ threshold energies measured for the previous systems. The kinetic shift for this reaction is 20 kcal/mol and represents one third of the observed threshold energy of 64 kcal/mol. Obviously, the major source of uncertainty in the CID threshold energies, even for these small biomolecules, lies in the modelling of the transition state.

Using the vibrational frequencies determined for the $\mathbf{a_1}$ transition state, an upper limit threshold energy of 37.7 kcal/mol is obtained for the $\mathbf{y_1}$ ion. The dissociation energy for the $\mathbf{y_1}$ ion, therefore, lies at least 6 kcal/mol below the energy barrier for the formation of the $\mathbf{a_1}$ ion. This threshold energy can be compared to a reaction endothermicity of 30.9 kcal/mol calculated (using MNDO generated heats of formation) by Wysocki and coworkers[26] for the formation of the $\mathbf{y_1}$ ion from the protonated dipeptide, $H_2NCH_2CONHCH(C_2H_5)COOH$. This peptide is very similar to glycylglycine and the reaction endothermicities are expected to be similar as well. If this calculated value is to be believed, the true activation energy for the formation of the $\mathbf{y_1}$ ion lies somewhere between 31 and 38 kcal/mol.

b. $^{+}H(H_2NCH_2CONHCH_2COX)$, where $X=NH_2$, $HNCH_2COOH$ and $-(HNCH_2CO)_2-OH$.

The appearance curves of the dominant CID fragment ions generated from protonated glycylglycinamide (Gly-Gly-NH_2) are shown in Figure 6.11. The most striking feature of Figure 6.11 is the very low onset energy for the ion produced by the loss of NH_3 (m/z 115). Using eq. 6.1 to fit the data, a threshold energy of 21.4 kcal/mol is obtained.

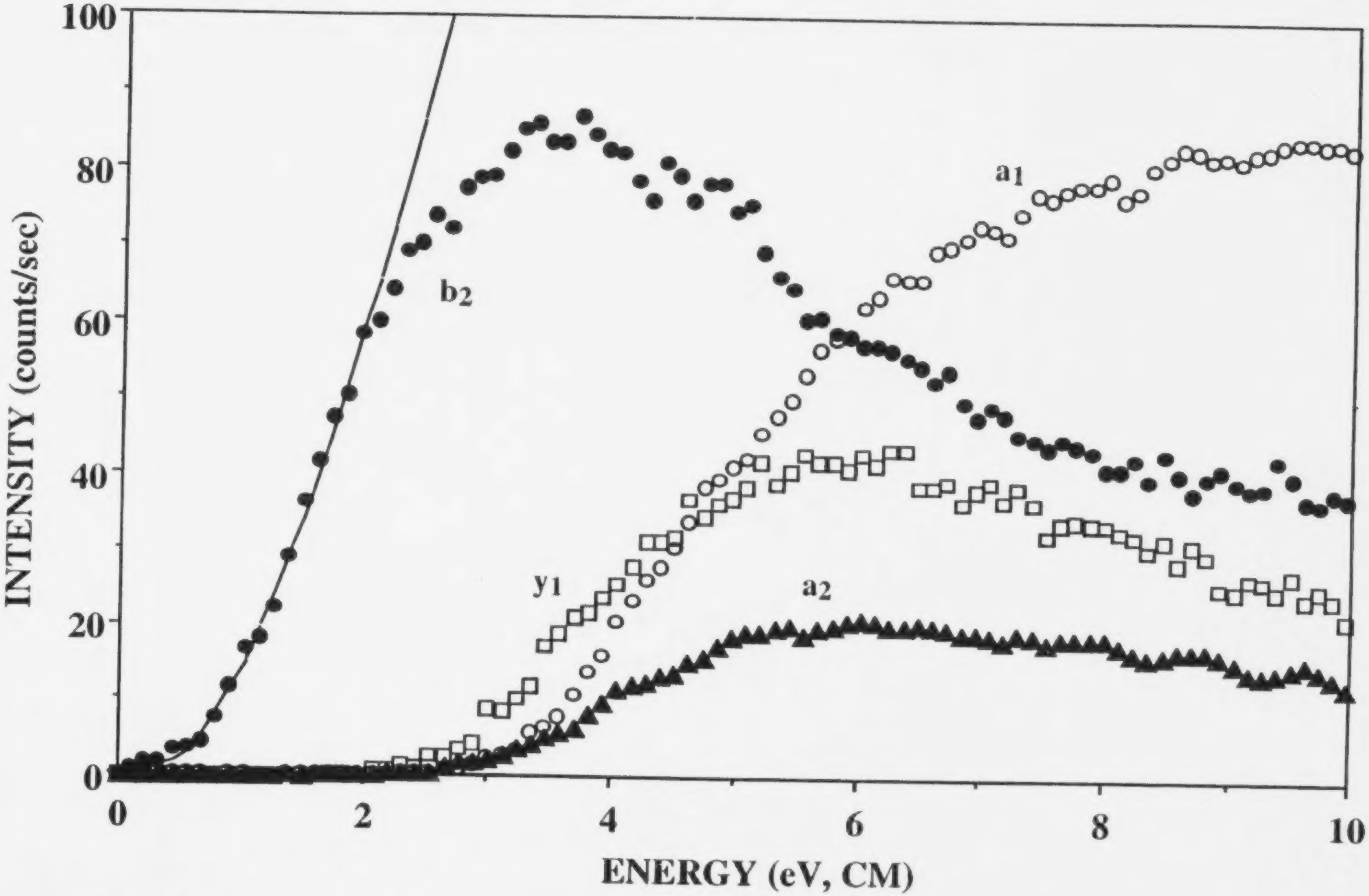

Figure 6.11 Appearance curves of the b_2 (●), a_2 (▲), y_1 (☐)and a_1 (○) fragment ions from CID of (Gly-GlyNH$_2$)H$^+$.The calculated curve (solid line) for the b_2 ion, fitted from 1.0 to 2.5 eV, corresponds to n=1.52 and E_o=0.93 eV (21.4 kcal/mol) (eq. 6.1).

Although loss of NH_3 can conceivable occur from either end of the peptide, it is believed that this ion is in fact a **b_2** ion, involving loss of NH_3 from the C-terminus. This assignment can be made on the basis of recent results by Harrison and co-workers[4a], where it was found that the loss of HX was a dominant dissociation process in the metastable spectrum of FAB-generated peptides with the general structure: $^+H(H_2NCHRCONHCHR'CO\text{-}X)$ where X= OH, NH_2, Gly and Ala and the side groups (R) were hydrogen atom or alkyl groups. The kinetic energy release (KER) associated with the resulting **b_2** ions was found to be small, $T_{1/2}$=0.02-0.03 eV, indicating that there is essentially no reverse activation energy associated with the loss of HX. As previously noted by Harrison[4a], the fact that the loss of NH_3 is not accompanied by the loss of CO (as was observed in the analogous reaction involving glycinamide) indicates intramolecular stabilization of the transition state. Such stabilization would explain the low activation energy observed for this reaction. Based on comparative KER and CID studies, the authors concluded that the **b_2** ions are protonated substituted oxazalones (shown below). The loss of NH_3, therefore, is accompanied by bonding between the carbonyl oxygen and the C-terminal carbonyl carbon. In order to determine the kinetic shift-corrected threshold energy, the vibrational frequencies of a guessed transition state **TS(b_2)**[27] (shown below) were evaluated semi-empirically. Using these frequencies, a threshold energy of 20.4 kcal/mol is obtained.

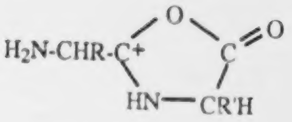

protonated oxazalone

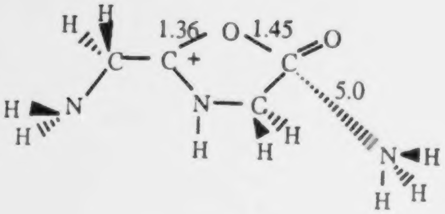

T.S(b$_2$)

Harrison *et al*[4a] also found that the dissociation of the **b$_2$** ions occurs by loss of CO to give the corresponding **a$_2$** ion. The kinetic energy release for this reaction is quite large, $T_{1/2} \approx 0.5$ eV. Based on calculations, the authors predicted that the loss of CO from the oxazalones proceeds via ring opening to give the acyclic acylium ion, from which loss of CO is exothermic. For the **b$_2$** ion, $HCONHCH_2CO^+$, the energy barrier associated with ring opening and loss of CO was calculated to be 1.49 eV, or 34 kcal/mol[4a]. From the present results, the threshold energy measured for the **a$_2$** ion (eq. 6.1) is 69 kcal/mol. An approximate activation energy of 48 kcal/mol for the loss of CO from the **b$_2$** ion is obtained by subtracting the **b$_2$** threshold energy (obtained using eq. 6.1) from the **a$_2$** energy. This is expected to represent an upper limit to the true activation energy since the **a$_2$** ion, with its much larger threshold energy, is expected to exhibit a larger kinetic shift than the **b$_2$** ion. Also observed in Figure 6.11 are the **y$_1$**[28] and **a$_1$** ions, formed by cleavage of the first amide bond. The relative energy dependence of the cross sections of these two ions is very similar to that observed with Gly-Gly, with the **y$_1$** ion having an earlier onset energy but with the **a$_1$** ion exhibiting a larger cross section at higher energies. The threshold energies for the **y$_1$** and **a$_1$** ions, obtained using eq. 6.1, are 69 and 82.3 kcal/mol. These energies are 15 and 17 kcal/mol higher than the respective onset energies measured from the CID of glycylglycine. This energy offset is attributed to a kinetic shift due to the pressence of the competing reaction leading to the **b$_2$** ion which kinetically supresses the other dissociation reactions.

The CID breakdown graph of protonated Gly-Gly-Gly is shown in Figure 6.12. The **b$_2$** ion is again found to be the lowest energy process, however the onset energy, 54.5 kcal/mol (eq. 6.1)[29] is considerably higher than that measured for glycylglycinamide, 21.4 kcal/mol. Although we have not attempted to model kinetic shift for this reaction, this increase of some 33 kcal/mol in the observed threshold energy is believed to reflect an increase in the kinetic shift due to the addition of the extra glycine residue and not a change in activation energy. The **a$_1$** ion, which has the second lowest onset energy, exhibits a relatively small cross section up to ~4.5 eV, above which it increases much more rapidly with collision energy indicating that additional reaction pathways are contributing to its ion intensity. This is expected since the immonium ion (**a$_1$**) is a major decomposition product of all of the larger fragment ions. At a collision energy of approximately 2.5 eV, the onset of the **y$_1$** and **y$_2$** ions is observed. Initially, the **y$_2$** ion cross section increases much faster with collision energy compared to the **y$_1$** ion. The neutral lost in the formation of the **y$_2$** will be the aziridinone as previously discussed. In the case of the **y$_1$** ion, the hydrogen atom that is transferred can orginate either from the terminal nitrogen or from the adjacent amide nitrogen. The neutral that is formed will then either correspond to a diketopiperazine or a substituted aziridinone molecule. There is experimental evidence that the diketopiperazine, which is expected to be thermodynamically more stable than the tight three membered cyclic

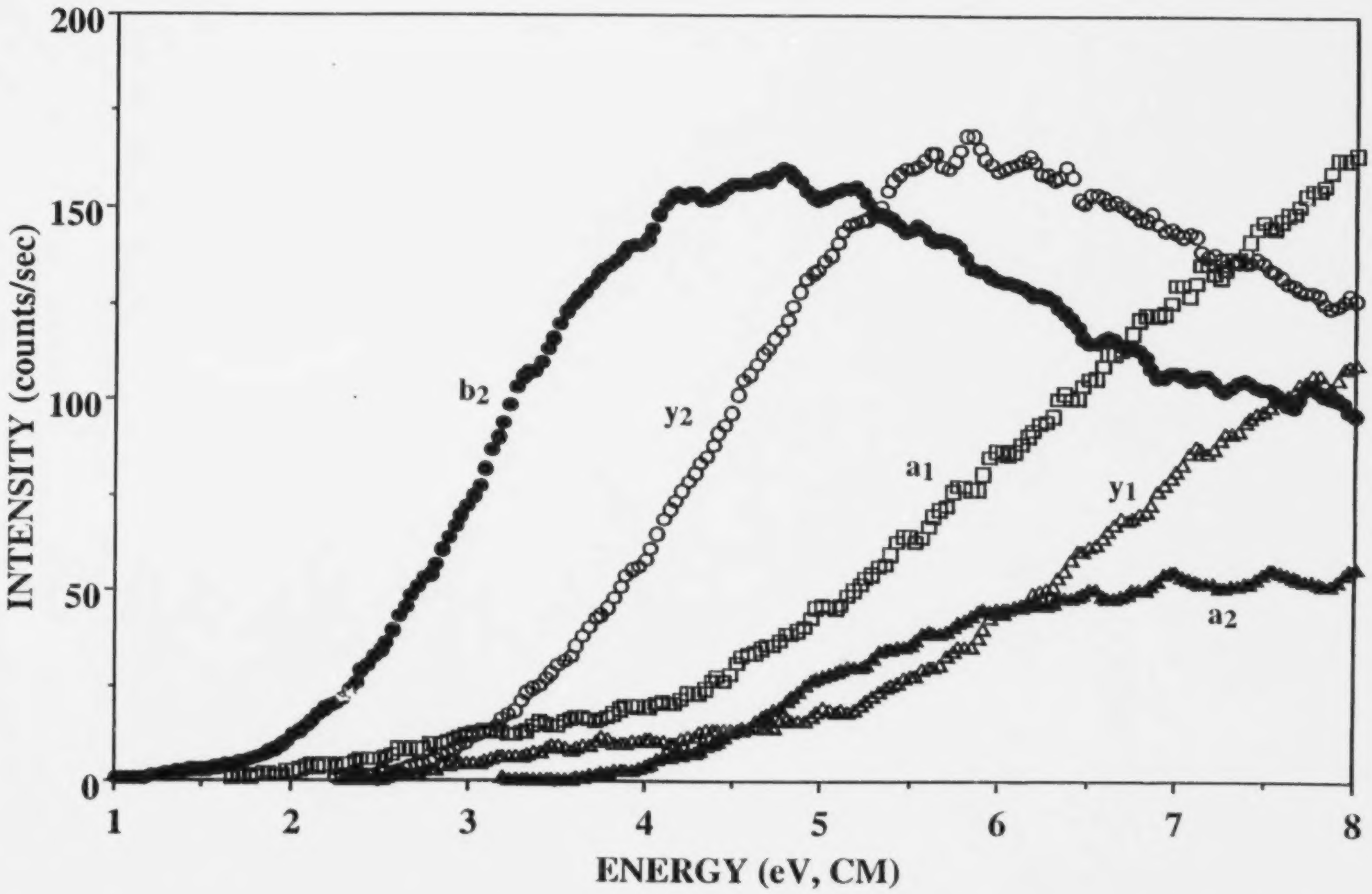

Figure 6.12 Appearance curves of the b_2 (●), y_2 (○), a_2 (▲), a_1 (□)and y_1 (△) fragment ions from CID of (Gly-Gly-Gly)H+.

aziridinone, is in fact the neutral that is lost in the formation of the $\mathbf{y_1}$ ion from tripeptides[21]. The small initial cross section observed for the $\mathbf{y_1}$ ion is likely due to the much faster reaction occuring at that same amide bond leading to the $\mathbf{b_2}$ ion. At ~5 eV one observes a sharp increase in the $\mathbf{y_1}$ appearance curve; this is due to the decomposition of $\mathbf{y_2}$ into $\mathbf{y_1}$ and $\mathbf{a_1}$ ions. Using eq. 6.1 to fit the data, the $\mathbf{y_2}$ threshold energy is found to be 73.1 kcal/mol. Due to the kinetic shift and kinetic supression of this pathway by the $\mathbf{b_2}$ reaction, this threshold energy substantially overestimate the true activation energy which is expected to be < 38 kcal/mol, based on the glycylglycine results.

It is interesting to compare the relative ion abundances obtained from our low energy experiments with those obtained from high energy CID[30]. Under high energy conditions, the $\mathbf{b_2}$ ion is found to be the dominant ion produced, with the only other significant fragment being the $\mathbf{y_2}$ ion. The relative ion abundances at high energy therefore correspond to what we observe at very low collision energies (see Figure 6.12). A survey of the the high energy CID spectrum of other protonated tripeptides reveals that the $\mathbf{b_2}$ and $\mathbf{y_2}$ ions are always observed as major fragment ions[28].

The largest system examined to date is protonated Gly-Gly-Gly-Gly which contains three amide bonds at which cleavage can occur. The breakdown graph for this ion is shown in Figure 6.13. The two dominant low energy fragment ions are the $\mathbf{y_2}$ and $\mathbf{b_2}$ ions which originate from cleavage of the middle amide bond. Somewhat surprisingly, it is the $\mathbf{y_2}$ ion that has the lowest observed onset energy, in contrast to what was observed with Gly-Gly-Gly. It is not clear whether this lower observed onset energy for the $\mathbf{y_2}$ ion is the result of a lower activation energy or

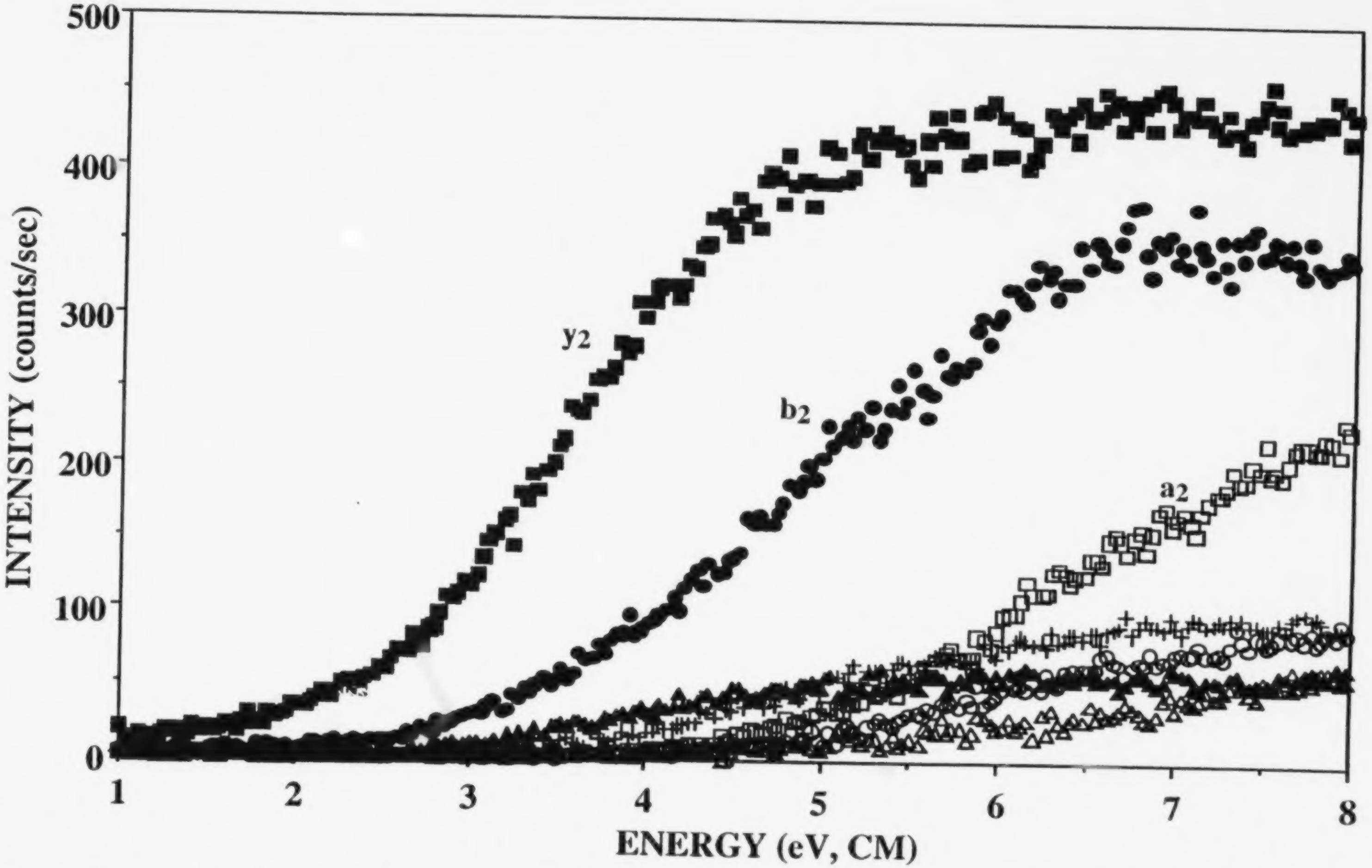

Figure 6.13 Appearance curves of the b_2 (●), y_2 (■), a_2 (□), b_3 (▲), y_3 (+), a_1 (△)and y_1 (○) fragment ions from CID of (Gly-Gly-Gly-Gly)H^+.

whether this reflects faster dissociation kinetics (i.e. a smaller kinetic shift). The threshold energies of the **y_2** and **b_2** ions, determined using eq. 6.1, are 63 and 79 kcal/mol respectively[31]. The **y_1**, **y_3**, **a_1** and **b_3** fragment ions are also observed, and exhibit similar onset energies. The reaction cross sections for these fragment ions are much lower than observed for the **b_2** and **y_2** ions suggesting much slower dissociation kinetics for cleavage of the amide bonds at either end of the peptide compared with the middle bond. It is not clear why CID leads preferential cleavage at the middle amide bond and this question deserves further investigation. The relative ion abundances in Figure 6.13, differ substantially with those observed in the metastable[4a] and CID[32] spectum of the FAB-generated peptide. In both cases, the **y_2** ion is observed as the major fragment ion, similar to our results, however, the **b_4** and to a lesser extent the **b_3** ions are also observed in large abundance. The **b_4** ion, which is formed by the loss of H_2O, is especially interesting since we observe it only as a very minor fragment ion. Loss of H_2O is in fact a common process in the decomposition of FAB-generated polyglycines and alanines[4a,30]. The low abundance of this ion under our experimental conditions suggest that much higher internal energies are required to generate significant amounts of this ion.

Conclusions

The present work details our first attempt to quantify the dissociation energetics of small protonated peptides using energy-resolved CID. At low collision energies (<10 eV, CM), ions with the general structure, $^{+}H(H_2N\text{-}CH_2\text{-}CO\text{-}X)$ are found to dissociate primarily at the C-X bond. For all X's studied, the immonium ion (or **a_1** ion) was observed as a major fragment ion. The energetics for this reaction were found to be insensitive to the nature of X, with threshold energies lying between 44 and 50 kcal/mol. When X was NHMe or $NHCH_2COOH$ a second dissociation pathway is found to operate, leading to XH_2^+ ($\mathbf{y_1}$) as a fragment ion. Due to uncertainty in the structure of the transition state leading to this fragment ion, only upper limits to the true activation energy were determined. In both cases the threshold energies were found to lie below the activation energy measured for the complementary reaction leading to the $\mathbf{a_1}$ ion.

The lowest energy CID fragment ion observed for ions with the general structure Gly-Gly-X, is found to be the $\mathbf{b_2}$ ion, corresponding to the loss of neutral HX. In the case of glycylglycinamide, the threshold energy for this reaction was measured to be 20.4 kcal/mol. The very low threshold energy is consistent with the $\mathbf{b_2}$ ions undergoing cyclization, leading to a protonated oxazalone structure.

The observed onset energies for the fragment ions of precursors larger than glycinamide are found to be significantly affected by kinetic shifts due to lifetime effects. For example, the kinetic shift observed for the $\mathbf{a_1}$ ion produced from glycine is 0.5 kcal/mol, while for glycylglycine it increases to 21 kcal/mol. An additional source of error stems from the competitive nature of the dissociation process. Fast processes, with large relative rate constants, tend to kinetically supress other pathways which may be energetically accessible but proceed at a slower rate. As a result of these two factors, the uncertainty associated with CID threshold energies increases as the size of the ion and number of fragment ions increases.

References

1. Hunt, D.F.; Yates, J.R.III; Shabanowitz, J.; Winston, S.; Hauer, C.R. *Proc. Natl. Acad. Sci. U.S.A.* **1986**, *83*, 6233.
2. Somogyi, A.; Wsysocki, V.H.; Mayer, I. *J. Am. Soc. Mass Spectrom.* **1994**, *5*, 704.
3. Poppe-Schriemer, N.; Ens, W.; O'Neil, J.D.; Spicer, V.; Standing, K.G.; Westmore, J.B.; Yee, A.A. *Int. J. Mass Spectrom. Ion Process.* **1995**, *143,* 65.
4. (a) Yalcin, T.; Khouw, C.; Csizmadia, I.G.; Peterson, M.R.; Harrison, A.G. *J. Am. Soc. Mass Spectrom.* **1995**, *6*, 1164; (b) Yalcin, T.; Csizmadia, I.G.; Peterson, M.R.; Harrison, A.G. *J. Am. Soc. Mass Spectrom.* **1996**, *7*, 233.
5. Meot-Ner, M.; Dongre, A.R.; Somogyi, A.; Wysocki, V.H.; *Rapid Commun. Mass Spectrom.* **1995**, *9*, 829.
6. Price, W.D.; Schnier, P.D.; Williams, E.R. *Anal. Chem.* **1996**, *68*, 859.
7. Armentrout, P.B. "Thermochemical Measurements by Guided Ion Beam Mass Spectrometry" in Advances in Gas Phase Ion Chemistry" 1992, Vol. 1, p.83. Adams, N. and Babcock, L.M., Eds., JAI Press Inc., Greenwich, Conn. U.S.A.
8. Sunderlin, L.S.; Wang, D.; Squires, R.R. *J. Am. Chem. Soc.* **1993**, *115*, 12060; Mazinelli, P.J.; Paulino, J.A.; Sunderlin, L.S.; Wenthold, P.G.; Poutsma, J.C.; Squires, R.R. *Int. J. Mass Spectrom. Ion Process.* **1994**, *130*, 89.
9. Kebarle, P. *Annu. Rev. Phys. Chem.* **1977**, *28*, 445.

10 Klassen, J.S.; Blades, A.T.; Kebarle, P. *J. Phys. Chem.* **1995**, *99*, 15509; Blades, A.T.; Klassen, J.S.; Kebarle, P. *J. Am. Chem. Soc.* **1995**, *117*, 10563.

11 . (a) Klassen, J.S.; Anderson, S.G.; Blades, A.T.; Kebarle, P. *J. Phys. Chem.* in press; (b) Anderson, S.G.; Blades, A.T.; Klassen, J.S.; Kebarle, P. *Int. J. Mass Spectrom. Ion Process.* **1995**, *141*, 217.

12 . Dalleska, N.F.; Honma, K.; Armentrout, P.B. *J. Am. Chem. Soc.* **1993**, *115*, 12125.

13 . Loh, S.K.; Hales, D.A.; Lian, L.; Armentrout, P.B. *J. Phys. Chem.* **1989**, *90*, 5466.

14 . Schmidt, M.W.; Baldridge, K.K.; Boatz, J.A.; Elbert, S.T.; Gordon, M.S.; Jensen, J.H.; Koseki, S.; Matsunaga, N.; Ngyuen, K.A.; Su, S,J.; Windus, T.L.; Dupuis, M.; Montgomery, J.A. *J.Comput. Chem.* **1993**, *14*, 1347.

15 . (a) Meot-ner, M.; Field, F.H. *J. Am. Chem. Soc.* **1973**, *95*, 7207; (b) Tsang, C.W.; Harrison, A.G. *J. Am. Chem. Soc.* **1976**, *98*, 1301; (c) Dookeran, N.N.; Yalcin, T.; Harrison, A.G. *J. Mass Spectrom.* **1996**, *31*, 500.

16.. Beranová, S.; Cai, J.; Wesdemiotis, C. *J. Am. Chem. Soc.* **1995**, *117*, 9492.

17. (a) Bouchonnet, S.; Hoppilliard, Y. *Org. Mass Spectrom.* **1992**, *27*, 71; (b) Jensen, F. *J. Am. Chem. Soc.* **1992**, *114*, 9533; (c) Bouchoux, G.; Bourcier, S.; Hoppilliard, Y.; Mauriac, C. *Org. Mass Spectrom.* **1993**, *28*, 1064.

18. The HF energies (in atomic units) calculated using a 3-21G basis set are: E(**Ic**)=-281.552329, E(**Id**)=-281.55077, E(**Ie**)=-281.574730.

19. The HF energies calculated using a 3-21G basis set are: E(**IIa**)=-261.9110653, E(**IIb**)=-261.876203, E(**IIc**)=-261.8330618 a.u..

20. Mueller, D.R.; Eckersley, M.; Richter, W.J. *Org. Mass Spectrom.* **1988**, *23*, 217.

21 Cordero, M.M.; Houser, J.J.; Wesdemiotis, C. *Anal. Chem.* **1993**, *65*, 1594.

22. The calculated AM1 energies are: E(**IIIa**)=-45.423633, E(**IIIb**)= -45.410295, E(**IIIc**)=-45.37007 a.u..

23. The vibrational frequencies of the transition state associated with the dissociation of the protonated dimer (**IIIe**) are expected to resemble those of the products, aziridinone and protonated methylamine, plus five low energy frequencies associated with translational and rotational degrees of freedom in the products. The vibrational freqencies for the products were obtained from calculations, while the five low energy frequencies were estimated to lie between 10 and 30 cm^{-1}, thus leading to the upper and lower limits of 24 and 13 cal/deg mol for $\Delta S^{\ddagger}$.

24. Lias, S.G.; Liebman, J.F.; Levin, R.D. *J. Phys. Chem. Ref. Data* **1984**, *13*, 695.

25. Zhang, K.; Zimmerman, D.M.; Chung-Phillips, A.; Cassady, C.J. *J. Am. Chem. Soc.* **1993**, *115*, 10812.

26. McCormack, A.L.; Somogyi, Á.; Dongré, A.R.; Wysocki, V.H. *Anal. Chem.* **1993**, *65*, 2859.

27. The geometry of the **TS(b_2)** was obtained, using semiempirical calculations (AM1), by varying the C-NH_3 bond length and optimizing the remaining degrees of freedom. The energy maximum (E=-69.993005 au) was located at a bond length of 5.0 Å.
28. In assigning this ion as a **y_1** type it is understood that the -$NHCH_2CONH_2$ group is treated as one residue.
29. No detailed search for the lowest energy geometry of protonated Gly-Gly-Gly was performed, the internal energy distribution of the precursor ion was evaluated using the vibrational frequencies of a single local minima obtained from semiempirical calculations. The average internal energy obtained with these frequencies is 7.2 kcal/mol. This is close to what one would have estimated based on the average internal energies obtained for protonated glycine, 1.7 kcal/mol, and glycylglycine, 4.4 kcal/mol.
30. Kulik, R.W.; Heerma, W. *Biomed. Environ. Mass Spectrom.* **1989**, *18*, 910.
31. The average internal energy of the precursor ion was estimated to be 10 kcal/mol.
32. Yeh, R.W.; Grimley, J.M.; Bursey, M.M. *Biol. Mass Spectrom.* **1991**, *20*, 443.